UNIVERSITY OF ADELAIDE LIBRARY 27/4/04

Surface Mixers for Destratification and Management of *Anabaena circinalis*

by

David Milton Lewis

March-2004

A Thesis Submitted for the Degree of

Doctor of Philosophy

School of Civil and Environmental Engineering

The University of Adelaide

Australia

"Philosophy is written in this grand book the universe, which stands continually open to our gaze, but the book cannot be understood unless one first learns to comprehend the language of mathematics, and its characters are triangles, circles, and other geometric figures, without which it is humanly impossible to understand a single word of it; without these, one wanders about in a dark labyrinth."

Galilei, Galileo (1618)

ABSTRACT

In 1998, the South Australian water utility SAWater and the Cooperative Centre for Water Quality and Treatment commenced project 2.5.1, entitled Destratification for Control of Phytoplankton, for which this research forms a part. The major objective of the project was to assess a novel method for destratification and control of cyanobacteria, in particular *Anabaena circinalis* Rabenh. *ex* Born. *et* Flah, with the use of raft-mounted mechanical surface mixers with draft-tubes, hereafter referred to as surface mixers.

The primary aims of destratification are to maintain aerobic conditions to prevent the release of iron, manganese and nutrient from the sediment, and to control excessive growth of nuisance phytoplankton, in particular cyanobacteria. The overall objectives for this research were to:

1. Ascertain if the surface mixers could be used as an effective management tool to improve water quality in lakes and reservoirs.
2. Quantify the hydrodynamic behaviour of the surface mixers.
3. Use numerical modelling techniques to extend the assessment of the surface mixers beyond the analysis of field data.

This thesis describes the investigation undertaken used to quantify the impact of the surface mixers upon the thermal structure and phytoplankton assembly. The surface mixers are essentially large impellers with a diameter of 4.9 m, which are suspended below the surface water at a depth of 1.8 m that pump water from the surface down through a 13 m draft-tube (suspended below the impeller). A critical factor to assess the surface mixers was to understand the hydrodynamics imparted by the large diameter, high Reynolds number impeller-induced swirling jet upon the water column. Historically, analysis of jets generated by impellers has been either restricted to laboratory scale experiments or based upon limited field observation. The investigation of the impeller-induced swirling jet at this scale was unique and provided the opportunity to determine if the published literature on impeller-induced

swirling jets were relevant to large-scale impellers. The surface mixers generate a very large swirling jet that can change from being purely momentum driven to buoyancy driven over relatively short time periods (hours to days) depending on the meteorological conditions.

The surface mixers were installed, and subsequent field investigations were carried out in Myponga Reservoir, South Australia. The monitoring of the meteorological conditions and thermal structure of the water column was achieved with two meteorological monitoring stations. The phytoplankton assemblage was also monitored with integrated phytoplankton samples from 0 to 5 m below water surface collected regularly (daily, weekly or monthly, depending on the season) for identification and enumeration. This had inherent limitations, which restricted the ability to recommend the use of surface mixers in other water bodies. Consequently, the use of numerical modelling was employed so that the surface mixers could be assessed under different operating conditions. Surface mixers of this scale and configuration had not been modelled before, so the development of an appropriate surface mixer algorithm was undertaken, and validated against field data.

The primary contributions from this research have been to provide insight into the capabilities of surface mixers, quantify the characteristics of large impeller-swirling jets, determine the effects of their impact upon cyanobacteria growth and destratification capabilities, and has enhanced the role of numerical modelling for reservoir management.

It was concluded that the surface mixers are able to remove buoyant cyanobacteria from the surface water and transport them to below the draft-tube depth, and limit the severity of stratification. The penetration of the surface mixer jet was found to be a function of the surface water temperature and the ambient water temperature at the exit point of the draft-tube. Consequently, during periods of excessive solar insolation, the jet issuing from the draft-tube becomes buoyant and is not able to reach the sediment surface, thus limiting the destratification capabilities and reducing the time that entrained cyanobacteria remain below the surface.

The characterisation of the surface mixer flow showed that the large diameter, high Reynolds number impeller-induced swirling jet fully develops at shorter distances than jets reported in the literature, during both stratified and isothermal conditions. The radial spread for the surface mixer flow under isothermal conditions is approximately three times that of a non-swirling jet. The entrainment into the jet has been analysed and can be predicted under isothermal and stratified conditions. This enabled the development of the surface mixer algorithm that describes the diffusion of the efflux, which allows the surface mixers to be assessed in any water body under varying meteorological conditions and enables informed decisions to be made.

STATEMENT OF ORIGINALITY

This work contains no material that has been accepted for the award of any other degree or diploma in any university or other tertiary institution and, to the best of my knowledge and belief, contains no material previously published or written by another person, except where due reference has been made in the text.

I give consent to this copy of my thesis, when deposited in the University Library, being available for loan and photocopying.

Date: 8/4/04

David Milton Lewis

ACKNOWLEDGMENTS

Throughout the entire project I have received continuous guidance and support from my supervisors, Dr Martin Lambert (School of Civil and Environmental Engineering, University of Adelaide) and Dr Justin Brookes (Cooperative Research Centre for Water Quality and Control, CRCWQT). I am honoured to work with these two outstanding academics and thank them for their input, encouragement and assisting with my professional development. Also, I would like to acknowledge the Cooperative Research Centre for Water Quality and Treatment for funding project 2.5.1, for which this thesis forms a part, and in particular I would like to thank Dr Dennis Steffensen and Mr Michael Burch for their support and giving me the opportunity to be part of the project team.

I have also had the privilege to collaborate with several world-class researchers during the course of the project that gave invaluable suggestions and provided opportunities for exploration of new ideas. I would like to express my gratitude to Associate Professor George Ganf from the School of Earth and Environmental Sciences, University of Adelaide; Professor Colin Reynolds, Dr Alex Elliott and Dr Tony Irish from the Centre for Ecology and Hydrology, UK; and Dr Jason Antenucci from the Centre for Water Research, University of Western Australia.

I would like to thank the many people who assisted with the extensive fieldwork carried out at Myponga Reservoir. Firstly, my fellow PhD student Rudi Regel, for his insight into freshwater ecology; Leon Linden and Dr John Vítkovský for their assistance with all the measurements; Dr Bradford Sherman for advising me to read the manual; Dr Jason Cassells for surveying Myponga River and the catchment; Mr Allan Brown, Mr Rod Boothey and Mr Vivien Pigeon who manage the reservoir operations, and Mr Gregory Atkins, Mr Jeffrey Hiorns and Mr Steven Huskinson for laboratory support.

Finally, I would like to thank my wife Joanne and my parents for their patience and encouragement throughout my PhD studies.

LIST OF PUBLICATIONS

The publications produced during this research are listed below. These represented the developmental nature of the research.

JOURNAL PAPERS

Lewis, D.M., Elliott J.A., Brookes, J.D., Lambert, M.F., Irish, A.E., and C.S. Reynolds, (2003). The effects of artificial mixing and copper sulphate dosing on phytoplankton in a simulated Australian reservoir. *Lakes and Reservoirs: Research and Management.* **8**, 31 - 40.

Linden, L., **Lewis, D.M.**, Burch, M.D. and J.D. Brookes, (2003) Nutrient load is determined by high flow episodes in the Mediterranean Myponga Reservoir. *Marine and Freshwater Research* (In Review).

Antenucci, J., Brookes, J.D. and **D.M. Lewis,** (2003). The use of mechanical destratification for the management of water quality in reservoirs. *Water*, (In Review).

Lewis D.M., Elliott J.A., Lambert M.F., and C.S. Reynolds (2002) The simulation of an Australian reservoir using a phytoplankton community model (PROTECH). *Ecological Modelling.* **150(1-2)**, 107 - 116.

Brookes, J.D., **Lewis, D.M.**, Linden, L., and M.D. Burch, (2002) On-line monitoring of reservoirs for risk management: linking reservoir data and treatment for improved management. *Water*, **29**(5), 20 - 27.

Lewis, D.M., Antenucci, J.P., Brookes, J.D., and M.F. Lambert, (2002) Surface mixing for destratification: simulating the impact. *Water*, **29**(5), 27 - 29.

CONFERENCE PAPERS

Lewis, D.M., Brookes, J.D. and M.F. Lambert, (2003). Numerical models for cyanobacteria management. *Fifth Asia-Pacific Conference on Algal Biotechnology. Focus: Algae for Human and Environment. P.R. China*. October 2003.

Brookes, J.D., **Lewis, D.M.** and L.G. Linden, (2002). Predicting, detecting and managing cyanobacteria in source water. *American Water and Wastewater Association. Water Technology Congress, Seattle*. November 2002.

Lewis, D.M. (2002). Artificial mixing and algal growth. *Third Postgraduate Student Conference, Cooperative Research Centre for Water Quality and Treatment; Reynella, Australia*. October 2002, 135 – 140.

Lewis, D.M., Antenucci, J.P., Brookes, J.D., and M.F. Lambert, (2001) Numerical simulation of surface mixers used for destratification of reservoirs. *International Congress on Modelling and Simulation, MODSIM 2001, Canberra, Australia.* December 2001, 311 - 317.

Lewis, D.M., Antenucci, J.P., Brookes, J.D., and M.F. Lambert, (2001) Numerical simulation of surface mixers used for artificial mixing in reservoirs. *Environmental Engineering Research Event. Noosa, Queensland, Australia*. November 2001, CD-ROM.

Regel, R.H., Brookes, J.D., **Lewis, D.M.**, Ganf, G.G., and M.D. Burch, (2001) Time scale of 'events' and threats to water quality within lakes and reservoirs. *Proceedings of the International Water Association 2nd World Water Congress, Berlin*. October 2001, CD-ROM.

Lewis, D.M. (2000). Turbulent transport of phytoplankton in artificially destratified reservoirs. *Second Postgraduate Student Conference, Cooperative Research Centre for Water Quality and Treatment; Daylesford, Australia*. October 2000, 17 – 22.

CONSULTANCY REPORTS

Billington, A., Cresswell, T., **Lewis, D.M.** and D. Walker, (2003). Investigating thermal stratification in the Torrens Lake. Prepared for the Torrens Catchment Water Management Board (pp 34).

Lewis, D.M., Regel, R.H., Ganf, G.G. and J.D. Brookes, (2002). Determination of flow generated by artificial mixing devices in the Torrens Lake. Prepared for the Torrens Catchment Water Management Board.

Linden, L.G., Burch, M.D., Brookes, J.D., Baker, P., Sherman, B.S. and **D.M. Lewis,** (2002). Artificial destratification and water quality in Happy Valley Reservoir. Report to SAWater Operations (pp 65).

Baker, P, Burch, M.D., Brookes J.D., Cenzato, D.M., **Lewis, D.M.** and G.G. Ganf, (2000). Torrens Lake monitoring, research and management of cyanobacterial growth 1999/2000. Prepared for Adelaide City Corporation and Torrens Catchment Water Management Board (pp 95).

Brookes, J. D., Burch, M. D. and **D.M. Lewis,** (1999). Transport time of pathogens from inflow to outflow at Myponga Reservoir. Report to Bulkwater Division, SAWater.

TABLE OF CONTENTS

LIST OF FIGURES

LIST OF TABLES

1. INTRODUCTION

Water quality in lakes and reservoirs is severely affected by the natural occurrence of vertical density stratification that occurs in temperate zones, which experience significant contrasts in seasonal meteorological conditions. Stratification creates a thermal and density structure in the water column that is characterised by a surface mixed layer (*SML*) that is effectively separated from deeper hypolimnetic water by a sharp density gradient, known as the metalimnion. The metalimnion prevents surface induced mixing penetrating to the hypolimnion that can become anoxic due to chemical reduction processes and biological respiration. The stable stratified water column can also favour the growth of nuisance scum forming phytoplankton species. Artificial mixing (destratification) with the aid of mechanical devices is often used to limit the occurrence of stratification, thus improving water quality. The primary aims of destratification are to maintain aerobic conditions to prevent the release of iron, manganese and nutrient from the sediment (Ismail *et al.*, 2002), and to control excessive growth by nuisance phytoplankton species e.g. *Anabaena circinalis*.

The research undertaken and reported in this PhD thesis provides a comprehensive evaluation of the capabilities of prototype raft-mounted mechanical surface mixers with draft-tubes, hereafter referred to as surface mixers (Fig. 1.1), used for the control of cyanobacterial growth and destratification. The surface mixers pump surface water (top 1.2 m), via a large diameter (4.9 m) impeller fixed to a pontoon, through a 13 m draft-tube, which extends through the metalimnion, into the hypolimnion to break down and inhibit the formation of the vertical density structure. The scum-forming cyanobacteria are also removed from the surface water by the pumping of the surface mixers, with the aim to inhibit growth by limiting the light available for photosynthesis.

1.1 OBJECTIVES AND ACHIEVEMENTS

The central objective for this work was to determine if the surface mixers could be used as an effective management tool to improve water quality in lakes and reservoirs. Historically, analysis of various types of surface mixers has been either restricted to

laboratory scale experiments or based upon limited field observation. An important aim of the project is to provide information for the design of surface mixers used for destratification and control of cyanobacterial growth, so that informed judgement can be made when determining the most appropriate method to manage water storages when considering the use of surface mixers.

The primary contribution of this work has been to provide insight into the capabilities of surface mixers and the effects of their impact upon cyanobacteria growth and destratification, and has enhanced the role of numerical modelling for reservoir management. Additionally, a significant contribution to the understanding of large diameter, high Reynolds number swirling jets has been achieved. Non-swirling jets have only radial and axial velocities, whereas a swirling jet also has tangential velocity. The swirling jet generated by the surface mixers is axisymmetric and could not be described by non-swirling axisymmetric jet theory (Albertson *et al.*, 1950). The introduction of swirl to an axisymmetric jet causes several large-scale effects on the flow field that are not present in a non-swirling jet (Petersson *et al.*, 1996). The surface mixers generate a very large swirling jet that can change from being purely momentum driven to buoyancy driven over relatively short time periods (hours to days) depending on the meteorological conditions. Traditionally, swirling jet theory has been largely restricted to laboratory studies and this research provided an ideal platform to investigate these jets at full-scale in the field.

The surface mixers are located in two South Australian primary drinking water supply reservoirs. Preliminary design, manufacture and installation of the surface mixers (undertaken by WEARS Pty Ltd) do not form part of the reported research. Prior to the commencement of this research the South Australian Water Utility, SA Water, installed the surface mixers during late 1998. Two surface mixers are deployed in Myponga Reservoir, and used in conjunction with an existing aerator. Another surface mixer was installed at Happy Valley Reservoir and was also used in conjunction with an aerator, which formed part of a concurrent project focused on developing a management plan for SA Water (Linden *et al.*, 2002). *Anabaena circinalis* is the dominant planktonic cyanobacteria in both reservoirs and is known to produce geosmin which causes taste and odour problems. This species is the focus of management strategies that traditionally involved algicide dosing ($CuSO_4$) and more

recently artificial destratification with the installation of surface mixers that complement the existing aerators.

To fully assess the impact of the surface mixers upon the physical, chemical and biological parameters, required that they be operated independently of the aerators so as to eliminate the effect of the aerators. The management procedures at the two reservoirs restricted the operational flexibility of the artificial mixing systems and subsequently the surface mixers could only be operated independently of the aerators from mid-autumn to early spring, which coincides with well-mixed conditions and are typically periods of insignificant cyanobacterial growth. This provided the impetus to undertake numerical modelling that assisted with the analysis of the surface mixers and to investigate the seasonal behaviour of the phytoplankton assemblage at Myponga Reservoir.

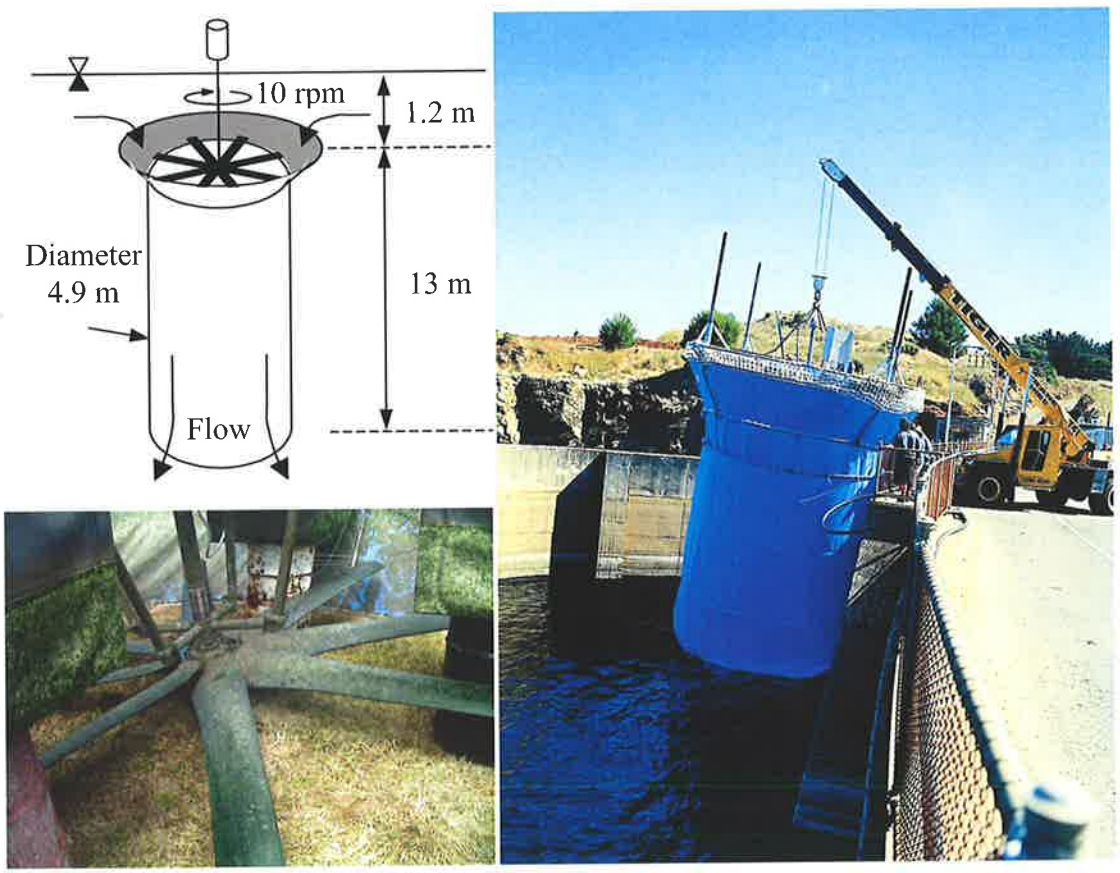

Figure 1.1 Surface mixer schematic, impeller blades and a surface mixer being lowered into Myponga Reservoir from the dam wall.

1.2 THESIS OVERVIEW

A literature review is presented in Chapter 2, which covers relevant aspects of artificial destratification and background on problems associated with excessive cyanobacteria growth. The literature review also provides an overview of jet and plume theory, which was required to understand the flow behaviour that was generated by the surface mixers. The numerical models used to investigate the phytoplankton assemblage and assess the impact of the surface mixers are also presented in Chapter 2. Chapter 3 presents the instrumentation and field methods used to investigate the limnological processes in Myponga Reservoir, which gave crucial insight into the capabilities of artificial destratification. Surprisingly, up until the mid-nineties, minimal monitoring of the impact of artificial destratification was undertaken, which limited the understanding of when and how artificial destratification should be employed (Schladow and Fisher, 1995). The data has been made available to water quality managers and researchers alike. The field data is assessed in Chapter 4 where important mechanisms unique to Myponga Reservoir are discussed and their implications to artificial destratification are highlighted.

The phytoplankton assemblage and artificial destratification operations at Myponga Reservoir were investigated with two one-dimensional hydrodynamic and aquatic ecological numerical models, which assume that first order balances of energy, momentum and mass are determined by vertical property variations. The code in both numerical models was extended to incorporate the simulation of the hydrodynamic action of the surface mixers, and $CuSO_4$ dosing. To justify using one-dimensional numerical modelling, where fluctuations in lateral directions are small compared with vertical variations (Hamilton and Schladow, 1997), drogue studies were undertaken at Myponga Reservoir investigating lateral mixing mechanisms. The results from this study are presented in Chapter 4.

Chapter 5 introduces the numerical phytoplankton growth model PROTECH (Phytoplankton RespOnses To Environmental CHange) and the subsequent improvements to the code that were necessary so that the model could be applied to Myponga Reservoir. PROTECH was developed in the United Kingdom to fulfil a commercial, decision-support role for management of water-supply storages where

phytoplankton growth can be problematic (Reynolds *et al.*, 2001). This research also provided the opportunity to test PROTECH by simulating a reservoir in the Southern Hemisphere, which had previously been used exclusively in the Northern Hemisphere. Additionally, a surface mixer algorithm based on preliminary flow measurements (Chapter 6) was incorporated into PROTECH. This allowed extensive numerical evaluation of the surface mixers, enabling their impact upon phytoplankton growth to be assessed.

Upon the successful work undertaken with PROTECH that culminated in the publication of two referred journal papers (Lewis *et al.*, 2002b; Lewis *et al.*, 2003), a University of Adelaide Small Research Grant was obtained to purchase a field-version acoustic velocimeter (*ADVField*) that was required to be able to adequately measure flow mechanisms within Myponga Reservoir (Chapter 3). To investigate the flow characteristics of the surface mixers with the *ADVField* a novel device was designed and manufactured, allowing the *ADVField* to be securely suspended below the surface mixer draft-tube (Chapter 6).

A comprehensive description of the surface mixer flow is presented in Chapter 6. The detailed flow measurements were used to develop an algorithm describing the entrainment, spread and penetration of the surface mixer efflux, which was integrated into an existing hydrodynamic numerical model DYRESM (DYnamic REservoir Simulation Model), presented in Chapter 7. The successful validation and application of the algorithm resulted in its permanent placement into DYRESM, which is freely available to researchers and water quality managers via the Internet (http://www.cwr.uwa.edu.au/). The development and validation of the surface mixer algorithm has been presented at two conferences and published in the conference proceedings (Lewis *et al.*, 2001a; Lewis *et al.*, 2001b).

To investigate the destratification capabilities and impact upon phytoplankton growth by the surface mixers, the aquatic ecological model CAEDYM (Computational Aquatic Ecosystem DYnaMics) was utilised. To initially validate CAEDYM, essential changes to the code and parameterisation was undertaken. These are presented in Chapter 8. To fully analyse the impact of the surface mixers and aerator at Myponga

Reservoir, the improved DYRESM model was coupled to the modified CAEDYM model and the following operational strategies investigated:

- No artificial mixing
- Surface mixers and aerator
- Aerator operation only
- Surface mixer operation only

The analysis of the numerical simulation is provided in Chapter 8.

The thesis is concluded (Chapter 9) with a discussion of the impact of the surface mixers on the physical, chemical and biological processes in reservoirs. To implement technology transfer from this research into the commercial sector, which focuses on water quality, and the wider community, two articles were published in the Australian Water Associations journal Water; see Brookes *et al.* (2002) and Lewis *et al.* (2002a).

1.2.1 Research program

The sequence and achievements of the research undertaken is summarised below:

- Literature review (Chapter 2).
- Deployment of meteorological monitoring stations at the two reservoirs (Chapter 3).
- Extensive drogue experiments at Myponga Reservoir investigating large basin scale mixing mechanisms (Chapter 4).
- Comprehensive water quality data monitoring and analysis (Chapter 4).
- Application modification and validation of the freshwater phytoplankton growth model PROTECH (Chapter 5).
- Examination of the phytoplankton community assemblage at Myponga Reservoir using PROTECH (Chapter 5).
- Measurements of the near and far field flow generated by the surface mixers (Chapter 6).
- Engineer novel methods to measure the efflux, far field and near-field flows around the surface mixers (Chapter 6).

- Detailed flow analysis of large diameter, high Reynolds number swirling jets generated by the surface mixers (Chapter 6).
- Development and incorporation of a surface mixer algorithm into the one-dimensional hydrodynamic model DYRESM (Chapter 7).
- Validation of the DYRESM surface mixer algorithm (Chapter 7).
- Simulation of Myponga Reservoir with the modified DYRESM-CAEDYM coupled hydrodynamic and ecological model (Chapter 8).
- Investigation of various management strategies used to control cyanobacterial growth, which explores the impact of artificial mixing and $CuSO_4$ dosing, through DYRESM-CAEDYM model simulations (Chapter 8).

1.3 Background

The quality of surface waters is compromised by the excessive input of nutrients that has occurred internationally for several decades (Psenner, 1994). The ramifications of the subsequent eutrophication are increased productivity and decreased biological variability and are widely reported in the literature (de Jonge *et al.*, 2002; Hodgkin and Hamilton, 1993). The problems associated with eutrophication can be exacerbated by the occurrence of stratification of surface waters that can further intensify the degradation of water quality (Reynolds, 1997b). Co-existence of eutrophication and stratification can provide favourable conditions of suitable temperature; adequate light, minimal turbulence and high nutrient concentration that favour the increased growth of scum-forming cyanobacteria in reservoirs, lakes and lowland rivers. The control of cyanobacteria growth in water supply reservoirs is of paramount importance to the water industry because these organisms can potentially produce toxins and compounds that taint the taste and odour of potable water.

The occurrence of cyanobacterial growth is largely dependent on climatic conditions. Growth can occur during late summer and early autumn in temperate zones, extend longer in sub-tropical climates, and can persist all year round during dry years in tropical and sub-tropical areas (Sivonen and Jones, 1999). During these periods, reservoirs and lakes can be stratified, which is characterised by an upper stratum of circulating water, the epilimnion. The epilimnion overlies a cooler region, the hypolimnion. The area between the epilimnion and the hypolimnion is characterised by a sharp thermal discontinuity, and is known as the metalimnion (Monismith and

Fong, 1996). A typical temperature profile for Myponga Reservoir highlighting these strata is shown in Fig. 1.2. Within the metalimnion a plane exists, known as the thermocline, where a maximum rate of decrease of temperature T with respect to depth z occurs, i.e.

$$d^2T/dz^2 = 0 \tag{1.1}$$

Within the epilimnion a diurnal or secondary thermocline can form during periods of high insolation. This diurnal effect decreases the depth of the *SML* from the 'parent' thermocline to the secondary thermocline and can intensify water quality problems. Stratification minimises vertical mass transfer and largely prevents surface induced mixing penetrating through the metalimnion to the hypolimnion. Subsequently the hypolimnetic water is effectively separated from the atmosphere (Schladow and Fisher, 1995), and can become anoxic due to chemical reduction processes and biological respiration. The anoxic hypolimnetic water develops high concentrations of hydrogen sulphide, phosphates, nitrates and various metals (Steichen, 1970). The epilimnion is relatively stable and ideal for increased phytoplankton growth and in particular buoyant cyanobacteria growth. Individual water bodies have unique seasonal populations of cyanobacteria and phytoplankton, dependent on meteorological and geochemical conditions. However, the general seasonal patterns are predictable and the principles relating to cyanobacteria and phytoplankton growth are exchangeable throughout the period. The excessive growth of cyanobacteria is likely to recur annually, in those water bodies that have a history of phytoplankton or cyanobacterial blooms, if there are minimal changes in the physical and chemical conditions (Sivonen and Jones, 1999).

The control of scum-forming cyanobacteria and water quality can be achieved by manipulation of the physical and geochemical conditions within the water column. There are a variety of techniques that can be utilised to improve water quality, including: (1) reducing the external nutrient load (catchment management), (2) accelerate nutrient outflow or prevent nutrient recycling, and (3) chemical controls, artificial destratification, dredging, sediment consolidation and other habitat

intervention (Cowell *et al.*, 1987). Artificial destratification is often used to improve water quality (Schladow and Fisher, 1995), and has been shown to reduce the growth of scum-forming cyanobacteria in reservoirs and lakes (Steel and Duncan, 1999; Steinberg, 1983; Visser *et al.*, 1995). The individual areas of physical mixing and phytoplankton dynamics have been well researched, but there is little and fragmented understanding about the interaction of these areas (Reynolds, 1999). This research provides an understanding of the effects of artificial mixing via surface mixers upon the interaction of the physical, chemical and biological processes.

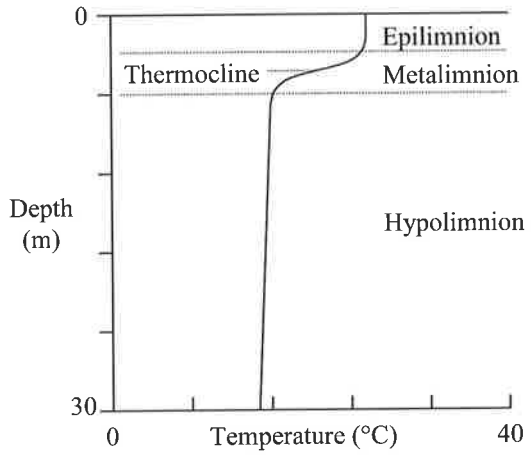

Figure 1.2 Typical temperature profile in Myponga Reservoir, showing the terminology of the various strata.

1.4 Artificial Mixing

Artificial mixing in water bodies is frequently employed to weaken density stratification that commonly occurs in lakes and reservoirs (Imberger and Patterson, 1989). Traditionally it is referred to as artificial destratification, which is used as a means to replenish oxygen levels in the hypolimnion and is commonly employed to avert significant stratification from occurring. One of the first reported uses of artificial destratification was by Hooper *et al.* (1952), who pumped hypolimnetic water into the epilimnion in a small lake. It is now recognised as an important management tool for drinking supply reservoirs (Steinberg, 1983). Artificial mixing is employed for varied uses, such as preventing winter fish kills, increasing productivity by circulating nutrients to the euphotic zone, reducing nutrient release from sediments, improving the downstream water quality, and controlling phytoplankton

and/or cyanobacterial blooms (Lorenzen, 1972; Sherman *et al.*, 2000; Tyson and Mobley, 1996).

Artificial mixing is generally undertaken during spring and summer so as to reduce the severity of stratification or breakdown strong seasonal thermoclines (Schladow and Fisher, 1995). Artificial mixing can also be undertaken to reduce the growth of scum-forming cyanobacteria, e.g. *Microcystis* (Visser *et al.*, 1996). Scum-forming cyanobacteria dominate during stable stratified periods as they benefit from being able to regulate buoyancy (by gas vacuoles), thus gaining a competitive advantage for resources, by being able to maintain their position in the euphotic zone, over non-buoyant phytoplankton, e.g. green algae and diatoms (Visser *et al.*, 1995). Non-buoyant algae have high sedimentation losses and during stratified conditions are unable to maintain their position in the euphotic zone.

Artificial mixing can impact phytoplankton growth, in particular cyanobacteria growth, by either reducing the internal nutrient load or increasing the depth of the *SML* (Sherman *et al.*, 2000). If the phytoplankton assemblage is maintained by an internal nutrient supply, artificial mixing can be used to limit nutrient availability by maintaining the dissolved oxygen levels in the hypolimnion, thus preventing reducing conditions occurring that lead to nutrient release from the sediment. If the nutrient loading is external, artificial mixing can be employed to increase the depth of the *SML* (z_{mix}) so that it is deeper than the euphotic zone (z_{eu}) and net photosynthetic production can be reduced (Kirk, 1994). Sherman *et al.* (1998) suggested that when $z_{mix}/z_{eu} > 3$ the growth of *Anabaena circinalis* can be limited.

Several investigations of the effects of artificial destratification upon phytoplankton growth have been reported in the literature. Using artificial destratification, Steinberg (1983) reported the successful biomass reduction of cyanophytes, in particular *Oscillatoria limnetica*, however the viable biomass of phytoplankton in the water column almost doubled, dominated by centric diatoms and cryptophytes. This was achieved in a small polytrophic and meromictic lake (max depth 11 m, volume 18 $x10^4$ m^3). Visser *et al.* (1996) found that artificial mixing in a hypertrophic lake (mean depth 18 m, volume $18x10^6$ m^3) during summer caused the phytoplankton assemblage to shift from a community dominated by cyanobacteria to a mixed

community of flagellates, green algae and diatoms. Cowell *et al.* (1987) determined the influence of whole lake (mean depth 4 m, surface area 21 $x10^4$ m^2) aeration upon the physical-chemical and biological parameters over a period of 2 years. Artificial mixing successfully eliminated the main undesirable effects of eutrophication including oxygen depletion, cyanobacterial blooms and low benthic diversity, but had no effect on the trophic state.

Artificial destratification assists large scale impoundment mixing, weakening the stratified conditions and can deepen the *SML*. Subsequently, buoyant cyanobacteria are removed from the euphotic zone, thus reducing their growth rate. To be effective, the artificial mixing device must be able to remove buoyant algae from the euphotic zone for extended periods (days) and generally this can only occur in deep water bodies (Reynolds, 1997b). The current research project focuses on surface mixers, but due to the presence of an aerator in Myponga Reservoir the impact of aerators are also discussed. The physical mechanisms of each device are presented below.

1.4.1 Bubble plume aerators

Bubble plume aerators release compressed air into the water body from a single or multi-port diffuser located at the bottom of a reservoir. As the air bubbles rise water is entrained creating a turbulent plume that in turn mixes the water column. Minimal oxygen transfer occurs from the air bubbles and the main oxygen transfer occurs at the surface.

The bubble plume aerator deployed in Myponga Reservoir has been successful in reducing the concentration of iron and manganese ions released from the sediment (Brookes *et al.*, 2000). This method is relatively expensive to operate due to the energy cost involved with compression of air and the inefficiency of the flow generation process. Nevertheless, the aerator at Myponga maintains aerobic conditions throughout the water column, and limits the degree of stratification for the majority of late spring and summer. The operational timetable of the aerator and surface mixers at Myponga Reservoir is shown later in Fig. 7.10.

1.4.2 Surface Mixers

The use of mechanical mixers for destratification is becoming increasingly popular; however, minimal research has been undertaken to determine the efficiency and

impact of mechanical mixers. The obvious benefits include the range and flexibility of mixers available and economic savings. The Oklahoma State University undertook studies in 1974 and 1978 on propeller-type lake destratification pumps to assess the effect of lake destratification upon water quality parameters (McLaughlin and Givens, 1978; Steichen, 1970). The objectives were to design, construct and test a device that could pump large volumes of water with low energy input, and establish the relationships among the system variables. Consequently, a low energy destratifier pump was developed by Quintero and Garton (1973). The pump was capable of moving 0.9 m^3s^{-1} from the surface to near the lake bottom, and was located in Ham's Lake, Oklahoma, which has a maximum depth of 9 m and surface area of 1.2 x 10^6 m^2. Steichen (1970) concluded that the pump was capable of intermittent deepening of the *SML* within the lake and maintained adequate dissolved oxygen concentration in the hypolimnion, but only caused minor changes in phytoplankton species predominating in the lake without impacting the growth of cyanobacteria. There was not sufficient data in the report to conclude why the growth of cyanobacteria was unaffected, but intuitively the reason is probably the inability to alter the light climate experienced by the plankton within the water body. During 1994, nine surface mixers were installed at Cherokee Dam to improve the dissolved oxygen content of hydro-turbine releases during the summer (Tyson and Mobley, 1996). The project was successful and the surface mixers remain in operation. However, no attempt was made to determine their effect, if any, on phytoplankton populations.

Traditionally, mixers have been used mainly in fluid bodies of relatively small scale (Petersson, 1996) but there is a potential for also using mixers in larger fluid bodies (Jonsson and Rissler, 1991; Stephens and Imberger, 1993). The research presented in the following chapters examines a jet that is 4.9 metres in diameter and has an outlet Reynolds Number (N_{Re}, Eq. 1.2) of $>10^6$ that is at least two orders of magnitude greater than discharges covered in the literature on jet analysis (see Fischer *et al.*, 1979).

$$N_{Re} = \frac{wD}{\nu} \tag{1.2}$$

In this definition of the Reynolds number, w is the mean discharge velocity and ν is the kinematic viscosity.

The results of this study enabled empirical relationships to be developed which reliably describe the hydrodynamic and geometric properties of large swirling jets. The publication of these results will enable large swirling jets with high Reynolds number generated from surface mixers to be effectively considered as a method of improving water quality in lakes and reservoirs.

2. LITERATURE REVIEW AND DESCRIPTION OF NUMERICAL MODELS

2.1 INTRODUCTION

The three main objectives for this research were to (1) ascertain if the surface mixers could be used for destratification (reviewed in Chapter 1) and to control the growth of cyanobacteria, (2) quantify the hydrodynamic behaviour of the surface mixers, and (3) use numerical modelling techniques to extend the assessment of the surface mixers beyond the analysis of field data. Consequently, the Literature Review is divided into three sections. The first deals with phytoplankton and cyanobacteria, followed by a review of jets and plumes, which is required to understand the fluid motions generated by the surface mixers giving insight into their capacity to destratify water bodies. The last section covers numerical modelling techniques used for the investigation of stratification and phytoplankton growth.

Artificial mixing techniques used in reservoirs to prevent stratification or destratify the water column and control phytoplankton biomass, include air-lift pumps, helixors, bubble curtains (aerators), jetted inlets and free jets. To control phytoplankton biomass with destratification the mixed conditions must reduce the light climate experienced by plankton, thus reducing their rate of photosynthesis. Artificial mixing vertically homogenises the water column and subsequently equalises the solute content. In some cases, these conditions can favour the growth of phytoplankton by alleviating the constraints of access to nutrients, and in the some cases light.

Due to the significant amount of physical, chemical and biological parameters affecting phytoplankton growth it is difficult to determine what conditions will result in the successful application of artificial mixing used for the control of phytoplankton growth (Lorenzen, 1972). A critical factor limiting phytoplankton growth is the depth of the *SML* relative to the penetration of irradiance that decreases exponentially with increasing mixed depth (see Chapter 4 Section 4.3).

The Urban Water Research Association of Australia (UWRAA) undertook a review of artificial destratification of water storages in Australia in December-1989 (McAuliffe

and Rosich, 1989). The report focused on the effectiveness of artificial destratification in controlling biological and chemical aspects of water quality. The use of artificial stratification in Australian water storages was determined to be of limited success as illustrated in Table 2.1.

Table 2.1 The degree of success achieved over specific water quality problems in Australian water storages listed in Appendix A (McAuliffe and Rosich, 1989).

Water Quality Problems	**Number of cases**		
	Success	**Limited Success**	**Failure**
Unpleasant tastes and odours	3 (25 %)	1	8 (67 %)
High phytoplankton levels	4 (16 %)	4 (16 %)	17 (68 %)
Undesirable algal species	4 (27 %)	4 (27 %)	7 (46%)
High iron, manganese or sulphides	12 (38 %)	10 (31 %)	10 (31 %)
Variable water quality	7	1	1
Low dissolved oxygen levels/release	23 (74 %)	1	8
Low temperature	-	-	1
High zooplankton/insect numbers	1	-	1
Fish kills	1	-	1
Dirty water complaints	1	-	1

Generally the control of colour and turbidity was successful, and to a lesser degree, the control of iron and manganese. The destratification systems were found to have minimal impact in controlling the growth of undesirable phytoplankton species, where the data in Table 2.1 indicates that 46 % of applications endeavouring to reduce these species levels failed to do so, and 27 % of the applications were of limited success. A conclusion that could be drawn from the work of McAuliffe and Rosich (1989) is the need to further understand the response of phytoplankton growth to water movement in water bodies. Each water body must be evaluated separately.

During 1988, three Flygt 4430 mixers were installed at Myponga Reservoir. The mixers had a mixer blade diameter of 2.5 m with a nominal flow rate of 4 $m^3 s^{-1}$. Each mixer was attached to the dam wall at adjustable depth and oriented from 0 – 45 degrees up from the horizontal (Velzeboer *et al.*, 1991). No detailed flow measurements were made to enable the flow to be characterised. Suter and Kilmore (1990) reported that the mixers were not successful in totally destratifying the reservoir, but limited local surface heating and reduced total algal biomass.

2.2 PHYTOPLANKTON AND CYANOBACTERIA

The contamination of water resources and drinking water by toxic substances, such as organic substances and heavy metals has been a major health concern in the twentieth century (Chorus and Bartram, 1999). Nutrient enrichment of water bodies (eutrophication) has been recognised as a growing concern since the 1950's, and cyanobacteria toxins have been identified as a significant problem affecting human and livestock health, arising as a result of eutrophication (Chorus and Bartram, 1999). Cyanobacteria are a group of photosynthetic plankton and the ability to understand and predict phytoplankton succession is essential to effectively manage our water resources.

In water bodies, the most commonly acknowledged factors affecting phytoplankton succession are temperature, nutrient availability and light conditions, which is explored in detail in Chapter 4. An additional, less researched, factor is turbulence. During the development of understanding of phytoplankton activities, such as growth, speciation and persistence, many ecologists ignored the fact that water is in continuous motion (Reynolds, 1997a). Fluid motion determines how phytoplankton is transported both vertically and horizontally, and subsequently exposed to a range of temperature gradients, light and nutrient availability. The literature indicates that spatial and temporal characteristics, and secondary effects of turbulence imposed on the water body are of greater importance to the phytoplanktonic cells than the actual intensity of turbulence (Reynolds and Irish, 1997). There is, however, increasing research being undertaken to determine the effect of turbulence intensity upon the phytoplankton cells. A PhD Student who was also part of the investigating team with the CRCWQT project 2.5.1 has undertaken the detailed analysis of turbulence effects upon phytoplankton growth; the reader is referred to the PhD thesis, entitled

Phytoplankton and turbulence at selected scales by Rudi Regel, School of Environmental Biology University of Adelaide, 2003. The ecology of the phytoplankton detected in Myponga Reservoir (Chapter 3) is investigated with the aid of numerical modelling. Chapters 5 and 8 provide further literature review and discussion on phytoplankton ecology.

2.2.1 Water movement

Variations in irradiance, photoadaption and photosynthesis on short time scales, have been shown to be important in physiological and modelling studies of phytoplankton (Patterson *et al.*, 1994). Photo-inhibition can occur when phytoplankton are entrained above the diurnal thermocline and fail to circulate (Brookes and Ganf, 2001; Kim and Watanabe, 1993). To accurately assess the importance of vertical mixing for phytoplankton the intensity, vertical extent, frequency and duration of mixing events must be quantified simultaneously with studies of phytoplankton physiology (MacIntyre, 1996). This will be examined at Myponga Reservoir in more detail in Chapter 4.

Spigel and Imberger (1987) investigated mixing processes relevant to phytoplankton dynamics. The description of mixing processes is fragmentary; nevertheless the physical processes that maintain phytoplankton in suspension are quantified. Humphries and Imberger (1982) introduced a dimensionless parameter ψ, the ratio of vertical turbulent velocity to phytoplankton velocity, which indicates the degree of relative entrainment for isotropic turbulence in mixed layers. It was shown that for sinking species in Burrinjuck Reservoir (NSW) $\psi < 1$, suggesting that turbulent diffusion controlled the distribution of diatoms and green algae. For positively buoyant *Microcystis aeruginosa*, ψ is frequently much larger than unity, implying that cell buoyancy is more significant than turbulent diffusion for vertical distribution of *Microcystis aeruginosa* colonies (Humphries and Imberger, 1982). Pasciak and Gavis (1974) reported that the rate at which a nutrient is taken up by an individual cell might be limited by two types of processes: biological properties of the cell itself, and the availability of nutrient and transport in the adjacent fluid. In conclusion Spigel and Imberger (1987) stressed the need for further research into the interactions between mixing, light penetration, nutrient uptake and productivity.

MacIntyre (1993) used profiles of temperature-gradient microstructure to characterize the magnitude and location of mixing zones, intensity of turbulence, and the possible exposure of phytoplankton to a fluctuating light regime in a turbid, shallow, productive lake. The profiles indicated that the mixing zone within the water column was divided into two regions, one with active turbulence and the other where turbulence was constrained by buoyancy. The upper layer, ranging from a depth of 0.3 to 1.5 m, was vigorously mixing whilst windy conditions were maintained, and phytoplankton were well-mixed and expected to experience continuous fluctuations in irradiance. The two regions in the *SML* were regularly comprised of frequent overturning events with varying timescales. The mixing times and circulation times for phytoplankton were assessed from these timescales.

To design experiments and model primary production in fluctuating light regimes the trajectories and mixing rates of phytoplankton are required. The coefficient of eddy diffusivity is used in phytoplankton growth and circulation models and is usually defined to be constant. MacIntyre (1993) indicates the inadequacy of parameterising the *SML* by one coefficient of eddy diffusivity and concludes that microstructure data used in conjunction with *SML* models would enable more practical models of phytoplankton trajectories to be developed. MacIntyre (1993) gives well-documented information for the consequence of vertical mixing for phytoplankton but does not attempt to relate this information to phytoplankton succession.

Lewis *et al.*, (1984) introduced a theory that represents the production and mixing relationship by two non-dimensional numbers. The first expresses the mixing-photoadaption ratio, and the second measures the degree of analogousness of light intensities within the *SML*. Subsequently when the mixing-photoadaption ratio is low and the ratio of the mixing length scale to the optical length scale is high, photoadaption proceeds at a rate that creates variations in light adaptation characteristics of planktonic communities within the water column. Lewis *et al.* (1984) focussed on the distribution of photoadaptive properties with depth and simplified the problem of assessing photosynthesis in the vertically mixed water column.

Phytoplankton mixing and growth interrelationships in the ocean have received a considerable amount of attention yet there are few comparable studies on lakes (Imboden and Wuest 1995). From July-1979 to January-1981 an intensive field study was undertaken at Lake Rotongaio, New Zealand. The seasonal succession of the major phytoplankton species was described. The phytoplankton biomass and dynamic behaviour seemed to be controlled directly by external events, where internally generated conditions had minimal effect (Viner, 1983). Specific interest was taken in the buoyant *Anabaena oscillarioides*, where rapid growth occurred during stratified periods. The decrease of *Anabaena oscillarioides* numbers coincided with the breakdown of stratified conditions even though adequate nutrients, light and temperature were available. Viner (1983) concluded that the dominance of *Anabaena oscillarioides* was independent of all environmental features in the lake except vertical mixing.

Berman and Shteinman (1998) investigated wind-induced turbulent movement and utilised data from a three-dimensional velocity fluctuation meter to compute the dissipation of turbulent kinetic energy (*TKE*) and the intensity of both horizontal and vertical turbulent mixing in the pelagic epilimnion of Lake Kinneret, Israel. Attention was focused in the epilimnion, as the fraction of lake volume below the diurnal mixed layer subject to turbulence was minimal, probably of the order of less than one percent (Spigel and Imberger, 1987). The turbulence was monitored from January-1992 to December-1996. Since 1994, sudden changes were observed in the seasonal and annual succession of phytoplankton, together with significantly high levels of primary production. *TKE* dissipation rates, vertical and horizontal turbulent movements were significantly different to previous years (1992-1993), and coincided with uncommon phytoplankton community composition occurring (1994-1996). Correlations were formulated between phytoplankton parameters (primary production, chlorophyll and the ratio of primary production to chlorophyll) and both the intensity of turbulent mixing in the vertical plane and the dissipation of *TKE*. Berman and Shteinman (1998) suggested that the altered turbulent climate, due to changing wind energy input, of Lake Kinneret posed an important factor in the determination of shifts in phytoplankton succession and the population of the algae group.

The study undertaken by Berman and Shteinman (1998) is one of the few studies to show unambiguous correlations between turbulence parameters and phytoplankton growth and succession. Further observational studies are required to parameterise the turbulent energy field with characteristics of the ambient phytoplankton. This will enable the delineation of the turbulence regime on phytoplankton growth in lakes and reservoirs. It is evident from the literature that the growth of cyanobacteria can be effectively controlled if the ability exists to mix the cyanobacteria to a greater depth than the euphotic depth of the water body. Subsequently the use of artificial mixing for control of cyanobacteria growth would only be effective in those water bodies where the *SML* depth can significantly exceed that of the euphotic depth.

2.2.2 Taste and odour compounds; geosmin, 2-MIB

Cyanobacteria have the ability to produce geosmin and 2-methyl isoborneol (2-MIB), which are earthy and musty smelling compounds (Chorus and Bartram, 1999). Several cyanobacterial genera produce geosmin and 2-MIB including *Anabaena*, *Aphanizomenon*, *Lyngbya*, *Microcystis*, *Planktothrix* (formally *Oscillatoria*; Reynolds, 1997a), *Phormidium*, *Schizothrix* and *Symploca* (Persson, 1983). The human taste threshold of geosmin is ~10 ng L^{-1} (Bowmer *et al.*, 1992), which corresponds to an *Anabaena circinalis* cell concentration of approximately 1000 to 2000 cells mL^{-1} (*Anabaena circinalis* has 0.72 pg Chl *a* $cell^{-1}$). The immediate risk to water quality managers experiencing excessive *Anabaena circinalis* growth is the production of geosmins.

2.2.3 Cyanobacterial toxins

Many species of cyanobacteria can produce toxic secondary metabolites (Carmichael, 1992). The toxicity of cyanobacterial biomass in Australia has been well documented (Falconer, 2001) and the risks posed to humans and livestock is well recognised (Chorus and Bartram, 1999). Toxic cyanobacteria present a hazard to human populations that are exposed through drinking water or recreational activities (Falconer, 1999). The toxins include hepatotoxic peptides, neurotoxic alkaloids, a cytotoxic alkaloid, and saxitoxin derivatives, with allergens and lipopolysaccharides also present (Falconer, 1999). The use of $CuSO_4$ (see Section 2.2.5) to manage cyanobacteria blooms can exacerbate the presence of toxins through copper-induced lysis of the cyanobacteria cell. Furthermore, $CuSO_4$ can also destroy the organisms responsible for degrading cyanobacterial toxins.

Recreational exposures to water containing toxic cyanobacteria have caused illnesses ranging from acute pneumonia and hepatoenteritis to mild skin irritation and gastroenteritis (Falconer, 1999). International water safety guidelines for cyanobacterial toxins are available and were developed by the World Health Organisation (see Chorus and Bartram, 1999).

2.2.4 Grazing

Filamentous phytoplankton such as *Anabaena circinalis* is typically un-grazed by zooplankton, as the filaments obstruct the feeding appendages and congest the carapace (Giussani *et al.*, 1990; Gliwicz and Lampert, 1990). However, there have been reported occurrences of grazing with smaller filaments (< 1.5mm) (Holm *et al.*, 1983), although the feeding rate is significantly lower when compared with unicellular forms (Arnold, 1971). When filamentous phytoplankton is present within the phytoplankton assembly, inhibition of grazing of edible forms of phytoplankton can occur (Gliwicz and Lampert, 1990).

2.2.5 Copper Sulphate dosing

To control cyanobacteria growth, $CuSO_4$ is dosed when concentrations exceed 2000 cells mL^{-1}, and can potentially become problematic (Chorus and Bartram, 1999; Jones, 1997; Whitaker *et al.*, 1978). This form of control is indiscriminate and reduces the biomass of all phytoplankton. Whitaker *et al.* (1978) reported a decline in an *Aphanizomenon flos-aquae* bloom with a Chlorophyll *a* (Chl *a*) concentration of 48 – 55 μg Chl *a* L^{-1} to 2 – 4 μg Chl *a* L^{-1} (>99 % reduction) when $CuSO_4$ dosing was used. The $CuSO_4$ is active for limited time (generally < 15 minutes) depending on the concentration of dissolved organic carbon and forms inert complexes that may sediment out of the water column (Burch *et al.*, 1998). However, whilst phytoplankton biomass recovery is rapid during growth seasons, the successional development of the phytoplankton community can be altered or reset.

From the cited literature, it can be concluded that the potential exists for cyanobacteria growth to be controlled by manipulating their light environment. With the aid of surface mixers the buoyant cyanobacteria can be physically removed from the euphotic zone. However, the cyanobacteria must be in the dark for extended periods so as to minimise growth. To determine the mixing times generated by the surface mixers an understanding of the flow was required. In the next section a review

of jets and plumes is presented which provided insight into the hydrodynamic action of the water movement generated by the surface mixers.

2.3 THE SURFACE MIXERS - JETS AND PLUMES

The surface mixers are large propellers suspended below the reservoir surface, directed downwards. The action of the propeller drives an axisymmetric swirling jet of water towards the bottom of the reservoir through a suspended draft-tube. Upon release from the draft-tube (Fig. 1.1) the jet will either continue on its path or turn on itself, depending on ambient conditions, entraining surrounding water as the jet propagates through the water column. To characterise the flow field generated by the surface mixers, and develop an algorithm to simulate the surface mixers, an understanding of jets, plumes and the degree of swirl was required.

The jet issuing from the surface mixer draft-tube will depend on three specific parameters (Fischer *et al.*, 1979):

- Jet parameters
- Environmental parameters
- Geometrical parameters

The jet parameters include the initial velocity distribution, turbulence level, mass and momentum flux, and the flux of tracer substance e.g. heat or phytoplankton concentration. Environmental factors comprise such ambient variables as degree of stratification, turbulence intensity, and currents. These parameters need to be quantified to determine their effect upon the jet dynamics. The geometrical parameters relevant to jet examination are the jet shape and orientation, proximity to boundaries, and buoyancy characteristic i.e. positive or negative buoyancy.

The aforementioned parameters enter a single problem when describing the hydrodynamics of the surface mixers. An appropriate method to describe axisymmetric jets and plumes is to use limiting asymptotic solutions for simple flows and combine these solutions into generalised descriptions of more complex flows (Ghazzawina, 1994). To assess the surface mixer flow the vertical jet region must be investigated. This section presents representative literature on existing knowledge of

non-swirling and swirling buoyant and non-buoyant jets. The coordinate system that was used for defining the flow parameters for the surface mixers is shown in Fig. 2.1.

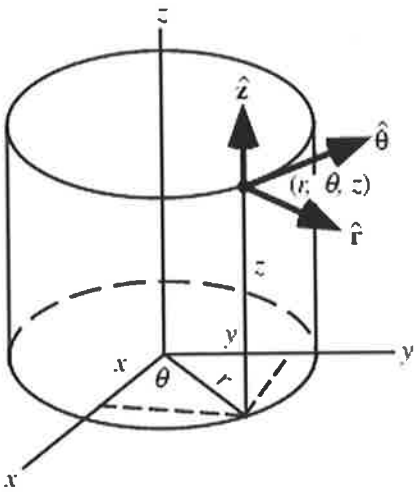

Figure 2.1 Cylindrical polar components (r, θ, z); u, v, and w are the velocities in the radial, tangential, and axial directions respectively.

Depending on ambient conditions the surface mixers can produce two different types of flow, which both have jet characteristics, namely a simple jet and a buoyant jet. Both jet types have volume flux, and either momentum flux or buoyancy flux. The generalised descriptions of these three important jet parameters are defined below:

Volume flux, μ ($m^3 s^{-1}$)

$$\mu = \int_A w dA \tag{2.1}$$

Momentum flux, m ($m^4 s^{-2}$)

$$m = \int_A w^2 dA \tag{2.2}$$

Buoyancy flux, β ($m^4 s^{-3}$)

$$\beta = \int_A g' w dA \tag{2.3}$$

where A (m^2) is the cross-sectional area of the jet, w (m s^{-1}) is the time-averaged velocity in the axial direction, g' (m s^{-2}) is the effective gravitational acceleration (defined in Eq. 2.4) and $\Delta\rho$ (kg m^{-3}) is the density difference between the jet and ambient fluids.

$$g' = g\frac{\Delta\rho}{\rho} \tag{2.4}$$

These parameters are a function of the axial location and it is often more convenient to describe the jet in terms of the initial values of volume flux Q, momentum flux M, and buoyancy flux B. For a round jet, these are given by:

$$Q = \pi r^2 w \tag{2.5}$$

$$M = \pi r^2 w^2 \tag{2.6}$$

$$B = g(\Delta\rho_0/\rho)Q \tag{2.7}$$

Jet characteristics are governed by these variables providing that the jet flow is fully turbulent ($N_{Re} > 4000$). The Reynolds number (N_{Re}) for a round jet can be defined as:

$$N_{Re} = M^{1/2}\nu \tag{2.8}$$

The following section discusses simple jets issuing into stagnant isothermal receiving fluid. Under these flow conditions the jet properties will be a function of the axial distance from the jet orifice z (m), and the initial values of Q and M.

2.3.1 Simple Jet

Time-averaged measurements of turbulent jets have shown that a Gaussian distribution of tracer concentration and axial velocity develops approximately six jet diameters downstream of the jet orifice. In this region the jets are termed 'self-similar', because at any cross section of the jet, the tracer distribution or time averaged velocity can be expressed in terms of a maximum value that is measured along the jet centreline. The velocity core of the jet is undergoing an unsteady decay in the zone from the jet orifice to the development of the Gaussian profile. This zone is defined at the zone of flow establishment (*ZFE*). The zone downstream of the *ZFE* where the jet expands and the mean velocities and tracer concentrations decrease is known as the zone of established flow (*ZEF*). The jet development in these two zones is shown in Fig. 2.2. Due to the self-similarity of the jet in the *ZEF* the mean velocity distribution can be described by the relationship:

$$w = w_m f\left(r/r_w\right) \tag{2.9}$$

where r (m) is the radial distance from the jet centreline and r_w is the value of r where w reduces to a specified fraction of the axial velocity along the jet centreline, w_m (often chosen to be either $0.5w_m$ or $e^{-1}w_m$). Similarly, the tracer concentration within the jet can be defined as:

$$C = C_m f\left(r/r_T\right) \tag{2.10}$$

where r_T is the value of r as for r_w, and C_m is the tracer concentration along the jet centreline. Usually f is of the Gaussian form. Subsequently Eq. 2.10 becomes:

$$C = C_m e^{\left(-(r/r_T)^2\right)} \tag{2.11}$$

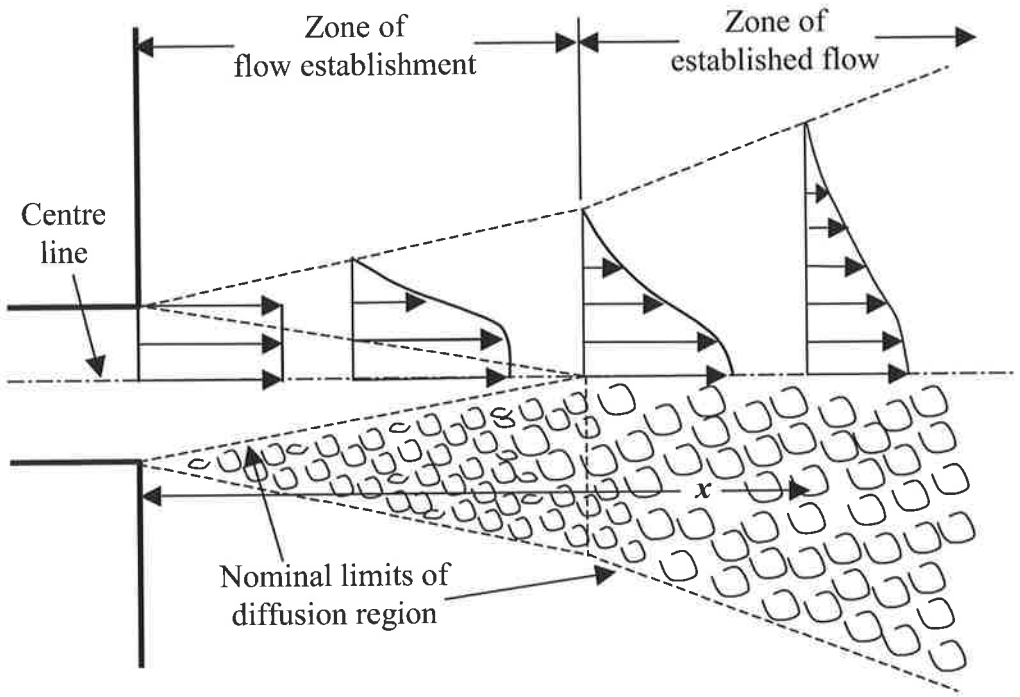

Figure 2.2 Schematic representation of jet diffusion. Reproduced from Albertson *et al.* (1950).

When describing round asymmetric jet dynamics a characteristic length scale l_Q (m) is defined:

$$l_Q = \frac{Q}{M^{1/2}} \tag{2.12}$$

Dimensional analysis implies that the jet properties are a function of z/l_Q, Q and M. Turbulence intensity measurements undertaken by Crow and Champagne (1971), Rosler and Bankoff (1963) and Sami *et al.* (1967) indicated that for a simple jet an asymptotic solution exists at a distance downstream of the jet at $z/l_Q \sim 10$, whereupon the jet reaches equilibrium and the turbulence reaches a state of steady decay. Subsequently, the jet parameters w_m, C_m, r_w, r_T, μ and m are a function of z/l_Q. Consider w_m, which has dimensions of length/time therefore using dimensional analysis,

$$w_m \, Q/M = f\left(z/l_Q\right) \tag{2.13}$$

Using the argument of Fischer *et al.* (1979), as $z \to 0$, $w \to M/Q$ which implies that $f(z/l_Q) \to 1$ for $z \sim l_Q$. And, where $z/l_Q >> 1$ requires that either:

$z \to \infty$ with Q and M fixed

$Q \to 0$ with z and M fixed

$M \to \infty$ with z and Q fixed

Consequently, for $z >> l_Q$, all properties of the jet are defined as functions of z and M (for turbulent flow). Therefore, $wQ/M \to a_1 l_Q/z$ for $z >> l_Q$, where a_1 is an empirical constant. Experimental results from six investigators suggest a value for a_1 of 7.0 ± 0.1 satisfies the decay of a simple jet. Therefore,

$$w_m \frac{Q}{M} = 7.0 \frac{l_Q}{z} \tag{2.14}$$

Using dimensional analysis and experimental observation, expressions can be derived for jet dilution, radial spread and mean tracer concentration dissipation in the *ZEF*:

$$\frac{\mu}{Q} = 0.25 \frac{z}{l_Q} \tag{2.15}$$

$$\frac{r_w}{z} = 0.107 \tag{2.16}$$

$$\frac{r_T}{z} = 0.127 \tag{2.17}$$

2.3.2 Pure Plumes

The description of a pure plume is simplified, as there is no initial volume or momentum flux to consider. Subsequently all plume flow variables are a function of

the initial buoyancy flux B, distance from the origin z, and the kinematic viscosity of the fluid ν. Consider the time-averaged centreline axial velocity:

$$w_m = f(B, z, \nu) \tag{2.18}$$

Using dimensional analysis, an expression for w_m for a round plume (Fischer *et al.*, 1979) is given by:

$$w_m \left(\frac{z}{B}\right)^{1/3} = f\left(\frac{B^{1/3} z^{2/3}}{\nu}\right) \tag{2.19}$$

The right-hand side (RHS) of Eq. 2.19 is a form of Reynolds number. If $z >> \nu^{3/2} B^{-1/2}$ the flow is fully turbulent and the viscous effects become negligible, consequently the left-hand side (LHS) becomes constant giving:

$$w_m = C_1 \left(\frac{B}{z}\right)^{1/3} \tag{2.20}$$

Rouse *et al.* (1952) determined that $C_1 \approx 4.7$. Using a similar argument for w_m and using empirical constants, the momentum and volume flux respectively are given by:

$$m = C_2 B^{2/3} z^{4/3} \tag{2.21}$$

$$\mu = C_3 B^{1/3} z^{5/3} \tag{2.22}$$

where $C_2 \approx 0.35$ and $C_3 \approx 0.15$. Combining Eqs 2.21 and 2.22, the volume flux for a round plume can be expressed in terms of m and B giving:

$$R_p = \mu \frac{B^{1/2}}{m^{5/4}} \tag{2.23}$$

R_p is called the jet Richardson number, where $R_p = C_3 C_2^{-5/4} \approx 0.557$.

2.3.3 Buoyant Jet in an Isothermal Environment

During warm periods, the water pumped through the surface mixers will be warmer than the homogenous receiving water at the exit of the draft-tube. Therefore, under these conditions the flow was expected to have the same attributes as a buoyant jet discharged into an isothermal environment. Consequently, the jet parameters were examined under these conditions.

A buoyant jet has characteristics of a simple jet or a pure plume depending on the distance from the jet orifice. The jet-like characteristics depend upon the initial volume and momentum fluxes, whilst the plume-like characteristics are dependent of the initial buoyancy flux. The density difference between the jet and the receiving fluid can be either positive or negative, subsequently it is important to consider the jet orientation. Initially the relationships for a vertical positively buoyant jet discharged upward are discussed.

Consider a flow for a round jet with momentum and buoyancy but no volume flux; then the characteristic length scale is given by:

$$l_M = \frac{M^{3/4}}{B^{1/2}} \tag{2.24}$$

The ratio of l_Q to l_M is the initial jet Richardson number:

$$R_0 = \frac{l_Q}{l_M} = \frac{QB^{1/2}}{M^{5/4}} \tag{2.25}$$

The ratio of R_0/R_p indicates if the buoyant jet will be jet or plume-like. As R_0/R_p approaches or exceeds 0.5 the buoyant jet can be considered a fully developed plume at the end of the *ZFE*. The dimensional arguments used for pure jets by Fischer *et al.* (1979) is applied to buoyant jets, leading to the following expressions for dilution:

$$\overline{\mu} = \frac{\mu}{Q}\left(\frac{R_0}{R_p}\right) \tag{2.26}$$

$$\zeta = c_p\left(\frac{z}{l_Q}\right)\left(\frac{R_0}{R_p}\right) \tag{2.27}$$

where the plume growth coefficient $c_p \approx 0.254$, and ζ is the dimensionless distance from the jet orifice. Consequently, the dimensionless buoyant jet volume flux $\overline{\mu}$ becomes:

$$\overline{\mu} = \zeta \quad (\zeta << 1) \tag{2.28}$$

$$\overline{\mu} = \zeta^{5/3} \quad (\zeta >> 1) \tag{2.29}$$

Asymptotic solutions for dilution in a round vertical turbulent jet compared to the experimental data of Ricou and Spalding (1961) are shown in Fig. 2.3.

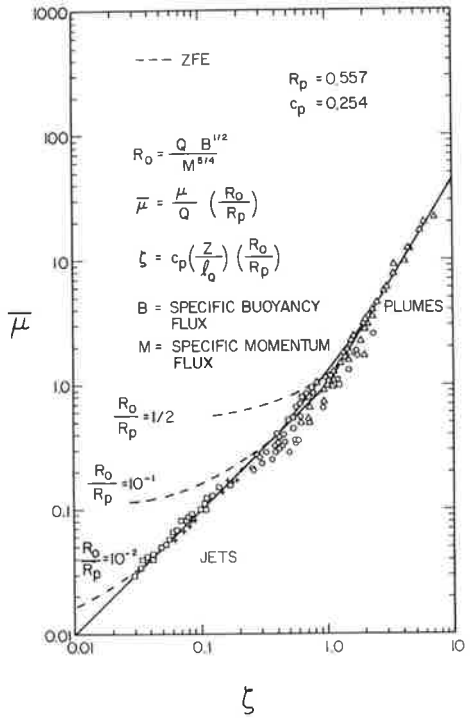

Figure 2.3 Vertical dilution in a round turbulent buoyant jet. ζ is the dimensionless distance from the jet orifice (Eq. 2.27) and $\bar{\mu}$ is the dimensionless volume flux (Eq. 2.26) . Reproduced from Fischer *et al.* (1979).

The jet Richardson number R_0, governs the behaviour of the buoyant jet but requires an implicit specification of the jet discharge direction. However, a positively buoyant jet pointing downwards will be identical to a negatively buoyant jet pointing upwards. A positively buoyant jet pointing downwards must satisfy a relationship of the form:

$$z_t \frac{M^{1/2}}{Q} = f(R_0) \tag{2.30}$$

Application of integral analysis on flow reversing jets is not appropriate since the entrainment involves flow previously discharged (List, 1982; Rodi, 1982).

Turner (1966) showed that the terminal height of a buoyant jet discharged into an isothermal environment could be defined by dimensional consistency as:

$$z_m = CM^{3/4}B^{-1/2} \tag{2.31}$$

where C is a constant. Using the experimental data of Turner (1966) the mean value for C was calculated to be 1.43. Baines *et al.* (1990) reasoned that the total volume flux entrained by the buoyant jet in the region between the region z and the terminal height z_m can be expressed as:

$$Q_{Entrained} = \frac{M^{5/4}}{B^{1/2}} f\left(\frac{zB^{1/2}}{M^{3/4}}\right) \tag{2.32}$$

It is convenient to express Eqs 2.31 and 2.32 using the buoyancy and velocity at the jet orifice and the orifice radius r_0. Subsequently:

$$\frac{z_m}{r_0 Fr} = Constant \tag{2.33}$$

$$\frac{Q_{Entrained}}{Q_0 Fr} = f\left(\frac{z}{r_0 Fr}\right) \tag{2.34}$$

where Fr is an internal Froude number defined by:

$$Fr = \frac{w_0}{\sqrt{r_0 g'}} = \frac{Q_0}{\pi r_0^{5/2} g'^{1/2}} \tag{2.35}$$

From Eq. 2.25, the jet Richardson number can be expressed as a densimetric Froude number, which is the inverse of Eq. 2.35, i.e.

$$R_0 = \left(\frac{\pi}{4}\right)^{1/4} \frac{1}{Fr} \tag{2.36}$$

The use of the Richardson number leads to simpler expressions and has a value between 0 and 1.

2.3.4 Buoyant Jet in a Stratified Environment

When a thermal gradient existed in the hypolimnion, the surface mixer jet effectively discharged into a stratified environment, and so an understanding of the jet behaviour during these conditions was required. Based on Taylor's hypothesis (Morton *et al.*, 1956), the entrainment for a round jet can be determined from:

$$\left(\frac{d}{dz}\right)\left(\pi r^2 w_m\right) = 2\pi\alpha r w_m \tag{2.37}$$

where r is the radius of the jet and αw_m is the entrainment volume at r. Eq. 2.37 states that the rate of change of volume flux in the jet as function of downstream distance is proportional to the rate of inflow by entrainment. The three main assumptions are (a) the axial velocity and buoyancy are similar at all heights, (b) the rate of entrainment at any depth is proportional to a corresponding characteristic velocity, and (c) the fluids are incompressible and local density differences are small compared to the reference density. The entrainment coefficients for jets and plumes reported in the literature are (Fischer *et al.*, 1979):

$$\alpha_{Jets} = 0.0535 \pm 0.0025 \tag{2.38}$$

$$\alpha_{Plumes} = 0.0833 \pm 0.0042 \tag{2.39}$$

When the environment is density stratified the entraining fluid density at a given level is higher than that at the next level so that the buoyancy flux in a rising buoyant jet will reduce. At a point the buoyancy flux will become negative. An expression for the entrainment coefficient was suggested by Priestley and Ball (1955), who found that the entrainment coefficient is proportional to the square of the local Richardson number of the jet:

$$\alpha = \alpha_{Jets} - (\alpha_{Jets} - \alpha_{Plumes})\left(R/R_p\right)^2 \tag{2.40}$$

In density-stratified flow, the entrainment coefficient calculated in Eq. 2.40 becomes negative when R^2 equals $\alpha_{Jets} R_p^2/(\alpha_{Jets} - \alpha_{Plume})$. To avoid this, Fischer *et al.* (1979) suggested the following function:

$$\alpha = \alpha_j \exp\left[\ln\left(\frac{\alpha_p}{\alpha_j}\right)\left(\frac{R}{R_p}\right)^2\right] \tag{2.41}$$

Using Eq. 2.41 to calculate the entrainment coefficient for buoyant jets with different values of the stratification number N (Eq. 2.42), asymptotic solutions for the jet dilution can be derived and are plotted in Fig. 2.4.

$$N = \frac{M^2 g}{B^2}\frac{1}{\rho_0}\frac{d\rho}{dz} \tag{2.42}$$

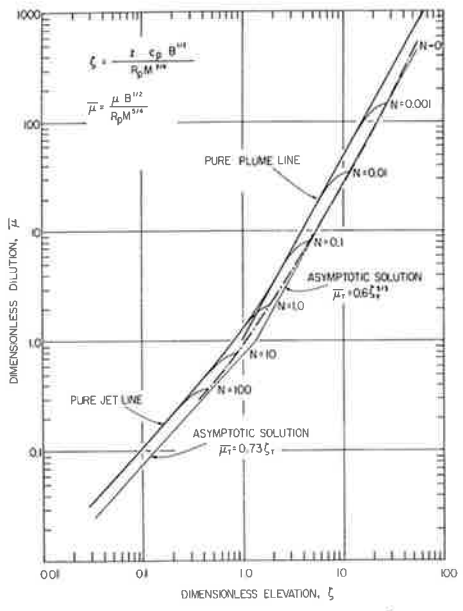

Figure 2.4 Dilution in turbulent buoyant jets in a linearly stratified environment. The dimensionless dilution and elevation parameters are given by Eqs 2.43 and 2.44 respectively. Reproduced from Fischer *et al.* (1979).

$$\bar{\mu} = \frac{\mu B^{1/2}}{R_p M^{3/4}} \tag{2.43}$$

$$\zeta = \frac{z C_p B^{1/2}}{R_p M^{3/4}} \tag{2.44}$$

2.3.5 Swirling Jets

A mixer was installed on Myponga Reservoir during 1990 to ascertain its performance and effect on water quality (Velzeboer *et al.*, 1991). The mixer was essentially an upward lifting pump, which drew cold water from the hypolimnion and deposited it at the surface. The mixer was modelled as a rising plume with no reference to swirling jets, which is applicable to the surface mixers being studied.

The action of the existing surface mixer impeller creates a swirling jet, which exits the draft-tube at a specified depth. The diameter of the jet at the draft-tube exit is 4.9m with a flow rate of 3.5 m^3s^{-1} (Chapter 6), which has a Reynolds number in the order of 10^6. Historically, the study of swirling jets has been diverse and often reflected the application of interest (Petersson, 1996), e.g. propulsion of airborne and marine vehicles (Hamill and Johnston, 1993; Hamill *et al.*, 1999; Hyun and Patel, 1991). Whereas, the study of swirling jets has predominately been restricted to laboratory scale models (Billant *et al.*, 1998; Park and Shin, 1993; Peterson and Bayazitoglu, 1992). Chapter 6 contains a review of swirling jets, with the focus on incompressible swirling turbulent jets, with some reference made to non-swirling jets and the importance of scale.

2.4 NUMERICAL SIMULATION

To gain insight into the specific action of the surface mixers and the limnological behaviour of Myponga Reservoir, numerical modelling was used (Chapters 5, 7 and 8). In general, lakes and reservoirs are in a continuous state of flux on time scales ranging from microseconds to years. The productivity, in particular the phytoplankton assemblage, of the lake or reservoir changes as the physical, chemical and biological states change. Subsequently the water quality within the lake or reservoir is also in a

state of flux. As mentioned there are numerous management practices in place that address these issues, but often manifest with very mixed results (Reynolds, 1997a). Each water body has unique qualities that require specific management practices to adequately maintain the water quality. Consequently, hydrodynamic and/or ecological numerical modelling may be an effective tool that may be employed to evaluate the effectiveness of a proposed water quality management plan.

The principle role of numerical modelling of lakes and reservoirs is to give insight into the origins and mechanisms of water quality issues (Hamilton, 1999). There are many models available that can be utilised to assist with management strategies. These models range from zero-dimensional to three-dimensional scales, where the complexity of the model varies accordingly. Physical, chemical and biological processes are simulated within the numerical model generating an output in time and space.

Small to medium sized water bodies often exhibit a one-dimensional structure that can be adequately modelled with first order balances of energy, momentum and mass, which are determined by vertical property variations. The assumption of one dimensionality is used because fluctuations in lateral directions are small compared with vertical variations (Hamilton and Schladow, 1997).

2.4.1 One Dimensionality

Density stratification in lakes and reservoirs can inhibit vertical movement whilst horizontal density variations are rapidly dampened by horizontal advection and convection. Small to medium lakes and reservoirs can experience this phenomena and subsequently one-dimensional modelling can be used to predict the physical structure. It is necessary to validate the one-dimensionality of a lake or reservoir and this is achieved with the use of the Lake Number L_N (Imberger and Patterson, 1989). The Lake Number is categorised by the stratification stability and the magnitude of the wind. A typical density profile for a lake or reservoir is shown in Fig. 2.5. The stratification depicted in Fig. 2.5 is subjected to a wind field that provides a surface friction velocity u^*.

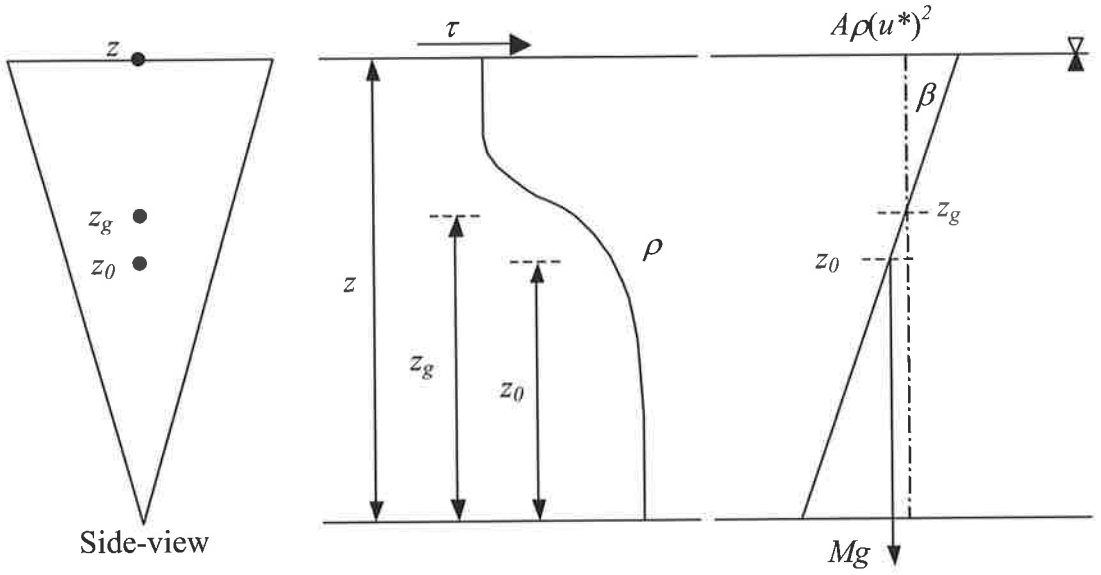

Figure 2.5 Lake Number variables, z is the height of the water column, z_0 is the centre of gravity of the water mass with a density stratification $\rho(z)$ at height z, and $A(z)$ is the water body surface area. M is the total mass of water and β is the angle subtended to the vertical by the line segment connecting the centre of mass to the centre of volume, z_g. Based on Antenucci and Imerito (2000).

As a wind stress τ acts on the surface layer a net force results that acts to overturn the density structure of the water column. Considering the moment around the water bodies centre of volume z_g at equilibrium, gives:

$$\left(z - z_g\right) \int_{A(z)} \rho_0 \left(u^*\right)^2 dA = \left(z_g - z_0\right) Mg\beta \tag{2.45}$$

Rearranging Eq. 2.45 gives the Lake Number:

$$L_N = \frac{\left(z_g - z_0\right) Mg\beta}{\int_{A(z)} \rho_0 \left(u^*\right)^2 dA\left(z - z_g\right)} \tag{2.46}$$

and z_0 is defined by:

$$z_0 = \frac{\int_0^z \rho(z) z A(z) dz}{\int_0^z \rho(z) A(z) dz} \tag{2.47}$$

The thermocline at height z_T, corresponding to the centre of the metalimnion, reaches the surface when maximum deflection occurs and β is defined by:

$$\beta = \frac{z - z_T}{\sqrt{A(z)}} \tag{2.48}$$

Substituting Eq. 2.48 into Eq. 2.46 gives:

$$L_N = \frac{(z_g - z_0) Mg \left(1 - \frac{z_T}{z}\right)}{A^{1/2} \left(1 - \frac{z_g}{z}\right) \int_{A(z)} \rho_0 (u^*)^2 dA} \tag{2.49}$$

The wind stress is assumed to be constant over the entire water surface; therefore Eq. 2.49 can be reduced to:

$$L_N = \frac{(z_g - z_0) Mg \left(1 - \frac{z_T}{z}\right)}{A^{3/2} \left(1 - \frac{z_g}{z}\right) \rho_0 (u^*)^2} \tag{2.50}$$

The restoring force is greater than the disturbing force for $L_N >> 1$ and the deflection of z_0 is minimal. Subsequently the density structure of the water body is approximately horizontal and the assumption of one-dimensionality is valid. In real terms a Lake Number greater than 1 implies severe stratification dominates the forces imposed by the surface wind stress. The ramification of severe stratification is that minimal turbulent mixing occurs in the metalimnion and/or the hypolimnion, as defined in Chapter 1. The validity of the one-dimensional assumption must be

extended to other disturbing factors such as inflow and the effects of the Earth's rotation. Consider the disturbance force due to inflows; an inflow lake Number L_{Ni} criterion is developed:

$$L_{Ni} = \frac{(z_g - z_0)Mg\left(1 - \frac{z_T}{z}\right)}{A^{1/2}uQ\left(\frac{z_g - z_i}{z}\right)} \tag{2.51}$$

where u is the inflow speed and z_i is the depth of the inflow. Similarly, when $L_{Ni} >> 1$, one-dimensionality is valid, and the stratified conditions dampen the horizontal instability induced by the inflows. The Earth's rotation can induce horizontal movement in a water body and is defined by the ratio (Patterson *et al.*, 1984):

$$R = \frac{\hat{R}_i}{B} \tag{2.52}$$

where B is the maximum width of the lake or reservoir and $\hat{R}_i$ is the internal Rossby radius of deformation defined as,

$$\hat{R}_i = \frac{\sqrt{g'h}}{f} \tag{2.53}$$

where h is the surface layer depth and g' is the effective gravity defined in Eq. 2.4. Subsequently for $R > 1$ the water bodies one-dimensionality is valid.

To investigate the hydrodynamic and ecological impact of the operation of surface mixers in Myponga Reservoir two existing one-dimensional numerical models were utilised. The chosen models were:

1. PROTECH, a phytoplankton growth model developed at the Centre for Ecology and Hydrology, Windermere Laboratory, United Kingdom.

2. DYRESM-CAEDYM, a coupled hydrodynamic and ecological model developed by the Centre for Water Research, University of Western Australia, Australia.

To adequately utilise these models significant alterations and additions to the code were required. In both models algorithms simulating the action of the surface mixers and $CuSO_4$ dosing were incorporated. These are presented in Chapters 5, 7, and 8. PROTECH is presented first, which is expanded upon in Chapter 5. DYRESM and CAEDYM are reviewed separately.

2.5 PROTECH

The one-dimensional numerical model used to simulate the phytoplankton assemblage in Myponga Reservoir was PROTECH. The model was developed by Reynolds and Irish (1997), rigorously tested (Elliott *et al.*, 2000a; Elliott *et al.*, 2000b) and validated against data from Blelharn Tarn (N 54°24', W 2°58') located in the north-west of England, U.K. (Elliott *et al.*, 2000a). This model was developed to fulfil a commercial, decision-support role for management of water-supply storages where phytoplankton growth is problematic (Reynolds *et al.*, 2001). PROTECH simulates the *in-situ* dynamics of phytoplankton in lakes, reservoirs and rivers and is sensitive to environmental state variables (temperature, light, day-length, and nutrient supply). The objective of the model is to simulate phytoplankton response to the state variables from which response to environmental change can be made. The model is designed around a series of regression equations used to describe the performance of common phytoplankton in controlled laboratory conditions of insolation and temperature in terms of phytoplankton cell morphology (Reynolds, 1989). The potential individual growth rate for up to eight species is calculated against the temperature and daily insolation, with nutrient availability, grazing, motility, and changing light conditions taken into account.

The model was adapted to investigate the impact of artificial mixing upon species-specific phytoplankton dynamics esp. *Anabaena circinalis*. PROTECH has an aerator algorithm incorporated, written as an override to sub-critical Monin-Obukhov calculations, which normally permits stratification to develop. The Monin-Obukhov equation predicts the *SML* depth as the point of balance where the buoyancy caused

by heating is balanced by its dissipation through the work of wind forcing (Reynolds *et al.* 2001). An algorithm for the surface mixers was incorporated into PROTECH and the generated results were compared with field data collected from Myponga Reservoir. Chapter 5 describes the mathematical formulae used in the model and details the additional algorithms used to improve the model and addresses the implications of the research undertaken with PROTECH. A comprehensive publication of the theory and mathematical development of PROTECH is presented in Reynolds *et al.* (2001) and further detailed descriptions of the incorporated equations can by found in Elliott *et al.* (2000b) and Elliott *et al.* (2000c).

2.6 DYRESM-CAEDYM

The combined use of the hydrodynamic numerical model DYRESM and the ecological model CAEDYM was used to simulate Myponga Reservoir, to assess the impact and optimise the use of artificial mixing for destratification and control of cyanobacteria growth. To determine the effectiveness of the surface mixers an algorithm describing the flow was required to be incorporated into DYRESM. Field measurements and flow analysis enabled the implementation of the surface mixer algorithm (Lewis *et al.*, 2001a; Lewis *et al.*, 2001b; Lewis *et al.*, 2002a), presented in Chapter 6. Upon successful validation of the DYRESM simulation of Myponga Reservoir the aquatic ecosystem model CAEDYM was utilised to investigate the fate of dissolved oxygen and the growth of three phytoplankton species, namely diatoms, chlorophytes and cyanophytes. To validate CAEDYM against Myponga Reservoir field data improvements to the code were required and extensive parameterisation was necessary, which is presented in Chapter 8.

2.6.1 The Hydrodynamic model DYRESM

The hydrodynamic numerical model DYRESM as developed by Imberger *et al.* (1978) is based on fundamental energy, mass, and momentum equations describing the one-dimensional structure detected in small to medium lakes and reservoirs. The model divides the water body into horizontal layers. The layers are Lagrangian, which are able to expand and contract thus accommodating volumetric change due to inflow, outflow, and evaporation (Fig. 2.6), as opposed to a fixed grid approach, e.g. PROTECH (Chapter 5), which would be defined as a Eulerian Scheme. The thickness of the layers also changes when vertical movement

accommodates the bathymetry of the water body. Consequently no numerical diffusion is considered (Fischer *et al.*, 1979).

DYRESM is used to predict the variation of water temperature and salinity with depth and time (Antenucci and Imerito, 2000). The density stratification occurring in reservoirs and lakes inhibits vertical motion whilst horizontal density variations defuse expeditiously by lateral and longitudinal convection, which occurs at a faster rate than vertical advection. An additional function of DYRESM is to provide a one-dimensional hydrodynamic platform for CAEDYM (Section 2.6.2).

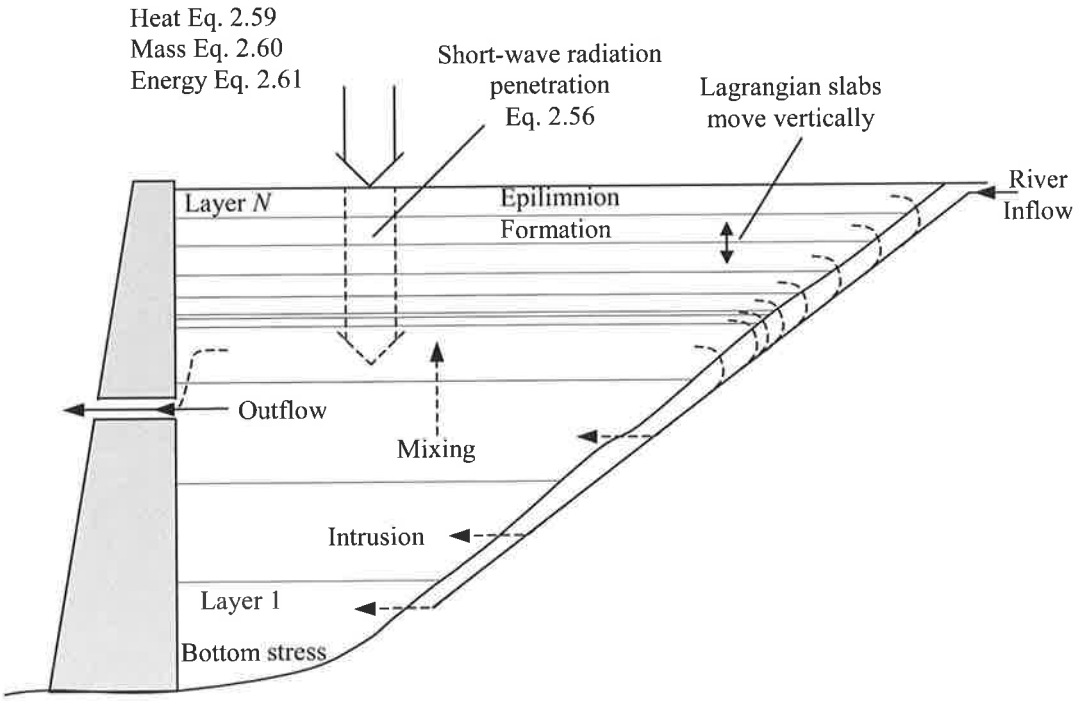

Figure 2.6 Schematic diagram of DYRESM, based on Imberger and Patterson (1981).

The layer structure accommodates the seasonal behaviour found in lakes and reservoirs where conditions can change rapidly between isothermal and stratified. During stratified conditions the biogeochemical properties in the *SML* are relatively constant so that only one layer is required. Whereas across the metalimnion large vertical gradients exist so that many layers are required. Conversely isothermal conditions require minimal layers as the water body is well mixed. The layer volume, area and thickness relationship calculates the volume and area as a function of layer thickness or the thickness and area as a function of layer volume. The layers are

numbered from the bottom up, shown in Fig. 2.6. Intuitively, the smaller the number of layers prescribed to a simulation run, the less the actual run-time. However to achieve adequate resolution and avoid an excessive number of layers developing, the upper and lower thickness limits are preset.

As the water bodies' temperature decreases the density usually decreases, except under special circumstances where the water temperature is less than 4°C, such as during ice cover when inverse stratification at the surface is observed. In contrast, as the salinity increases the density increases. The water layer density (kg m^{-3}), given its temperature (°C), salinity (psu), pressure (bar) is calculated using the equation of state for the density of salt water (Antenucci and Imerito, 2000),

$$\rho(T,S,P)=\frac{\rho(T,S,0)}{\left(1-P/K(T,S,P)\right)} \tag{2.54}$$

To ensure that the layer structure is stable the individual layer densities are checked from the top down. If the upper layer density is higher than the immediate layer below, the two layers are amalgamated and the layer properties are conserved via appropriate governing equations. The process is repeated for all layers culminating in a stable structure.

In a typical lake or reservoir the majority of energy is inputted via heat, mass and momentum exchange at the surface. The heat exchange occurs due to short and longwave radiation, sensible heat transfer and evaporation. Momentum exchange is induced by wind stress, and the change in mass in the surface layer (layer number N) is due to rain and the latent heat flux. Meteorological data may be input into DYRESM either on a sub-daily or daily time-step. The shortwave radiation Q_{SW} is input to the model directly. Shortwave radiation will penetrate the water body to significant depths and is a function of the light attenuation coefficient η. Commonly a relationship given by Eq. 2.55 adequately fits measured data:

$$\frac{Q_Z}{Q_{SW}} = e^{-\eta(H-z)} \tag{2.55}$$

where Q_Z is the radiation remaining at depth z. In DYRESM 55 % of the incoming solar radiation is assumed to be non-penetrative, with the residual 45 % being dispersed throughout the water column layers as found experimentally by Gates (1966), and is calculated according to:

$$\Delta Q_{SW_j} = Q_{SW_j}\left(1 - e^{-\eta(z_j - z_{j-1})}\right) \tag{2.56}$$

The penetrative shortwave radiation has a wavelength < 700 nm and between 400 and 700 nm the shortwave radiation is defined as the Photo-synthetically Active Radiation (*PAR*). The following heat fluxes are all absorbed in the water surface layer, i.e. non penetrative. The net longwave radiation can be inputted either as incoming longwave, net longwave or cloud cover data. The heat flux due to conduction, known as the sensible heat transfer Q_{SH} is calculated within the model by:

$$Q_{SH} = C_S \rho_A C_P U(T_A - T_S)\Delta t \tag{2.57}$$

where the sensible heat transfer coefficient C_S = 0.0013, and the specific heat of air at constant pressure C_P = 1003 J kg^{-1} K^{-1}, the density of air ρ_A = 1.2256 kg m^{-3}, U is the wind speed at the water surface, the air temperature T_A and water surface temperature T_S, and Δt is the time-step. The loss of heat due to evaporation Q_{LH} is given by:

$$Q_{LH} = min\left(0, \frac{0.622}{P} C_L \rho_A L_E U(e_a - e_s(T_S))\Delta t\right) \tag{2.58}$$

where the latent heat transfer coefficient C_L = 0.0013, the latent heat of evaporation of water L_E = 2.453E-6 J kg^{-1}, P is the atmospheric pressure in milli-bars, e_a is the air vapour pressure and e_s is the saturation vapour pressure at the water surface. No

condensation effects occur in the numerical model so that $Q_{LH} \leq 0$. The total non-penetrative energy Q_{NP} received in the surface layer is given by:

$$Q_{NP} = Q_{LW} + Q_{SH} + Q_{LH} \tag{2.59}$$

where Q_{LW} is the longwave energy flux. There are three methods of calculating Q_{LW} within DYRESM depending on the method of data input; incident longwave radiation, percentage cloud cover or net longwave radiation. The change in mass across the surface layer is given by,

$$\Delta M_i = \underbrace{\frac{-Q_{LH} A_N}{L_w}}_{\text{latent heat mass flux}} + \underbrace{\frac{\rho_N A_N R_h \Delta t}{N_d}}_{\text{rain mass flux}} \tag{2.60}$$

where L_w is the latent heat of evaporation of water and R_h is the daily total rainfall and N_d is the number of seconds in a day. The properties of the rain are assumed to be the same as in the surface layer. Wind stress along the water surface causes momentum exchange into the water column and is included in DYRESM. The wind energy available to mix is defined as E_{stir} and is available only to the surface layer and given by Imberger and Patterson (1981):

$$E_{stir} = \eta_S \rho_i A_i (u*)^2 \Delta t \tag{2.61}$$

where η_s is the wind stirring efficiency ρ_N the surface layer density, A_N the area of he surface layer and $u*$ is the shear velocity calculated by:

$$u* = \left(\frac{C_D \rho_a}{\rho_N} \right)^{1/2} u_a \tag{2.62}$$

where u_a is the wind velocity at a reference height of 10 m.

Mixing within the layer structure is undertaken with three specific mechanisms, wind mixing, convective overturn and shear transfer between layers. The available kinetic and potential energies of the individual layers, starting at the surface layer, are used to determine if adjacent layers will mix. If adequate energy is available the layers will mix, with any excess energy used to determine if subsequent layers are able to mix. The amalgamation of layers ceases when there is insufficient energy left, which is carried over to the next time step. The epilimnion height (h_E) and property values are those for the surface layer. The hypolimnion height (h_H) and properties are that of the layer immediately beneath the epilimnion.

The magnitude of the bottom stress is calculated to allow for resuspension of sediment within CAEDYM. The stress is calculated using the water velocities in the epilimnion and the hypolimnion. The epilimnion velocity (u_E) is equal to the surface layer velocity calculated from:

$$u_N = \frac{(u*)^2}{\Delta z_N}\Delta t \tag{2.63}$$

Subsequently the hypolimnion velocity is calculated by:

$$u_H = \begin{cases} \dfrac{u_E h_E}{h_H} & \forall\ h_E < h_H \\ u_E & \forall\ h_E \geq h_H \end{cases} \tag{2.64}$$

Using the drag coefficient C_D the bottom stresses for the epilimnion and hypolimnion can be calculated from:

$$\tau_E = C_D \rho_E u_E^2 \tag{2.65}$$

$$\tau_H = C_D \rho_H u_H^2 \tag{2.66}$$

The mechanisms of hypolimnetic mixing are separated into boundary and internal mixing. To simulate the action of the benthic boundary layer, aliquots from each hypolimnetic layer are mixed into the lowest epilimnion layer, the thermocline layer (Antenucci and Imerito, 2000). Starting at layer 1, internal mixing is achieved by removing a percentage of each layer and mixing it with the layer above.

The inflow to the water body is modelled by inserting the volume into the layer of equal density, taking into account the associated entrainment as the inflow passes layers of greater density. The layer structure is maintained within the limits set by the user and amalgamation of layers occurs accordingly. Outflow will occur with withdrawal and overflow events. The water is removed from the corresponding layer to the withdrawal height; if the volume of this layer is less than the withdrawal volume then water is extracted from layers above the withdrawal height.

DYRESM incorporates a bubble plume algorithm used to simulate an aerator employed for destratification. The plumes generated by the aerator diffuser are modelled with buoyant plume equations assuming that the plumes are non-interacting and axisymmetric. The initial volumetric flow rate of entrained water is calculated with:

$$Q_P = \alpha \frac{6\pi}{5} b_1 L_R B^{1/3} z_1^{5/3} \tag{2.67}$$

where α is the entrainment coefficient (within the range 0.04 – 0.14), b_1 is a constant (= 4.7, Fischer *et al.*, 1979) and L_R is the ratio of plume radius to plume length (= 0.1). The initial buoyancy flux is calculated with:

$$B = \underbrace{gQ_{Air}\left(\frac{P_{Air}}{P_{Diffuser}}\right)^{0.71}}_{\text{Corrected free flow rate}} \tag{2.68}$$

Note that the free airflow rate is corrected for adiabatic compression at the diffuser height (assuming the air is an ideal gas). To calculate subsequent entrainment, the airflow rate is adjusted in each layer to account for the adiabatic expansion of the air bubbles. A combined buoyancy flux of the entrained water and air bubbles is calculated by:

$$B_i = gQ_i - g\left(\frac{\rho_i - \rho_P}{\rho_i}\right)Q_P \tag{2.69}$$

where ρ_i is the density of the current layer. Subsequently the entrained volume in layer i is calculated by:

$$Q_{Pi} = \alpha\frac{6\pi}{5}b_1 L_R B^{1/3}\Delta z^{5/3} + Q_{Pi-1} \tag{2.70}$$

The insertion of the entrained water into a neutrally buoyant layer occurs when Eq. 2.69 becomes negative.

The development and process parameterisations of DYRESM have been described extensively in the literature (Hamilton, 1999; Hamilton and Schladow, 1995; Hamilton and Schladow, 1997; Hocking *et al.*, 1988; Imberger, 1982; Imberger *et al.*, 1978; Imberger and Patterson, 1981; Patterson *et al.*, 1984; Schladow and Hamilton, 1995; Spigel and Imberger, 1980).

2.6.2 The Aquatic Ecological model CAEDYM

CAEDYM is an autonomous ecological model that can be linked to hydrodynamic models, e.g. DYRESM, but can be run independently to assess specific temporal ecological processes (Herzfeld and Hamilton, 2000). CAEDYM is a general ecosystem simulation model with the capability to simulate the biogeochemical processes of phytoplankton, zooplankton, fish, jellyfish, seagrass and macrophytes, macroalgae and macroinvertebrates, dissolved oxygen, biological oxygen demand, nutrient dynamics, tracer/colour, pH, iron, manganese and aluminium. The main biogeochemical state variables are shown in Fig. 2.7.

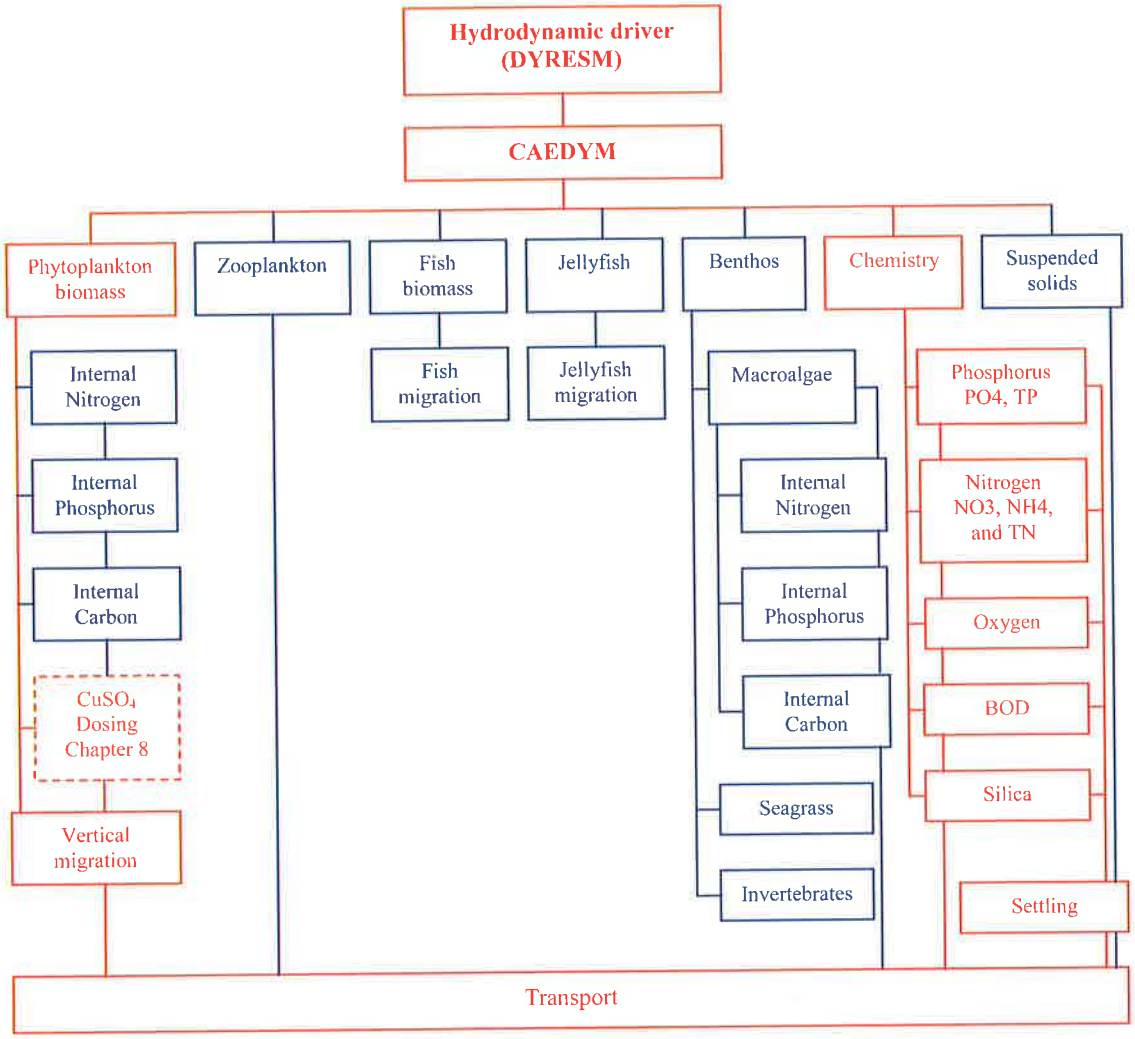

Figure 2.7 CAEDYM biogeochemical state variables. The part of the CAEDYM used in the modelling investigation (Chapter 8, where the $CuSO_4$ dosing algorithm is introduced) is denoted in red. Based on the flowchart developed by Herzfeld and Hamilton (2000).

The model is designed to offer substantial flexibility for the user with the choice of state variables. Consequently CAEDYM was an ideal choice to assess artificial mixing in Myponga Reservoir and the subsequent impact on phytoplankton succession and dissolved oxygen dynamics. The description of the model will be limited to these two processes. An extensive description of CAEDYM has been produced by Herzfeld and Hamilton (2000).

The phytoplankton groups modelled with CAEDYM were freshwater cyanophytes that were represented by the genus *Anabaena circinalis*, chlorophytes represented by

Scenedesmus, and diatoms represented by *Nitzschia*. Total Chl *a* concentration represents the biomass of each phytoplankton group. The generalised maximum growth rate at 20°C is a function of *PAR*, phosphorus, nitrogen, silica, carbon and temperature that is represented by:

$$r' = r_{20^\circ C} \times min\{f(l), f(N), f(P), f(Si), f(C)\} \times f(T) \tag{2.71}$$

where $f(T)$ is a temperature function described by Eq. 2.74, $f(C)$ is used for explicitly modelling the internal carbon, and $f(Si)$, $f(P)$, $f(N)$ and $f(I)$ represent limitation by silica, phosphorus, nitrogen and *PAR* respectively. Light limitation is modelled with the Webb model (Webb and Newton, 1974), which ignores photo-inhibition, and is given by:

$$f(l) = 1 - e^{\left(-I/I_k\right)} \tag{2.72}$$

where I is the incoming irradiance and I_k a parameter for the initial slope of the associated *PI* curve. Michaelis-Menten kinetics is used to simulate nutrient limitation of phytoplankton growth. For phosphorus limitation the Michaelis-Menten term is:

$$f(P) = \frac{PO_4}{PO_4 + K_P} \tag{2.73}$$

where K_P is the half saturation constant for phosphorus on growth rate. The equation for the bio-available dissolved carbon takes the same form as Eq. 2.73 with K_P replaced with the half saturation constant for carbon K_C. The half saturation constant for nitrogen (K_N) is set to zero for nitrogen fixing cyanobacteria. $f(P)$ is plotted as a function of [PO_4] in Fig. 2.8. The qualitative features of Fig. 2.8 show that the limitation rate is proportional to the concentration of phosphorus, and as nutrient concentration increases the limitation order decreases from one to zero.

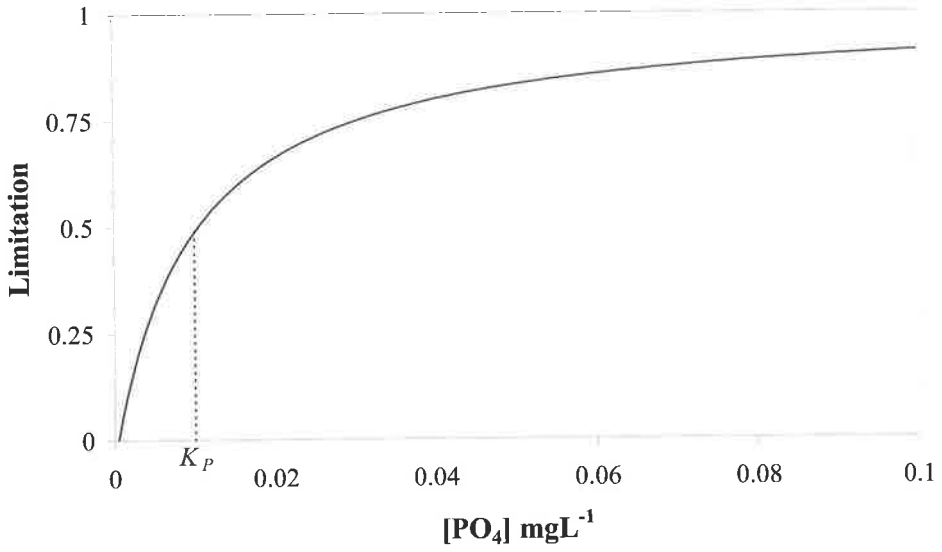

Figure 2.8 Michaelis-Menten nutrient limitation for dissolved inorganic phosphorus.

Maximum growth for phytoplankton occurs at an optimum temperature T_{opt}. For $T < T_s$ (the standard temperature), temperature limitation to growth is calculated by:

$$f(T) = \vartheta^{T-20} \tag{2.74}$$

where ϑ is a non-dimensional temperature multiplier. When the temperature increases above T_{opt}, $f(T)$ reduces to zero where the temperature is defined as T_{max}. The temperature limitation equation for $T > T_s$ has the form:

$$f(T) = \vartheta^{T-20} - \vartheta^{k(T-a)} + b \tag{2.75}$$

where k, a and b are unknown and which are solved by using the boundary conditions:

$$T = T_s, \quad f(T) = 1$$
$$T = T_{opt}, \quad \partial f(T)/\partial T = 0$$
$$T = T_{max}, \quad f(T) = 0$$

There are several options for simulating vertical migration and settling of phytoplankton in CAEDYM:

1. Stokes settling velocity
2. Constant settling velocity
3. Motile without light inhibition
4. Motile with light inhibition
5. Motile based on carbon accumulation

The respiration of the phytoplankton uses a lumped term that includes respiration, excretion and natural mortality. The respiration term (R), a fraction of the biomass, is calculated by:

$$R = k_r \vartheta^{T-20} \tag{2.76}$$

where k_r is a respiration rate coefficient. The type of salinity environment is defined as freshwater for Myponga and consequently there is no limitation by salinity. The respiration term can be adjusted to account for grazing.

The modelled reactions of dissolved oxygen in the water column are associated with the following processes:

- Sediment chemistry
- Air/water surface exchange
- Phytoplankton photosynthesis and respiration
- Nitrification

There are two options to model the utilisation of oxygen at the sediment surface, either with a static model or a dynamic model where the oxygen flux at the sediment surface is related to dynamic oxygen budgets in the sediment surface (see Herzfeld and Hamilton, 2000). In the static model for the sediment, oxygen flux is a function of the adjacent ambient water temperature and dissolved oxygen concentration.

The flux of oxygen across the air-water boundary is modelled using the method presented in Wanninkhof (1992):

$$F = k(C_a - C_w) \tag{2.77}$$

where F is the oxygen flux (positive into water column), k is the oxygen transfer coefficient , C_a the concentration of oxygen in the air boundary layer, which is a function of temperature and salinity, and C_w the oxygen concentration in the water surface boundary layer.

Many improvements and parameter determination of the code were required to validate CAEDYM against Myponga Reservoir data as detailed in Chapter 8. The methods used to validate the numerical modelling investigations are presented in Chapter 3.

2.7 SUMMARY

A study of phytoplankton succession in an artificially destratified reservoir coupled with a detailed examination of the effect of artificial mixing using a combination of an aerator and surface mixers has not been reported in the literature. The field investigation undertaken at Myponga Reservoir, subsequent research and numerical modelling reported in this thesis will help close the gap in the literature and provide a significant data set that consists of concurrent monitoring of physical, biological and chemical parameters. The reported use of CAEDYM for the study of phytoplankton growth and succession is limited. This Ph.D. research will provide an independent assessment of CAEDYM, and apply the model to an artificially destratified reservoir.

Currently there is minimal literature available relating to the hydrodynamics and diffusion of impeller-induced swirling jets. The literature relating to these jets has been restricted to laboratory-scale studies (Chapter 6) and a need exists to extend the study of these jets at full-scale in the field. This Ph.D. research will enable the detailed examination of full-scale impeller-induced swirling jets, and provide a comparison with results published for laboratory-scale investigations.

3. METHODS – DATA COLLECTION AND ANALYSIS

3.1 INTRODUCTION

Myponga Reservoir was the site for the field study to investigate the impact of the surface mixers upon stratification and cyanobacterial growth. To understand and quantify the effect of the surface mixers upon the limnological processes in Myponga Reservoir extensive physical, chemical and biological field monitoring and experimentation was undertaken.

To characterise the limnological conditions in Myponga Reservoir, field data was collected at various time scales, ranging from seconds to weeks, depending on the specific parameter being measured. The equipment used and methods undertaken to collect and assess field data are described in this chapter.

Myponga Reservoir (S 35°24', E 138°25') is situated 70 km south of Adelaide on the Fleurieu peninsula, South Australia (Fig. 3.1). The reservoir is a flooded river valley impounded by a concrete arch-dam (Fig. 3.2) with a ski-jump spillway that was completed in 1962. It is a highly managed water body with regular algicide ($CuSO_4$) dosing and prolonged artificial mixing.

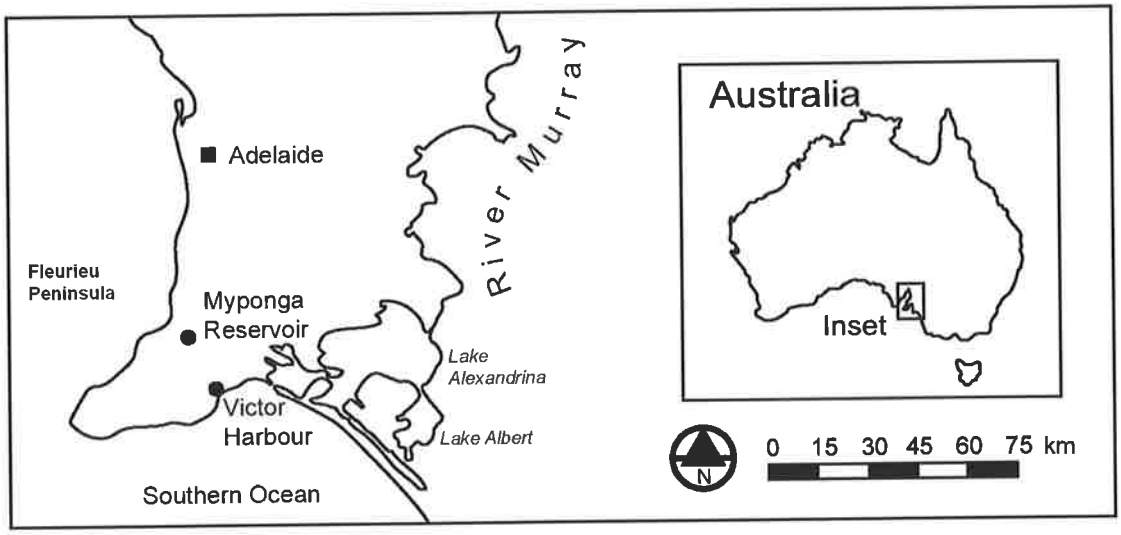

Figure 3.1 Location of Myponga Reservoir.

The reservoir supplies a Dissolved Air Flotation (DAF) water treatment plant that provides filtered water to the majority of the inhabitants of the Fleurieu Peninsula. The water column in Myponga Reservoir is extremely coloured and has a relatively high light attenuation coefficient ($k_d \sim 1.5$ m^{-1}). The reservoir has a capacity of 26800 ML at a full supply level of 211.7 m A.H.D. (Australian Height Datum), and a maximum depth of 36 m. The mean retention time based on abstraction is approximately 3 years. The area of water-spread is 2.8 km^2 and the catchment is 124 km^2, which is of mixed land use, including, improved pasture for dairy, beef and hay production, with patchy remnant vegetation. Recent estimations of dominant land use are 62% grazing and 24% dairying (Thomas *et al.*, 1999). Water is removed from the reservoir via an off-take valve, located on the dam wall, at 195.2 m A.H.D.

Figure 3.2 Myponga Reservoir, the bubble plume generated by the aerator is visible in the foreground. The off-take tower can be seen atop the dam wall.

As well as supplying beachside suburbs from McLaren Vale to Victor Harbor, water from the Myponga Reservoir is used to supplement the Happy Valley Reservoir and is transported to meet the distribution network via a large trunk main.

Artificial mixing at Myponga is achieved with the use of a multi-diffuser aerator and two surface mixers, which was shown to reduce the internal nutrient load (Section 4.6), and hence the total nutrient load is dominated by catchment sources. The aerator is located adjacent to the dam wall at a depth of 30 m (Fig. 3.3). The aerator diffuser has 160 outlets over a length of 200 m and delivers air at 120 Ls^{-1} via a 100 kW compressor. The two surface mounted mechanical mixers, which were deployed in 1999, pump water downward through a 13m draft-tube at a rate of 3500 Ls^{-1} (see Section 6.2.1). The aerator and mixers are operated between October and March each year. The algicide dosing is undertaken to limit the growth of *Anabaena circinalis* thus reducing the risk of taste and odour problems from the associated production of geosmin, and generally consists of one application in early January at a dose rate of 2 mg L^{-1}. No artificial mixing is undertaken during algicide treatment.

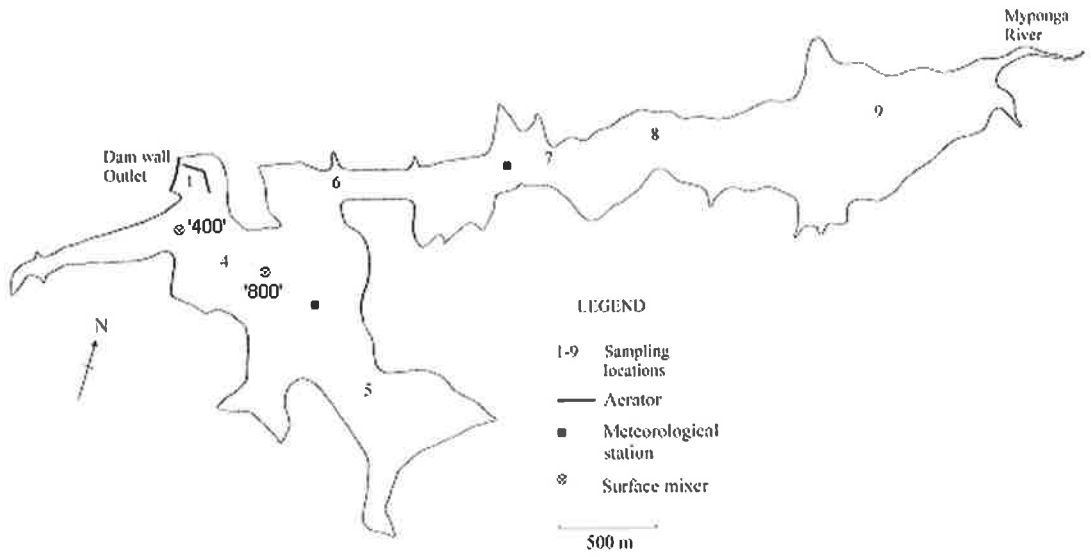

Figure 3.3 Myponga Reservoir with aerator, surface mixers ('400' and '800'), meteorological stations and phytoplankton sampling locations.

Integrated phytoplankton samples were collected over the depths 0 to 5 m using a 5 m hosepipe. Frequency of sampling was daily, weekly or monthly, depending on the season and was undertaken for the project from October-1998 to March-2001 for identification and enumeration (described in Section 3.2); the phytoplankton sampling locations are shown in Fig. 3.3. The main inflow to Myponga Reservoir is Myponga River where an event dependent flow sampler was deployed. The flow sampler was

activated during flood events and nutrient concentrations (μg L^{-1}) were obtained (Section 3.1.2). Inflow rate (m^3 s^{-1}) was recorded every 10 minutes and daily abstraction volumes (m^3 d^{-1}) are recorded. Two permanent meteorological monitoring stations were installed on Myponga Reservoir in June-1999. The meteorological stations are described in section 3.3.

3.2 SAMPLING PROGRAM

The sampling program was conducted as part of a large inter-disciplinary study by the CRCWQT to examine the effectiveness of surface mixers to erode stratification in the surface layer and control the growth of cyanobacteria. The program started in October-1998 and concluded in April-2001. Historical data collected prior to this period was sampled from Location 1, adjacent to the dam wall, analysed by the Australian Centre for Water Quality (AWQC) according to the methods outlined below and provided by SAWater.

3.1.1 Phytoplankton

Depth integrated samples for phytoplankton identification and enumeration were collected from five sites (sites 1, 4, 5, 6, and 7; Fig. 3.3), preserved with Lugol's iodine and counted within a Sedgewick rafter chamber. Cell counts were performed weekly between October and April and monthly between May and September.

Chl *a* concentrations were determined by filtering one litre of sample onto GF/C filters and extracting the pigment in cold ethanol (-20 °C), in the dark, for a minimum of 24 hours. Absorption at 665 nm and 750 nm were measured using a Varian Cary 1 Spectrophotometer and Chl *a* concentration calculated using the equation from Lorenzen (1967).

3.1.2 Nutrients

Nutrient concentrations were determined weekly on samples collected at site 4 from the surface, 10 m, 20 m, and 30 m, and from Myponga River, which is the main tributary. For the period 1998-2001 chemical analyses included nitrate and nitrite (NOx), ammonia (NH_4), Total Kjeldahl Nitrogen (TKN), filterable reactive phosphorus (FRP; filtered through a 0.22 μm filter) and Total Phosphorus (TP).

Nutrients analyses were carried out by standard methods in an ISO 9001 NATA certified laboratory (Australian Water Quality Centre, Accreditation No. 1115, Chemical testing). Soluble nutrients were defined as those that passed through a 0.22 μm polyethersulfone filter (Acrodisc #4652, Pall Gelman Laboratory, MI, USA), filtered the same day as collected, usually within 2 hours.

An accumulated flow triggered auto-sampler (ISCO) was used to sample peak flow events at the gauging station in Myponga River. Sampling of the peak river flows was required to be optimised to sample the flows effectively while operating within budget. Initially (2-May-2000) the auto-sampler was programmed to sample when the accumulated flow in the previous 24 hours exceeded 25 ML and then sampled every 10ML of flow until the gauge height of the river at the sample point subsided to 1.5 m. On 27-June-2000 the auto-sampler was reprogrammed to sample after 35 ML flow in 24 hours and then sample every 20 ML until the gauge height decreased to 1.5 m. On 20-July-2000 the auto-sampler was again reprogrammed to sample after 90 ML flow in 24 hours and then every 40 ML until the gauge height was 1.75 m. Operation of the auto-sampler was monitored using telemetry and samples were collected and analysed as soon as possible after rainfall events, usually within 24 hours. The sampler was located in a cold-shed so bacterial transformation was assumed to be minimal.

3.1.3 Light attenuation

Down welling irradiance was measured at 10 cm intervals through the euphotic zone with an underwater light meter (LiCor UQW 3946). Irradiance was log transformed and the attenuation coefficient calculated by linear regression with respect to depth (Kirk, 1983).

3.3 METEOROLOGICAL STATIONS

Two raft-mounted meteorological monitoring stations were installed at Myponga Reservoir, one in the main basin and the other in the side arm, named Met 1 and Met 2 respectively. The meteorological data, described below, was logged every 10 minutes for all instruments. The logged data was downloaded at weekly intervals using telemetry and stored in database format. Measurement Engineering Australia

Pty Ltd (MEA) supplied and undertook the calibration of the instrumentation prior to installation on the reservoir.

The instrumentation installed on the meteorological stations monitored the following:

- Thermistor chain (°C) at discreet depths through the water column (see Appendix A)
  - Met 1: 24 of 3K3D Negative Temperature Coefficient Thermistor (3000Ω @ 25 °C), Betatherm Ireland.
  - Met 2: 25 of 3K3D Negative Temperature Coefficient Thermistor (3000Ω @ 25 °C), Betatherm Ireland.
- Wind speed (ms^{-1}) and direction (°) at 1.8 m above the air-water interface
  - Met 1: WM-IIIA Wind Sensor, Climatronics USA.
  - Met 2: Model 034 Wind Sensor, Met One Instruments USA.
- Relative humidity (%) and Air temperature (°C)
  - Met 1: HMP45A Humidity and temperature probe, Vaisala Oyi Finland.
- Incoming solar radiation (Wm^{-2})
  - Met 1: Middleton EP09 Secondary Standard Pyranometer, Carter-Scott Design Australia.
- Net radiation between the water surface and atmosphere (Wm^{-2})
  - Met 1: Middleton CN1-R Net Pyrradiometer, Carter-Scott Design Australia.

The meteorological data coupled with biological monitoring was used to investigate the phytoplankton succession and understand the unique limnological attributes of Myponga Reservoir that was required to assess the impact of the surface mixers, Chapters 4 and 6. The data set was also used as input and validation for the numerical modelling investigations described in Chapters 5, 7 and 8.

3.4 DROGUE STUDIES

To investigate the hydrography and associated movement of phytoplankton in Myponga Reservoir, drogue studies were undertaken. Drogues (Fig. 3.4) are commonly used to investigate large-scale movements in water bodies (Boyd *et al.*, 2001; Hindell *et al.*, 2003; Redalje *et al.*, 2002) and to give insight into the transport

of phytoplankton and nutrient from littoral zones and throughout deeper regions in water bodies (Cotonnec *et al.*, 2001; George, 2000; Hoge *et al.*, 1998).

The drogues used for Myponga Reservoir were constructed from 25 mm PVC conduit with associated elbows and junctions (that were filled with lead weight ensuring the drogues were negatively buoyant), which were covered in water resistant material. Two sizes of drogues were manufactured, one with 0.75 x 0.75 m panels and the other with 0.5 x 0.5 m panels. Each drogue was attached to a 200 mm diameter white foam buoy with fishing line, which allowed for the drogues to be set at a range of depths (1 to 6 m) in the water column. The results of the drogue studies are presented in Chapter 4.

Figure 3.4 The drogues used to investigate the hydrography in Myponga Reservoir. The surface area of the individual square panels on the large drogue is 0.5625 m^2 and the small drogue 0.25 m^2.

3.5 SURFACE MIXERS

The surface mixers, model SMDI-5, (Fig. 3.5) were manufactured by Water Engineering And Research Solutions Pty Ltd. (WEARS); Queensland, Australia. The SMDI-5 is a 5 m-diameter pontoon mounted impeller fitted with an adjustable length draft-tube designed to pump surface water from the water surface to the depth of the draft-tube (~14.2 m).

The draft-tube is suspended below the pontoon via four adjustable poles, which also serve to adjust the water inlet depth to the impeller (Fig. 3.5).

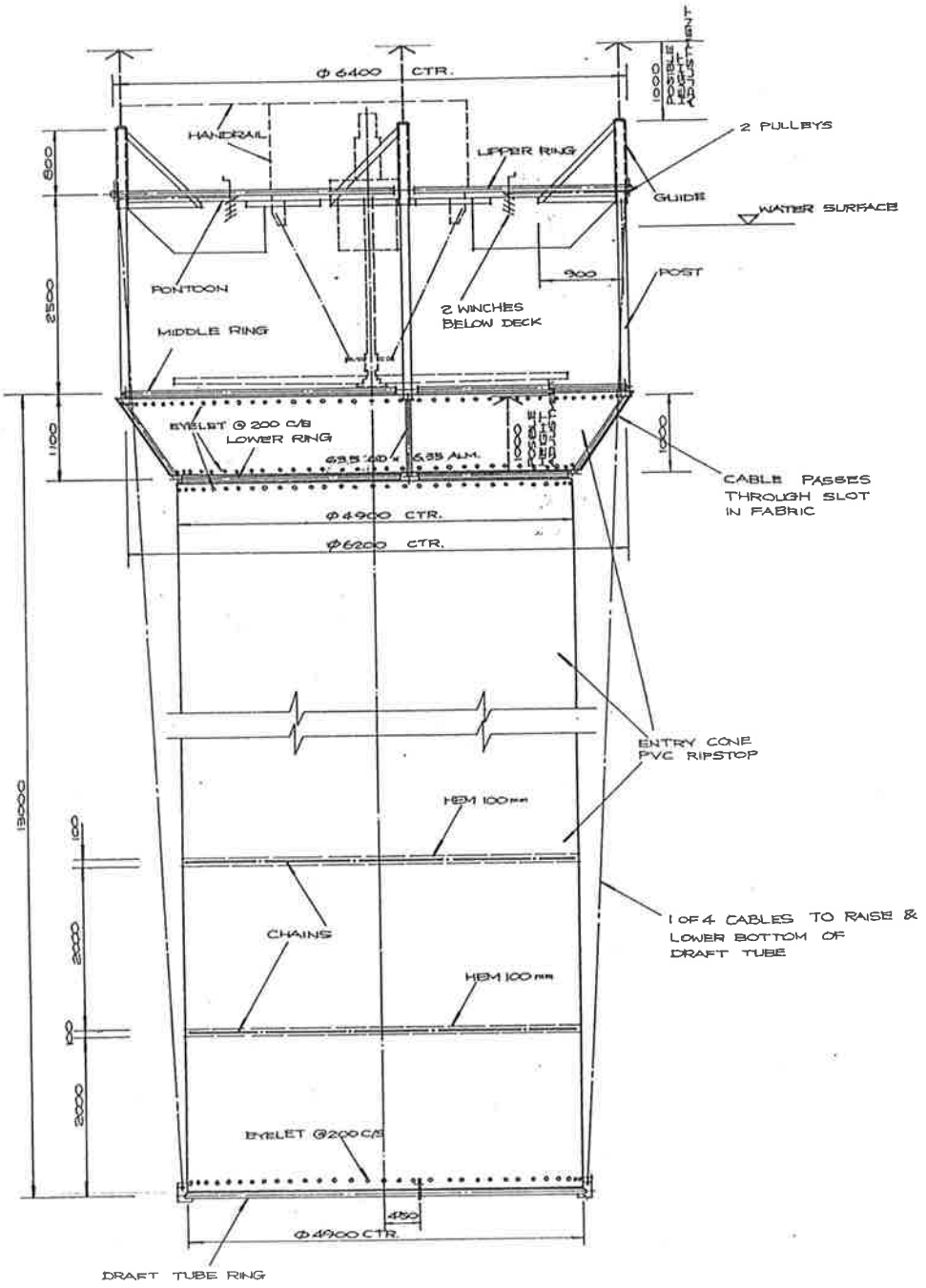

Figure 3.5 WEARS SMDI-5 Surface mixer (reprinted with permission).

The pontoon is manufactured with four aluminium-floating chambers and stainless steel (316L) structure materials. The impeller is driven by a variable speed Genat and Wood 4 kW 3-phase motor (model 4030-D120) coupled to a Genat and Wood flange mounted helical gearbox. Variable speed is provided by a 4 kW Allen Bradley variable speed drive (model 1305-BA090). All electrical equipment is IP56 (Australian/New Zealand Standard 3008.1.1:1998, 3008.1.2:1998) rated. Mooring of the surface mixers is achieved with 4x125 kg concrete anchors via adjustable stainless steel mooring cable.

3.6 ACOUSTIC DOPPLER VELOCIMETER

A field-version and a laboratory-version Acoustic Doppler Velocimeter (*ADVField* and *ADVLab* respectively) were used to measure the flow generated by the surface mixers. The *ADVLab* is used with a desktop personal computer in a laboratory setting (the processor card is installed inside the computer) and the *ADVField* is an autonomous unit.

The Acoustic Doppler Velocimeter (*ADV*) uses acoustic doppler technology to measure three-dimensional flow in a sampling volume (approximately 0.3 cm^3) located 5 cm from the probe (Fig. 3.6). Consequently the *ADV* measurements minimised disturbance to the surface mixer flow whilst providing accurate point measurements of the velocity field. Data can be acquired at sampling rates up to 50 Hz. With no zero offsets, the *ADV* can measure flow velocities from less than 0.001 ms^{-1} to over 2.5 ms^{-1}.

The 10 MHz *ADVField* (Fig. 3.6) probe consists of the acoustic sensor, mounting stem and a Signal-Conditioning Module (*SCM*). The acoustic sensor is the assembly of three acoustic receivers and one acoustic transmitter. A sacrificial zinc anode is attached to the stem for corrosion protection. The *ADV* normally reports velocity data in a Cartesian (*XYZ*) coordinate system. A high frequency cable connects the *SCM* to a digital processor.

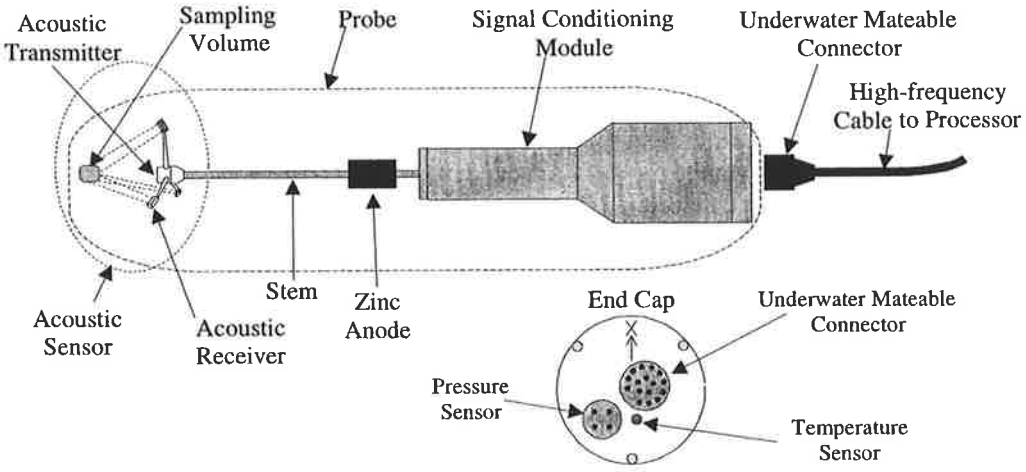

Figure 3.6 10 MHz *ADVField* Probe with sensors.

The *SCM* also contains compass, tilt, pressure, and temperature sensors. The compass-tilt sensor allows the *ADV* to report velocity data in Earth coordinates (East-North-Up or *ENU*), regardless of instrument orientation. The probe *X*-axis is painted red and corresponds to the compass bearing.

The optimum sampling rate corresponds to a time interval between samples that is twice the integral time scale of the flow (Hyun and Patel, 1991). Subsequently the optimum sampling rate is a compromise between minimising the amount of data to be collected and maximising the convergence rate to obtain statistically stable estimates of the mean flow properties.

The *ADV* calculates two quantities to determine the efficiency of the measurement, namely the Signal-to-Noise Ratio (*SNR*) and the Correlation Coefficient (*COR*). The *SNR* is the ratio of signal strength to the background acoustic noise level inherent in the *ADV* instrument. The values are given in decibels (dB) relative to the noise level. For collection of instantaneous velocity data a *SNR* of 15 dB or higher should be maintained. For measuring mean velocities, the *SNR* ratio should be 5 dB or higher. Low *SNR* ratios are usually caused by a low concentration of scatterers, particles in the flow that reflect acoustic signals back to the probe receivers, in the sample volume.

The *ADV* probe actually measures the velocity of the scatterers in the flow. Micro-bubbles of air can be effective scatterers as can organic and inorganic particles. A correlation score is calculated for each sample stored in the *ADV* file, for each of the three signal beams; values are expressed in percent, with 100 % being a perfect correlation. Correlations of 70 to 100 % are typically considered good. Low correlation values may indicate problems related to turbulence, signal strength, scatterer density, excessive air bubbles, or problems with the probe itself.

One significant advantage of the *ADV* is that there is no minimum measurable velocity, with no potential for a zero offset or zero drift. The lowest *ADV* velocity range, ±3 cm s^{-1}, will yield good results for flows down to about 0.1 cm s^{-1}. The *ADV* has been used to measure calibrated flows as low as 0.04 cm s^{-1} and has shown excellent performance at even lower levels where no reference is available. The *ADV* is reported to be accurate to within 1 % for velocities greater than 0.0025 m s^{-1}, see http://www.sontek.com.

3.1.4 *ADV* data analysis

To analyse the data collected by the *ADVLab* and *ADVField*, a reliable method of post-processing was required. To ensure that the technical limitation of the *ADV* does not affect the quality of the data, filtering is required. Filtering can be achieved by exploiting the *SNR* and correlation score *COR* parameters supplied in the recorded *ADV* data file. In addition to providing the time-averaged velocity data, the post-processing needed to provide turbulence characteristics, namely the root-mean-square of the turbulent velocity fluctuations and the covariance. Consequently a customised software package was used for the post-processing of the *ADV* data. The *WinADV* software program (Wahl, 2000) was utilised for this purpose. *WinADV* provides a platform to view and process data recorded with the *ADVLab* and *ADVField* (Wahl, 2000). The data handling options used for the investigation of the surface mixer flow were:

- Filtering of data to exclude erroneous and poor-quality data
- Sampling options to define the range of samples being analysed

3.7 HYDROLAB

Water quality parameters were measured using a Hydrolab multi-probe, which measures multiple parameters simultaneously including: temperature, pH, conductivity, dissolved oxygen, depth, turbidity, chlorophyll fluorescence, and Global Positioning System (*GPS*) coordinates. The Hydrolab multi-probes incorporate multiple sensors in a single housing. Two types of Hydrolab's were used for data collection, the DataSonde 4a® and MiniSonde 4a® Multi-probes, which were connected to a Surveyor 4a® Data Display with *GPS* or to a laptop computer using proprietary software, depending on the measurements undertaken.

The DataSonde 4a® is designed for *in-situ* and flow-through applications and measures up to 15 or more parameters. It comes with seven built-in expansion ports for field-replaceable sensors. The MiniSonde 4a® has four built-in ports. Both units are available with battery packs and memory to use for long-term monitoring and profiling applications. The Surveyor 4a® provides data logging and display. Connected to either the DataSonde 4a® or MiniSonde 4a®, the Surveyor 4a® displays water quality parameters in real time or automatically stores or downloads documents. The high-resolution screen displays the water quality data in real-time graphical form or tabular format. *GPS* coordinates were also recorded.

The Hydrolab's and *ADVLab* were cast from the boat with an instrument winch for near to far field monitoring, and when profiling beneath the surface mixer draft-tube the DataSonde 4a® was attached to the *ADVField* extendable traversing mechanism arm (Section 6.2.4) adjacent to the *ADVField* (Fig. 3.7).

Figure 3.7 *ADVField* and DataSonde 4a® mounted on the *ADVField* extendable traversing mechanism arm.

The instrument arrangement shown in Fig. 3.7 enabled the profiling of water quality parameters to be measured simultaneously within the surface mixer flow. The MiniSonde 4a® was located in the surface mixer inlet to monitor inflow temperature whilst profiling was undertaken on the surface mixer efflux. Results from the *ADVField*, *ADVLab* and Hydrolab's profiling are presented in Chapters 4, 6 and 7. Measurements were recorded at 50 Hz for 2-minute intervals every 500 mm through the water column. The near to far-field profiling process was repeated at numerous distances from the surface mixer ranging from 1 to 500 m. The measurements were time-averaged using the 2-minute sampling time to ensure that the required draft-tube radial, tangential and vertical flow was detected.

3.8 NUMERICAL MODELLING VALIDATION TECHNIQUES

The use of numerical modelling requires that validation be undertaken to ensure that the models predictions are comparable with the measured event (McKinion and Baker, 1982). Numerical models and data vary greatly in complexity and there is no universal validation technique that is applicable across all modelling situations

(Mayer and Butler, 1993). General overviews of validation processes are found in many simulation texts (Bratley *et al.*, 1987; Jørgensen, 1986; Mayer and Butler, 1993).

The validation techniques used to assess the individual outputs from PROTECH; DYRESM, and DYRESM-CAEDYM were the use of the Pearson's product moment correlation coefficient (R^2) (Mayer and Butler, 1993) and *P-value*, and the modelling efficiency (*EF*) (Loague and Green, 1991). The R^2 value obtained from linear regression analysis is a useful general statistical method, and the *EF* is a statistic based on the coefficient of determination and directly compares model predictions with measured data. The methods are described below, where x_i represents observed values, $\hat{y}_i$ simulated values, and n the number of data points.

3.8.1 Pearson's product moment correlation coefficient

The Pearson product moment correlation coefficient (Eq. 3.1) is a dimensionless number with a range from -1.0 to 1.0 inclusive. R reflects the extent of a linear relationship between two data sets. In the case of modelling, one data set would be the observed data (independent variables) and the other data set would be simulated data (dependent variables).

R^2 is the square of the Pearson product moment correlation coefficient through data points. R^2 can be interpreted as the proportion of the variance in field data to the variance in the simulated data, i.e. quantifies the goodness of fit. R^2 is has a value that ranges from zero to one, and is the fraction of the variance in the two variables that is shared, e.g. if $R^2 = 0.59$, then 59% of the variance in x_i can be explained by variation in $\hat{y}_i$. Similarly, 59% of the variance in $\hat{y}_i$ can be explained by variation in x_i.

$$R = \frac{n\left(\sum x_i \hat{y}_i\right) - \left(\sum x_i\right)\left(\sum \hat{y}_i\right)}{\sqrt{\left[n\sum x_i^{\,2} - \left(\sum x_i\right)^2\right]\left[n\sum \hat{y}_i^{\,2} - \left(\sum \hat{y}_i\right)^2\right]}} \tag{3.1}$$

3.8.2 *P-value*

The *P-value* indicates the probability that random sampling would result in a correlation coefficient as observed in the investigated data sets, i.e. the probability that

a variate would assume a value greater than or equal to the observed value strictly by chance:

$$P(z \geq z_{observed}) \tag{3.2}$$

If the *P-value* is small (<< 0.01), the correlation is not coincidental. Normally the confidence level is set to 95 %. Therefore for *P-value* << 0.01 implies that the modelled population lies somewhere within the measured range. If the *P-value* is large (> 0.05), the data does not give any reason to conclude that the correlation is real. This is not the same as saying that there is no correlation at all, but there is not any compelling evidence that the correlation is real and not a coincidence.

3.8.3 Modelling Efficiency

The modelling efficiency (Eq. 3.3) gives an overall measure of model performance, which relates the observed data to the 'perfect fit' line as opposed to the 're-calibration' of the model. A model that results in a negative value cannot be recommended, and an *EF* value of one indicates a perfect fit (Mayer and Butler, 1993).

$$EF = 1 - \frac{\sum (x_i - \hat{y}_i)^2}{\sum (x_i - \bar{x}_i)^2} \tag{3.3}$$

where $\bar{x}$ is the observed mean.

3.9 SUMMARY

The aforementioned methods of field data and acquisition, and analysis, were used for analysis of the limnology in Myponga Reservoir, presented in Chapter 4. This is followed by the numerical investigations using the PROTECH model, which are validated using the methods presented in section 3.8. The detailed flow analysis of the surface mixers is discussed in Chapter 6. Further numerical modelling investigations are presented in the chapters following the analysis of the surface mixers.

4. ANALYSIS OF MYPONGA FIELD DATA

4.1 INTRODUCTION

The previous chapter presented the methods of field data acquisition at Myponga Reservoir. In this chapter an interpretation of the collected physical and biological data is presented. Understanding the limnology in Myponga Reservoir allowed the characteristics of the physical processes to be understood and how these processes affect the diversity of phytoplankton biota and growth characteristics. When altering the 'natural' state of Myponga Reservoir, a degree of confidence was required that the subsequent alterations by the use of the surface mixers were favourable. Additionally, analysis of the water body assisted future phytoplankton management procedures by providing insight into the inter-relationships of phytoplankton and the dynamic limnological environment.

An important limnological characteristic is time-scale of events, especially when considering phytoplankton ecology. Phytoplankton ecology and community composition is determined by the rate of resource delivery and the rate of habitat change. If we consider the major resource requirements to be light and nutrients, and the habitat to be the degree of mixing relative to light penetration, then the magnitude and composition of the phytoplankton community is determined by meteorological and physical features, which vary with space and time. Processes that occur at scales ranging from the microhabitat to global processes all impact phytoplankton habitat and physiology. Similarly, processes may impact the phytoplankton instantaneously or they may take a period of weeks for the impact to be observed in the phytoplankton community.

Limnological processes in lakes and reservoirs are relatively well understood (Imberger and Patterson, 1989; MacIntyre, 1993; MacIntyre, 1996; MacIntyre *et al.*, 2002; Wells and Sherman, 2001). With respect to habitat change in a lake or reservoir the relevant physical processes include wind mixing, which deepens the *SML* and transports cells vertically (Imberger and Patterson, 1989; Patterson, 1991). Lateral transport processes, such as differential cooling (Monismith *et al.*, 1990), can

transport phytoplankton cells between site-specific habitats. If there are differences in stratification and nutrient supply at different sites within a reservoir then this may result in different species being favoured and lead to "patchiness" in the phytoplankton community. However, if there are processes that result in basin scale circulation and significant flux of phytoplankton between sites then this patchiness may be overcome and the phytoplankton community would appear homogeneous throughout the reservoir.

Many lakes and reservoirs in temperate zones exhibit one-dimensional physical structure where time-scales in horizontal motion far exceed those in vertical motion. The water in the shallow littoral zones is able to exchange rapidly with the interior in these water bodies. Consequently, the phytoplankton assemblage can become homogeneous throughout their respective growth cycles when one-dimensional structures exist, as the time-scale for horizontal mixing exceeds that of the phytoplankton growth. Generally the bathymetry in lakes and reservoirs that display one-dimensional structures are reasonably uniform (e.g. basin shaped), and experience relatively homogeneous meteorological forcing.

The geomorphological characteristics at Myponga Reservoir (Fig. 3.3) suggest that two separate habitats for phytoplankton growth might exist due to the side arm bathymetry being significantly different from the main basin. The location of the side arm is effectively situated perpendicularly from the main basin and joined by a narrow channel. The differing topography around each region would cause the meteorological forcing to be dissimilar in either location, e.g. wind forcing. The inflow to the side arm is seasonal with minimal inflow occurring annually from November to February (see Fig. 4.2). It is during this period that the water movement between the side arm and main basin is limited to convective currents driven by meteorological forcing, i.e. differential cooling and heating.

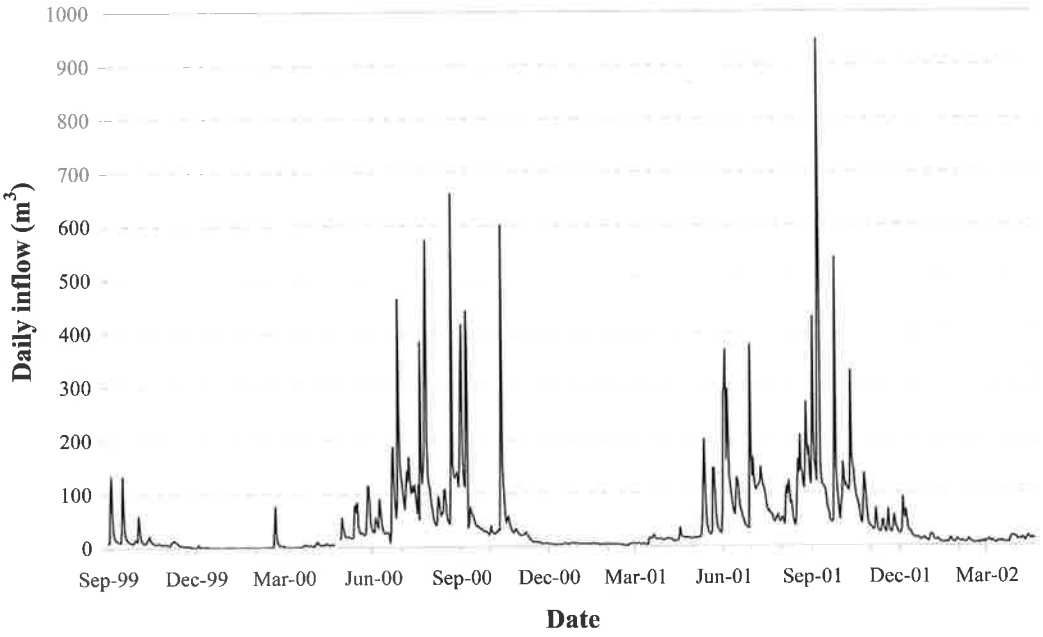

Figure 4.1 Daily inflow to Myponga Reservoir from 1999 to 2002. Note the insignificant inflow that occurs annually from November/December to March/April.

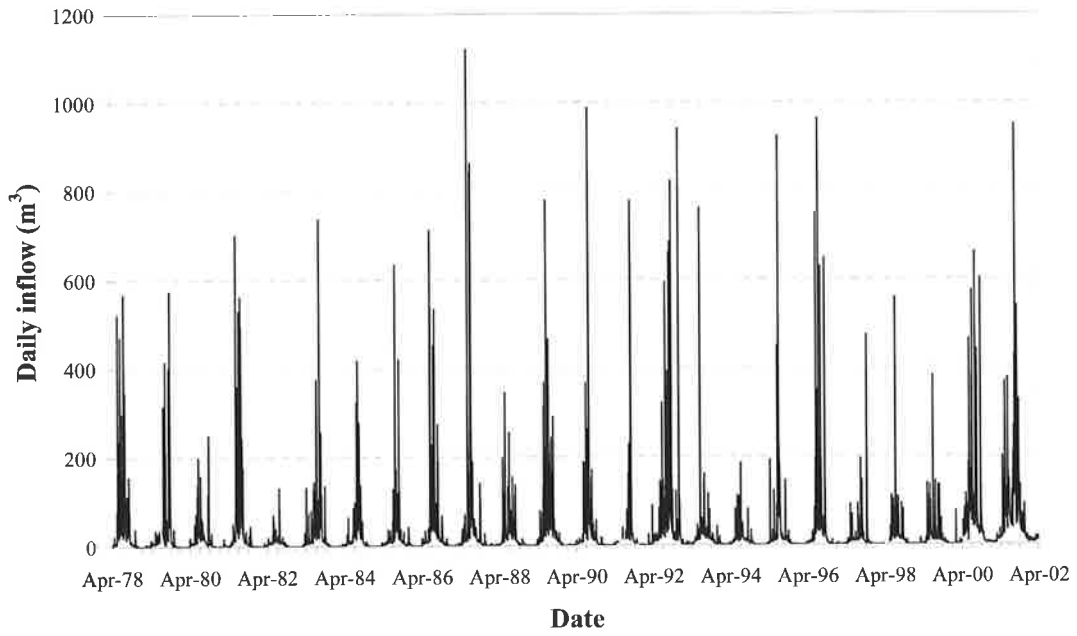

Figure 4.2 Daily inflow to Myponga Reservoir from 1978 to 2002.

The different heating and cooling rates across the water surface presented two potential problems, would the phytoplankton assemblage in the side arm differ from

the main water body, and would the action of the aerator and surface mixers influence the side arm. During the warmer months the bathymetry of Myponga Reservoir could potentially lead to a diversity of microenvironments for phytoplankton as well as locations with different rates of biological and chemical behaviour.

The phytoplankton assemblage was monitored at several locations (Fig. 3.3) for identification and enumeration, and to monitor for heterogeneity (see Table 4.1 for identified species in Myponga Reservoir).

Table 4.1 Myponga Reservoir phytoplankton assemblage ($^{1 \rightarrow 3}$ denotes dominant groups).

Chlorophytes[1]	**Cryptophytes**[3]	**Cyanophytes**	**Diatoms**[2]	**Dinophytes**	**Euglenophytes**
Ankistrodesmus	*Chroomonas*	*Anabaena circinalis**	*Cyclotella*	*Peridinium*	*Euglena*
Chlamydomonas	*Cryptomonas*	*Anabaena (straight) spp.*	*Flagellate Green SP4*	*Glenodinium*	
Chlorella		*Aphanocapsa*	*Melosira*		
Dictyosphaerium		*Microcystis incerta*	*Navicula*		
Golenkinia		*Oscillatoria*	*Nitzschia*		
Oocystis		*Phormidium*	*Synedra*		
Scenedesmus		*Planktolyngbya*			
		Planktothrix			

An analysis of a drogue study and interrogation of field data is presented to investigate these issues. An additional aim of the data collection was to provide an extensive data set that could be used for further investigation into limnological processes in Myponga Reservoir for future projects.

4.2 DROGUE STUDY

The forced vertical mixing of surface water with deeper water (or vice versa) in a stratified water body causes a new layer being formed at the depth of the thermocline, that moves horizontally and radially away from the mixing device, known as a radial intrusion. The radial intrusion will theoretically penetrate until a physical barrier (e.g. the shoreline) is encountered. Therefore it could be expected that the radial intrusions generated by the surface mixers and aerator in Myponga Reservoir will travel up the side arm. The velocities in the intrusions are inversely proportional to radial distance from the source of the intrusion. Intuitively the velocity of the radial intrusion travelling through the side arm entrance would be orders of magnitude less than that

at their source. Therefore the intrusions would not be expected to cause any significant mixing along the side arm. However, the near field intrusions generated around the mixing devices would deepen the *SML*, that in turn would create instability in the water column resulting in horizontal motion, therefore causing the water in the side arm to interact with the main basin. To observe the water transfer between the side arm and the main basin drogues were placed in either location, and their movement tracked.

Additionally, the difference in bathymetry between the relatively shallow side arm and deeper main basin suggests that the side arm will cool and heat at faster rates than the main basin. Consequently, if drogues were placed at selected locations in the side arm and main basin during periods of significant diurnal temperate changes (i.e. late autumn) the action of differential cooling and heating should be observed with the drogues travelling through the side arm entrance to and from the main basin.

The drogue study was used to qualify basin exchange between the two locations. The manufacture and deployment techniques for the drogues are presented in Chapter 3 and the results from selected studies are shown in Table 4.2. The results give a qualitative representation of basin exchange. The trajectories of the motion of the drogues are shown in Fig. 4.3, which should be viewed as ideal due to the impracticalities of following the drogues during their entire voyage. The trajectories, distances and velocities presented are used for the sole purpose to show that basin exchange occurs.

The *GPS* positions of drogues 1, 3 and 6 were recorded at launch and retrieval only, drogues 2, 4, 5 and 10 at three locations, drogues 7 and 9 at four locations and drogue 8 at five locations. The wind potentially interfered with the travel of drogues 1, 2, 3, and 5, whilst the other drogues traversed in significantly different directions to the prevailing wind (see Table 4.2).

Table 4.2 Drogue deployment description and averaged trajectory distance, velocity and direction.

Drogue			Depth (m)	Date	Δt hh:mm	Minimum distance (m)	Average velocity (ms^{-1})	Mean direction (°)	
ID	Size (m^2)	Line (Fig. 4.3)						Drogue	Wind
1	0.5	Black	6	4-Oct-00	17:45	1365	0.02	124	135
2	0.75	Red	8	3-Nov-99	01:42	513	0.08	231	190
3	0.5	Brown	16	2-Oct-00	21:36	701	0.01	332	256
4	0.5	White	2	2-Nov-99	23:15	786	0.01	232	130
5	0.5	Yellow	3.5	16-Nov-99	19:40	934	0.01	270	246
6	0.75	Green	10	5-Nov-99	02:28	218	0.02	231	70
7	0.5	Light green	3.5	2-Nov-00	06:14	730	0.01	61	278
8	0.75	Blue	10	11-Nov-99	19:38	418	0.01	19	164
9	0.5	Purple	3.5	12-Nov-99	20:02	1512	0.02	244	81
10	0.5	Pink	2.5	2-Nov-00	18:40	1336	0.02	67	130

Drogues 2, 3, 4, 5 and 6 traversed through the channel connecting the side arm to the main basin. Drogue 3 travelled from the main basin into the channel and the other 4 drogues travelled in the opposite direction. The time taken for travel through the channel in either direction ranged from ~2 to 23 hours suggesting that interchanges between the 2 locations occur dielly. This is supported by the fact that differential cooling and heating follows a diurnal pattern. The drogue study conclusively demonstrated that 'natural' large-scale circulation patterns occur in Myponga Reservoir, and the water in the side arm and main basin interchanges dielly during periods of insignificant inflow.

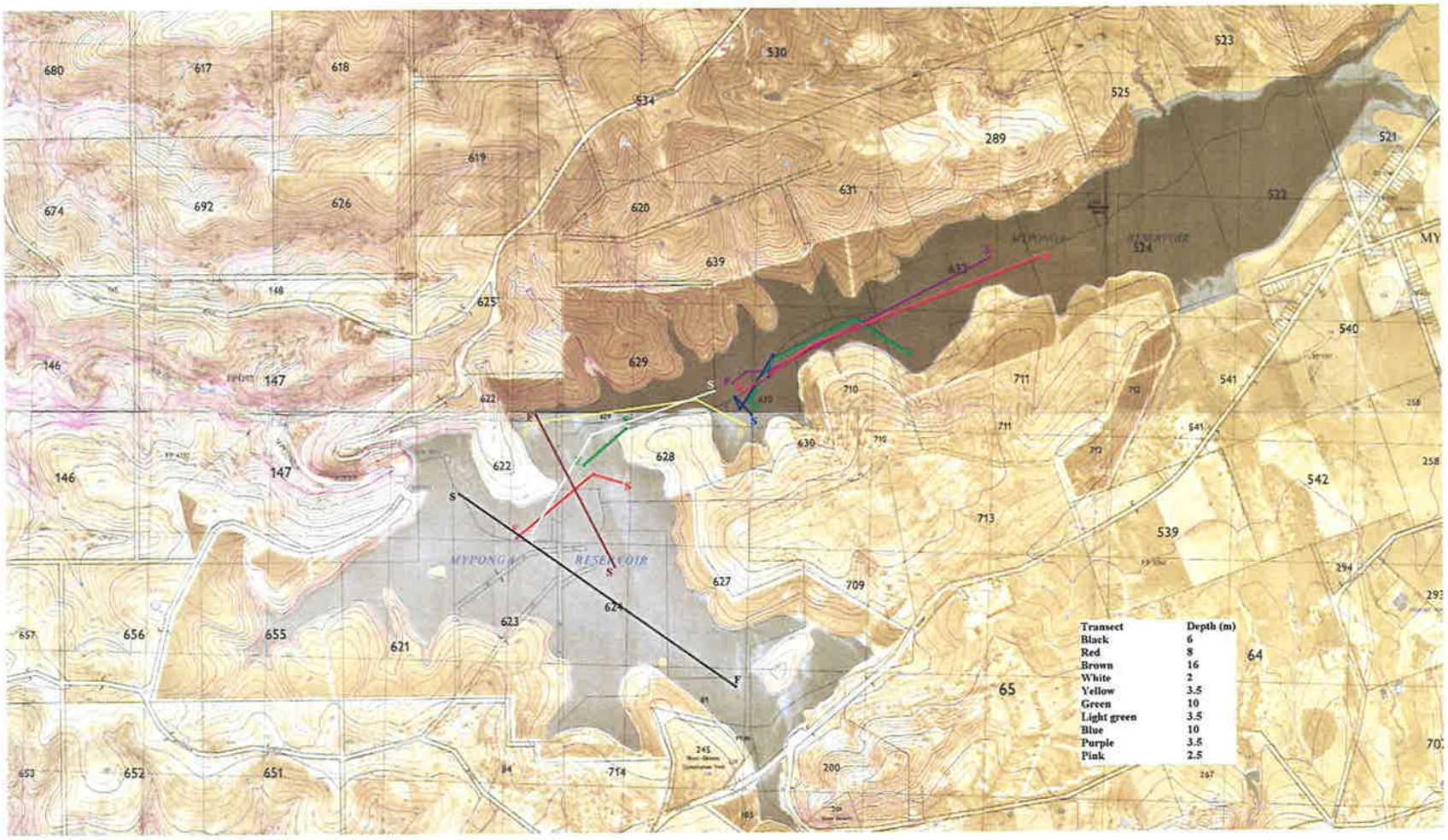

Figure 4.3 Trajectories of drogues deployed in Myponga Reservoir to qualify basin exchange between the side arm and main basin. The trajectories are colour coded and correlate with the data in Table 4.2. 'S' represents the position of drogue deployment and 'F' the conclusion.

4.3 EUPHOTIC DEPTH

The coloured nature of the water in Myponga Reservoir caused by tannin input manifests in a very shallow euphotic depth. The euphotic depth (z_{eu}, m) is defined as the depth at which the irradiance measured at that depth (I_z) is 1% of the irradiance at the reservoir surface (I_0). The light irradiance at depth z is calculated by:

$$I_z = I_0 e^{-\eta z} \tag{4.1}$$

where η is the attenuation coefficient (m^{-1}). Light attenuation coefficient and euphotic depth were calculated from light profiles using a LiCor underwater Radiometer. The measured light data and calculated euphotic depth is shown in Fig. 4.4 for the period from November-1998 to April-2000, which proved to be relatively constant throughout this period.

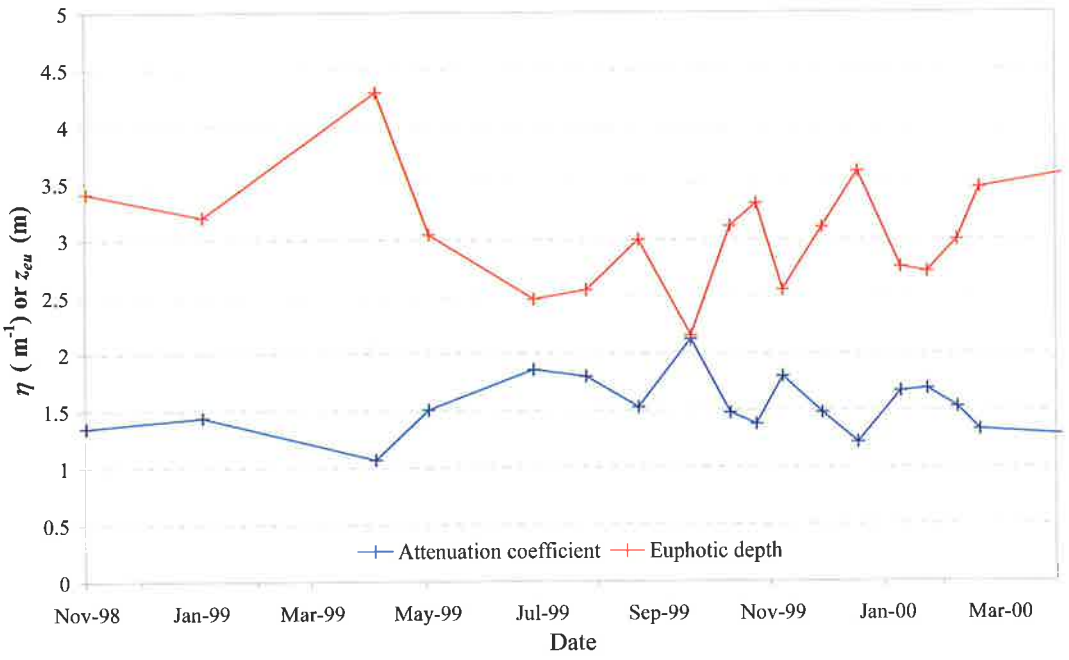

Figure 4.4 Light attenuation and euphotic depth taken at location 4 (refer Fig. 3.3).

4.4 METEOROLOGICAL AND THERMISTOR DATA

The meteorological data collected at Myponga Reservoir is presented in Figs 4.7 and 4.8 as mean monthly values from September-1999 to February-2002. Throughout this period the aerator and surface mixers were operated annually from October to April. The meteorological conditions at Myponga Reservoir are typically that of a temperate region where annual cycles of heating and cooling occur. The maximum average monthly air temperatures, ranging from 18 to 23 ^{o}C, occurred during January and February coinciding with periods of high solar insolation when the average net monthly radiation peaked at 230 W m^{-2} (Fig. 4.7).

The maximum loss of heat due to evaporation and conduction, latent heat and sensible heat respectively, occurred from December to February coinciding with high insolation and wind speeds. The average relative humidity peaked at > 80 % mid-year, coinciding with the winter rains. The inter-annual meteorological cycles are reasonably consistent.

The objective for the collection of meteorological data was to quantify the meteorological forcing that causes the reservoir to stratify and leads to optimal conditions for nuisance cyanobacterial growth. During periods of high insolation and low wind the reservoir is likely to stratify. Maximum daily air temperatures, minimum relative humidity and high insolation occurs mid-January at Myponga Reservoir, giving rise to stratified conditions. These meteorological conditions consistently occur each year as seen in the data (Figs 4.7 and 4.8), which requires the intervention of artificial mixing to minimise stratification. The thermistor data recorded at Met 1 from September-1999 to September-2000 is shown in Fig. 4.5.

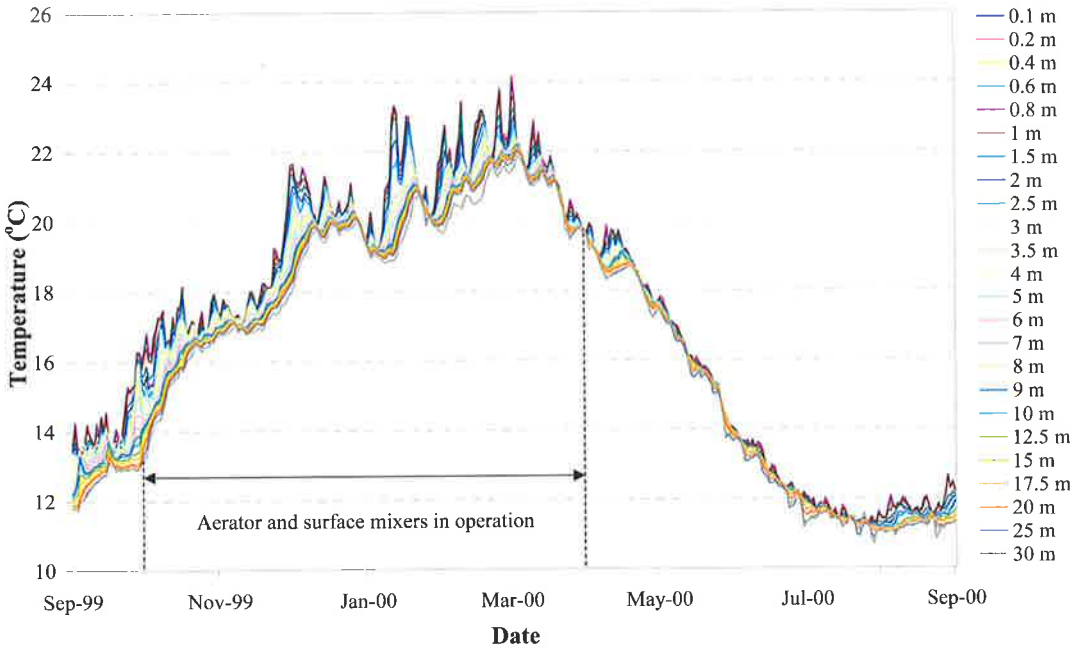

Figure 4.5 Myponga Reservoir thermistor data taken for Met 1 from September-1999 to September-2000. Separation of traces represents persistent stratification.

The thermistor data enabled the degree of stratification to be monitored throughout each season. During summer the average daily temperature difference between the top and bottom of the water column rarely exceeds 4 °C. Although stratified conditions exist whilst the surface mixers and aerator are in operation, the degree of stratification is relatively weak ($\Delta T \leq 4\,^{\circ}C$) and persists for short periods of up to one to two weeks (Fig. 4.5).

The heating and cooling of the reservoir follows the pattern of solar insolation, shown in Fig. 4.7, where maximum insolation occurs during January-February and minimum insolation during June-July. The reservoir exhibits polymictic behaviour throughout each year when artificial mixing is operated during the heating cycle, exhibiting weak stratification most of the time with short (days to weeks) periods of significant stratification. Reservoirs in temperate zones are typically monomictic displaying stratified conditions during the summer and well-mixed conditions during the winter. Myponga Reservoir would be monomictic without the use of the aerator and surface mixers. This is discussed in more detail in Chapter 7.

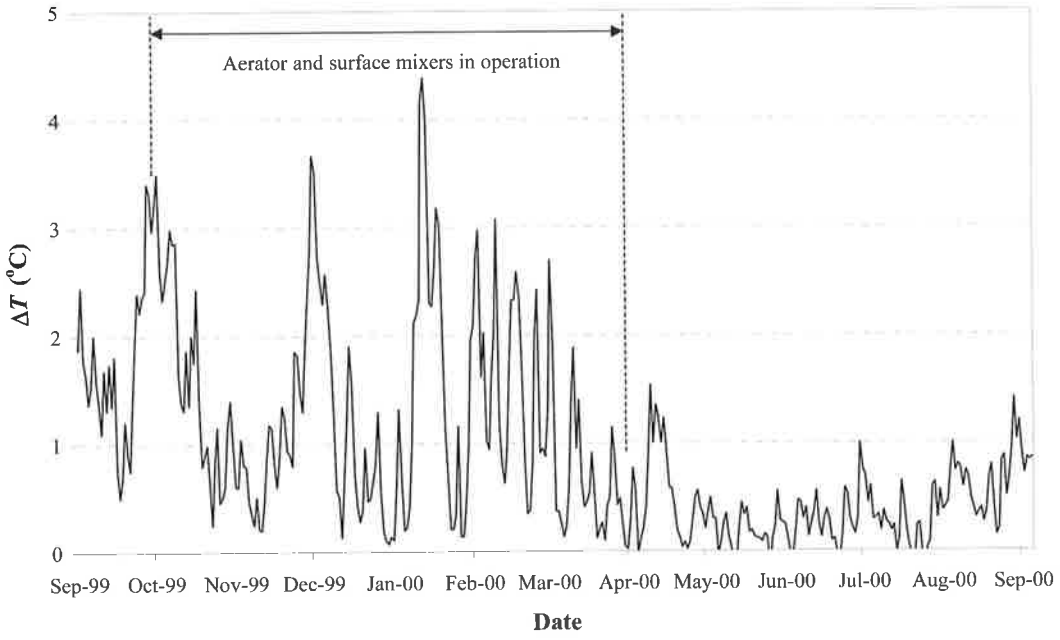

Figure 4.6 Temperature difference between the water surface and 30m depth from September-1999 to September-2000.

Artificial mixing reduces the intensity of stratification, which can be demonstrated by considering the average daily temperature difference between the water surface and the 30m thermistor on Met 1 (ΔT); the data is plotted in Fig. 4.6. During periods of high insolation the maximum ΔT reached is ~4.4°C, which was limited to a period of a couple of days with the *SML* reduced to ~1.5 m (Fig. 4.9).

Without the use of artificial mixing, permanent stratification would occur and historical data (Appendix B) shows that ΔT exceeds 10°C. The numerical modelling investigation presented in Chapter 7 gives insight into the severity of stratification and associated water quality issues that would occur in Myponga Reservoir without the use of artificial mixing.

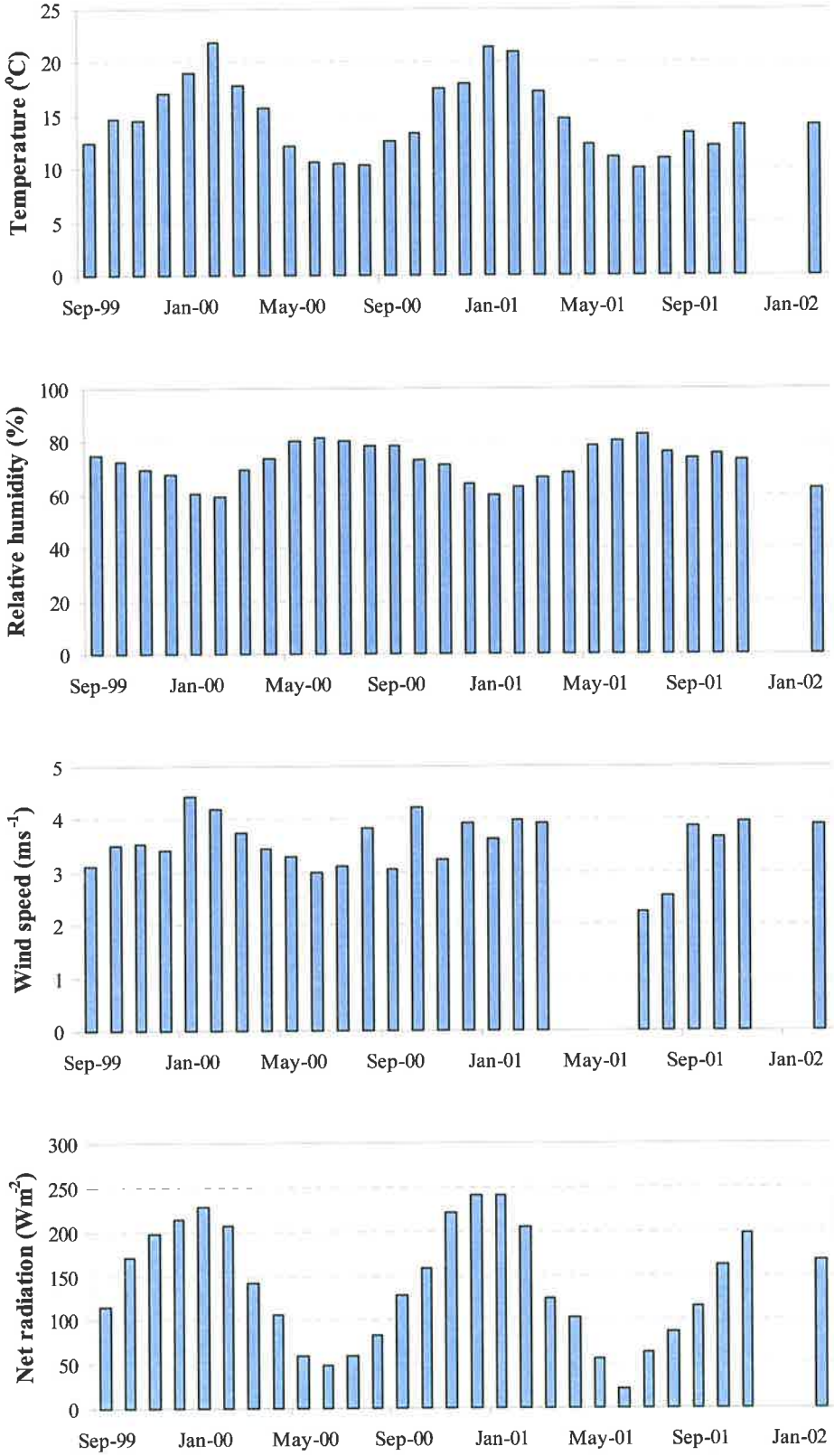

Figure 4.7 Monthly meteorological parameters for Myponga Reservoir from September-1999 to February-2002 (note that the wind vane on Met 1 was not in operation from April to June-2001).

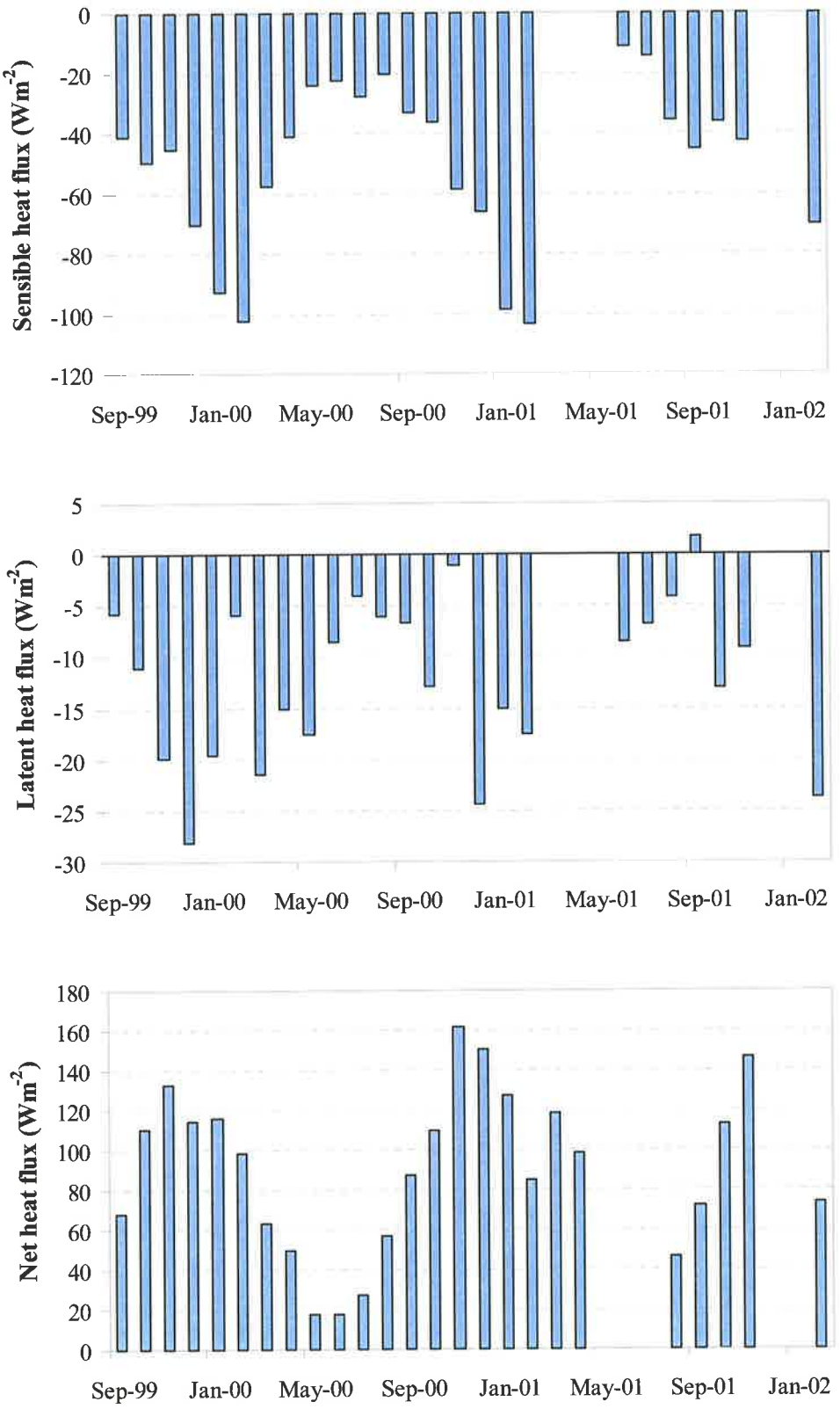

Figure 4.8 Monthly sensible, latent, and net heat fluxes calculated from Myponga Reservoir meteorological and water column observations (note that the wind vane on Met 1 was not in operation from April to June-2001).

4.4.1 Surface mixed layer

Using the thermistor data from both Meteorological Stations the *SML* in the side arm and main basin was calculated for the period January-2000 to April-2000 coinciding with high solar insolation. Using the thermistor data, the *SML* depth was defined as the depth where the ΔT between adjacent thermistors was greater than 0.1 °C. The data plotted in Fig. 4.9 show that the *SML* was maintained below the euphotic depth for most of this period whilst the aerator and surface mixers were in operation. The *SML* was less than the euphotic depth for short periods ranging from 1 to 10 days. The longest period was 10 days, when excessive insolation occurred and calm conditions persisted. The data taken at both locations demonstrates that the reservoir does have one-dimensional characteristics with the *SML* following a similar pattern. The discrepancy in the daily average *SML* depth data can be attributed to the different rates of cooling and heating at either site.

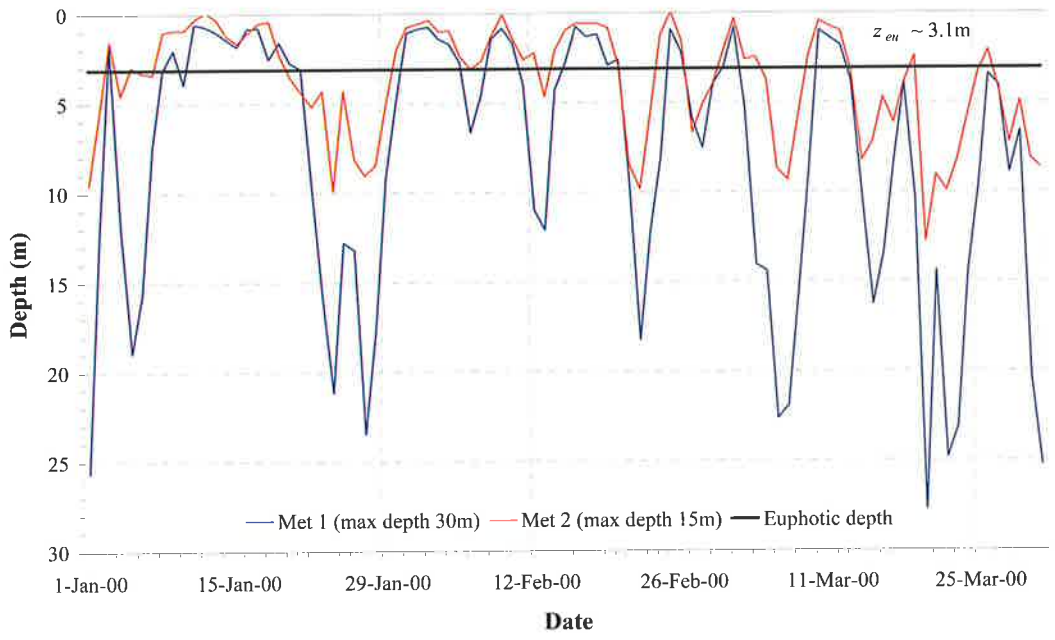

Figure 4.9 Daily average *SML* depth at Met 1 and 2. The average euphotic depth for this period is ~ 3.1 m.

Maintaining the *SML* below the euphotic depth is desirable thus limiting the light climate experienced by buoyant cyanobacterial species, thereby reducing their rate of photosynthesis and subsequent growth. The thermistor data gives good insight into the

operational capabilities of the aerators and surface mixers. Well-mixed conditions are generally maintained throughout the summer periods, with severe stratification restricted to very short periods when excessive insolation and calm conditions persist.

The growth of *Anabaena circinalis* is light limited when the ratio of the *SML* depth to the euphotic depth (z_{mix}/z_{eu}) is greater than 3 (Sherman *et al.*, 1998), which effectively causes the *Anabaena circinalis* cells to be removed from the light environment. The ratio z_{mix}/z_{eu} and average daily air temperature from September-1999 to September-2000 are plotted in Fig. 4.10. The growth of *Anabaena circinalis* occurred during January-2000, corresponding to stable conditions, high ambient temperature and $z_{mix}/z_{eu} << 3$ for an extended period (~12 days).

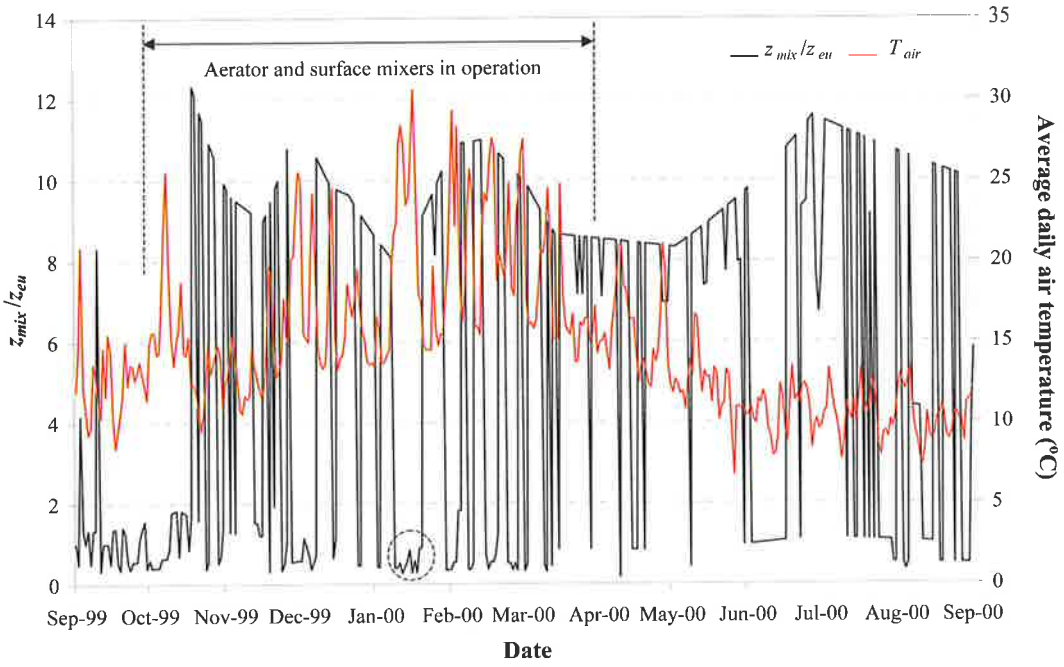

Figure 4.10 z_{mix}/z_{eu} and daily air temperature from September-1999 to September-2000. During January-2000 (indicated with a dashed circle) the growth of *Anabaena circinalis* occurred.

4.4.2 Mixing, light penetration and cyanobacterial growth

The light harvesting potential of phytoplankton and cyanobacteria is determined by their photo-physiology and the hydrodynamics and optical properties of the water-body. Typically the bloom-forming species such as *Anabaena* spp and *Microcystis aeruginosa* are confined to water bodies where the euphotic depth is 0.5-3.5 times the mixed depth (Reynolds and Walsby, 1975).

The light dose phytoplankton would receive whilst travelling through a water column with a *SML* depth z_{mix} can be calculated and growth rate inferred from growth irradiance curves, a model is presented to demonstrate the effect. For the model a mean daily solar radiation of 335 W m^{-2}, which is 58 mol photons m^{-2} d^{-1} of *PAR* (400-700 nm) is used, which is representative of mid-summer irradiance at this latitude.

The instantaneous solar irradiance at the water surface (I_0) can be expressed as a function of the maximum irradiance at solar noon (I_{max}) and the day length (DL):

$$I_0 = I_{\max} Sin(\pi / DL) \tag{4.2}$$

The sum of I_0 calculated at ten-minute increments for a day length of 15 hours and I_{max} of 1750 µmol m^{-2} s^{-1} gives a daily average *PAR* of 57.55 mol m^{-2} d^{-1}.

The amount of light that is reflected from the water surface is dependent upon the solar elevation, which is a function of the day of the year, the time of day and the geographical latitude (Kirk, 1994; Walsby, 1997). The equations to determine the reflection and sub-surface irradiance are given in Walsby (1997). Further corrections for reflectance can be made to account for wind roughening of the water surface (Walsby, 1997), however, the smooth water reflectance value was considered satisfactory for this model of light dose in different Z_{eu}/Z_{mix} conditions. Having accounted for reflection from the water surface the average sub-surface daily light dose for January was 47.8 mol m^{-2} day^{-1}.

The daily light dose an alga would experience is also determined by the mixing characteristics of the water body and can be calculated using the equation of Riley (1957):

$$I_{avg} = I_U \frac{\left(1 - e^{(-k_d z_{mix})}\right)}{(k_d z_{mix})} \tag{4.3}$$

where I_U is the sub-surface irradiance, k_d the attenuation coefficient.

The mean light dose experienced by an alga circulating within the euphotic zone would be 10.28 mol m^{-2} day^{-1}. The daily light dose exposure under different physical conditions of light penetration and mixed depth is given in Table 4.3. This can be used in conjunction with the light-dependent growth estimates from Reynolds (1997a) redrawn as Fig. 4.11.

Table 4.3 Modelled mean daily light dose (mol m^{-2} day^{-1}) experienced by phytoplankton circulating through various mixed depths in water-bodies with different euphotic depth and a sub-surface light intensity of 47.8 mol m^{-2} day^{-1}.

Mixed depth (m)	**Euphotic depth (m)**			
	1	**2**	**3**	**4**
1	10.28	18.68	24.43	28.39
2	5.19	10.28	14.85	18.68
3	3.46	6.91	10.28	13.40
4	2.60	5.19	7.77	10.28
5	2.08	4.15	6.23	8.28
6	1.73	3.46	5.19	6.91
7	1.48	2.97	4.45	5.93
8	1.30	2.60	3.89	5.19
9	1.15	2.31	3.46	4.61
10	1.04	2.08	3.11	4.15

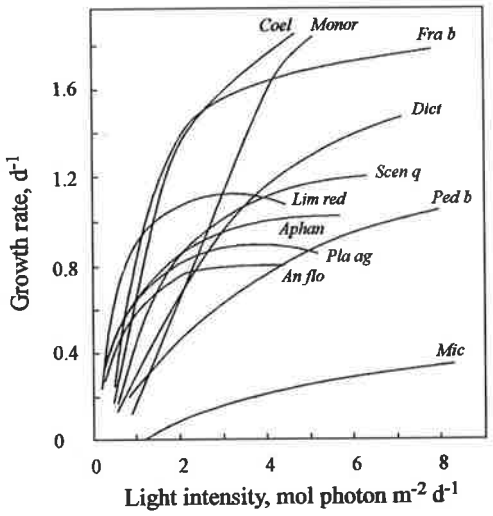

Figure 4.11 Light dependence of growth rate at 20°C, as a function of intensity, for a selection of phytoplankton (*An flo* = *Anabaena flos-aquae*, *Aphan* = *Aphanizomenon flos-aquae*, *Coel* = *Coelastrum microporum*, *Dict* = *Dictyoshaerium pulchellum*, *Fra b* = *Fragilaria bidens*, *Lim red* = *Limnothrix redethrix*, *Mic* = *Microcystis aeruginosa*, *Monor* = *Monoraphidium minutum*, *Ped b* = *Pediastrum boryanum*, *Pla ag* = *Planktothrix agardhii*, *Scen q* = *Scenedesmus quadricauda*). Taken from Reynolds (1997a).

During mid-January-2000, the growth of *Anabaena circinalis* occurred in Myponga Reservoir (Fig. 4.10). To illustrate the different growth rates of *Anabaena circinalis* in the side arm and main basin during this period, the mean daily light dose was calculated using Eq. 4.3 and coupled with growth rate light dependence data for *Anabaena circinalis*, taken from Brookes *et al.* (1999a), to determine the daily growth rate *r'*. The initial conditions for the modelled growth were k_d = 1.56 and I_u = 47.8 mol m^{-2} day^{-1}. The z_{mix} data for either location was calculated from the respective meteorological station thermistor data recorded between 3-January-2000 and 10-January-2000 (Fig. 4.9). A starting population of 50 cells mL^{-1} of *Anabaena circinalis* in either location was assumed to be present on the 3-January-2000. The daily concentration of cells was calculated using Reynolds (1984):

$$N_t = N_{t-1}e^{r'} \tag{4.4}$$

where N is the concentration of cells (cells mL^{-1}), and t is the time-step (days).

The final concentration of *Anabaena circinalis* in either location on the 10-January-2000 was considerably different with a resulting population of 6095 cells mL^{-1} in the side arm and 2363 cells mL^{-1} in the main basin, shown in Table 4.4. The difference in concentration occurred due to the different light environment experienced by the plankton in each location, which was attributed to the different daily average z_{mix}/z_{eu} ratio and daily light dose at either location during the modelled period. From the 4-Jan-00 to the 7-Jan-00 the growth rate in the main basin was approximately 33 % less than that in the side arm.

Table 4.4 Modelled growth rate and concentration of *Anabaena circinalis* in the side arm and main basin at Myponga Reservoir.

Date	Side arm				Main basin			
	z_{mix}/z_{eu}	I_{avg}	r'	N	z_{mix}/z_{eu}	I_{avg}	r'	N
3-Jan-00	0.5	6.2	0.59	50	0.6	15.8	0.72	50
4-Jan-00	1.5	6.8	0.61	92	3.9	2.6	0.47	80
5-Jan-00	1.0	10.4	0.66	178	6.1	1.6	0.41	122
6-Jan-00	1.1	9.4	0.65	341	5.0	2.0	0.44	189
7-Jan-00	1.1	7.7	0.62	636	2.4	4.1	0.54	324
8-Jan-00	0.3	7.1	0.61	1174	1.0	9.7	0.65	623
9-Jan-00	0.3	34.1	0.82	2674	0.7	14.5	0.71	1264
10-Jan-00	0.3	34.1	0.82	6095	1.3	7.8	0.63	2363

The significant difference in the *Anabaena circinalis* concentrations shown in the modelled data at either location was not evident in the field data (described in section 4.7) as the hydrodynamic exchange between the side arm and main basin homogenise the population.

4.4.3 Wind

The frequency of wind direction, directional dependence of wind run and mean wind speed are shown in Fig. 4.12. The wind run is a product of mean wind speed and frequency for any given direction. The monitoring of wind forcing gives insight into the stability of stratification where internal waves are affected by wind direction, with the greatest effect occurring on the major axes of the reservoir where horizontal motions significantly affect stratification.

The mean wind speed measured at Met 1 was strongest (up to 8 m s^{-1}) for winds blowing in a north-westerly direction. The highest recorded mean wind speeds (~4 m s^{-1}) at Met 2 also blow in a north-westerly direction. The mean wind velocity blowing in any other direction at both stations was usually 3 to 4 m s^{-1}. The predominating wind direction and largest wind run at either met station was in a south to south-easterly direction. The dominant wind induced mixing upon the main basin was along its longest fetch, which is fortuitous as this imparts the most mixing energy into the water column. The dominant wind mixing in the side arm was across the fetch.

The data shows that the wind at Myponga Reservoir is a significant factor pertaining to the stability of the water column. The stress experienced by the water surface is significant when the wind velocity is greater than 4 m s^{-1} where the energy imparted by the wind contributes to the breakdown of stratification and the subsequent deepening of the thermocline by production of turbulent kinetic energy into the *SML* (Reynolds, 1984). With an understanding of the seasonal wind activity at Myponga Reservoir the operation of the aerator and surface mixers could be reduced by capitalising upon the natural wind mixing phenomena.

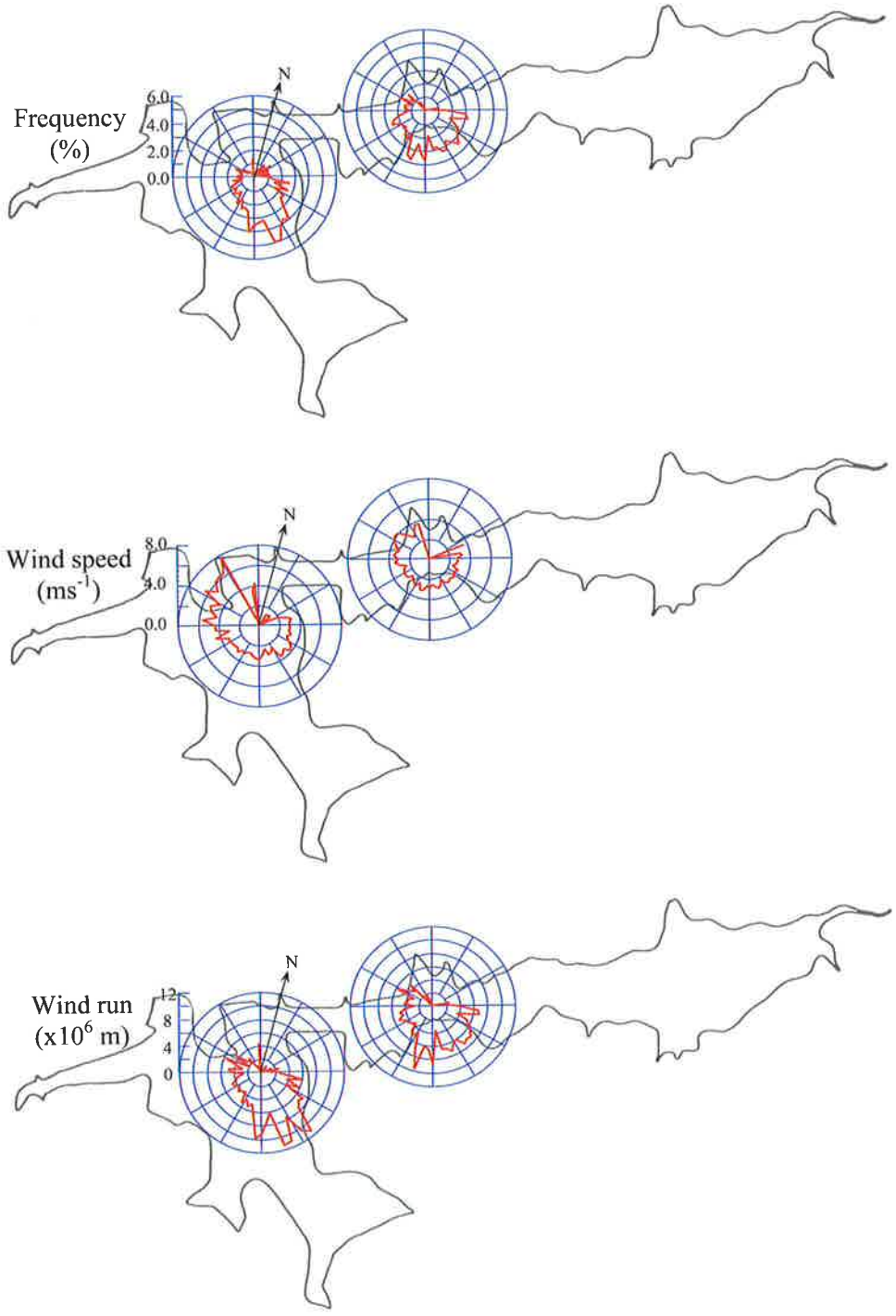

Figure 4.12 Directional dependence of wind speed, wind frequency and wind run at Myponga Reservoir from September-1999 to February-2002. Data shows the direction to which the wind was blowing and the centre of the concentric cycles is the location of the meteorological stations.

4.5 HEAT BUDGET

The integrity of the field data was checked by undertaking a heat budget from 1-September-1999 to the 1-September-2000, coinciding with the majority of the numerical modelling investigations presented in Chapters 5 and 7. To calculate the heat budget for Myponga Reservoir, the daily change in storage heat content was determined. This was compared with the daily energy exchange from the sum of the heat content of the inflow, outflow, rain and the heat fluxes across the water surface.

Theoretically the change in daily heat content should be equal to the sum of the daily energy exchange. The calculations do not account for heat flux through the sediment surface that is seasonally significant in temperate zones. Sediments of lakes and reservoirs absorb significant amounts of heat during warmer months and radiate heat during cooler months. Heat flux across the sediment is dynamic, occurring in both directions and can occur on time scales as short as a day. Little data exist to demonstrate this phenomenon (Wetzel, 2001). Based on data presented in Wetzel (2001) heat flux through the sediment attributes ~8 % in deep lakes (average depth 12.1 m) and ~38% in shallow lakes (mean depth 1.7 m). As the heat budget was taken over a period of one year, the sediment heat flux was assumed to average out over the four seasons and was not included in calculations.

4.5.1 Heat budget calculations and bulk aerodynamic formulas

Using the bathymetric map of Myponga Reservoir where the water body was divided up into layers with a thickness of 3 m, the daily heat content of the storage was evaluated. The volume in each layer was calculated, and using the thermistor chain data the mean temperature for each layer was known. The daily heat content for each layer was estimated (Eq. 4.5) using the thermistor data taken at 0600 to minimise the effects of surface heating and cooling.

$$H_n = \rho_n C_{p_n} V_n \tag{4.5}$$

where n is the layer number, ρ is the density (kg m^{-3})and C_p is the heat capacity (J kg^{-1} $^oC^{-1}$) both as a function of the mean temperature for layer n, and V is the

volume (m^3) of layer n. Eq. 4.5 was also used to calculate the heat content of the rainfall input, inflow and outflow. To calculate the latent and sensible heat fluxes the following bulk aerodynamic equations (Fischer *et al.*, 1979; MacIntyre *et al.*, 2002) were used:

$$E = \rho_A L_V C_E U_{10}(T_S - T) \tag{4.6}$$

$$H = \rho_A C_{p_A} C_H U_{10}(Q_S - Q) \tag{4.7}$$

where E is the latent heat flux (J), H is the sensible heat flux (J), ρ_A is the density of the air (kg m^{-3}) at the air-water interface, L_V is the latent heat of vaporisation (J kg^{-1}), U_{10} is the wind speed at 10 m above the water surface (m s^{-1}), T_S is the temperature at the water surface (°C), T the air temperature (°C), C_{pA} is the specific heat of air (J kg^{-1} $°C^{-1}$), C_E is the latent heat transfer coefficient, C_H is the sensible heat transfer coefficient, Q_S is the specific humidity at saturation pressure at T_S (kg water moisture/kg air-water moisture), and Q is the specific humidity of the air. As the heat budget was calculated with measured parameters taken at 0600 on each day, the thermal inertia of the water was disregarded, therefore assuming the atmospheric stability was constant, and constant values for C_E and C_S were used, therefore $C_E \sim C_S = 0.00145$ (Hicks, 1972).

The values for net longwave (H_{LW}) and shortwave radiation (H_{SW}) were taken from the measurements taken at Met 1. To calculate the heat budget the following energy balance was used:

$$\Delta H = H_{SW} + H_{LW} + H + E + H_{Rain} + H_{Inflow} - H_{Outflow} \tag{4.8}$$

The results for the monthly heat budget calculations confirm the integrity of the field data where the measured heat input across the reservoir surface is accounted for in the closure of Eq. 4.8 (Table 4.5). The reduced net surface heat flux that occurred from January to March-2000 coincided with increased mean wind velocities that resulted in

increased evaporation. The discrepancies in the data represent an error either in the measured radiation data or the water budget or most likely a combination of both. The largest error is -0.60×10^{13} J, which is equivalent to 2.8 % of the change in monthly heat content. The large amount of heat associated with inflows and outflows makes heat budget calculations relatively sensitive to inflow and outflow temperatures. The inflow temperature is measured at ~0.5 m below the surface in Myponga River at a location ~2 km upstream of the side arm, which introduces some error into the heat budget. Also, the outflow is located adjacent to the aerator and the temperature of the outflow would not be representative of the mean temperature at the same depth in the reservoir. The limited inflow and outflow temperature data will limit the accuracy of the heat budget calculations.

Table 4.5 Myponga Reservoir heat budget calculations. Heat contents are instantaneous value on the day. Fluxes are cumulative during the preceding month.

Date	**Heat content ($x10^{13}$ J)**	**Net monthly ($x10^{13}$ J)**					
		ΔHeat content	**Surface heat flux**	**Inflow**	**Outflow**	Rainfall	**Discrepancy**
1-Sep-99	100.45						
1-Oct-99	121.12	20.68	20.06	4.65	4.60	0.71	-0.14
1-Nov-99	142.44	21.32	24.08	2.49	5.22	0.51	-0.55
1-Dec-99	152.55	10.11	14.29	0.84	5.10	0.28	-0.19
1-Jan-00	142.24	-10.31	-2.72	0.20	8.04	0.46	-0.22
1-Feb-00	130.93	-11.31	-0.57	0.05	10.78	0.13	-0.14
1-Mar-00	132.40	1.48	8.35	1.76	9.94	1.27	0.03
1-Apr-00	108.50	-23.91	-17.22	0.37	7.26	0.42	-0.21
1-May-00	87.06	-21.44	-18.32	1.23	3.90	0.16	-0.60
1-Jun-00	73.32	-13.74	-17.95	5.49	1.89	0.54	0.07
1-Jul-00	73.96	0.64	-7.54	8.88	1.35	0.65	0.004
1-Aug-00	95.14	21.18	3.36	19.25	1.76	0.23	0.11
1-Sep-00	117.24	22.10	9.93	13.51	1.56	0.41	-0.20

The heat content of the reservoir is a function of reservoir depth where a discrepancy in depth data of ±0.03 m could contribute errors of the same magnitude as the

discrepancies in the heat budget. The radiometers used to measure shortwave and longwave radiation data had a calibration accuracy of 3 %. The inherent accumulated instrumentation errors over a period of a month were also of the same magnitude of the discrepancies in the heat budget. In conclusion, the heat budget is accurate when compared with the limitations in measured data. There are no significant discrepancies in the results and the integrity of the data set was deemed to be satisfactory.

4.6 CHEMICAL ANALYSIS

Nutrient loads are important to reservoir management from the perspective of eutrophication and associated phytoplankton problems. An intensive analysis of the nutrient load was undertaken by Linden *et al.* (2003), which concluded that the nutrient loading at Myponga Reservoir originated externally with the majority of nutrients being supplied via Myponga River. The nutrient loading for Myponga Reservoir is shown in Fig. 4.13.

Annual retention of nutrients in 1999 and 2000 was estimated from the annual catchment load and the annual load lost to outflow, Table 4.6. Significant differences in the proportion retained are observed in these years of differing hydrology (Linden *et al.*, 2003). The nutrient data was used to provide input files for the numerical modelling of phytoplankton growth, presented in Chapters 5 and 8.

Table 4.6 Annual nutrient retention of Myponga Reservoir (Linden *et al.*, 2003).

Loadings (kg)	Year	TP	FRP	NH_4	NO_x	TKN
Annual Catchment Load	1999	2518	1283	546	1351	11516
	2000	5485	2307	1100	1192	28662
Annual Load lost	1999	466	182	193	714	7805
	2000	608	306	240	924	6923
Annual load Retained	1999	2052	1102	353	637	3712
	2000	4877	2001	861	268	21739
Annual Load Retained (%)	1999	81.5	85.8	64.7	47.1	32.2
	2000	88.9	86.7	78.2	22.5	75.8

Based on the nutrient concentrations present in Myponga Reservoir during 1999 and 2000 the system is categorised as eutrophic, where the annual mean TP and TN concentrations exceed 16 $\mu g\ L^{-1}$ and 393 $\mu g\ L^{-1}$ respectively (Wetzel, 2001). Dissolved oxygen levels have been maintained above 4 $mg\ L^{-1}$ since the aerator was installed in 1994 (Brookes *et al.*, 2000). As a consequence of this, the release of iron and manganese from the sediment has been successfully inhibited. Interrogating the field data does not give insight into the impact of the surface mixers upon dissolved oxygen concentration in the water column, as the aerator could not be switched off. Consequently, numerical modelling was undertaken to investigate this aspect (Chapter 8).

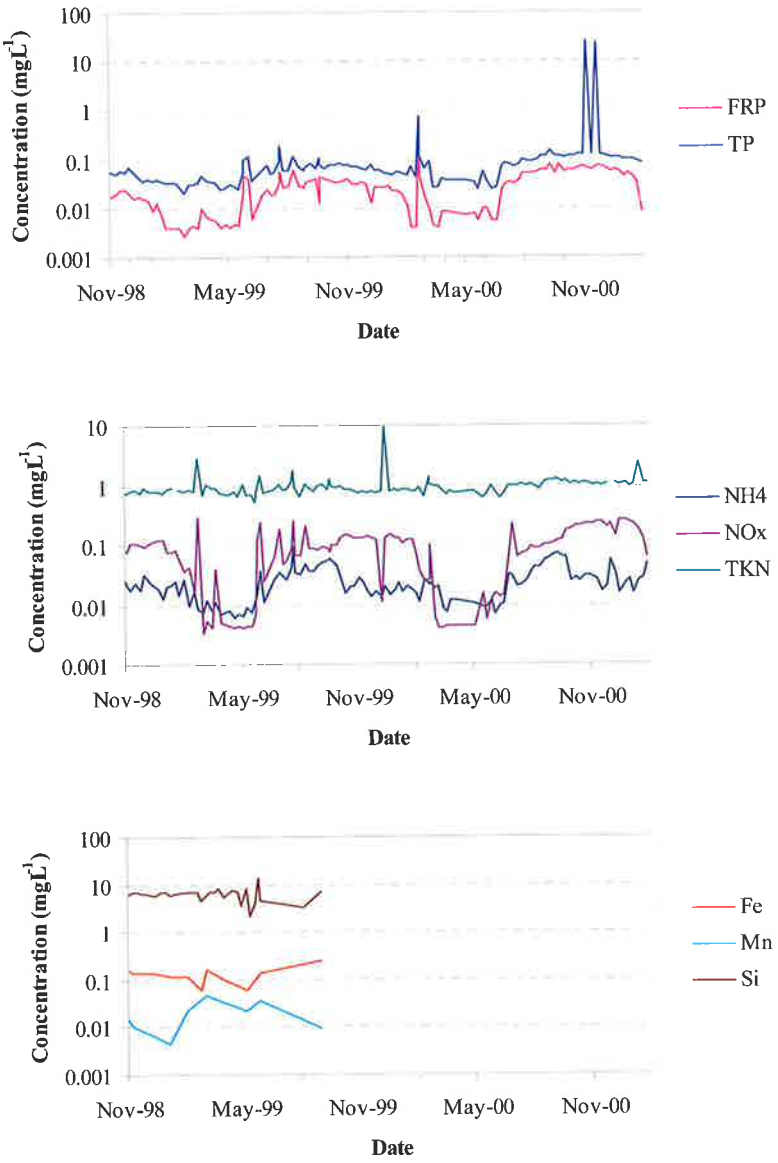

Figure 4.13 Nutrient loading for Myponga Reservoir from November-1998 to February-2001.

4.7 PHYTOPLANKTON COMPOSITION

The phytoplankton assembly at Myponga Reservoir was intensively monitored from November-1998 to April-2001. Integrated phytoplankton samples from 0 to 5 m were regularly taken (daily, weekly or monthly, depending on the season) for identification and enumeration; the phytoplankton sampling locations are shown in Fig. 3.3. Species-specific cell counts (cells mL^{-1}) were converted into Chl *a* concentrations (μg Chl *a* L^{-1}) using values from Reynolds (1984). The total Chl *a* concentration at

five sampling locations for this period is presented in Fig. 4.15. The seasonal spatial variation of Chl *a* is minimal with similar patterns and concentrations being observed at all five locations throughout each year. The bathymetry of Myponga Reservoir suggests that the phytoplankton assembly would be heterogeneous, but the data shows the growth of individual species occurs at similar time scales and magnitudes within the reservoir at all locations. The Chl *a* data strengthens the argument that horizontal mixing occurs on very short time-scales in Myponga Reservoir, resulting in a homogenous assembly.

The phytoplankton assemblage in Myponga Reservoir is presented by taxonomic functional groups using biovolume analysis. Biovolume is calculated for a single cell from each detected species by measuring the lineal dimensions and accounting for the characteristic geometrical shape (Hillebrand *et al.*, 1999). The total biovolumes for each functional group was calculated from the sum of the specific cell concentrations multiplied by the corresponding single cell volume. The presentation of the phytoplankton assemblage as functional group biovolumes allows simplified analysis of the phytoplankton succession, described in section 4.7.1 and presented in Fig. 4.16.

4.7.1 Myponga Reservoir phytoplankton succession and dominance

Examination of the observed phytoplankton succession at Myponga Reservoir is compared to an established paradigm that is based on Lewis (1979) and Ganf (1980), shown in Fig. 4.14. The theory of the succession paradigm is based on the physical and chemical environment experienced by the phytoplankton assembly. The dominant phytoplankton species in any assembly will have favourable morphological, physiological and behaviour characteristics that can maximise growth under the prevailing physical and chemical environment.

Green algae detected at Myponga Reservoir (chlorophytes – *Ankistrodesmus*, *Dictyosphaerium*, *Scenedesmus*, and *Oocystis*) have relatively high growth rates and are physically small (refer Chapter 5), requiring higher light intensities for survival but can cope with variable light environments. They are non-motile, thus require mixed conditions allowing growth rates to exceed sedimentation loss. Green algae do

not pose water quality hazards; however high biomass creates filtration issues, e.g. filter clogging.

The Cyanobacteria (cyanophytes – *Anabaena circinalis*, *Anabaena* (straight) spp., and *Aphanocapsa*) dominate during stratified conditions where they capitalise on their ability to regulate buoyancy allowing them to access light and nutrient as required to optimise growth. The physical characteristics at Myponga Reservoir do not favour the growth of cyanobacteria and only very short periods exist when the conditions are favourable for cyanobacterial growth, discussed in section 4.7.2.

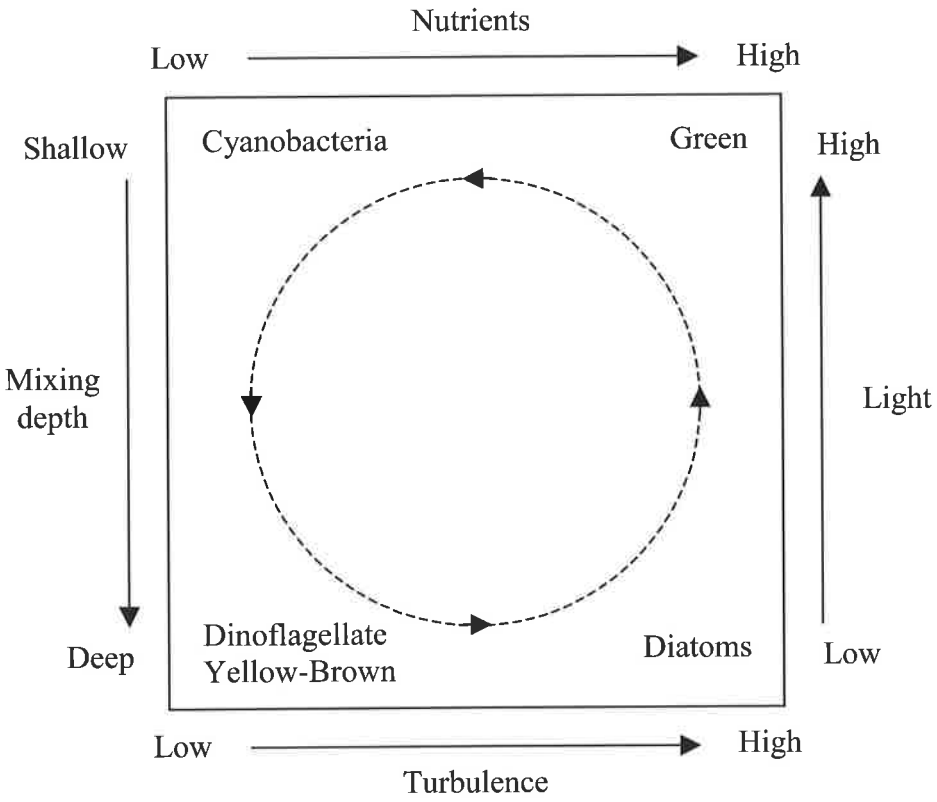

Figure 4.14 Phytoplankton succession hypothesis

Dinoflagellates and yellow-brown algae (Cryptophytes – *Chroomonas*, *Cryptomonas*, and *Peridinium*) have flagella, which provides motility and subsequently can tolerate mixed conditions, enabling them to access growth resources as required. The final dominant group detected are diatoms (Bacillariophytes – *Cyclotella*, and *Nitzschia*) that are composed of amorphous, opaline silica (Carter-Lund and Lund, 1995) and are

non-motile. Consequently the diatoms are highly susceptible to sedimentation losses, and therefore persist during extended periods of strongly mixed conditions.

The phytoplankton assemblage during the monitored period at Myponga is dominated by diatoms, followed by yellow-brown and green algae (Fig. 4.16). With the aid of Fig. 4.14 coupled with the phytoplankton data, the physical conditions at Myponga Reservoir can be hypothesised to be well-mixed with poor light conditions. The phytoplankton species biovolume data (Fig. 4.16) shows minimal spatial variation of phytoplankton biomass, alluding to a well-mixed environment; this is also evident from the species-specific cell counts shown in Appendix B, which are relatively constant at the sampling locations.

The relative standard deviation for the simultaneous total Chl *a* concentrations recorded at sampling sites 1, 4, 5, 6 and 7 between November-1998 to April-2001 ranged between 0.6 and 0.02 with a mean of 0.2. The comparatively low mean relative standard deviation supports the conclusion that the phytoplankton assembly is reasonably homogeneous due to the mixed state of Myponga Reservoir. Over the three years significant phytoplankton growth occurred during the summer with anomalous growth occurring November-2000, which was attributed to unseasonal meteorological conditions in Myponga Reservoir. During November-2000 the net heat flux was exceptionally high with a mean monthly value of 162 W m^{-2} and a low mean monthly wind speed of ~3 m s^{-1}.

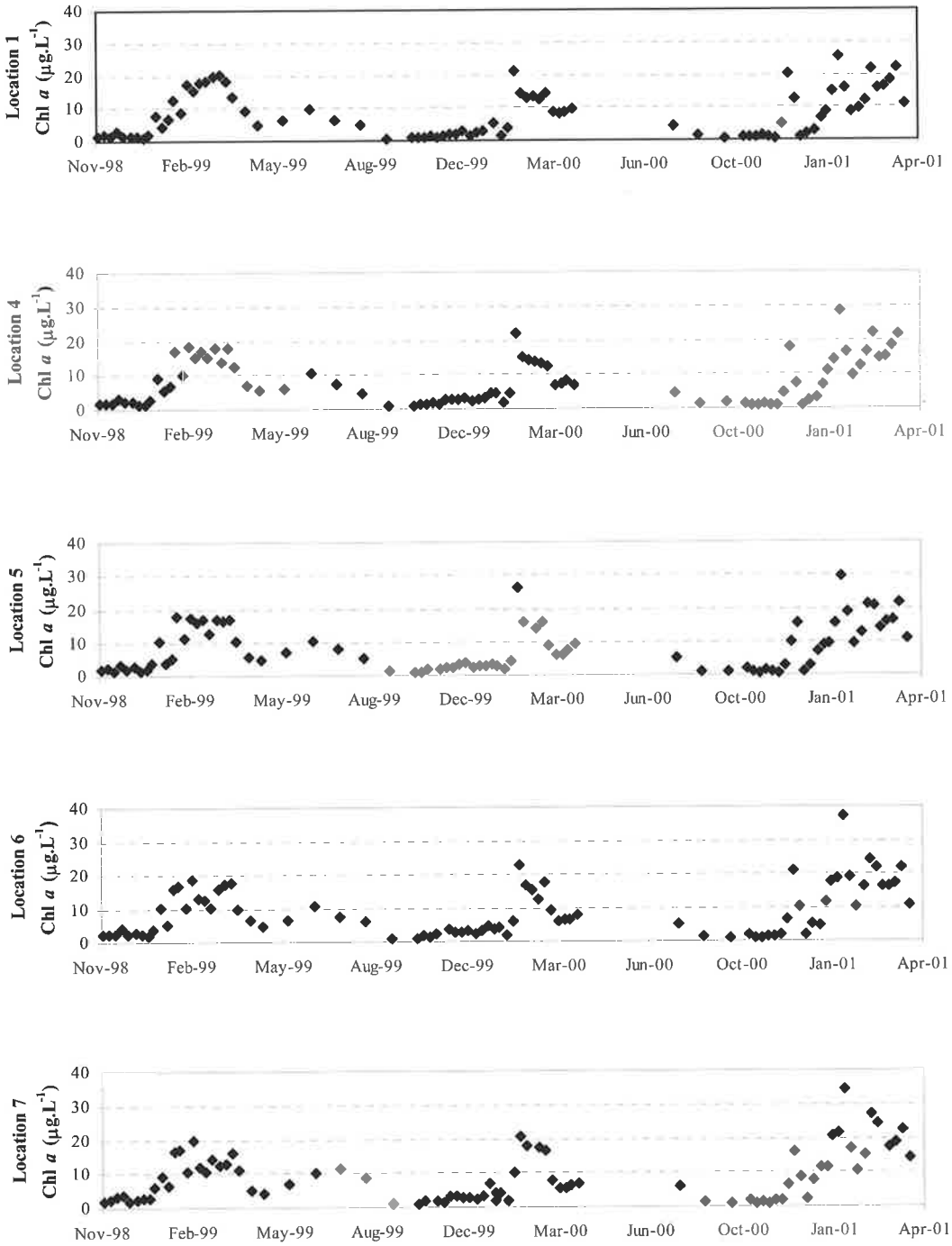

Figure 4.15 Total Chl *a* concentrations at 5 sampling locations at Myponga Reservoir.

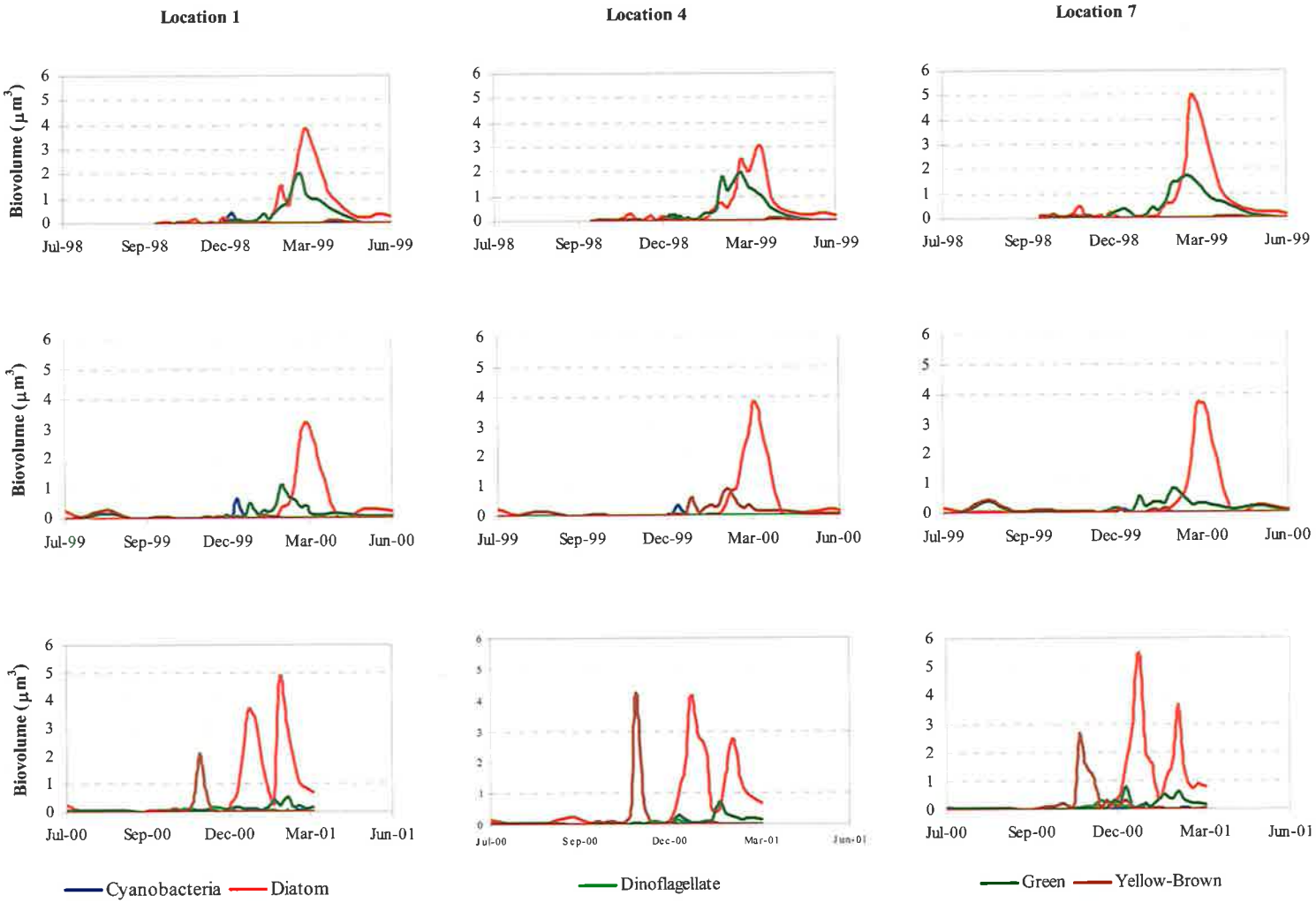

Figure 4.16 Comparison of species biovolumes at 3 separate sampling locations

4.7.2 Cyanobacteria growth

The growth of cyanobacteria (*Anabaena circinalis*) at Myponga Reservoir occurs only during periods when permanent stratification can occur. Examination of Fig. 4.16 reveals that the growth of *Anabaena circinalis* is restricted to short periods during late spring and summer. During January-2000, when high insolation occurred and the surface mixers and aerator were operating continuously, the reservoir was permanently stratified for a period of 18 days (Fig. 4.17).

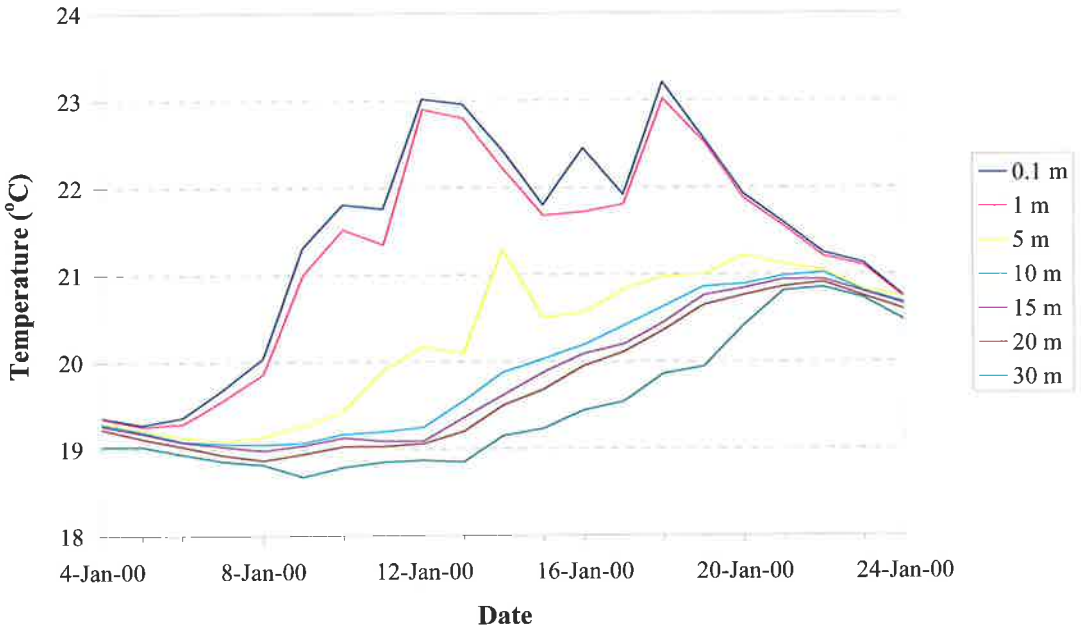

Figure 4.17 Temperature isotherms for Myponga Reservoir from 4-January-2000 to the 24-January-2000.

On 4-January-2000 the average *Anabaena circinalis* concentration was approximately 40 cells mL^{-1}, and the water body was well mixed at a temperature of ~19.4 °C. On 6-January-2000 a temperature differential of 0.3 °C (between 0 and 30 m) existed where the daily net radiation was ~260 W m^{-2}.

The concentration of *Anabaena circinalis* increased to ~ 4000 cells mL^{-1} by the 10-January-2000, which corresponded to a day of strong stratification where the *SML* was reduced to ~1.0 m with a ΔT = 3 °C and the daily net radiation peaked at

~325 W m^{-2}. Due to excessive insolation and wind velocities << 4 m s^{-1}, the mixing via the aerator and surface mixers was unable to prevent permanent stratification developing. During periods of high insolation, the rate of vertical transport of heat through the water column is higher than the rate that the aerator and surface mixers are able to mix the *SML* and deepen the depth of the thermocline. Subsequently the threat of excessive exponential growth *Anabaena circinalis* occurred and $CuSO_4$ dosing was invoked to inhibit further growth. During $CuSO_4$ dosing on 11-January-2000 the surface mixers and aerator were switched off.

The mean *Anabaena circinalis* concentration was reduced to approximately 40 cells mL^{-1} by 18-January-2000. The surface mixers and aerator were reactivated on 12-January-2000. The reduced impact of the surface mixers and aerator during this period can be visualised by considering the severity of stratification on 12-January-2000, notably the shallow *SML* (Fig. 4.17). Insolation decreased and by 24-January-2000 the reservoir returned to a well-mixed state, but overall heating had occurred and the temperature of the water column had increased to 20.7 °C from 19.3 °C.

4.7.3 Homogenous phytoplankton assemblage

The physical processes which could be contributing to the relative homogeneity in phytoplankton distribution are wind-driven circulation of surface water, the river flow intrusion, the intrusion from the destratification systems, differential cooling and the return flows associated with these phenomenon. During summer and autumn, when the phytoplankton biomass is maximal, the river does not flow and hence can be excluded as a mechanism contributing to homogeneity of the phytoplankton population for much of the year. Horizontal exchanges generated by differential cooling have been observed in other reservoirs with complex bathymetry and large horizontal temperature gradients, such as Wellington Reservoir (Monismith *et al.*, 1990) and Chaffey Reservoir (Wells and Sherman, 2001).

Differential cooling and heating was clearly evident at Myponga Reservoir, but was the reverse of that observed in Wellington Reservoir. In Myponga Reservoir the destratification systems aid in heat dissipation and the surface temperatures in the main basin are lower than in the side arm. On 10-January-2000 at 16:00 the

destratification units were turned off. The main basin of the reservoir had been cooling in the afternoon, from a surface maximum of 22.2 °C. The maximum surface temperature in the side arm was 25.3 °C. Differential heating is evident at Met 1 from 16:50 (Fig. 4.18). Using Eqs 3 and 5 of Monismith *et al.* (1990) the approximate "spin up time" for the convection to occur can be calculated.

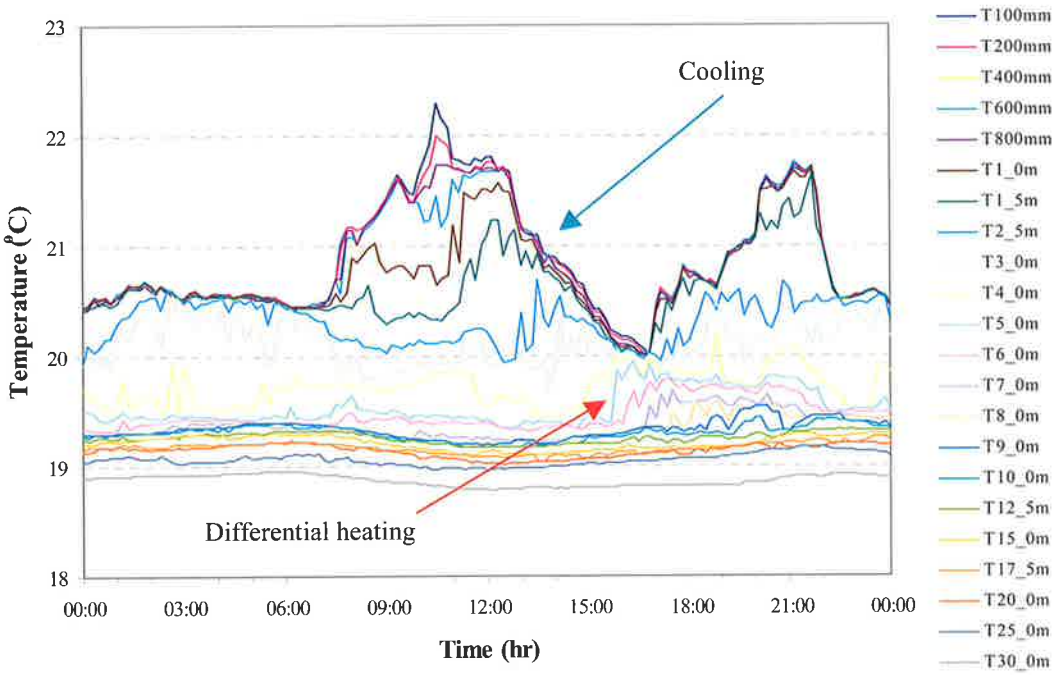

Figure 4.18 Differential heating event in Myponga Reservoir on the 10-January-2000.

The velocity scale for convective motions (m s^{-1}) can be approximated by $(\propto \Delta\theta g H)^{½}$ where $\propto$ is the thermal expansivity of water (1.4 x 10^{-4} deg^{-1}), $\Delta\theta$ is the longitudinal temperature gradient, g is the gravitational acceleration (9.8 m s^{-2}) and H is the depth length-scale for convective motions. For a temperature difference at 16:50 of 5 °C, and a depth of intrusion from the side arm of 2 m, the velocity of the convection is 0.12 m s^{-1}, which over a distance of 1300m (Met 2 to Met 1, Fig. 3.3) equates to a spin up time of 3.08 hours. This time-scale is very short relative to the time it takes for significant growth to be observed in the phytoplankton community (many hours to days). It is plausible that phytoplankton responses to site-specific habitat differences are not observed at Myponga Reservoir because large-scale lateral water movement overcomes heterogeneity between sites, which was observed in the low relative

standard deviation for the simultaneous total Chl *a* concentrations recorded at the individual sampling sites.

4.8 CONCLUSIONS

The extensive physical, chemical and biological data collected at Myponga Reservoir gave important insight into the limnological processes that occur within the water body. Myponga Reservoir is well-mixed from late April to late September without the use of artificial mixing. From October to May artificial mixing was in operation, maintaining relatively well-mixed conditions. During periods of high insolation, diurnal stratification occurs and permanent stratification is restricted to a couple of weeks when excessive insolation and stable conditions occur.

The *SML* at Myponga Reservoir is maintained below the euphotic depth for the majority of the summer period with the use of the aerator and surface mixers. Due to the coloured nature of the water body the euphotic depth is relatively shallow (~3.1 m), thus providing a restrictive light environment for phytoplankton growth. Due to substantial wind mixing, differential heating and cooling, horizontal mixing in Myponga Reservoir occurs on diurnal time-scales, which enables the water in the side arm and main basin to be well-mixed creating relatively homogeneous habitats for phytoplankton growth.

The maximum Chl *a* concentration detected is approximately 38 μg Chl *a* L^{-1}, Fig. 4.15, which supports the categorisation of Myponga Reservoir as a eutrophic system. There is a lag between nutrient delivery to the reservoir and utilisation of the resource for cyanobacteria growth, which requires the right combination of light, heat and nutrient that occurs rarely due to artificial mixing. The bulk of the nutrient load comes from Myponga River as the internal nutrient load was suppressed by artificial destratification (Brookes *et al.*, 1999b; Linden *et al.*, 2003).

The integrity of the field data meteorological monitoring instrumentation was validated by a heat budget. The discrepancies in the heat budget can be attributed to instrument error and limitations with heat content calculations. The shortfall with the data was that it did not give insight into the sole use of the surface mixers used to destratify the reservoir and control cyanobacterial growth. To adequately assess the

surface mixers numerical modelling was undertaken and presented in Chapters 5, 7 and 8. The field data was used for validation of intensive numerical modelling investigations. The extensive data collection gave essential insight into the limnological processes at Myponga Reservoir, which was required to determine the impact of the surface mixers upon the ecosystem.

5. MODELLING THE PHYTOPLANKTON ASSEMBLAGE IN MYPONGA RESERVOIR

5.1 INTRODUCTION

To fully assess the impact of the surface mixers and $CuSO_4$ dosing on the phytoplankton assemblage, and particularly *Anabaena circinalis*, in Myponga Reservoir, numerical modelling was employed. The need to use numerical modelling was motivated by the inherent difficulties of obtaining sufficient field data that provided insight into the operational capabilities of the surface mixers under replicated environmental conditions. The investigation of natural systems was problematic because significant phytoplankton growth events occur only during a particular combination of chemical, physical and biological conditions and it is difficult to obtain sufficient replicate data during these events.

The role of numerical modelling to assist the management of water bodies is well recognised with proven hydrodynamic models available (Hamilton, 1999). Hydrodynamic models incorporating aerators have greatly assisted the development of operational strategies and the optimisation of the aerator design (Patterson and Imberger, 1989). The effect of aerators on water quality has been modelled extensively (Imteaz and Asaeda, 2000; Patterson, 1991); however surface mixers of the type used at Myponga Reservoir had not previously been modelled.

The one-dimensional model PROTECH was used to simulate the phytoplankton assembly, which required significant alterations to the code to accommodate an algorithm for the surface mixers. PROTECH had never been applied to a water-body in the Southern Hemisphere and this work offered an opportunity to validate the model in a climate it had not been previously applied. This work provided an ideal platform to extend the capabilities of PROTECH and test the universality of the phytoplankton growth algorithms.

The main objective for using PROTECH was to examine phytoplankton response to the action of the surface mixers and use of algicides. To achieve this, additional subroutines were incorporated into PROTECH that were validated against field data

using regression analysis and the modelling efficiency (Jørgensen, 1995b; Rykiel, 1996). The incorporation of phytoplankton control strategies into PROTECH increases its application in dealing with risks associated with nuisance phytoplankton.

Special attention was paid to the simulated performance of the scum-forming cyanobacteria, whose functional group is represented in PROTECH by the character of *Anabaena circinalis*. The algicide dosing is undertaken to limit the growth of *Anabaena circinalis* thus reducing the risk of taste and odour problems from the associated production of geosmin. No artificial mixing is undertaken during algicide treatment so that the majority of the phytoplankton population floats into the surface water and is exposed to Cu^{++} ions. Artificial mixing at Myponga is achieved with the use of a multi-diffuser aerator and two surface mixers (described in Chapter 3).

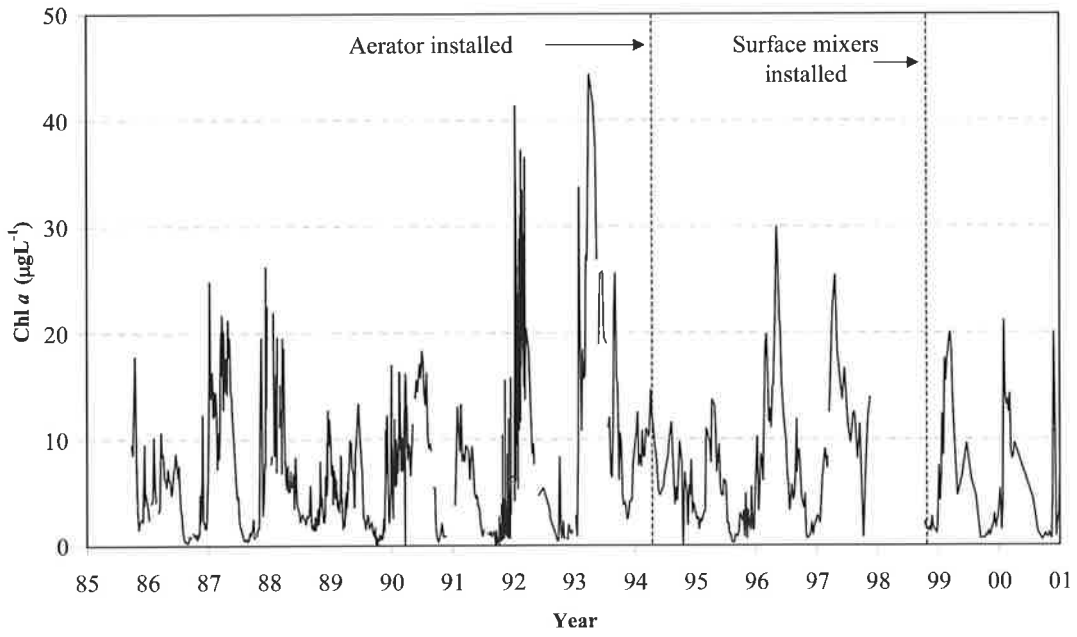

Figure 5.1 Total Chl *a* at Myponga Reservoir from 1985 – 2001, indicating installation of a bubble plume aerator.

To validate PROTECH against Myponga Reservoir field data, significant changes to the model code were required. Subroutines were added to simulate $CuSO_4$ dosing and artificial mixing via the surface mixers. The total Chl *a* concentration in Myponga Reservoir from 1987 to 2001 is shown in Fig. 5.1, which includes the installation periods of the aerator and surface mixers. It should be noted that Fig. 5.1 does not

give insight into the succession of phytoplankton and indicates only a measure of the total Chl *a*, which is attributed to phytoplankton biomass. The objective of this study was to determine the effect of the surface mixers and $CuSO_4$ dosing upon the phytoplankton succession and in particular how the growth of *Anabaena circinalis* is affected when transported through the surface mixers, and consequently the action of the aerator was not included in the PROTECH simulation. However, the aerator has a significant impact upon the phytoplankton assembly as it successfully controls the release of iron and manganese from the sediment and has adequate destratification abilities (Brookes *et al.*, 2000). The combined and individual use of the aerator and surface mixers, and their impact on the phytoplankton assembly is analysed in Chapter 8.

5.2 DESCRIPTION OF MODEL AND METHOD

The validation data used was collected from Myponga Reservoir from September-1999 to September-2000; see Chapter 4. The use of PROTECH was limited to the duration of my visit to the Centre for Ecology and Hydrology Windermere, UK, from September-2000 to December-2000.

PROTECH has been developed to simulate the *in-situ* dynamics of phytoplankton in lakes, reservoirs and rivers. The objective of the model is to simulate phytoplankton responses to environmental change. The model is designed around a series of regression equations used to describe the performance of common phytoplankton in controlled laboratory conditions of insolation and temperature in terms of phytoplankton cell morphology (Reynolds, 1989).

The potential individual growth rate for up to eight species is calculated against the temperature and daily insolation, with net population change being a function of nutrient availability, grazing, and changing light conditions taken into account. The basic state variable equation that determines the daily change in Chl *a* concentration for each phytoplankton species is,

$$\frac{\Delta X}{\Delta t} = (r' - S - G - D)X \qquad (5.1)$$

where r' is the growth rate (day^{-1}) defined as a proportional increase over 24 h, S is the loss due to settling out of the water column, G is the loss due to grazing of species with a maximal linear dimension < 50 μm (see Table 5.1) and D is the loss due to dilution due to the inflow and outflow of water within the water body (Elliott *et al.*, 2000a). The routine is repeated for each of up to eight species with daily iterations. Species-specific growth rate (r') is a function of cell morphology and the achievable net growth rate is:

$$r' = min\{r'_{(\theta,I)}, r'_P, r'_N, r'_{Si}\} \tag{5.2}$$

where $r'_{(\theta,I)}$ is the growth rate as a function of temperature and diurnal photo-period ($r'_{(\theta,I)}$ is further adjusted to include dark respiration), and r'_P, r'_N, and r'_{Si} are the growth rate as functions of phosphorus, nitrogen and silicon concentrations respectively (Elliott *et al.*, 2000a).

Thus, PROTECH is based on an assumption that all species grow to the best of their abilities at all times, but always strictly within the selective constraints of the environment (Reynolds, 1989). Moreover, as the intention has been to simulate rates of cell replication and of population increase in individual phytoplankton species, the development of the model avoided the precedent of other attempts to simulate phytoplankton dynamics founded on rates of chlorophyll-specific photosynthesis and nutrient-uptake kinetics (Jørgensen, 1995a; Reynolds *et al.*, 2001).

An initial profile for the water column (containing temperature, nutrient concentrations and inoculum sizes for phytoplankton species) is defined for day 1 (which in this study was 1-September-1999). Daily wind speed, cloud cover, river inflow (including nutrient concentrations) and outflow data are inputted to the model and insolation is adjusted according to the day of the year and latitude.

Simulated fluctuations in *SML* depth and stratification use physical rules based upon the Monin-Obukhov length calculations and Wedderburn number analysis (Imberger and Hamblin, 1982). The Monin-Obukhov length is defined as the height at which the

Wedderburn number equals 1. The overall or layer Richardson number (*Ri*) determines the stability of the flow such that for $Ri >> 1$ the flow is stable. Turner (1973) determined that when a large shear is applied across a density interface whereupon the gradient *Ri* falls below a critical value of approximately 0.25, Kelvin-Helmholtz waves will grow and become unstable producing turbulent mixing. A typical Richardson number is described as:

$$Ri = \frac{g(d\rho/dz)}{\Delta\rho(du/dz)^2} \tag{5.3}$$

where, g = acceleration of gravity, ρ = density, u = horizontal velocity, z = depth. The Richardson Number expresses the accumulated buoyant resistance as a function of the density difference between adjacent layers of water, relative to the dispersive energy available (Reynolds *et al.*, 2001).

The stability of the *SML* is influenced by the aspect ratio (downwind length, L, and thickness, h_m). Multiplying the Richardson number by the aspect ratio gives the Wedderburn Number, W (Reynolds *et al.*, 2001):

$$W = Ri(L/h_m) \tag{5.4}$$

A stable structure exists when $W \geq 1$. As the loss of heat increases, or the work of wind increases, $W < 1$, and the layer thickness will increase. Equilibrium is re-established when $W = 1$. The Wedderburn term is used to accommodate the Monin-Obukhov length. For each 24-hour time-step, the Monin-Obukhov equation is used to calculate the mixed layer thickness, h_b, as a function of heat flux and wind stirring. The mixed layer thickness is determined at the point where the buoyancy flux is balanced by the momentum flux caused by the dissipation of wind mixing according to Eq. 5.5 (Imberger and Hamblin, 1982):

$$h_b = \frac{2\sigma\rho_w(u*)^3}{g\gamma E*} \tag{5.5}$$

where, σ is the specific heat of water, ρ_w is the surface water density, u^* is the wind friction velocity, γ is the temperature dependent coefficient of expansion, and E^* is the shortwave radiation passing through the surface layer.

The starting water column profiles of temperature, nutrients and phytoplankton are changed at the start of each time-step as a result of *SML* changes. Prior to the phytoplankton being submitted to growth and grazing calculations, species-specific movement attributes are addressed. Distinction is made between non-motile and the swimming or buoyancy-regulating species (Reynolds *et al.*, 2001). The water column profiles of temperature, nutrients, and phytoplankton are updated at the start of each time-step and the mixed-layer adjustment is completed. The biological functions (Eqs 5.1 and 5.2) are then used to calculate the new biomass and dissolved nutrient concentrations remaining at the end of the time-step, assuming no further vertical movements.

5.3 ALTERATION TO THE CODE

Initial adjustments to PROTECH were made in respect of local features. Myponga Reservoir bathymetric data was used to generate surface area and volume data for each 0.1 m PROTECH layer. The outflow depth was adjusted from a simple river over-spill to an abstraction point at depth (19.6 m from reservoir bottom). However, further changes were still necessary to complete the adaptation of PROTECH to adequately represent Myponga Reservoir.

5.3.1 Latitudinal and hemispherical adjustments

The net heat flux in PROTECH is calculated by determining the energy flux (*Esurf*; W m^{-2}) into the water body (based upon solar day-length and latitude) and the net heat loss (*Eloss*; W m^{-2}), which is calculated as a function of *Esurf*. In this investigation measured field values of *Esurf* and solar day-length (*h*) were used directly.

PROTECH does not have subroutines that calculate the heat losses in the water column due to radiation, conduction and evaporation, but uses a function that groups the losses to a single parameter (*Eloss*). *Eloss* is adjusted to allow for the rate of increased evaporation at the latitude of Myponga Reservoir during the highest anticipated air temperature (Lewis *et al.*, 2002b; Reynolds *et al.*, 2001). The simulated

and observed integrated surface temperature (0 to 5 m below surface) is shown in Fig. 5.2 for the modelled period. A linear regression was fitted to the data where an R^2 of 0.92 was obtained. The close match between simulated and observed results was further validated by the use of the modelling efficiency, where a value of $EF = 0.93$ was achieved. The results shown in Fig. 5.2 were deemed adequate and provided the basis to investigate the phytoplankton succession in Myponga Reservoir.

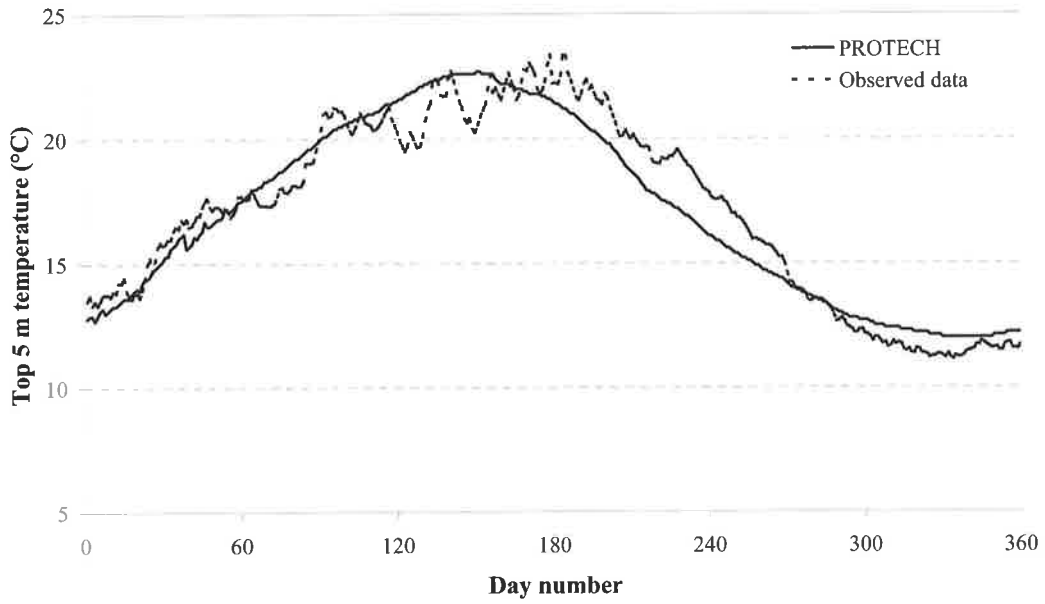

Figure 5.2 Temperature comparison with no artificial mixing in PROTECH.

5.3.2 Adapting the model life-forms for Myponga Reservoir

The eight most dominant phytoplankton genera found at Myponga Reservoir during the simulated period were *Scenedesmus*, *Cryptomonas, Anabaena circinalis, Pseudanabaena*, *Nitzschia*, *Chroomonas*, *Chlamydomonas* and *Monoraphidium*. The first three-phytoplankton types were included in the original PROTECH library and the remaining five required defining attributes. For this study, the properties of five new phytoplankton species were coded, having the properties of *Pseudanabaena*, *Nitzschia*, *Chroomonas*, *Chlamydomonas* and *Monoraphidium*. The morphological characteristics of these additional types (Table 5.1) were taken from Tikkanen and Willen (1992) and Reynolds (1984), with specific motility functions to describe observed behaviour (Lewis *et al.*, 2002b; Reynolds *et al.*, 2001). Although these

narrowly defined morphotypes would not be regarded as representing only the taxonomic species, their generic properties are those processed within PROTECH.

Table 5.1 The morphological and phylogenetic characteristics of the eight simulated phytoplankton species. An asterisk denotes the new species introduced to PROTECH. The last three columns signify simple logic statements (Elliott *et al.*, 2000b), where T = true and F = false.

Species	*C, S, R* strategist type	Surface Area (μm^{-2})	Volume (μm^{-3})	Maximum Dimension (μm)	Diatom	Grazed	Nitrogen Fixer
Pseudanabaena *	R	2538	2513	200	F	F	F
Nitzschia *	R	591	566	45	T	T	F
Chroomonas *	R	292	118	12	F	T	F
Scenedesmus	R	908	1000	80	F	T	F
Chlamydomonas *	C	112	60	5	F	T	F
Monoraphidium *	C	126	101	8	F	T	F
Cryptomonas	CS	1030	2710	21	F	T	F
Anabaena circinalis	CS	6200	29000	75	F	F	T

The input files used for the PROTECH simulation are provided in Appendix C.

5.3.3 Initial simulation without surface mixer or $CuSO_4$ dosing algorithms

PROTECH was run with the five new phytoplankton and three others from its data library (*Scenedesmus*, *Cryptomonas* and *Anabaena circinalis*), and total Chl *a* values produced from this simulation were compared to observed values as shown in Fig. 5.3. An *EF* value of 0.10 was calculated and when combined with visual inspection, showed that the simulated phytoplankton biomass during the summer was too high where the model over predicted the total Chl *a* by up to 100 %. To improve the simulated results, algorithms representing the $CuSO_4$ dosing and surface mixers were incorporated into the PROTECH code.

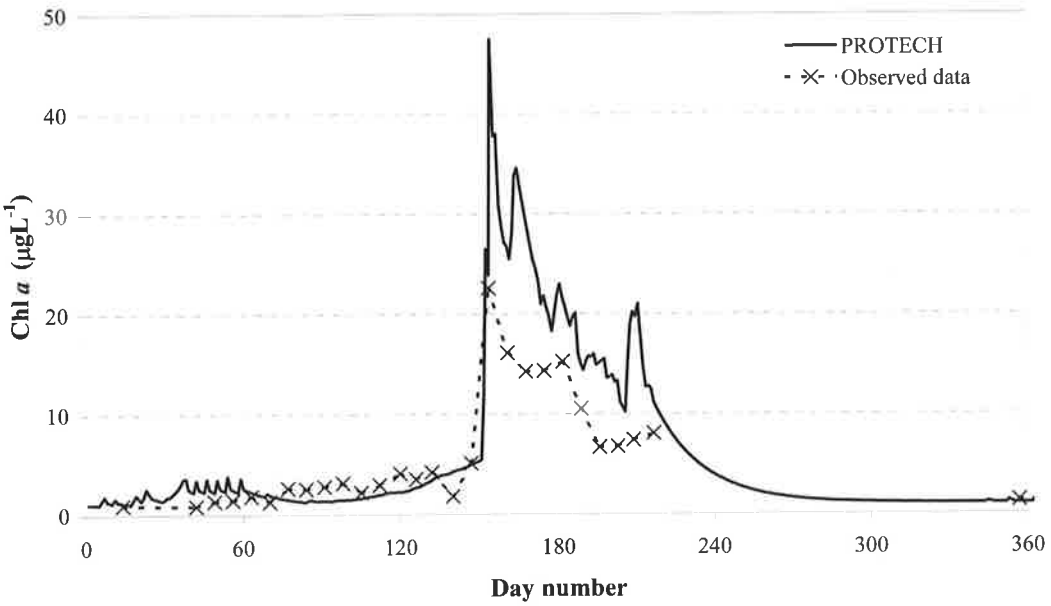

Figure 5.3 Total Chl *a* (µg Chl *a* L^{-1}) comparison with no $CuSO_4$ dosing and no artificial mixing in PROTECH.

5.3.4 Algicide dosing

The simulation of algicide dosing was achieved by adding an extra parameter (k_{CuSO_4}) to Eq. 5.1 to reduce the daily biomass, as shown in Eq. 5.6.

$$\frac{\Delta X}{\Delta t} = (r' - S - G - D)X.k_{CuSO_4} \tag{5.6}$$

As presented in Chapter 2, $CuSO_4$ dosing acts indiscriminately upon the phytoplankton assembly which is reflected in the simulation by reducing the phytoplankton biomass in the *SML* by a value of 90 % per day (Whitaker *et al.*, 1978) over a period of two days, inline with the dosing undertaken at Myponga Reservoir during the summer of 2000. Simulated and observed total Chl *a* values were compared again (Fig. 5.4) and there was an improvement in both the visual fit and *EF* value (0.24). The simulated $CuSO_4$ dosing reduced the maximum peak Chl *a* concentration by ~15 µg Chl *a* L^{-1}.

5.3.5 Surface Mixers

A new subroutine was incorporated into PROTECH to simulate the action of the surface mixers pumping water to the hypolimnion and the impact of this on phytoplankton growth. The depth to which the water was pumped was fixed at 14.2 m (the depth of the draft-tube exit) and with a flow rate of 7 $m^3 s^{-1}$, representing the combined flow generated by the two surface mixers.

Due to PROTECH operating on a 24-hour time step an additional daily outflow (Q_{smix}; $m^3 d^{-1}$) was incorporated, which represented the water removed by the surface mixers. The depth (n; m) to which Q_{smix} was abstracted from the surface was defined by:

$$\sum_{i=pdata}^{n} V(i) = Q_{smix} \tag{5.7}$$

where *pdata* is the top PROTECH layer and $V(i)$ is the volume in layer i.

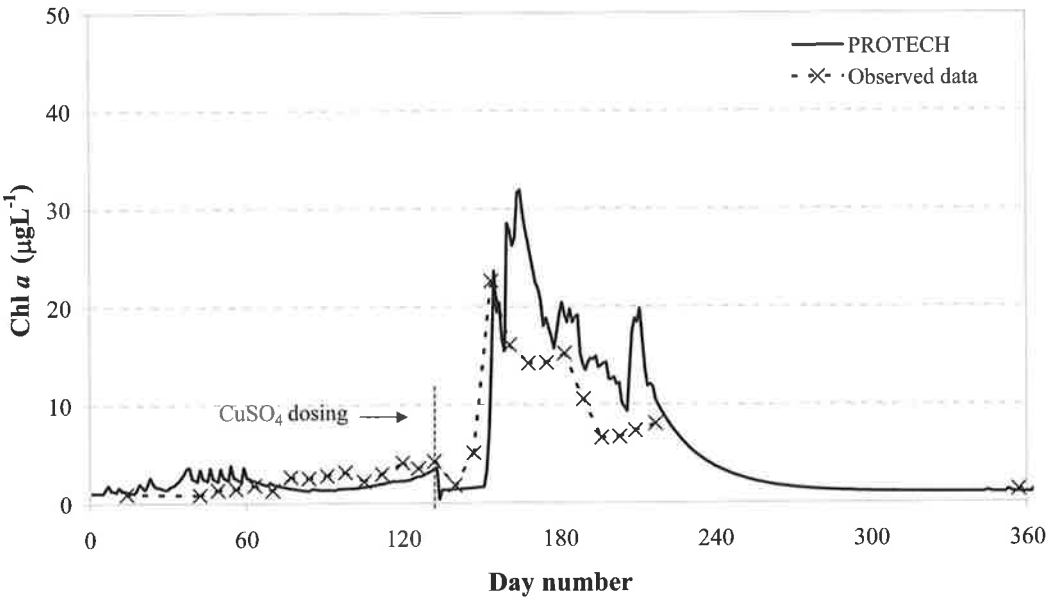

Figure 5.4 Total Chl *a* (µg Chl *a* L^{-1}) with simulated $CuSO_4$ dosing on PROTECH day 133 (11-January-2000), no simulated artificial mixing.

The calculation of the concentrations (C; µg Chl a L^{-1}) for each of the eight specific phytoplankton and nutrient in the water pumped through the surface mixers (Q_{smix}) was calculated by the following conservation equation:

$$C = \frac{\sum_{i=pdata}^{n} C(i)V(i)}{\sum_{i=pdata}^{n} V(i)} \tag{5.8}$$

The temperature (T; °C) of Q_{smix} was determined from the weighted mean of the individual layer water densities (ρ; kg m^{-3}):

$$T = f\left(\frac{\sum_{i=pdata}^{n} \rho(i)V(i)}{\sum_{i=pdata}^{n} V(i)}\right) \tag{5.9}$$

The composition calculations and abstraction of Q_{smix} occurred at the end of the iteration sequence within PROTECH. At the beginning of the next iteration, Q_{smix} is reintroduced to a PROTECH layer corresponding to a depth of 14 m from the surface, which mixes with the adjacent layers until a level of neutral buoyancy is obtained, using the relevant energy equations already incorporated in PROTECH that ensure a stable density structure exists at the end of each time step. The phytoplankton and nutrient concentration within each layer is adjusted accordingly. The surface mixers were operated between Day 31 and Day 213 (1-October-1999 and 31-March-2000) at Myponga Reservoir, and the algorithm was therefore used only during this period.

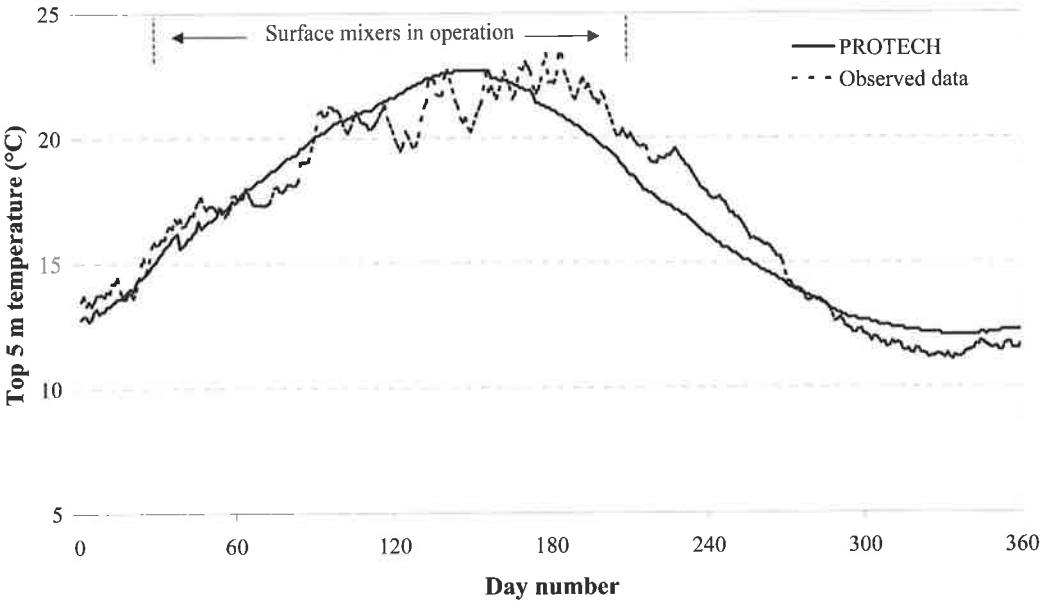

Figure 5.5 Temperature comparison with the addition of artificial mixing to PROTECH.

The simulation including the $CuSO_4$ dosing and surface mixer subroutines gave encouraging results when compared to the observed data. The temperature plot for the top 5 m of the water column was consistent with previous runs (Fig. 5.5; *EF*=0.92). However, the greatest improvement came from the correlation between observed and simulated total Chl *a* profiles, with surface mixer operation and $CuSO_4$ dosing, plotted in Fig. 5.6, where an *EF* value of 0.69 resulted. The high *EF* value corresponds to a reasonable goodness of fit between the simulated and observed data sets.

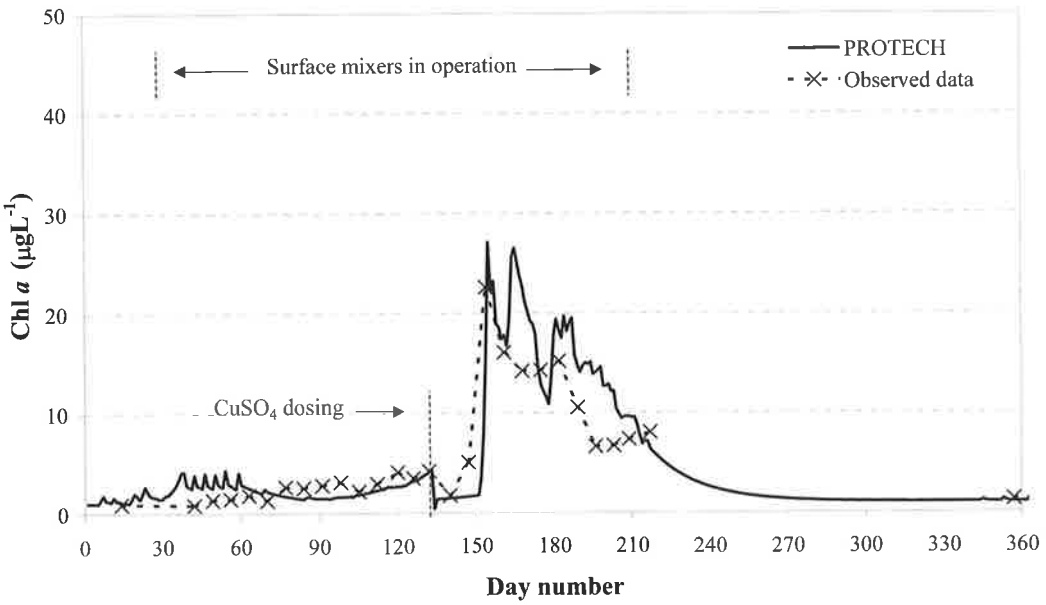

Figure 5.6 A comparison of observed and simulated total Chl *a* (µg Chl *a* L^{-1}), with simulated $CuSO_4$ dosing on PROTECH day 133 (11-January-2000) and simulated surface mixers between PROTECH days 31 and 214 (1-October-1999 to 1-April-2000), $EF = 0.69$.

5.4 Phytoplankton functional group classification

In order to highlight the ecological processes behind the successional changes simulated and observed, the eight PROTECH species were classified according to their functional typology (Fig. 5.7).

The adopted *CSR* (Competitors, Stress-tolerant, Ruderals) matrix (Reynolds, 1988; Reynolds, 1997b) is based on evidence that species-specific sensitivities to resources and energy availability are predicted by the morphology of the plankton and their characteristic features are summarised in Table 5.2.

Three functional types were identified in Myponga Reservoir. *C*-species denote invasive, ecological pioneers, which are small with high surface-to-volume ratios ($s/v > 0.5$ μm^{-1}) and which grow well at low temperatures (e.g. *Chlamydomonas* and *Monoraphidium*). *R*-species have the ability to saturate their growth-rate at lower insolation levels than other phytoplankton. They are tolerant of well-mixed-poorly-insolated environments (e.g. *Pseudanabaena*, *Nitzschia*, *Chroomonas* and

Scenedesmus). The third functional group, whose characteristics are intermediate between those of *C* and *S* species, includes *Anabaena circinalis* and *Cryptomonas*.

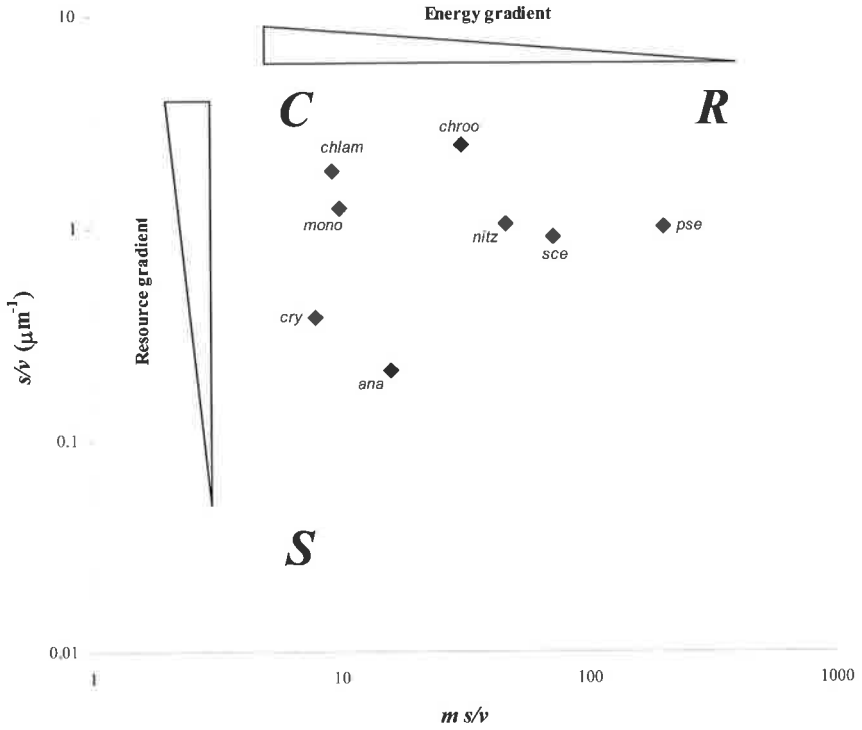

Figure 5.7 Strategic differentiation of primary life-history strategies (*CSR*) of 8 Myponga Reservoir phytoplankton species as a function of their morphology (*s* = surface area; *v* = volume; *m* = maximal linear dimension; values taken from cells, or where applicable, colonies). Resource (nutrients) and energy (light) gradients relevant to a specific morphological characteristic are superimposed upon the matrix (*ana* = *Anabaena circinalis*, *chlam* = *Chlamydomonas*, *chroo* = *Chroomonas*, *cry* = *Cryptomonas*, *mono* = *Monoraphidium*, *nitz* = *Nitzschia*, *sce* = *Scenedesmus*, and *pse* = *Pseudanabaena*). Modified from Elliott *et al.* (2000b).

Table 5.2 Morphometric and physiological characteristics of planktonic *C*, *R*, and *S* strategists. Reproduced with permission from Reynolds (1988).

Parameter	*C*	*R*	*S*
Unit Volume [μm^3]	5 – 5000	500 – 10E4	10E3 – 10E6
Surface area to volume ration s/v [μm^{-1}]	0.3 - 3.0	0.3 - 2.0	0.03 - 0.3
Maximal linear dimension M [μm]	3 – 80	10 - 300	30 - 500
Photosynthetic efficiency α [mmol C(mg Chl *a*) m^{-1}(mol photon)$^{-1}m^2$]	Up to 1.5	0.4 - 1.0	< 0.5
Projected area K_c [m^2 (mg Chl *a*)$^{-1}$]	< 0.012	> 0.011	< 0.013
Maximum growth rate (20 °C) r'_{max} [d^{-1}]	0.8 – 1.8	0.8 – 1.8	0.2 – 0.9
Cellular phosphorus uptake rate relative to r'_{max} [$\mu Mx10^{-9}$ $cell^{-1}$ d^{-1}]	0.2 – 0.5	0.1 – 0.7	0.4 – 0.9
Temperature sensitivity of r', Q_{10}	2.2 – 3.2	1.9 – 3.4	2.4 – 4.4
Threshold dose of exposure to saturating light intensity [h d^{-1}]	3 – 8	3 – 6	> 5
Motility	Variable	Mostly –ve	+ve
Minimum sinking rate [m d^{-1}]	Generally << 0.6	Generally 0.2 – 1.0	0
Susceptibility to grazing, Ψ	⟶ 1	Generally < 0.6	Generally < 0.3

Most of the annual phytoplankton biomass recorded in Myponga was from the *R*-type functional group (constituting nearly 100 % of the summer bloom). The individual simulated contributions of the *R*, *C*, and *CS* types respectively compared with observed data with artificial mixing and $CuSO_4$ dosing are shown in Fig. 5.8. The observed concentrations of *C* and *CS* types at Myponga are an order of magnitude lower than the concentration of the dominant *R* types. Subsequently, the simulation results do not show dramatic changes in the *C* and *CS* type concentrations under the modelling scenarios. Within the model seeding populations must be maintained and subsequently the results in Fig. 5.8 show that all 8 simulated species co-exist, however variability within the biomass is evident. The timing of the growth of the *C*

and *CS*-types during the summer period occurred later than the observed growth, but the magnitude of growth was reproduced in the model simulations.

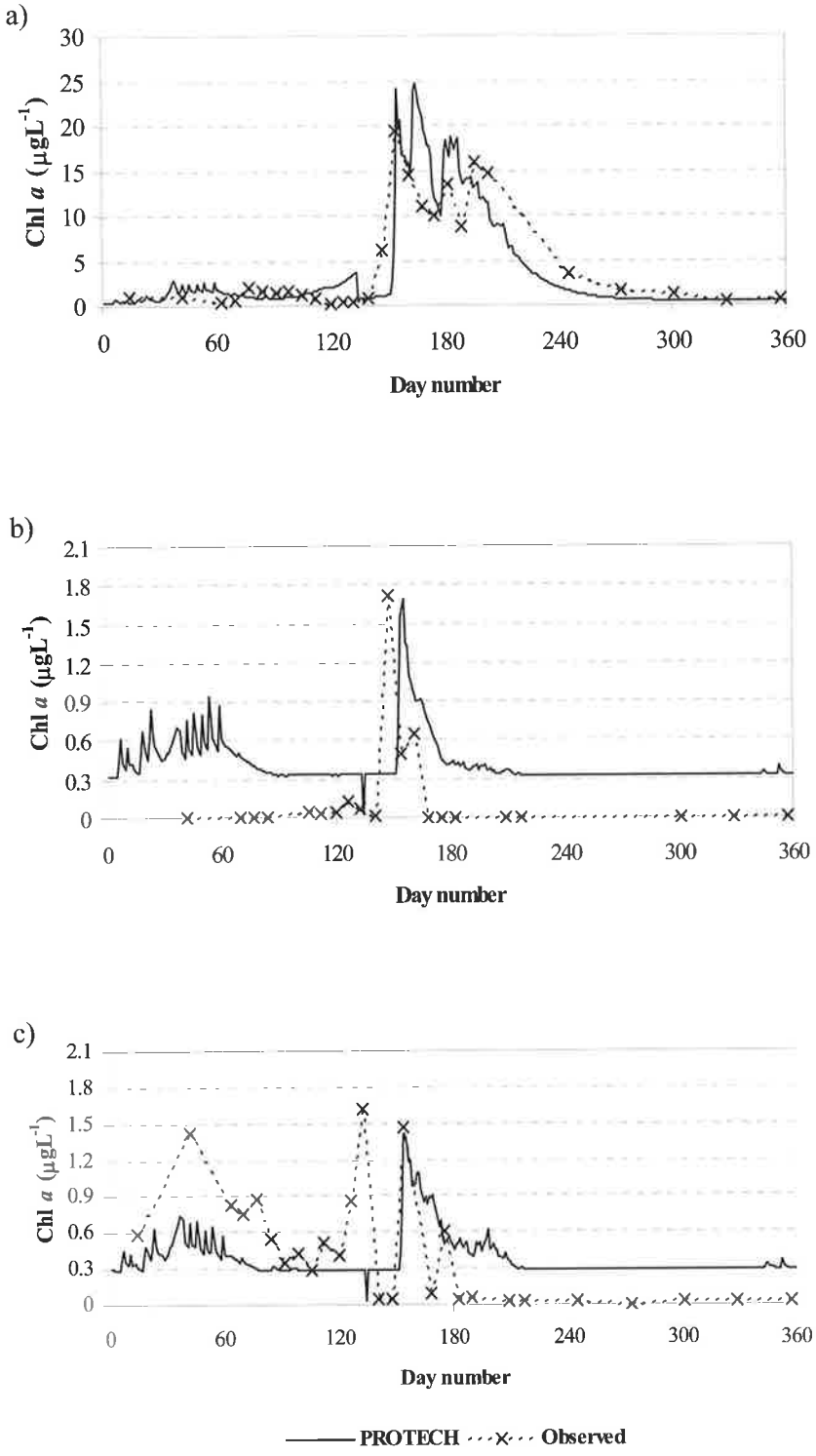

Figure 5.8 Simulated and observed data for individual species type: (a) *R*-type species, (b) *C*-type and (c) *CS*-type.

Due to the low observed concentrations of *C* and *CS*-types, which are inherently difficult to reproduce within a model simulation due to the magnitude of the modelled system, the validation of the succession of phytoplankton at Myponga Reservoir was based on the *R* type simulation which had an $EF = 0.61$. Consequently the following scenarios for Myponga Reservoir were analysed.

5.4.1 No artificial mixing and no $CuSO_4$ dosing

In the absence of these artificial controls, PROTECH simulated a similar annual pattern of phytoplankton biomass (i.e. a single summer bloom) as was observed in the field, Fig. 5.8 (a). A maximum total Chl *a* concentration of ~47 µg Chl *a* L^{-1} occurred during the summer bloom that was dominated by the *R*-type species. The growth of the *C* and *CS*-types was suppressed by the domination of the *R*-types. The major difference in the simulation was in the maximum biomass which was significantly greater than that simulated in the presence of artificial controls.

5.4.2 $CuSO_4$ dosing with no artificial mixing

The inclusion of 2 days of $CuSO_4$ dosing reduced the annual biomass of *R*-types by 18% and increased the *CS* and *C*-type biomass by 16 and 11 % respectively, Fig. 5.8 (b). However, the simulated community was still dominated by *R*-types and again conformed to the summer biomass pattern observed in the previous scenario.

5.4.3 Artificially mixed with no $CuSO_4$ dosing

The activation of the surface mixers in the absence of $CuSO_4$ dosing again reduced the maximum biomass when compared to the simulation using no artificial mixing and no $CuSO_4$ dosing, Fig. 5.8 (c). *C*-type biomass increased slightly and the reduction of *R*-type biomass was significantly less than that produced by the simulated action of just $CuSO_4$ dosing, but again the overall composition of the phytoplankton community was maintained. The action of the surface mixer did however reduce the *CS*-type biomass.

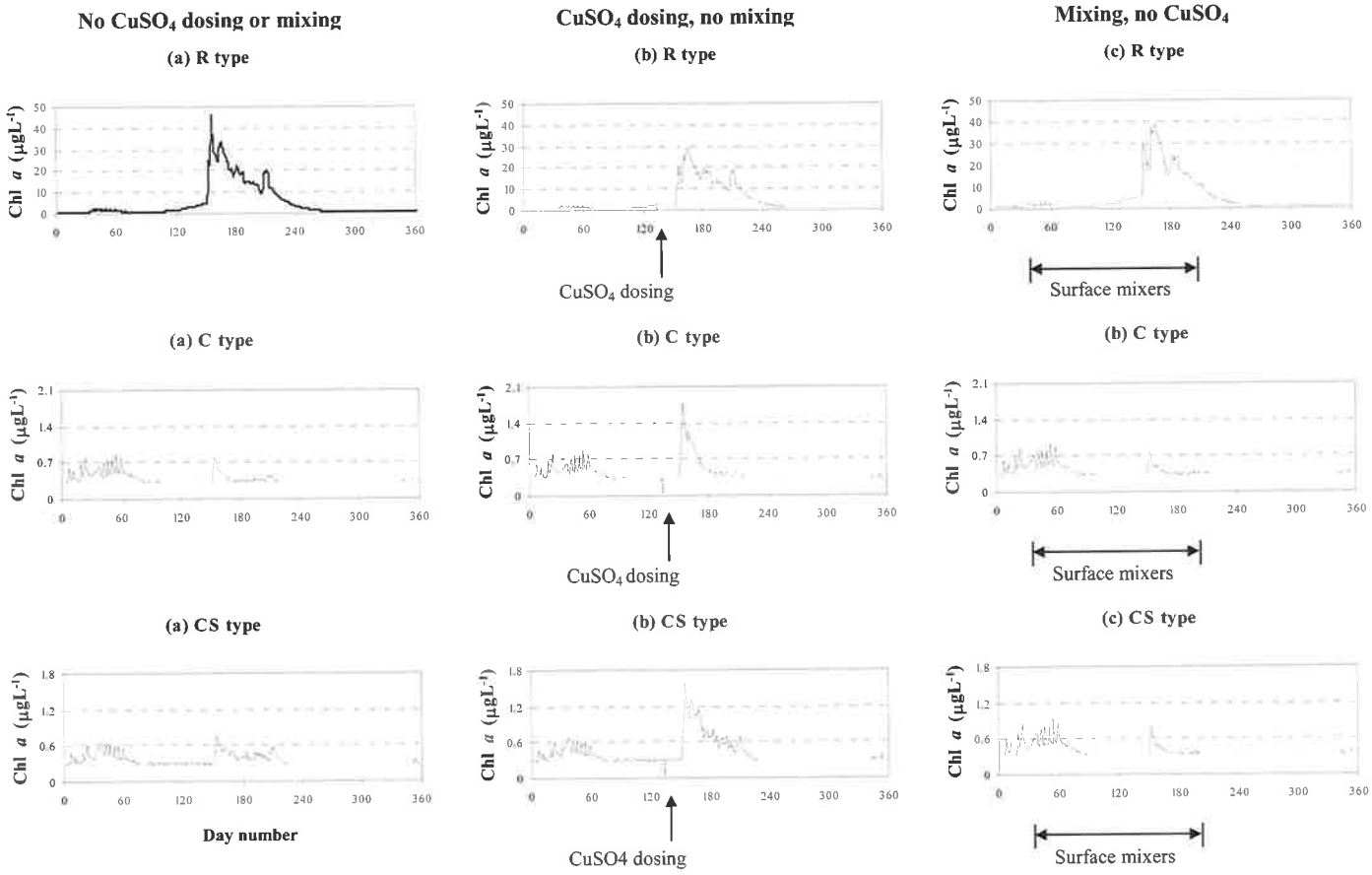

Figure 5.9 Simulated Chl *a* (µg Chl *a* L^{-1}) for individual species type with: (a) no $CuSO_4$ dosing and no surface mixers, (b) $CuSO_4$ dosing and no surface mixers and (c) surface mixers and no $CuSO_4$ dosing. The simulated $CuSO_4$ dosing occurred on PROTECH day 133 (11-January-2000) and simulated surface mixers operated between PROTECH days 31 and 214 (1-October-1999 to 1-April-2000).

5.5 Discussion

Many models have been written which simulate individual mechanisms of phytoplankton growth (Behrenfeld and Falkowski, 1997; Droop, 1973; Pahl-Wostl and Imboden, 1990), however few models exist that simulate growth in a hydrodynamic environment (Reynolds *et al.*, 2001). The linking of hydrodynamic and aquatic ecological models provides a more realistic prediction of what is occurring and what affect management may have.

The modelling of phytoplankton growth response to environmental change is a useful tool for management of water bodies. PROTECH provides accurate predictions of phytoplankton biomass composition and growth. Many process-based models have been developed which offer insight into specific processes e.g. photosynthetic production, nutrient uptake, and the carrying capacity provided by the physical conditions in the water column, external nutrient loads and by the internal bioavailability but offer no indication of timing and composition of the phytoplankton assemblage (Reynolds *et al.*, 2001).

As noted previously, Myponga Reservoir is subjected to intense regulation and has been for many years. Hence few data exist to describe its natural mixing free from chemical interference. The validation exercise was made considerably more difficult because data adequate for simulation were only available during years of significant management intervention. The inclusion of the $CuSO_4$ algorithm resulted in an improved modelling efficiency for the simulation of total Chl *a*.

The simulation of the vertical dimension within PROTECH is undertaken using simplified first principle processes that is unlike comprehensive hydrodynamic models such as DYRESM (Imberger and Patterson, 1981; Reynolds *et al.*, 2001). The scheme divides the body of the lake/reservoir into fixed 0.1m horizontal slabs, which can be instantly integrated with adjacent slabs in response to vertical mixing events. The fixed layer approach differs from the Lagrangian layers used in DYRESM where layer volumes are kept between prescribed limits by partitioning and amalgamation. DYRESM layer positions alter as rainfall, evaporation, inflow and outflow change the

stored volume, and the layer depth changes as they are moved vertically accommodating volume changes.

The surface mixer subroutine was readily incorporated into PROTECH taking advantage of the fixed layer method. The efflux from the surface mixer draft-tubes was inserted into a layer corresponding to a depth of 14.2 m whereupon mixing processes are invoked resulting in a stable water column. The surface mixer subroutine was limited, as it did not allow for the penetration of the efflux below the draft-tube exit. At the time when the PROTECH surface mixer algorithm was used, no data was available that gave insight for the penetration of the efflux.

This approach has been validated in two ways: temperature simulations were consistently realistic and the total Chl *a* results were improved dramatically by incorporating the effects of mixing. Statistical validation employing the modelling efficiency resulted in *EF* values greater than 0.5 being obtained (Fig. 5.6). The model simulations revealed important insight into the dynamics of phytoplankton in Myponga Reservoir. The most interesting was the persistent dominance of the *R*-type phytoplankton in all the simulations. Given the reservoir's highly mixed state and its shallow euphotic depth ($z_{eu} \sim 3.1$ m), this might be anticipated from the *CSR* matrix. The selection favouring this persistence can be visualised through the superimposition of a conceptual seasonal cycle over the matrix, Fig. 5.10.

The implication of the seasonal cycle remaining within the *R*-type niche is that even without $CuSO_4$ dosing and artificial mixing, *CS*-types, such as *Anabaena circinalis*, do not have the opportunity to grow to a level exceeding WHO guidelines for drinking water quality (Chorus and Bartram, 1999). However concentrations of geosmin can exceed the taste and odour threshold, 10 ng L^{-1} (Bowmer *et al.*, 1992), and require management intervention either within the storage or in the water treatment plant. Both controls did have an impact on the simulated maximum phytoplankton biomass but no discernible effect of the composition of the community; the control of that lies intrinsically with the light limiting environmental conditions.

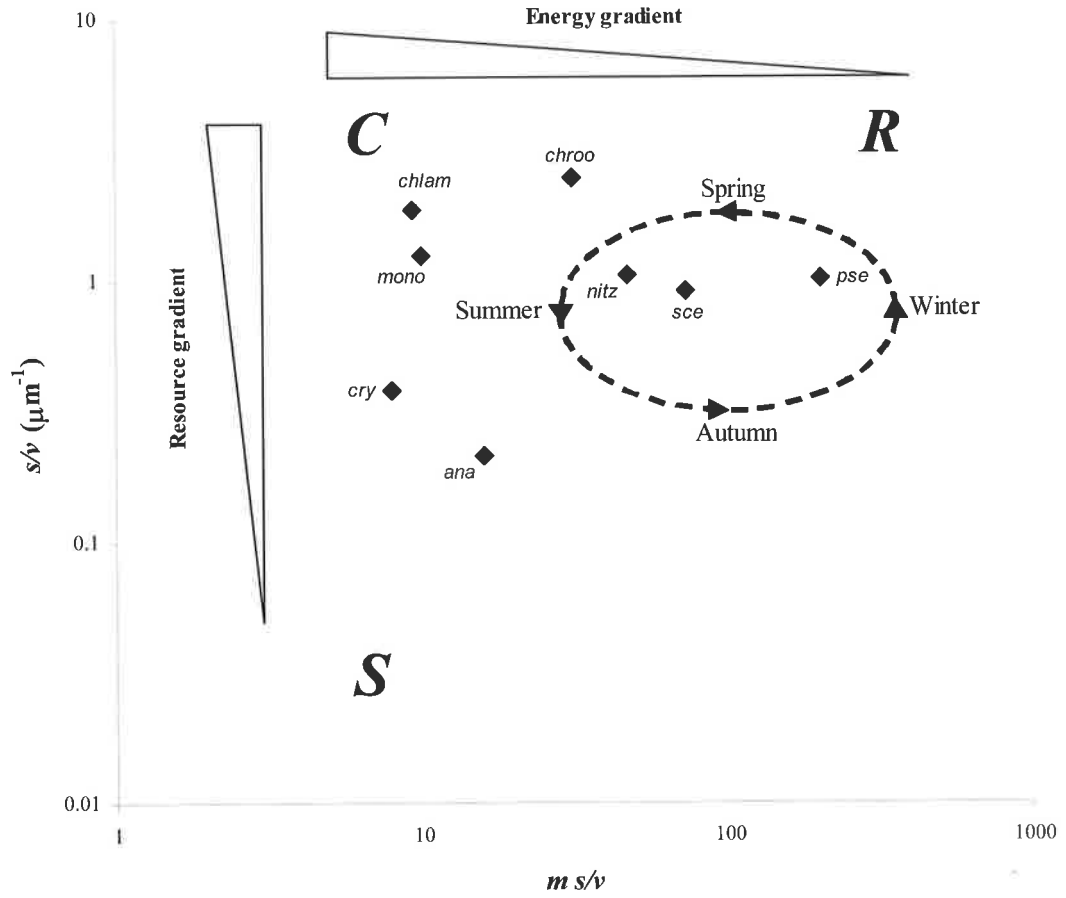

Figure 5.10 Illustration of the conceptional processes behind the phytoplankton observed in Myponga Reservoir depicting the seasonal cycle of change.

The simulated surface mixers had a similar effect to $CuSO_4$ dosing but it would be unwise to dismiss their role. Artificial mixing has functions beyond those simulated by PROTECH in the study, e.g. control of iron and manganese release from the sediment (Cowell *et al.*, 1987). To fully assess the impact of the surface mixers upon physical and geochemical conditions, further fieldwork, data analysis and numerical modelling was undertaken, see Chapters 6, 7 and 8.

5.6 Conclusions

Despite the site-specific complications of complex reservoir management strategies, PROTECH has been successfully modified to simulate the annual thermal and phytoplanktonic characteristics of Myponga Reservoir (Lewis *et al.*, 2002b). The flexibility of PROTECH was clearly demonstrated in the way that the model has the

ability to be applied to water bodies, radically removed from its origins in the United Kingdom.

This study has shown that artificial mixing via surface mixers has a significant effect upon total biomass in reservoirs. To further improve the surface mixer subroutine, the flow mechanisms and subsequent entrainment of algae and ambient water generated by the surface mixers needed to be incorporated using jet and plume equations, see Chapter 2. Due to PROTECH being unavailable for use outside of CEH Windermere, an improved surface mixer algorithm could not be incorporated. However, further numerical modelling using an enhanced surface mixer algorithm based on comprehensive field measurements was undertaken with the DYRESM-CAEDYM model presented in Chapters 7 and 8.

The adjustments made to PROTECH for hemispherical and latitudinal differences were achieved. By inputting measured shortwave radiation and solar day-length values, the switch from a Northern Hemisphere to a Southern Hemisphere solar climate required that the *Eloss* equations were adjusted for increased local net convective heat transfer, at the lower latitude. The success of these changes is evident from the resulting high *EF* values calculated for the temperature data. Additional algorithms should be included into PROTECH to calculate the surface energy fluxes. Extra input data would be required; namely incident or net longwave radiation and cloud cover or relative humidity.

The management practices put in place at Myponga Reservoir to control the phytoplankton community reduces the phytoplankton biomass but the most important factor regulating the current phytoplankton content is that it is light limited. PROTECH has successfully been able to reproduce this phytoplanktonic character of Myponga Reservoir and has shown that the community was dominated by *R*-type phytoplankton under all the simulated conditions tested. The action of $CuSO_4$ and artificial mixing reduced the simulated phytoplankton biomass but had insignificant effects upon the actual phytoplankton succession. Thus it was concluded that, regardless of the artificial controls imposed upon the reservoir, potentially harmful *CS*-types (*Anabaena circinalis*) would probably never be a significant health risk with the current physical and biological conditions in Myponga Reservoir.

6. THE SURFACE MIXERS – FLOW CHARACTERISATION

6.1 Introduction

The action of the surface mixer impeller generates a 4.9 m diameter high Reynolds Number axisymmetric swirling jet that is either dominated by momentum or buoyancy forces or a combination of both depending on ambient conditions. To predict the performance and impact of the flow generated by the surface mixers upon the physical structure of the water column and water quality, namely dissolved oxygen concentration and the phytoplankton assemblage, in Myponga Reservoir, a detailed analysis of the surface mixer flow characteristics was required.

The initial objective was to determine the fate of surface water that was transported through the surface mixers, which required detailed flow measurements. The field measurements were carried out on the '800' surface mixer, which has the furthest proximity to boundaries as shown in Fig. 3.3. The distance required for a typical jet to develop and achieve self-similarity (known as the zone of established flow, *ZEF*), where the jet expands and the mean velocities decrease, occurs up to a distance of 6 jet diameters downstream of the jet orifice (Fischer *et al.*, 1979). Using this relationship, the length of the *ZEF* for the jet exiting the '800' mixer would be up to 30 m below the draft-tube, implying that the surface mixer jet would not be able to fully develop before impeding upon the sediment surface in Myponga Reservoir. The flow data was analysed to determine if the characteristics for large diameter large Reynolds Number swirling jets differed to the smaller, lower Reynolds Number swirling jets reported in the literature (Pitts, 1991). As reported in Chapter 2, the analysis of swirling jets and plumes has been restricted to small-scale laboratory studies (e.g. Billant *et al.*, 1998; Peterson and Bayazitoglu, 1992; Petersson *et al.*, 1996).

The behaviour of the surface mixer jet under the draft-tube was investigated during quiescent isothermal and stratified conditions to determine how the characteristics of the jet changed with the inflow density. If the surface mixer jet became positively buoyant, it would be anticipated that the jet might not penetrate to the bottom of the

reservoir, therefore limiting the destratification abilities of the surface mixers, i.e. oxygenation of the hypolimnion. Additionally, during periods when the surface water in Myponga Reservoir was heating, the depth of the intrusion that developed from the surface mixer efflux needed to be quantified. This was necessary to determine if the intrusion impacted upon the depth of the *SML*, and deposited the phytoplankton that was transported through the surface mixers below the euphotic zone. Consequently, knowledge of the measured jet characteristics was essential to validate the mixing capabilities of the surface mixers used for destratification and control of cyanobacterial growth when deployed in the field.

A further important aim of the flow characterisation was to develop a surface mixer algorithm that could be incorporated into existing hydrodynamic models. This would enable the surface mixers to be adequately assessed when operated independently from the aerator in Myponga Reservoir.

To achieve these objectives *ADV* measurements of the radial, axial and tangential flow components were undertaken in the discharge from the surface mixer draft-tube. The swirling jet generated by the surface mixer impeller flows through the draft-tube, which restricts the development of the jet until the discharge point whereupon the jet could be characterised. Before the methods used to obtain the necessary data are described, the velocity characteristics of swirling flows are introduced.

6.1.1 Swirl flow characterisation

Near field characteristics of axisymmetric jets are greatly affected when these jets are generated with a swirling motion. Swirling flows are generated by the inducement of a spiralling motion where a tangential velocity component, v, is imparted to the flow by the use of, for example, impellers, rotating pipes, specially designed nozzles or twisted tapes (Petersson, 1996). In turbulent swirling jets the rotating fluid emerges from the orifice with radial, tangential and axial velocity components (u, v, and w). In the presence of swirl, large effects are observed in the flow-field, jet growth, entrainment and decay occur when compared to the non-swirling jet (Gupta *et al.*, 1984), described in Chapter 2.

The degree of swirl can be characterised by the non-dimensional swirl number S, representing the ratio of the axial flux of swirl momentum G_θ, to the axial flux of axial momentum G_x, multiplied by the equivalent jet orifice R (Gupta *et al.*, 1984).

$$S = \frac{G_\theta}{G_x R} \tag{6.1}$$

where,

$$G_\theta = 2\pi\rho \int_0^\infty R^2 \overline{v}\overline{w} dR \tag{6.2}$$

and,

$$G_x = 2\pi\rho \int_0^\infty R\left(\overline{w}^2 - \frac{\overline{v}^2}{2}\right) dR \tag{6.3}$$

The mean axial and tangential velocities are denoted by $\overline{w}$ and $\overline{v}$ respectively. The intensity of the swirl is weak if $S < 0.4$ and strong if $S > 0.6$ (Petersson *et al.*, 1996). The swirl number is usually given at the jet orifice. However, a local swirl number can be evaluated at any axial location using R as the local jet radius. Monotonic decrease of the swirl number will occur with increasing axial distance from the jet. For fixed axial velocity the penetration of the jet is barely affected in weakly swirling jets with small initial tangential velocity, but significant axial retardation occurs with high swirl. Initial axial/tangential velocity ratios greater than 1.5 cause stagnation of the swirling jet in the immediate vicinity (or within) of the jet orifice and the angle of spread will increase toward 90° (Morton, 1968).

The tangential velocity is a result of the swirl device. At the jet orifice the tangential velocity field changes rapidly whilst adjusting to the ambient conditions. Two types of swirl exist, specifically solid-body (forced vortex) rotation and free vortex (Fig. 6.1).

The maximum tangential velocity for solid-body rotation occurs at the outer edge of the vortex, whilst with a free vortex the maximum is found near the axis of rotation.

The combination of the forced and free vortex is common in viscous fluids and is known as the Rankine combined vortex. Initially, the jet possesses a swirl characteristic of a Rankine vortex (Pratte and Keffer, 1972), which has solid-body rotation in the jet centre and free vortex in the outer region (Gupta *et al.*, 1984). The swirl distribution created from a mechanical impeller has solid-body rotation in the centre and free vortex flow for the remainder of the tangential velocity distribution. Downstream of the jet orifice the swirl distribution will achieve self-similarity and rapidly decay in the form of a Rankine vortex that loses its direct influence on the flow (Petersson, 1996). Self-similarity occurs when the jet can be defined by a characteristic velocity and a local length scale (Townsend, 1976).

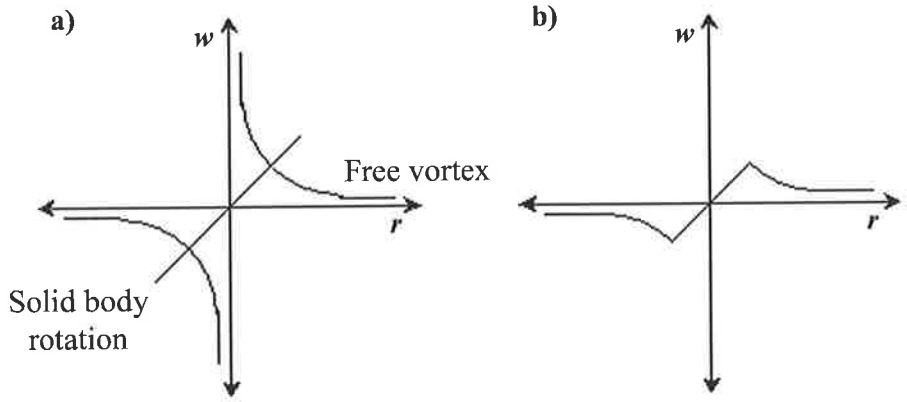

Figure 6.1 Distribution of swirl for (a) solid-body rotation and free vortex and (b) Rankine vortex (Petersson, 1996).

The swirl affects the radial distribution of the axial velocity. Under weak swirl the radial distribution is uniform and Gaussian like, with the maximum axial velocity occurring on the jet axis. As the swirl increases a low velocity core develops in the jet centre due to centrifugal force. Under extreme swirl ($S > 0.6$) the forces due to the axial adverse pressure gradient can cause axial recirculation. Typical axial velocity profiles with weak, moderate and strong swirl are shown in Fig. 6.2.

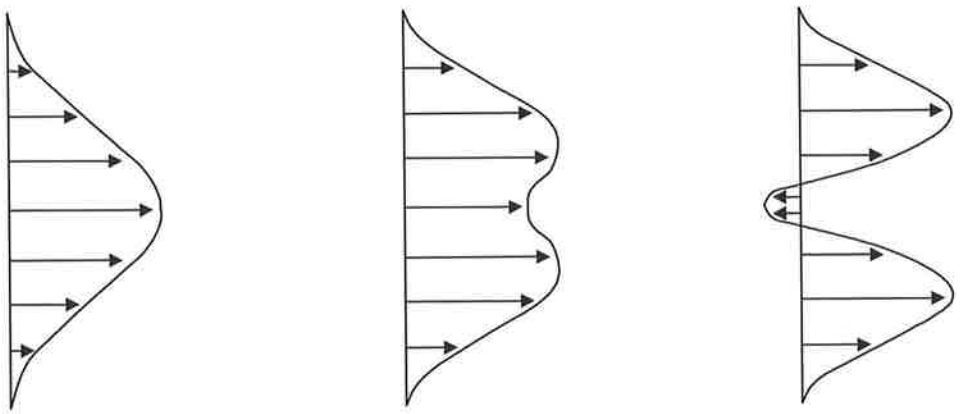

Figure 6.2 Characteristic mean axial velocity profile with (a) weak swirl ($S < 0.4$), (b) moderate swirl and (c) strong swirl ($S > 0.6$). Reproduced from Petersson (1996).

6.2 Techniques developed to measure jet characteristics in the field

The experimental strategy was to investigate the dilution, velocity distribution, turbulence levels, mass and momentum fluxes as functions of radial distance and depth for the surface mixers. The velocity measurements enabled detailed description of the jet dynamics to be determined. The spatial and temporal velocity and temperature parameters were measured with a field-version Acoustic Doppler Velocimeter, a laboratory-version Acoustic Doppler Velocimeter, a Hydrolab MiniSonde®, and a Hydrolab DataSonde®, described in Chapter 3.

The dynamics of the surface mixer mean flow in both the near and far fields was investigated during both isothermal and stratified conditions. High resolution measurements where made to investigate the development of the surface mixer flow to quantify the zone of flow establishment and the zone of established flow, radial spread, dilution, swirl and entrainment characteristics, decay of the centreline axial velocity, terminal penetration depth, and the zone of influence. To calculate the turbulent characteristics of the flow a high signal-to-noise ratio (*SNR*) was required. This was achieved by seeding using very fine dilute clay particles collected from the sediment that were deposited into the inlet of the surface mixer. An average *SNR* of ~15 dB was obtained.

To measure the flow entering and exiting the surface mixers, specialised brackets incorporating the *ADVLab*, *ADVField* and Hydrolab's were devised to mount either to the surface mixer structure or a boat. A schematic diagram of the surface mixer is shown in Fig. 3.5. There were three main methods of data acquisition, which are described below.

6.2.1 Inflow measurements

The inflow to the surface mixers was measured using the *ADVLab*. The *ADVLab* was attached to a purpose made bracket that could be attached to the top and middle surface mixer draft-tube rings spanning the inlet in the vertical dimension, shown in Fig. 6.3. At 0.1 m intervals the *ADVLab* was lowered through the water column from the surface to the bottom of the inlet. The sample rate was set at 25 Hz and the sample time at each point was 120 s. The inflow was measured at the four compass points (Fig. 6.4) at 0.1 to 0.2 m intervals from the surface to the bottom of the inlet. The inflow measurements were repeated for three different draft-tube inlet depths: 0 - 2 m, 0 - 1.5 m, and 0 - 1.2 m.

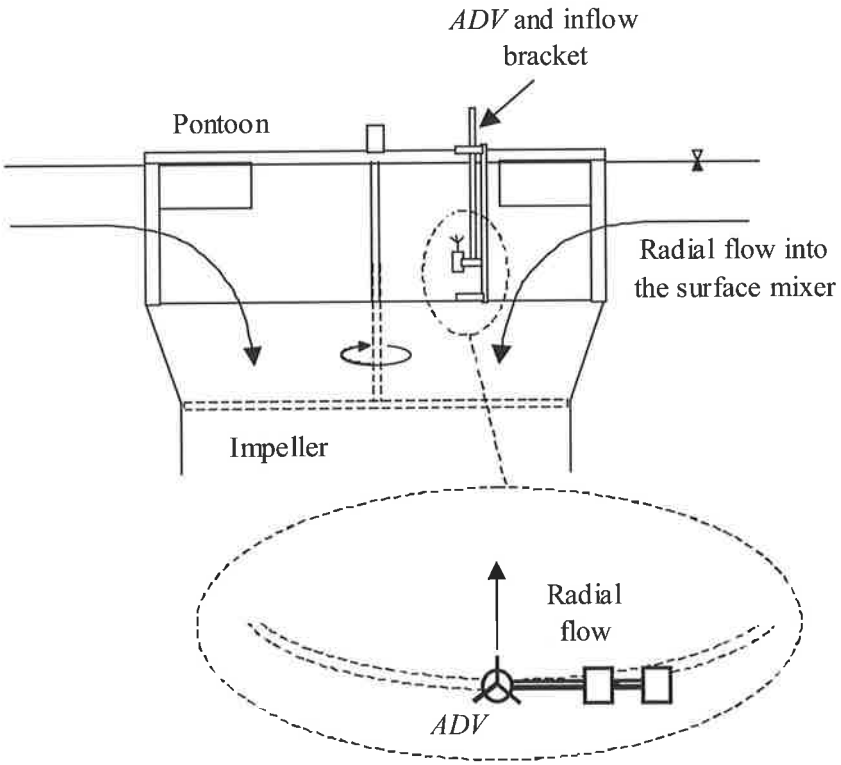

Figure 6.3 Inflow measurements, the *ADVLab* bracket is attached to the top and middle inlet rings to enable undisturbed flow measurements into the surface mixer. The bracket is able to be located at any angular position on the inlet circumference.

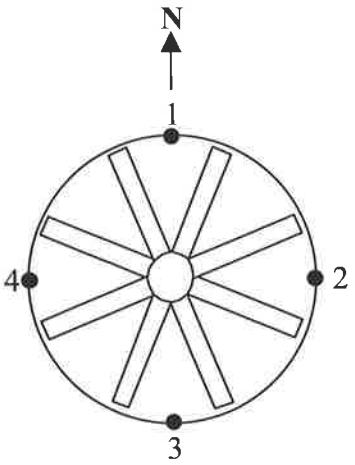

Figure 6.4 Inflow measurement locations, looking down on the surface mixer.

6.2.2 Zone of influence measurements

When measuring the radial zone of influence around the surface mixers the *ADVField* was cast from a boat. To prevent pitch and roll of the boat interfering with the *ADVField* measurement signal a novel anchor system was implemented whereupon the *ADVField* would measure the flow without being directly attached to the boat (Fig. 6.5). A spinnaker cleat was attached to an anchor and used to secure a float to which the *ADVField* was mounted.

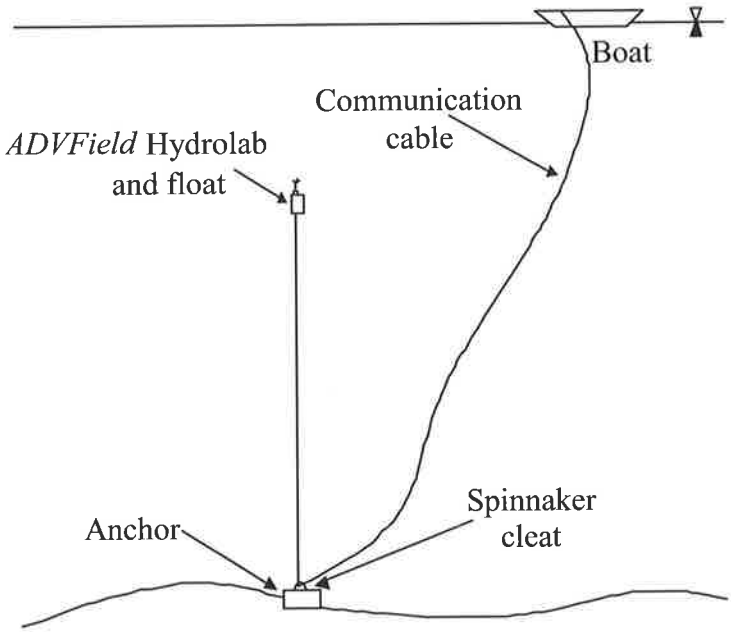

Figure 6.5 Surface mixer zone of influence flow data collection set-up. The arrangement allows the movement of the boat to be independent of the *ADVField*.

This arrangement allowed near to far field measurements to be undertaken at any location in Myponga Reservoir under any meteorological condition. The near to far field *ADVField* measurements were taken from the reservoir sediment surface to the water surface at radial distances from 3 to 400 m from the centreline of the surface mixer.

6.2.3 Efflux measurements – stage one

The surface mixer efflux was initially measured with a propeller meter (Braystoke BFM002, Valeport Limited) mounted to an aluminium bracket. The propeller meter provides an immediate flow measurement in the direction of its orientation, and measures flow accurately for angles ± 10 ° with a tolerance of ± 1.5 %, and due to buoyancy and swirl, flow angles in this instance were not vertical. The bracket was suspended below the surface mixer draft-tube and lowered at 0.1 m intervals at radial positions spanning at 0.2 m intervals from the jet centre to the extremity of the draft-tube. The details of the propeller meter are described in Chapter 3. The measurements obtained from this procedure were limited due to the propeller meter providing one-dimensional readings and the inability to accurately detect flow below 0.1 m s^{-1} without significant error. Therefore these restrictions limited the flow measurements to within ~2 m of the draft-tube exit.

6.2.4 Efflux measurements – stage two

To accurately measure the surface mixer efflux in three dimensions, throughout the full vertical extent of the water column below the draft-tube the *ADVField* was employed. The *ADVField* was located directly beneath the draft-tube at a minimum depth of 14.2 m. An extendable traversing mechanism was manufactured, which was mounted to the surface mixer structure. The vertical arm of the extendable traversing mechanism could span distances from ~ 14 to 30 m, was lightweight and transportable. The design was based on a drilling rig apparatus whereupon the vertical arm was made up of individual attachable 2 m lengths of aluminium tubing. At the bottom of the vertical arm a horizontal bracket was attached. At one end of the horizontal bracket the *ADVField* was mounted and at the other end a counterweight was attached to keep the extendable traversing mechanism stable. The *ADVField* extendable traversing mechanism mounted to the surface mixer is shown in Fig. 6.6.

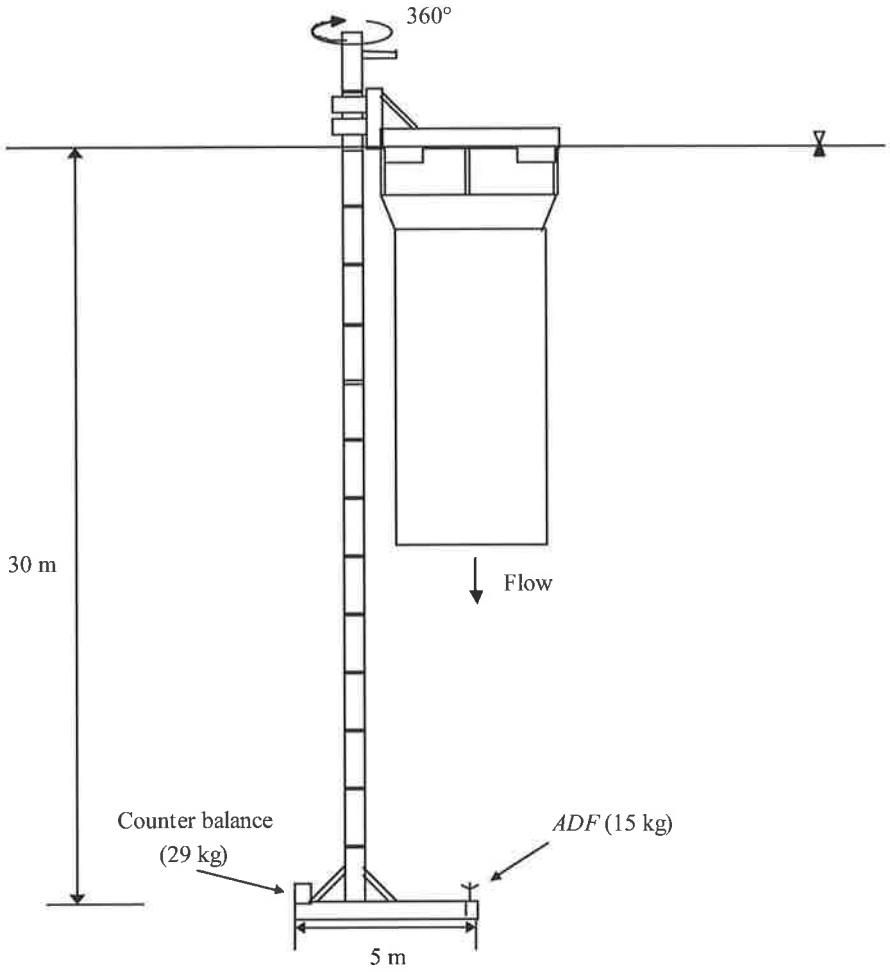

Figure 6.6 Efflux measurement and *ADVField* aluminium extendable traversing mechanism arm. The extendable traversing mechanism is able to be lowered through the water column via a winch mounted to the surface mixer pontoon, and rotated 360°.

Measurements below the draft-tube were taken from 14 to 30 m (below surface) at intervals of 0.5 m at the surface mixer centreline to a radial distance of ~ 7 m (at 0.2 m radial intervals). By turning the extendable traversing mechanism, the horizontal bracket arm was rotated, producing the measurement trajectory shown in Fig. 6.7.

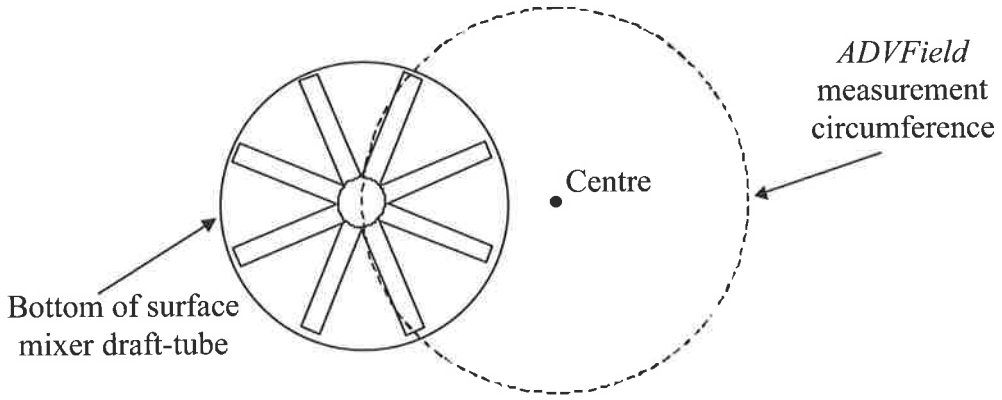

Figure 6.7 Location of *ADVField* measurements below surface mixer draft-tube (looking up).

6.3 Results

During the entire investigation the running conditions for the surface mixers were kept constant and are shown in Table 6.1. The inflow to the surface mixers was examined first to determine the amount of water being pumped through the draft-tube, with the measured volume flux and mean axial velocity values also shown in Table 6.1. Secondly, the analysis of the surface mixer outflow was undertaken under two conditions, stratified and isothermal. The isothermal flow analysis was carried out during August-2001 and under stratified conditions throughout February-2002. The results from the inflow experiments are presented first, then the outflow under isothermal and stratified conditions are analysed.

Table 6.1 Initial conditions for surface mixer flow analysis

Parameter	Value	Units
Impeller rotational speed, ϖ	10	rpm
Measured volumetric inflow, Q_{inflow}	3.5	$m^3 s^{-1}$
Measured mean axial velocity, $\overline{w}_{inflow}$	0.19	$m s^{-1}$
Momentum flux, M	0.65	$m^4 s^{-2}$
Draft-tube radius, $r_{outflow}$	2.45	m

6.3.1 Surface Mixer Inflow

The inflow radial velocity to the surface mixers was measured, using the method described in section 6.2.1, to determine the volumetric flow rate and optimum intake depth. The averaged radial velocity profiles measured at three different inlet heights are plotted in Fig. 6.8, where it is evident that the inlet velocity increases proportionally with reduced inlet depth.

The inlet depth was set to 1.2 m to generate the highest surface velocities to minimise the effects of the wind, which can cause the immediate surface water to be unaffected by the impeller and flow directly over the mixer inlet. This is evident when the inlet depth was set to 2.0 m and the top 0.5 m surface water flowed away from the surface mixer, shown as negative velocities in Fig. 6.8. The inlet measurements were recorded on the 24-January-2000 when the wind was blowing in a north-westerly direction with an average velocity of 4.1 m s^{-1}.

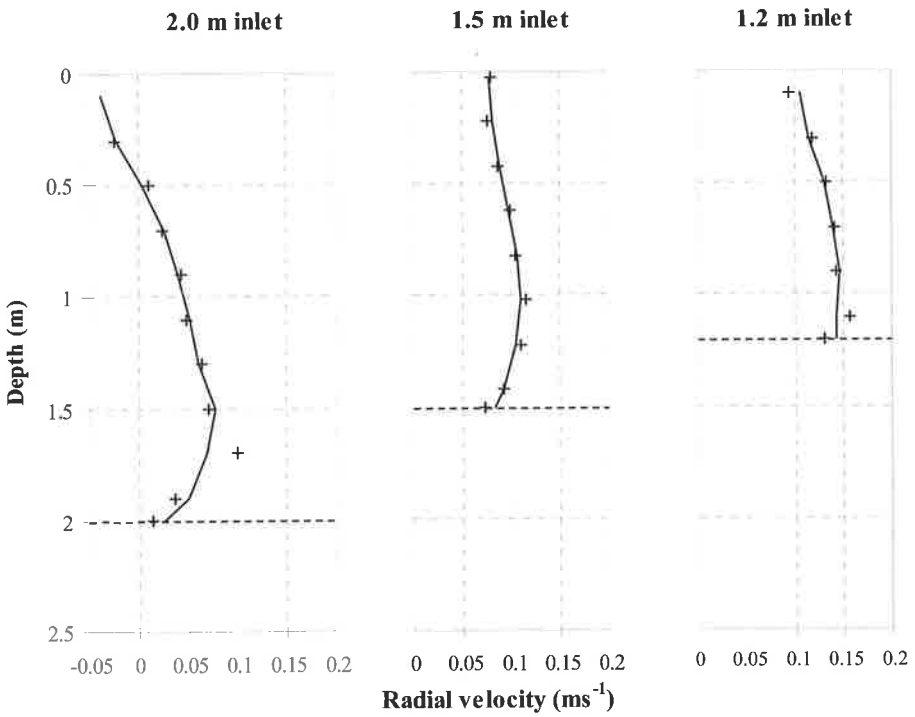

Figure 6.8 Averaged radial inflow velocities taken at three inlet heights (2.0, 1.5 and 1.2 m). The black dashed line corresponds to the depth of the intake (the height between the top and middle surface mixer draft-tube rings).

As the inlet depth was decreased, the overall inlet velocities increased from an average velocity of 0.04 m s^{-1} at an inlet depth of 2.0 m, to 0.12 m s^{-1} when the inlet depth was set to 1.2 m. The measured radial velocity data for an inlet depth of 1.2 m taken at the four compass points is shown in Fig. 6.9, where the velocity at a depth of 0.2 m is affected by the wind in the south and west profiles. The radial velocities at each depth were time averaged and then used to determine the volumetric flow rate for the surface mixers. At an intake depth of 1.2 m, the flow rate was determined to be ~ 3.5 $m^3 s^{-1}$, which was calculated using Eq. 6.4:

$$\overline{Q} = 2\pi r \int_0^{d_{inlet}} \overline{u}(z)dz \tag{6.4}$$

where, r is the radius of the inlet to the surface mixer draft-tube.

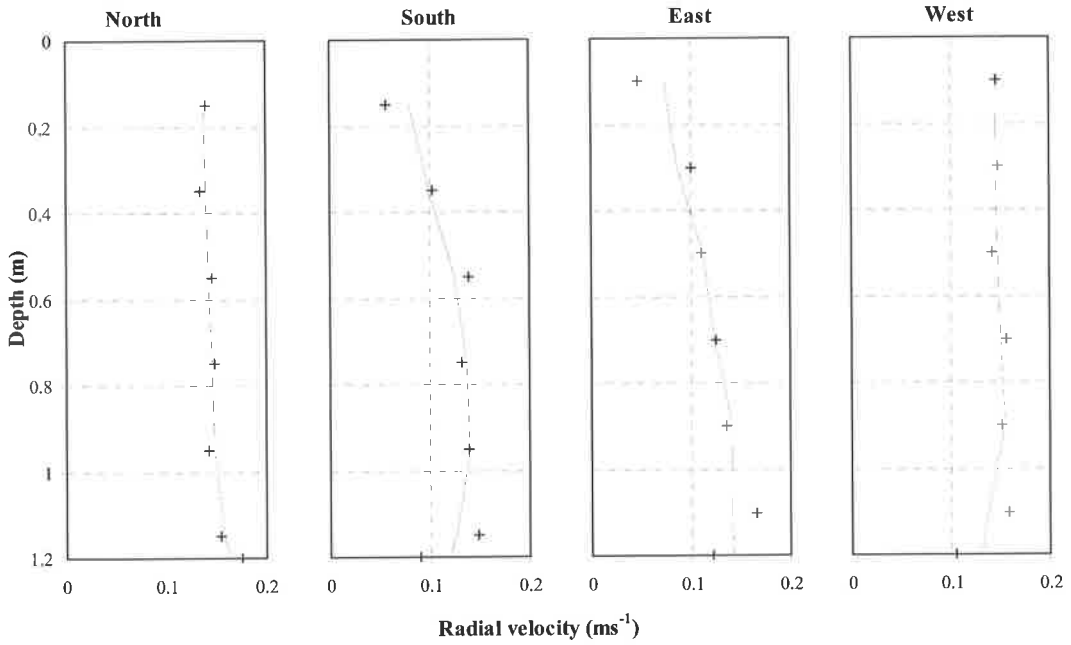

Figure 6.9 Inlet radial velocity with the intake depth set to 1.2 m. The positions of the 4 compass points correspond to Fig. 6.4.

6.3.2 Flow structure of the surface mixer efflux

The surface mixer impeller develops a weak swirling jet that spreads radially as the flow develops downstream from the draft-tube. Using the non-dimensional swirl number S (Eq. 6.1) the surface mixer jet swirl was characterised. It was determined

that in the *ZEF*, analysed in section 6.3.3, the jet had an average Swirl number of 0.20, indicating weak to moderate swirl. The local Swirl number calculated at each depth interval of 0.5 m in the *ZEF*, initially increases to ~0.28 at ~4.5 m below the draft-tube and then decreases to ~0.8 at a depth of ~13.5 m below the draft-tube. The radial spread and penetration of the jet are dependent on the ambient conditions. The surface mixer jet had a terminal penetration depth under stratified conditions and impinged on the sediment surface under weakly stratified ($\Delta T < 0.3$ °C, section 6.3.4) and isothermal conditions. When the jet impinged on the sediment surface radial deflection occurred and an intrusion layer formed along the sediment surface. At the terminal depth, a plume developed in the opposite direction that rose to a height of neutral buoyancy.

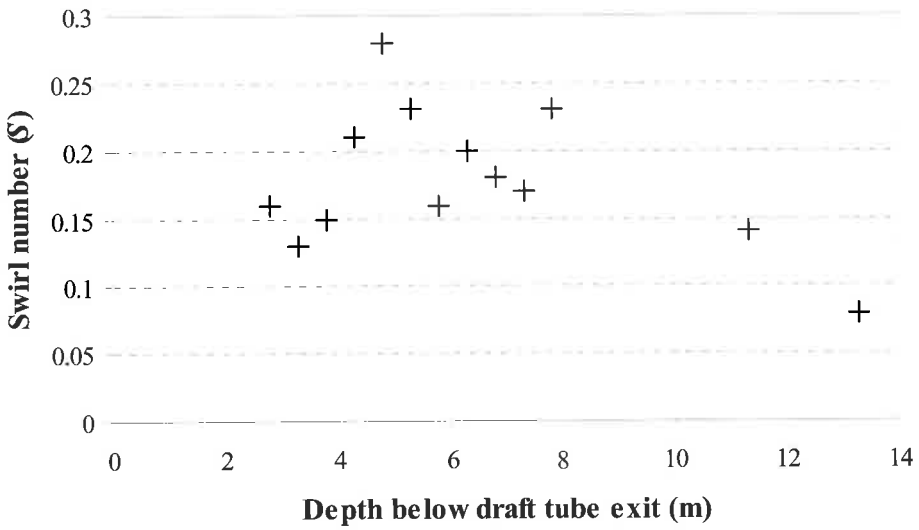

Figure 6.10 Swirl number, calculated for the surface mixer efflux in the zone of established flow.

6.3.3 Zone of flow under isothermal conditions

Under isothermal conditions the surface mixer jet can be divided into two different zones, the zone of flow establishment and the zone of established flow. The demarcation between these zones depends on the appearance of a Gaussian shaped mean axial profile and the steady decay of the jet centreline axial velocity (Albertson *et al.*, 1950). The *ZFE* for non-swirling round turbulent jets is typically in the region from the jet orifice to six-jet diameters (D) downstream (Fischer *et al.*, 1979). To

determine the commencement of the *ZEF* for the surface mixer jet the measured jet centreline axial velocity data was non-dimensionalised and plotted against non-dimensional distance (z/l_Q). The commencement of the *ZEF* for the surface mixer jet started at ~0.5*D* below the draft-tube outlet, where steady decay of the axial velocity was observed, Fig. 6.11. Q and M are the initial values of volume and momentum flux and l_Q is the characteristic length scale defined in Eq. 6.5:

$$l_Q = \sqrt{A} \tag{6.5}$$

where A is the initial cross sectional area of the jet. The corresponding value of z/l_Q for the approximate start of the *ZEF* for the surface mixer was obtained by fitting a linear regression to a plot of measured jet centreline axial velocity against distance from the draft-tube outlet (Fig. 6.12) giving the slope that represents z/l_Q. Subsequently, the *ZEF* starts at ~2.0 m below the draft-tube where w_mQ/M = 0.5561 l_Q/z (R^2 = 0.68, *P-value* = 3E-13).

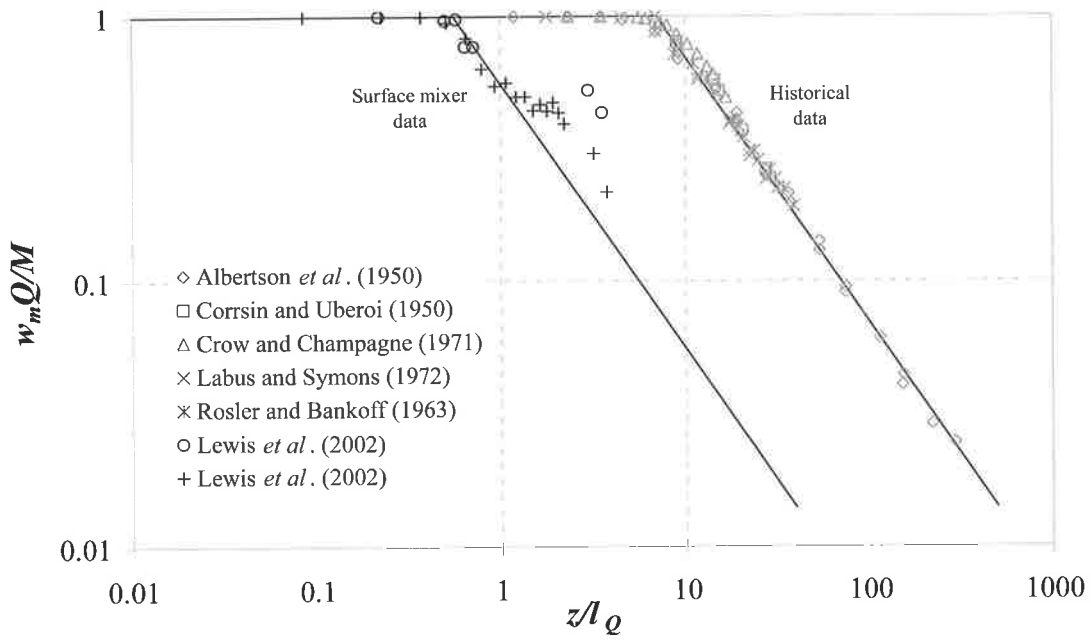

Figure 6.11 Mean axial velocity decay on the axis of the surface mixer swirling jet and a round turbulent jet (Fischer *et al.*, 1979).

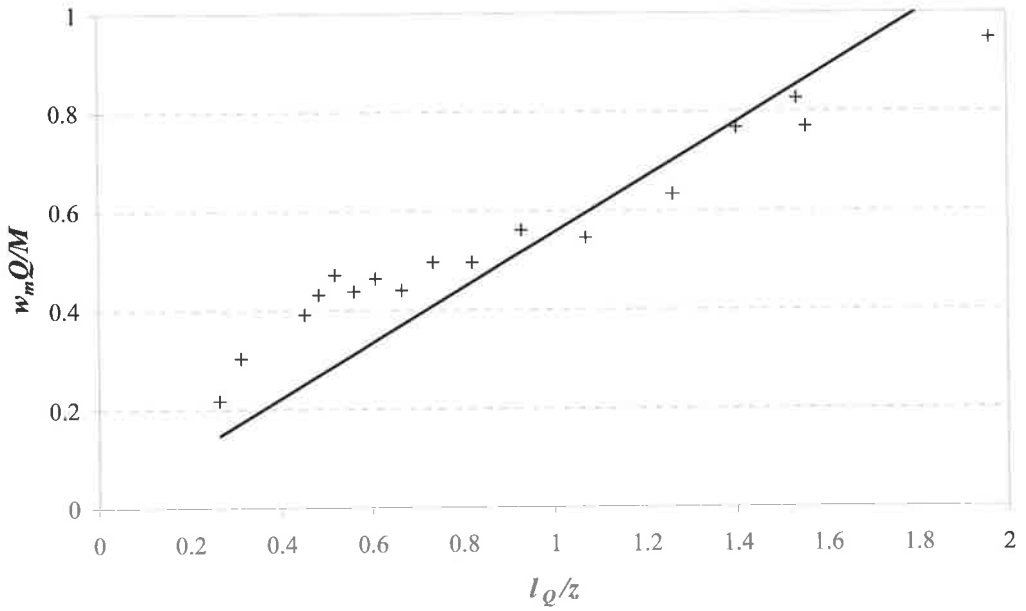

Figure 6.12 Mean axial velocity vs. axial distance from the draft-tube outlet $w_mQ/M = 0.5561\ l_Q/z$ ($R^2 = 0.68$, *P-value* = 3E-13).

The decay of the axial centreline velocity started at a considerably shorter distance than that of smaller radius jets reported and plotted in Fig. 6.11. As the surface mixer jet centreline velocity decreased the jet expanded thus conserving momentum, enabling the entrainment into the jet to be determined. To calculate the local entrainment coefficient (α) for the surface mixer jet in the *ZEF*, Taylor's entrainment hypothesis was used (Eq. 2.37). To calculate α the jet radius and jet volume were required as a function of depth. The jet radius was found at the location of the demarcation between the jet and ambient fluid that is defined as the radial distance r_e, where the measured axial velocity equals the mean axial centreline velocity multiplied by 0.37 (e^{-1}), i.e. $w(z) = w_m(z)/e$.

Subsequently the mean axial velocity distribution of the jet can be represented by:

$$w = w_m f\left(z/r_e\right) \tag{6.6}$$

The radial spread r_e of the jet is plotted in Fig. 6.13 where z is the distance from the draft-tube outlet. Using a linear regression fitted to the data shown in Fig. 6.13 the width parameter for the isothermal surface mixer jet was determined to be:

$$\frac{r_e}{z} = 0.199 \tag{6.7}$$

where $R^2 = 0.83$ (*P-value* = 0.0005) was obtained. Therefore the radial spread of the jet exiting the draft-tube was assumed to spread linearly during isothermal conditions at a half angle of 14.4° (Arc Tangent r_e/z).

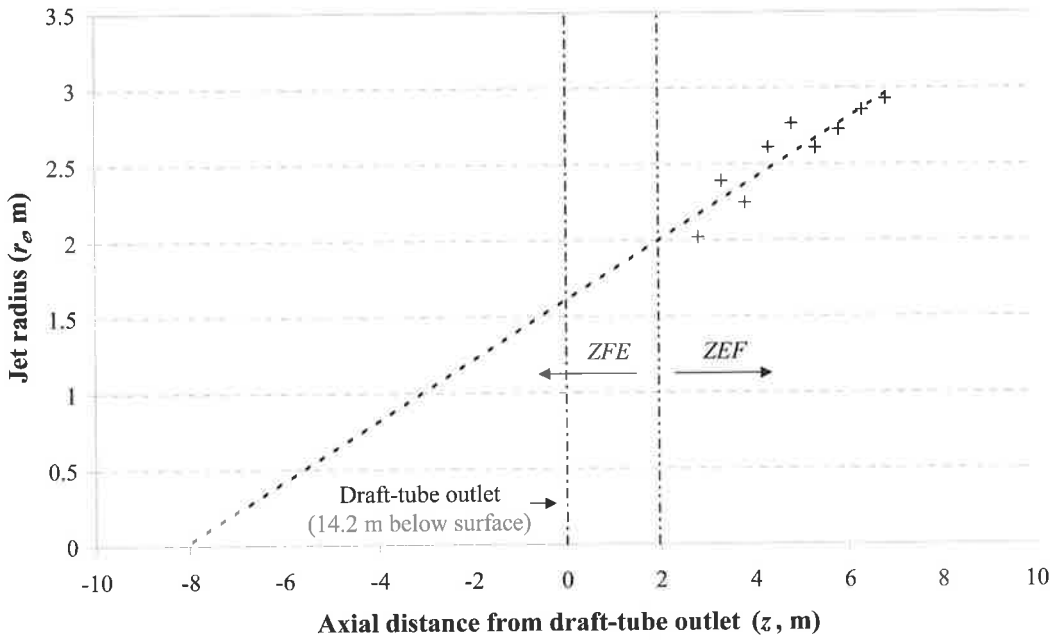

Figure 6.13 Radial spread of the surface mixer jet, $r_e/z = 0.199$ and $R^2 = 0.83$ (*P-value* = 0.0005).

The observed volumetric flow at each measured depth z ($Q_{Observed}$) was calculated by integrating the axial velocity data from the jet centre to the radial distance r_e. Iterative optimisation of the R^2 value for the observed volume flux and calculated volume flux data was used to determine the entrainment coefficient for the surface mixer jet. Eq. 2.37 was used to calculate the volumetric flow ($Q_{Calculated}$). A value of 0.07 for the entrainment coefficient was obtained from the iterative process where $Q_{Observed} = 1.02$ $Q_{Calculated}$ and $R^2 = 0.82$ (*P-value* = 0.0008), Fig. 6.14.

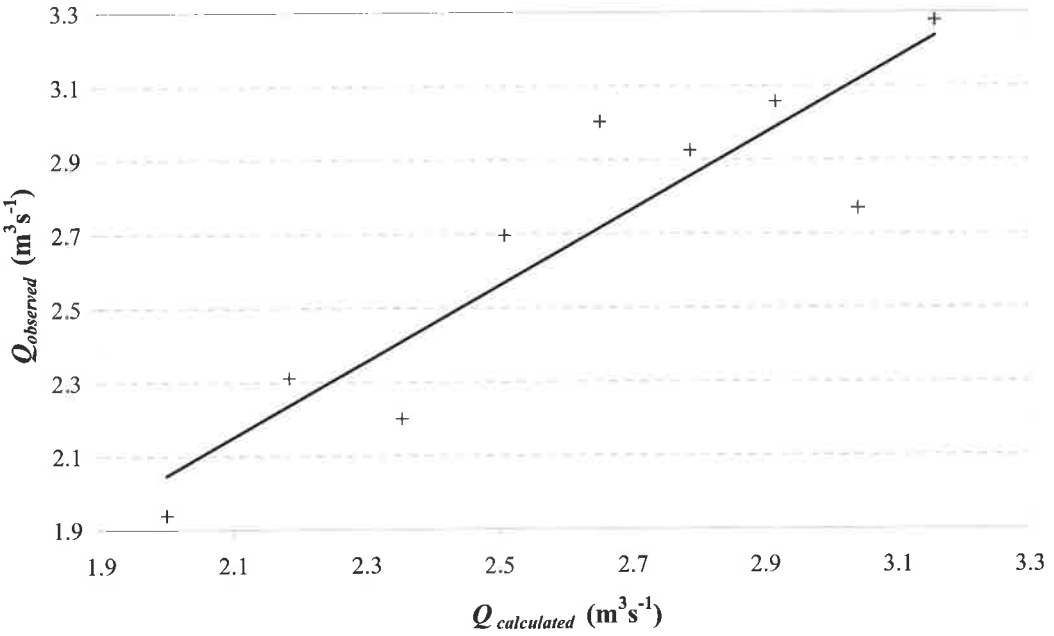

Figure 6.14 Observed vs. calculated volumetric flow used to determine the entrainment coefficient for the surface mixer jet under isothermal conditions, $Q_{Observed} = 1.02\ Q_{Calculated}$ ($R^2 = 0.82$, *P-value* = 0.0008).

6.3.4 Zone of flow under stratified conditions

Under stratified conditions and periods of surface heating, the surface mixer jet has a positive buoyancy flux due to the temperature difference between the jet and the ambient fluid. Under certain conditions the jet will not penetrate through the entire water column beneath the draft-tube, and a terminal depth will exist. The penetration depth is dependent upon two jet parameters being the momentum flux M (Eq. 2.6) and the buoyancy flux B (Eq. 2.7) as shown in Eq. 2.31.

To measure the terminal depth of the jet under stratified conditions the *ADVField* was lowered beneath the draft-tube until no significant downward axial flow along the jet centreline was detected (<0.001 m s^{-1}). With a temperature difference between the surface and draft-tube exit of ~1.31 °C no axial flow was evident 20.3 m below the water surface. Using Eq. 2.31 with the initial momentum flux and calculated buoyancy flux with ΔT = 1.31 °C, a terminal depth of 20 m below the water surface was calculated, which correlates well with the measured data.

Calculating the buoyancy flux for a range of ΔT from 0 to 10 °C and the initial conditions for the surface mixer, the terminal depth for the surface mixer efflux is plotted against ΔT (Fig. 6.15). Using Fig. 6.15 for the '800' surface mixer, where a maximum depth of 36 m occurs, a ΔT of 0.3 °C or greater will prevent the surface mixer efflux penetrating to the sediment surface.

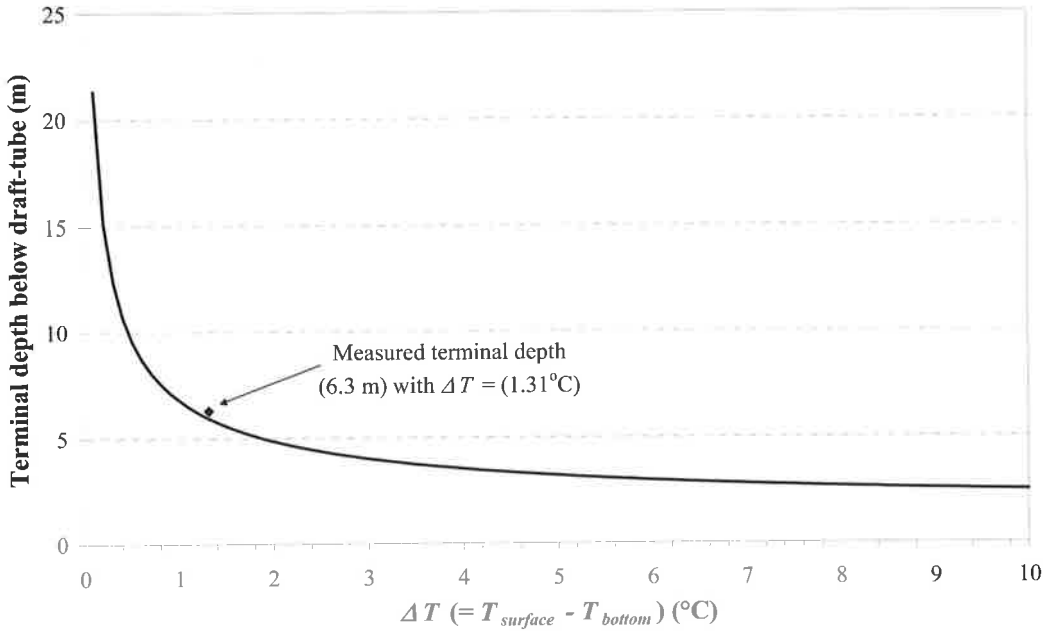

Figure 6.15 Predicted terminal depth of a buoyant surface mixer jet, using the initial conditions shown in Table 6.1.

To obtain a relationship to calculate the dilution of the surface mixer jet under stratified conditions a polynomial regression was fitted to the asymptotic solution ($R^2 = 1$) plotted in Fig. 2.4:

$$\overline{\mu}_T = 1\times10^5\zeta^4 - 0.0023\zeta^3 + 0.2322\zeta^2 + 0.6875\zeta \qquad (6.8)$$

where $\overline{\mu}_T$ is dimensionless dilution and ζ is dimensionless depth (Eq. 2.44). Using Eq. 6.8 the dilution of the surface mixer buoyant jet was calculated as a function of depth.

The surface mixer volume flux in the *ZEF* could not be calculated from the measured velocity profiles under permanently stratified conditions as the measured velocities were affected by the strong return flow originating at the terminal penetration depth. Consequently, the calculated volume flux under stratified conditions was compared to the measured volume flux under isothermal conditions to determine if there was any significant difference. Using the initial conditions from the measured data in Table 6.1 the comparison of the measured volume flux under isothermal conditions, the volume flux calculated using Eq. 2.37 and the volume flux determined using Eq. 6.8 is plotted in Fig. 6.16.

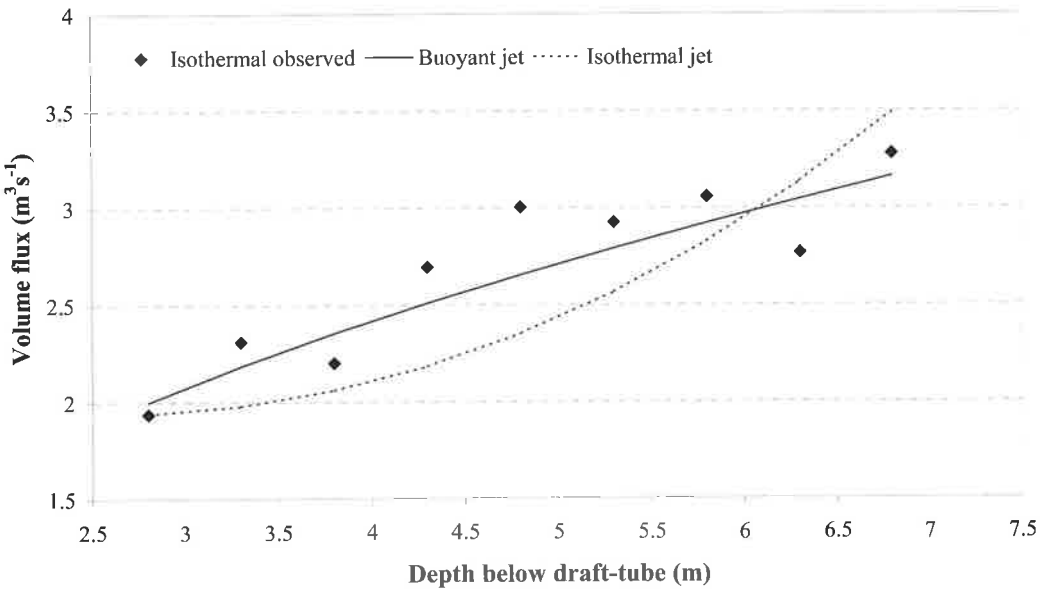

Figure 6.16 Measured volume flux compared with the calculated volume flux using the entrainment hypothesis, and the volume flux determined using Eq. 6.8.

The measured volume flux correlates sufficiently with both the volume fluxes calculated by Eq. 2.37 and Eq. 6.8 respectively; where $R^2_{\text{measured/Eq. 2.37}} = 0.82$ (*P-value* = 0.0008) and $R^2_{\text{measured/Eq. 6.8}} = 0.63$ (*P-value* = 0.001).

6.3.5 Detailed description of the swirling jet velocity components

The mean velocities have been separated into three distinct components, axial, tangential and radial. The presentation of the measured data shows only half of the jet as the flow was found to be axisymmetric. The following analysis was undertaken in

isothermal conditions and subsequently the only boundary effect to be accounted for was the jet impingement on the sediment surface. The distance between the draft-tube outlet and the sediment is approximately three times the diameter of the draft-tube orifice (3*D*). The limit of the *ADVField* measurements was 2.7*D*.

Mean axial velocity

Following the procedure of Pratte and Keffer (1972), the peripheral velocity of the impeller v_p (Eq. 6.9) is used to normalise the measured velocities shown in Figs 6.17 to 6.22, so that the surface mixer velocities could be compared with the results generated by Hyun and Patel (1991) and Petersson *et al.* (1996).

$$v_p = 2\pi r_0 \varpi \tag{6.9}$$

where ϖ is the rotational speed. The axial distance z measured from the exit of the draft-tube was normalised with the draft-tube diameter D, and the radial distance r from the jet centreline was normalised with the impeller radius r_0. The mean axial velocity within the zone of flow establishment is shown in Fig. 6.17. A contraction of the jet is evident at 0.1*D* where the jet has a radius of $r/r_0 \sim 0.81$, but no further contraction occurs downstream. The contraction occurs due to the initial entrainment of ambient water into the jet. For the surface mixer jet the contraction is not evident at 0.3*D* below the draft-tube outlet.

At distances less than 0.6*D* from the draft-tube outlet an obvious trough in the jet centre occurs. Centrifugal forces in the swirling jet and the blocking effect of the impeller hub culminate to create the trough. At 0.5*D* the maximum axial velocity occurs at $r/r_0 \approx 0.4$, which correlates well with literature where Petersson (1996) and Hyun and Patel (1991) found that the maximum axial velocity occurs at $r/r_0 \sim 0.5$, which corresponds to the position where the impeller blades produce maximum thrust.

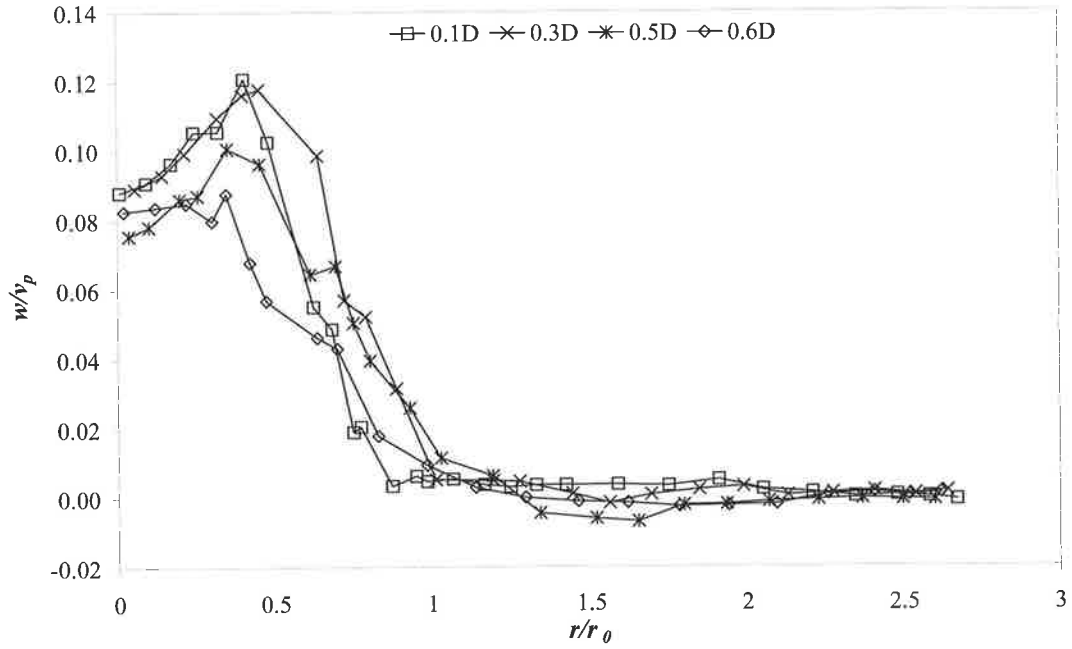

Figure 6.17 Mean axial velocity profiles in the *ZFE* at 4 locations beneath the draft-tube outlet ($z = 0.1D$, $0.3D$, $0.5D$, and $0.6D$).

The *ZEF* for the surface mixer jet started at a streamwise location of ~ $0.6D$ where a Gaussian profile developed and w_{max} occurred on the jet centreline. Using the radial spread based on the radial distance r_e where $w = w_{max}/e$, the *ZEF* started at ~ $0.6D$ (Section 6.3.3). The axial velocity profiles in the *ZEF* for the surface mixer jet are shown in Fig. 6.18. The steady decay of the centreline axial velocity is evident in the *ZEF* up to $2.7D$ below the draft-tube outlet (~27.5 m below surface) corresponding to the limit of the *ADVField* measurements, whereupon the jet impinged upon the sediment surface.

At radial distances $r/r_0 > 1$, negative velocities were observed in both the *ZFE* and *ZEF*. These occurred outside the jet radius and were attributed to turbulence within the entrainment region between the jet and the ambient water.

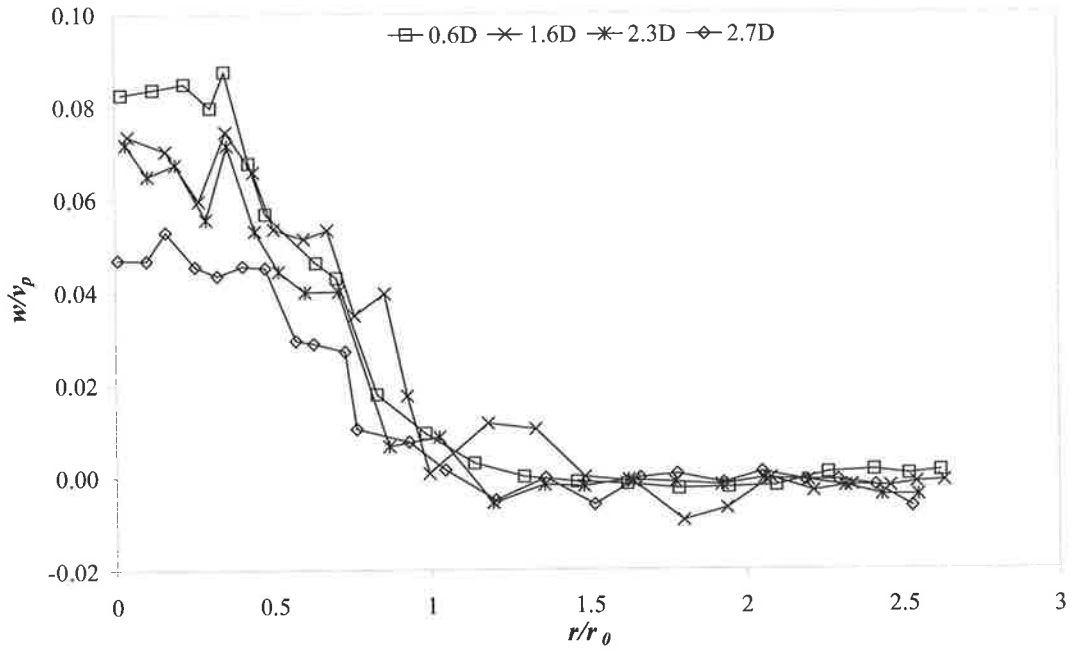

Figure 6.18 Mean axial velocity profiles in the *ZEF* at 4 locations beneath the draft-tube outlet (z = 0.6D, 1.6D, 2.3D, and 2.7D).

Mean tangential velocity

The mean tangential velocity for the surface mixer jet in the *ZFE* showed that v_{max} occurred at $r/R_0 \sim 0$ to 0.1 (Fig. 6.19), which is typical of free vortex rotation where the maximum tangential velocity occurs along the jet centreline. There are no distinct peaks in the profiles that can be attributed to the impeller blades or the impeller hub radius as detected by Petersson *et al.* (1996) and Hyun and Patel (1991), who reported that these peaks occur in the *ZFE* occurred at $r/R_0 \sim 0.65$ and $r/R_0 \sim 0.15$ respectively.

The tangential flow in the *ZEF* is typical of Rankine combined vortex rotation where the tangential velocity is ~0 m s^{-1} at the jet centreline which increases to a maximum at the jet radius (defined previously) then gradually decreases away from the jet (Fig. 6.20). At the limit of the *ADVField* measurements (2.7D) no significant decrease in swirl was detected.

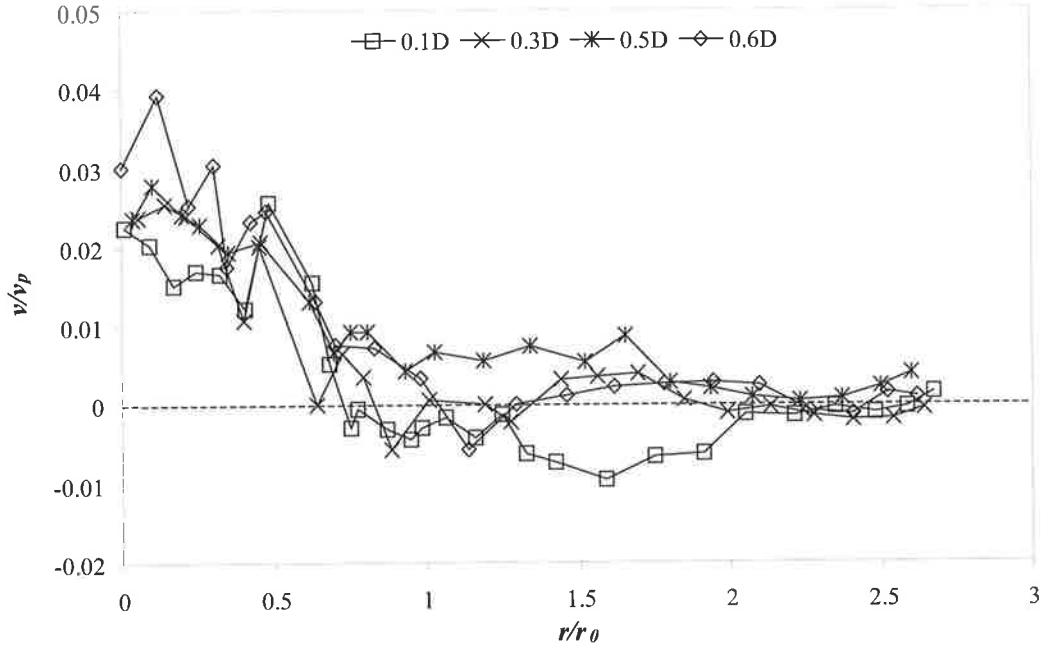

Figure 6.19 Mean tangential velocity profiles in the *ZFE* for the surface mixer jet showing free vortex rotation characteristics.

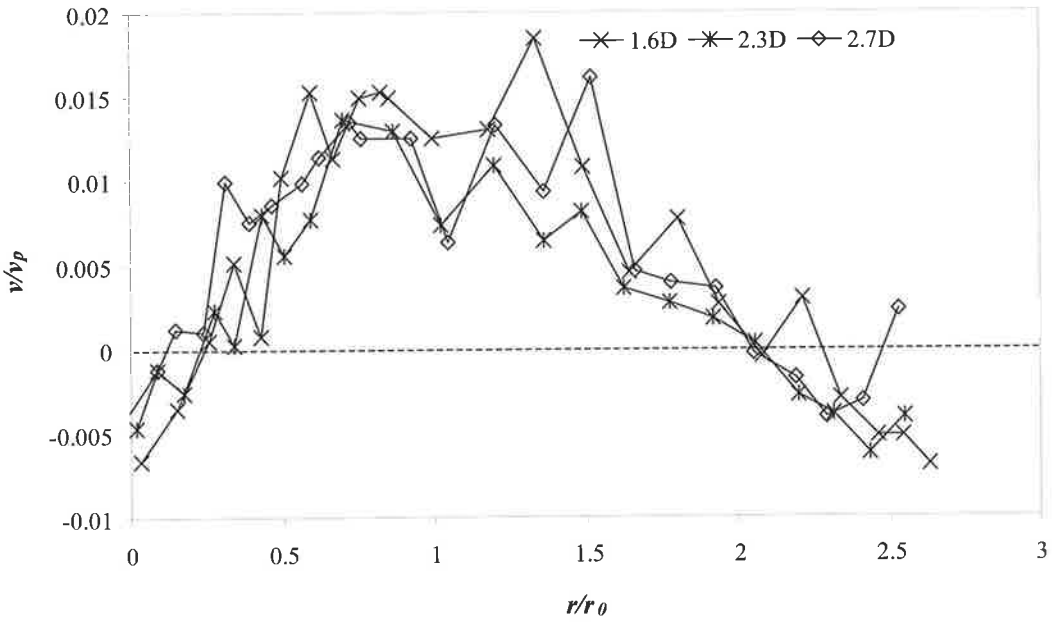

Figure 6.20 Mean tangential velocity profiles in the *ZEF* for the surface mixer jet that can be represented by Rankine combined vortex rotation.

Mean radial velocity

The surface mixer jet mean radial velocity profiles in the *ZFE* and *ZEF* are shown in Fig. 6.21 and Fig. 6.22 respectively. A positive velocity represents flow out from the jet centre. In the *ZFE* the radial velocity acted towards the jet centre that was attributed to the radial pressure gradient established by the swirl.

As the surface mixer jet spread in the *ZEF* and the radial velocities decreased to below 0.03 m s^{-1}, the magnitude of the radial velocity was difficult to detect due to the low and fluctuating velocity gradients. The negative radial velocities near the jet radius represent the entrainment into the jet. At the jet centre, symmetry implies that radial velocity should be zero. Although the velocities near the jet centre are low, flow was still detected due to the fluctuation of the jet.

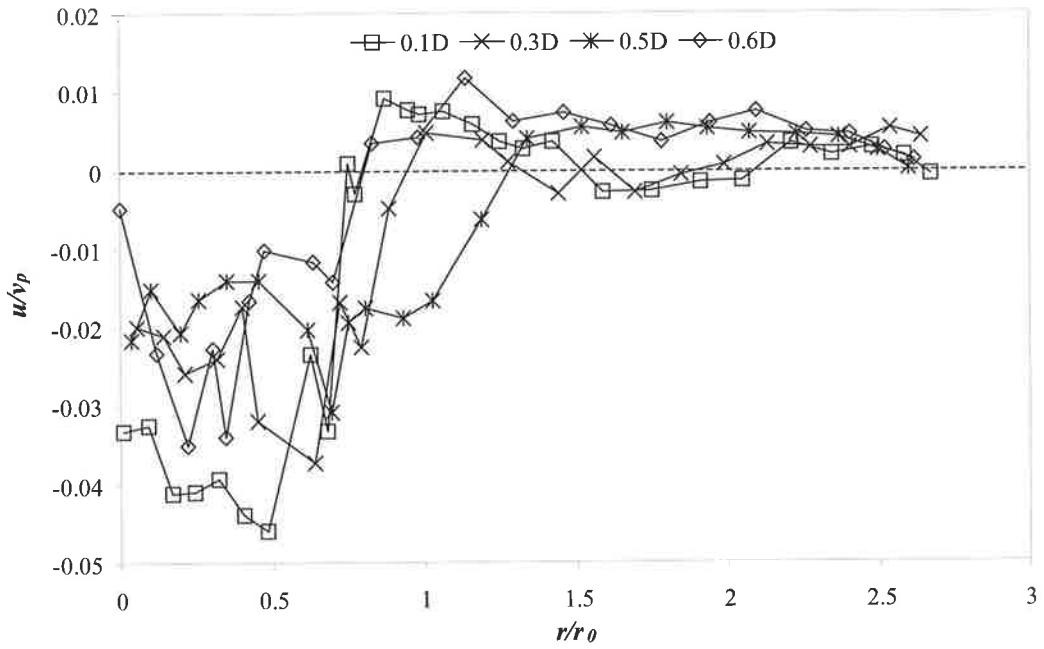

Figure 6.21 Mean radial velocity profiles in the *ZFE*.

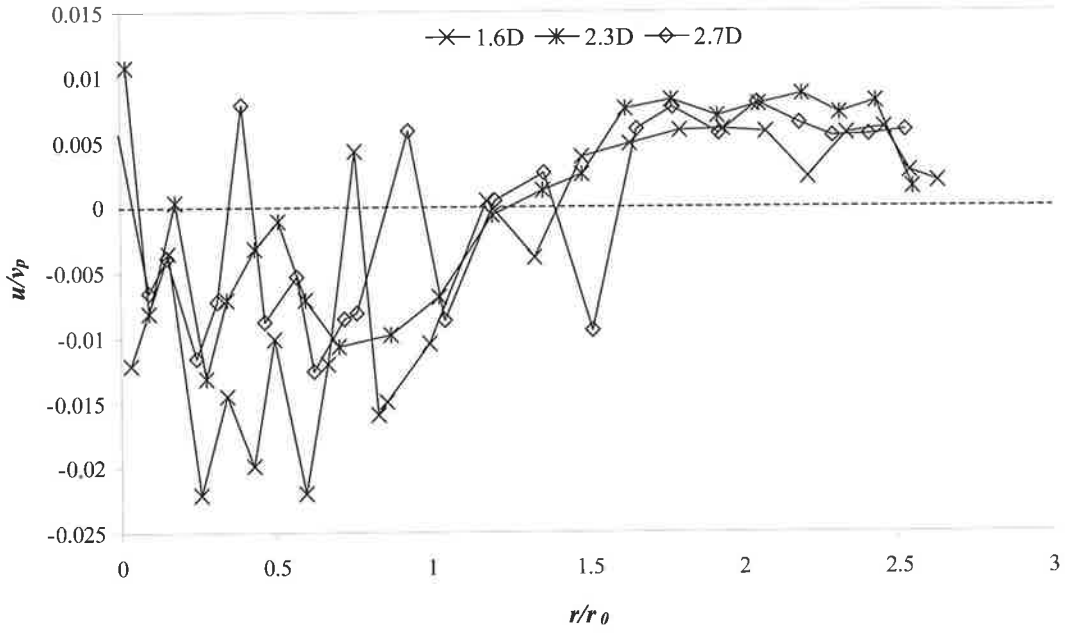

Figure 6.22 Mean radial velocity profiles in the *ZEF*.

Turbulent intensity

The turbulent intensity in the surface mixer jet was calculated from the measured mean velocities. The root-mean-square (*RMS*) turbulence in the axial direction is calculated by:

$$w_{rms} = \sqrt{\overline{(w')^2}} = \sqrt{\frac{\sum w^2 - \left(\sum w\right)^2 / n}{n-1}} \qquad (6.10)$$

where n is the number of samples. Eq. 6.10 was also used for the tangential and radial velocities. Turbulent intensity is related to the mixing energy stored in the velocity field (Petersson, 1996). The *RMS* turbulence results from this study were correlated against phytoplankton metabolic activity in a concurrent project undertaken by a fellow PhD scholar, Rudi Regel. Measurements of metabolic activity and viability of phytoplankton above and below the surface mixers revealed that transport and subsequent exposure to small-scale shear had no impact on the phytoplankton. The data is presented here for completeness and was found to be typical for an impeller generated swirling jet.

The turbulent intensities in the *ZFE* in the axial, tangential and radial directions at selected downstream locations are normalised with the peripheral velocity of the impeller and are plotted in Fig. 6.23. In the surface mixer jet the turbulent intensity was higher than the ambient and all three components demonstrated peaks in magnitude at $r/r_0 \approx 0.5$ to 0.8, corresponding to the location of maximum radial velocities.

As the flow developed in the *ZEF* the normalised off centre peak turbulent intensities reduced by ~0.5 (Fig. 6.24). The turbulence achieved self-similarity, i.e. the *RMS* turbulence does not vary with spatial scale, at a greater distance downstream than the mean velocities. The normalised turbulent intensities stabilise and the overall magnitude decreased in the streamwise direction. The normalised *RMS* turbulence values in the radial and tangential directions were approximately equal (~0.3), as expected due to symmetry (Pratte and Keffer, 1972). Beyond the jet radius in both the *ZFE* and the *ZEF* the *RMS* turbulence was non-zero. This was attributed to the entrainment flows generated outside the jet flow path.

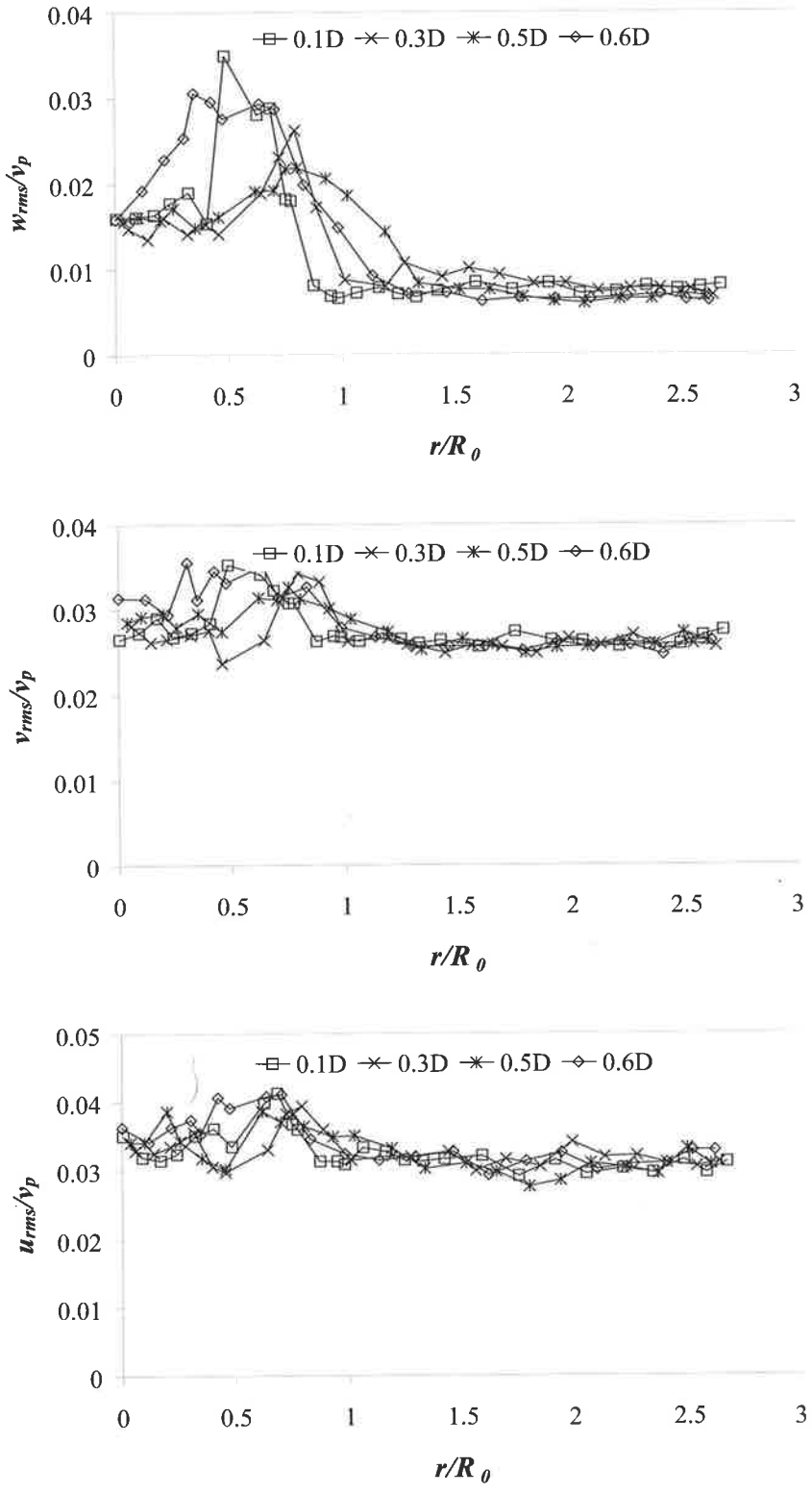

Figure 6.23 Turbulent intensity in the *ZFE*: a) axial, b) tangential, and c) radial directions.

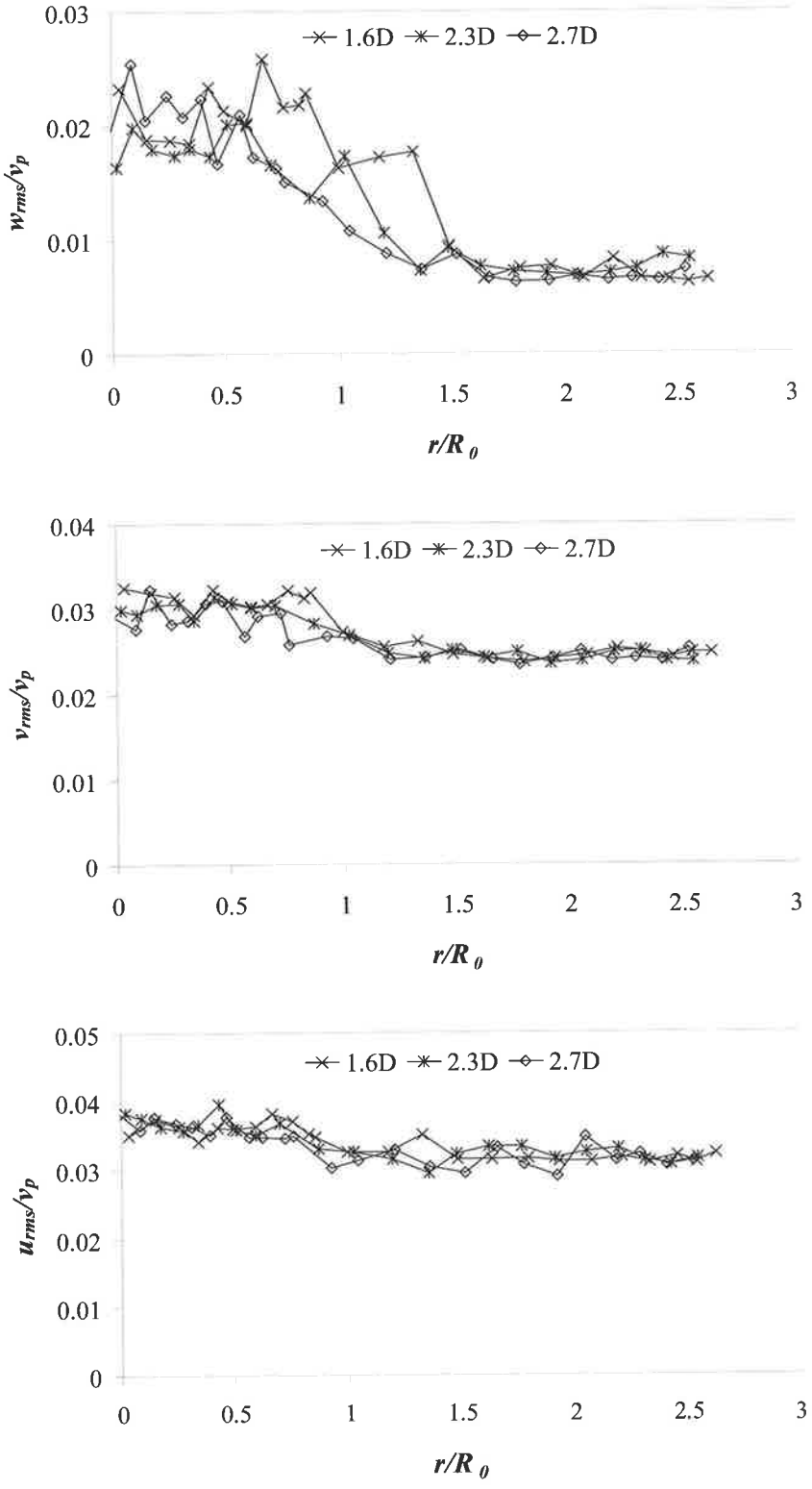

Figure 6.24 Turbulent intensity in the *ZEF*: a) axial, b) tangential, and c) radial directions.

6.3.6 Self-similarity and Decay

The *ZEF* for the surface mixer starts at approximately 0.6*D*, where the maximum axial velocity occurred on the jet centreline and the mean axial velocity profile kept the same form but became wider and lower as downstream distance increased. To investigate the approach towards self-similarity the axial velocity was normalised with w_{max} at selected streamwise locations. The radial location r was normalised with $(z + a)$, where a is the location of the virtual origin (see below). The non-dimensionalised axial velocity, w/w_{max}, is plotted against the non-dimensionalised radial distance, $r/(z + a)$, in Fig. 6.25.

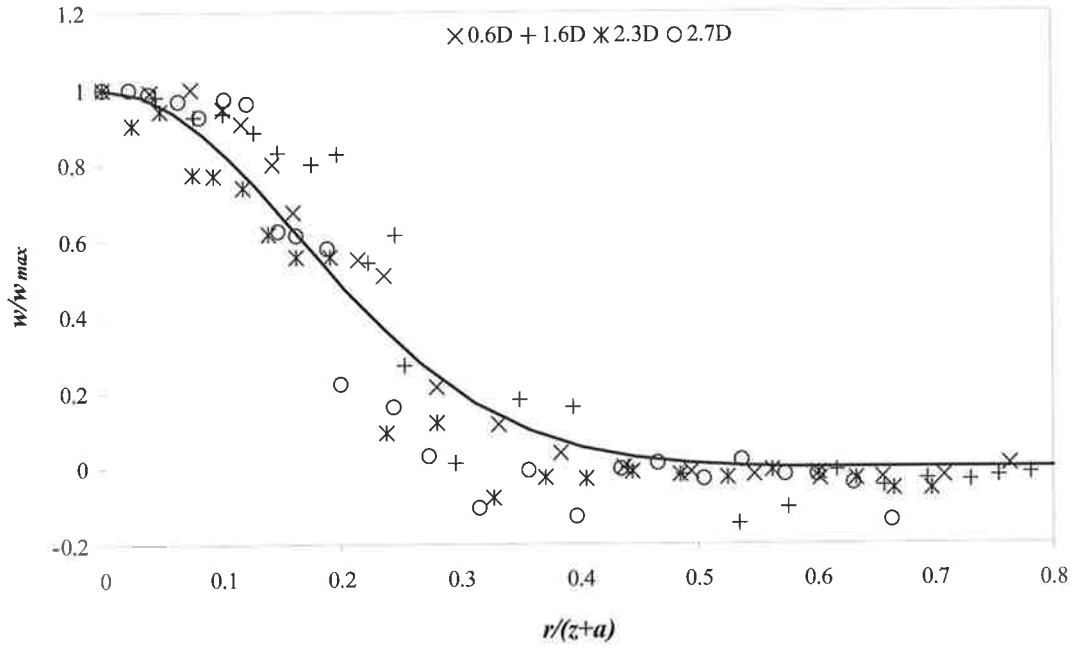

Figure 6.25 Normalised mean axial velocity profile in the *ZEF* with a least-squares Gaussian profile.

A least-square Gaussian curve was fitted to the data, and is given by:

$$\frac{w}{w_{max}} = e^{-k\left(r/(z+a)\right)^2} \tag{6.11}$$

where k is an empirical coefficient for swirling jets. The empirical constant for the Gaussian profile shown in Fig. 6.25 was determined to have a value of 18 ($R^2 = 94$),

thus allowing the axial velocity distribution to be determined in the *ZEF* at distances greater than 2.7*D*. Petersson *et al.* (2000) reported $k = 41$ for a swirling jet developed by an impeller ($\varpi = 1500$ rpm) in a closed tank. The value of k is independent of the impeller speed and as k increases the profile of the swirling jet becomes narrower (Petersson *et al.*, 1996).

Virtual origin

The virtual origin may be considered as a point source upstream of angular and axial momentum with zero mass that generates an equivalent jet in the *ZEF* as developed by the surface mixer. To determine the location of the virtual origin of the surface mixer jet a straight line was extrapolated back from the measured radial spread in the *ZEF* on the axis of symmetry, defined as the virtual origin (Figs. 6.13 and 6.27). The virtual origin, which is a function of the radial spread of the jet, was calculated to be ~6.2 m below the reservoir surface, giving a virtual origin ($a \sim 1.6D$) upstream the draft-tube orifice, which is similar to the results found by Petersson *et al.* (1996), which was located at 2*D*, Chigier and Chervinsky (1967) at 2.3 *D*, and Pratte and Keffer (1972) at 3*D*.

6.3.7 Far-field flow

The far-field flow pattern generated by the surface mixers (Fig. 6.26) is typical of a horizontal intrusion flow. Under both stratified and isothermal conditions the flow generated by the surface mixers will ultimately penetrate horizontally through the reservoir. If the reservoir is isothermal the surface mixer jet impinges and spreads radially along the sediment surface. Under stratified conditions the surface mixer flow is buoyant and will flow horizontally at a level of neutral buoyancy.

The radial velocity and temperature data in Fig. 6.26 was recorded along an eastern transect from the '800' surface mixer on the 20-February-2002 with a ΔT of ~1.2°C between the reservoir surface and bottom. The radial velocity in the intrusion generated by the surface mixers was clearly evident at 90 m from the surface mixer, and at 300 m the temperature profile shows a weakened *SML* that was also evident in the thermistor data at Met 1 (~400 m from the '800' surface mixer) that was attributed to natural cooling mechanisms.

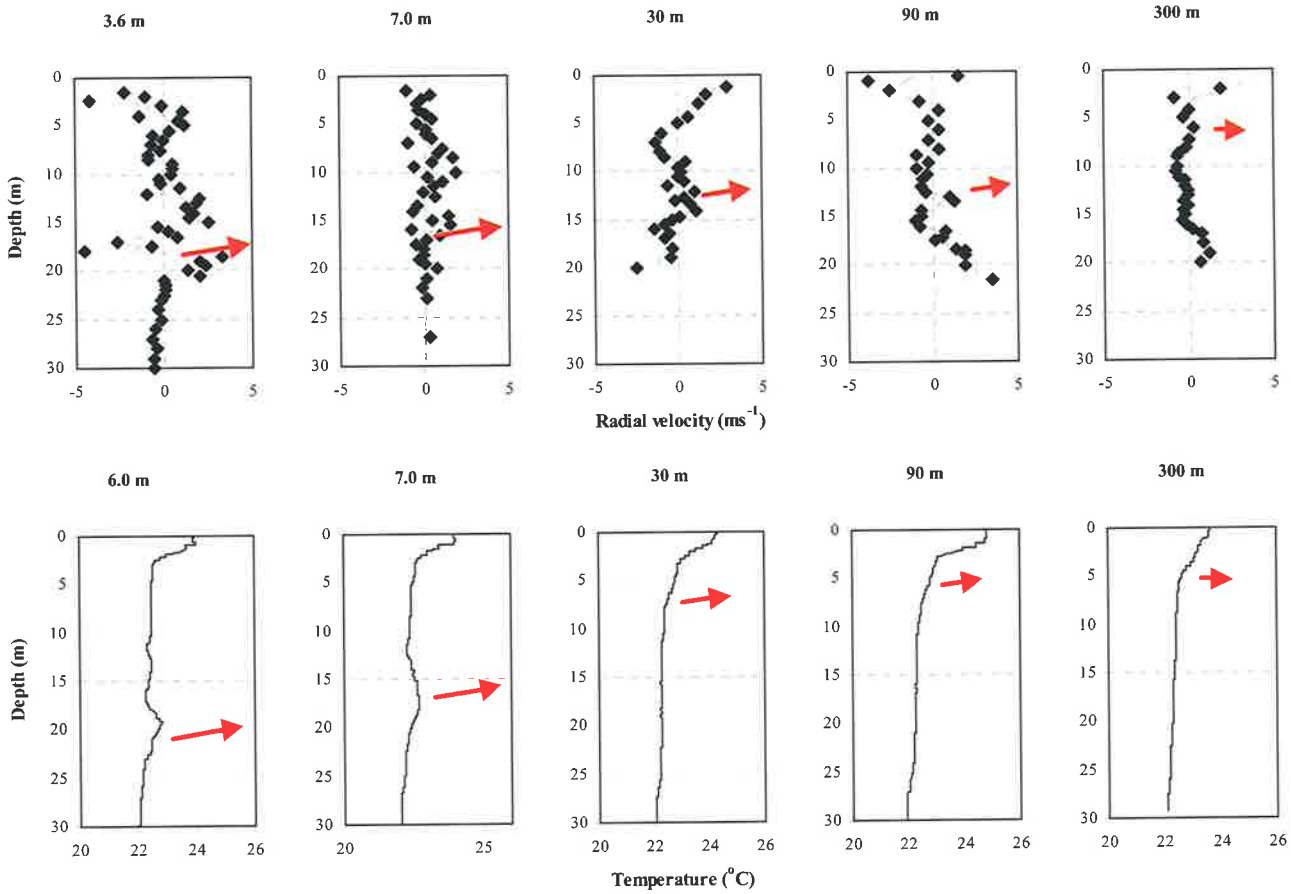

Figure 6.26 Far-field radial velocity (top row) and temperature (bottom row) profiles taken at the respective radial distance from the centre of the '800' surface mixer. The red arrows give a qualitative indication of the direction and magnitude of the intrusion flow generated by the surface mixer.

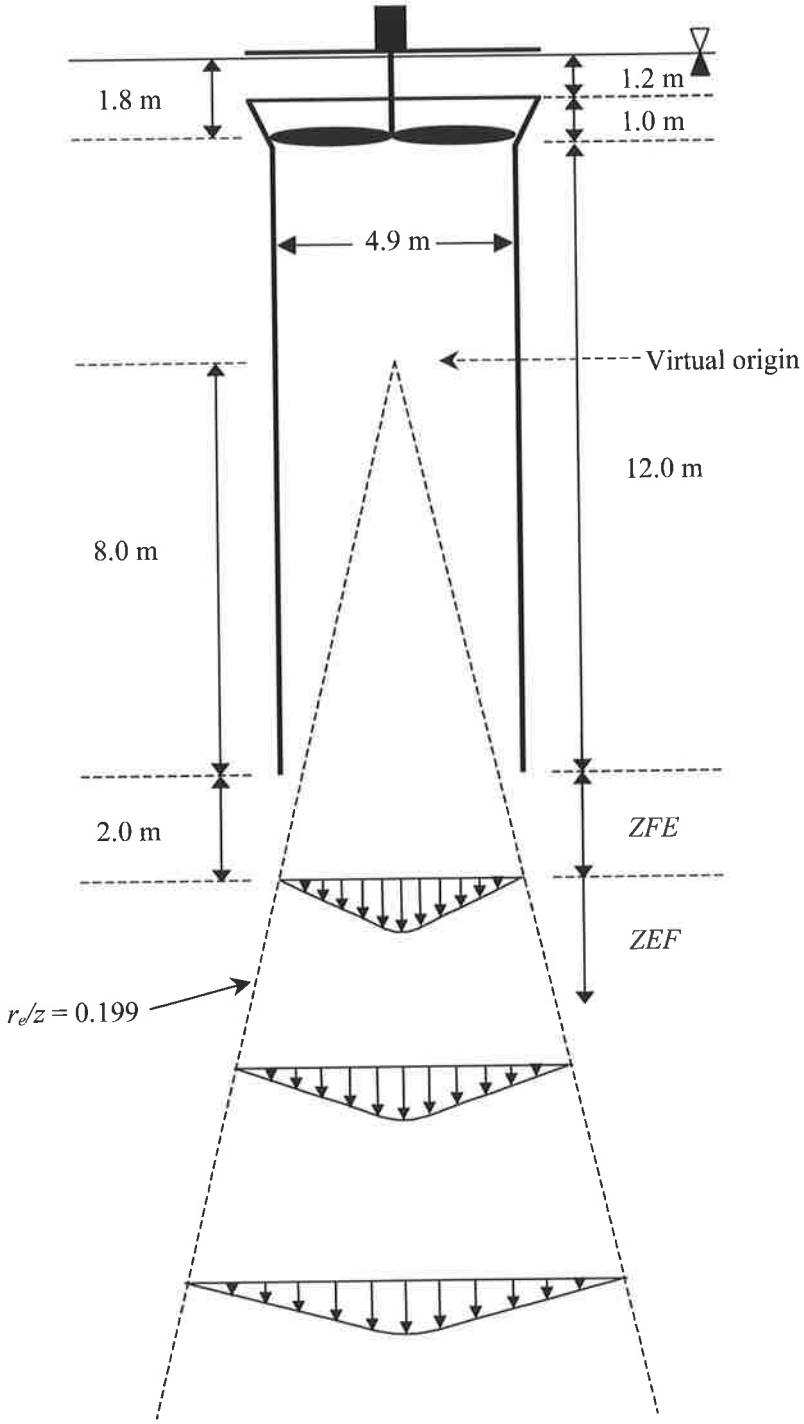

Figure 6.27 Virtual origin and spread of swirling jet exiting the surface mixer draft-tube. *ZFE* extends to 2 m below the draft-tube exit whereupon the *ZEF* is established.

6.4 CONCLUSIONS

The surface mixer efflux was examined during isothermal and stratified conditions in Myponga Reservoir by measuring the axial, radial and tangential velocities in near

and far-field locations. The surface mixers generated a large swirling jet with a Reynolds number in the order of 10^6 and a Swirl number of 0.2. Swirling jets of this magnitude have not been characterised prior to this study. The surface mixer efflux flow pattern is typical of a swirling turbulent jet generated by an impeller and the results compared favourably with the limited number of investigations that focus on the velocity fields generated by impellers (Chigier and Chervinsky, 1967; Petersson *et al.*, 2000; Pratte and Keffer, 1972).

Under isothermal conditions the streamwise flow quickly developed forming a typical Gaussian profile unique with axisymmetric swirling and non-swirling jets. The *ZFE* for the surface mixer flow was considerably shorter than that of swirling jets presented in the literature (Petersson *et al.*, 2000). The radial spread for the surface mixer flow under isothermal conditions was approximately three times that of a non-swirling jet and spread linearly at a half angle of 14.4°. The entrainment into the jet has been analysed and can be predicted under isothermal and stratified conditions. The entrainment hypothesis (Eq. 2.37) is adequate when the flow is isothermal and under stratified conditions the empirical relationships presented by Fischer (1979) (Fig. 2.4) accurately predict the dilution of the jet.

During stratified conditions the flow was difficult to characterise due to the return flow from the terminal depth where the flow literally turns on itself due to buoyancy. However, the terminal depth could be adequately predicted by using Eq. 2.31. The significant parameters characterising the surface mixer jet were the radial spread of the jet, length of the *ZFE*, commencement of the *ZEF* and the location of the virtual origin. These parameters are summarised in Fig. 6.27.

The results generated from this study enabled the fate of the surface water pumped through the surface mixers to be predicted under varying meteorological conditions. The analysis of the surface mixer flow enabled an algorithm to be developed that was incorporated into the one-dimensional lakes and reservoir simulation model DYRESM discussed in detail in Chapter 7.

7. DEVELOPMENT OF THE SURFACE MIXER ALGORITHM

7.1 INTRODUCTION

To aid informed choice when designing a destratification system for a water body, numerical models can be employed. Currently an aerator algorithm exists in the widely used hydrodynamic model DYRESM, described in detail in Chapter 2, enabling the impact of aeration systems upon the water body to be assessed during the design stage and for operational optimisation. The detailed surface mixer flow analysis (Chapter 6) was utilised to develop a surface mixer algorithm that was incorporated into DYRESM.

The aim of the surface mixer algorithm was to be able to determine the effectiveness of surface mixers under transient meteorological conditions, explore their destratification capabilities, and establish the impact of the surface mixers upon cyanobacteria growth, which is presented in the following chapter. To compliment DYRESM, the surface mixer algorithm needed to be universally applicable.

The development of the surface mixer algorithm was a two-stage process due to equipment limitations experienced during the course of the research. Based on initial flow measurements using a propeller meter mounted beneath the draft-tube an algorithm describing a plume was used to simulate the action of the surface mixers as a first approximation (Lewis *et al.*, 2001b). Subsequent *ADVField* measurements (Chapter 6) provided data that enhanced the algorithm thus taking into account entrainment due to the swirling characteristics, and penetration depth of the surface mixer efflux.

7.2 STAGE ONE - INITIAL FLOW ANALYSIS

Extensive near and far-field flow profiling was carried out during stratified and isothermal conditions around the '800' surface mixer at Myponga Reservoir to determine its flow field. The *ADVField* was suspended from a fixed mooring adjacent to the '800' surface mixer to measure the flow field, described in Chapter 3. Fig. 7.1 shows the vertical and radial flow through the water column at a radial distance of

3.8 m from the centre of the surface mixer, from 2.6 to 30 m below the surface. The profile was recorded on 28-August-2000, where a 2 °C temperature difference existed between the *SML* and the hypolimnion, signifying that the surface mixer efflux would be positively buoyant. Thus the flow exhibited buoyancy characteristics representing a buoyant plume. Negative horizontal flow is radially away from the surface mixer and negative vertical velocity is downwards. The horizontal flow generated by the surface mixer efflux is clearly evident (Fig. 7.1), where a radial intrusion has developed at a depth of approximately 17 m. The vertical flow shows an upward flow towards the surface mixer inlet from 13 m below the surface, and downwards flow from ~ 13 to 18.5 m. Beneath 18.5 no significant horizontal or vertical flow was evident.

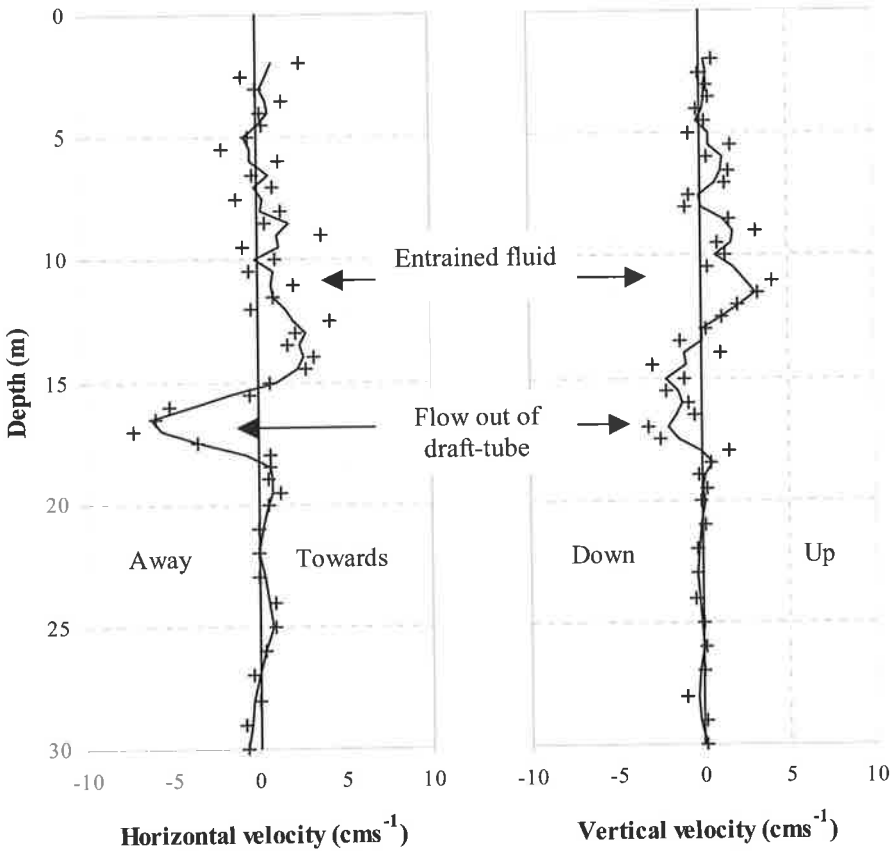

Figure 7.1 Near field *ADVField* measurements at 3.8 m from the centre of the surface mixer.

A plume is a flow that has the appearance of a jet, but is developed by a potential energy source, which provides the fluid with buoyancy (either negative or positive) relative to the ambient environment (List, 1982; Turner, 1966).

The initial flow measurements undertaken beneath the surface mixer draft-tube were carried out with a propeller meter (Section 6.2.3) mounted on a bracket and lowered underneath the draft-tube. Measurements were recorded across the diameter of the draft-tube at 0.3 m intervals. The measurements were recorded when a 4 °C temperature difference existed between the *SML* and the hypolimnion. The depth to which the flow penetrated below the draft-tube was ~1.8 m where no significant axial flow was detected (< 0.25 cm s^{-1}), shown in the velocity profiles plotted in Fig. 7.2. The flow profile measured immediately at the draft-tube exit showed a typical flow pattern downstream of an impeller. The data was limited due to not capturing the swirl and penetration of the flow. Nevertheless as a first approximation the results enabled an algorithm to be developed to simulate the action of the surface mixer.

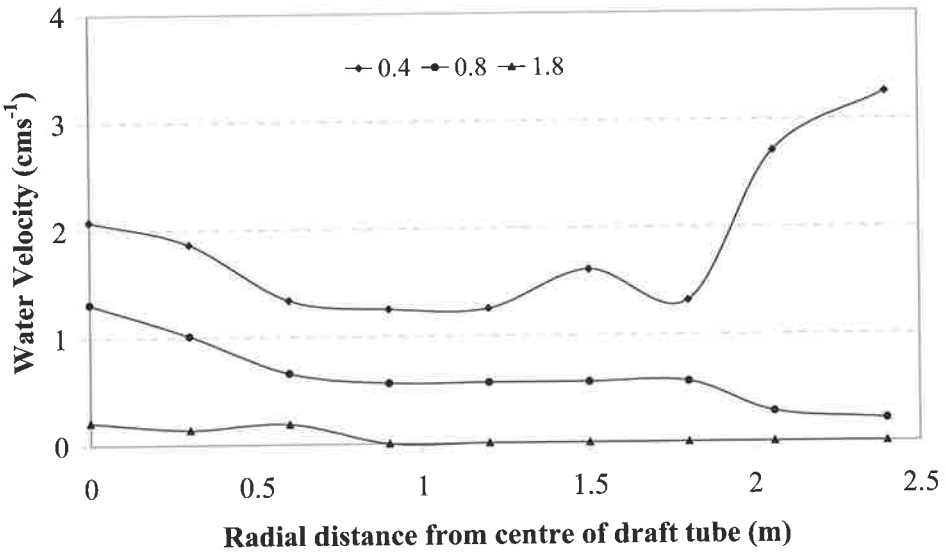

Figure 7.2 Averaged mean velocity exiting the '800' surface mixer measured at 0.4, 0.8 and 1.8 m directly below the draft-tube outlet, from the centre of the draft-tube to the outer radius.

Temperature profiling recorded on the 19-February-2000 and taken at regular intervals away from the surface mixer supported the buoyant plume hypothesis. See Chapter 2 for detailed information pertaining to the collection of this data. This was illustrated by the formation of a horizontal intrusion at a depth of ~ 17. 5 m, at a radial distance of 7 m from the centre of the surface mixer draft-tube, shown in Fig. 7.3. As radial distance from the centre of the draft-tube increased the radial buoyant

horizontal intrusion decreased in magnitude and raised to a level of neutral buoyancy at ~7 m below the surface at approximately 55 m from the centre of the '800' surface mixer.

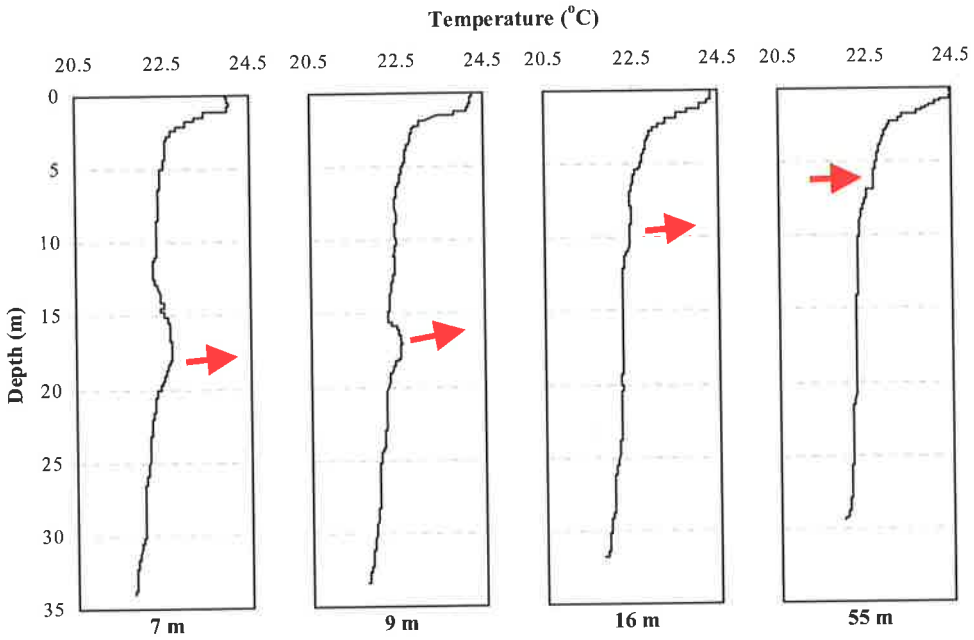

Figure 7.3 Temperature profiles taken on 19-February-2001, from left to right recorded at 7, 9, 16 and 55 m from the centre of the '800' surface mixer. The surface temperature was 24.5 °C and the bottom temperature was 21.8 °C.

7.2.1 Initial surface mixer algorithm

The initial surface mixer algorithm was based on a simple buoyant plane plume, with the plume geometry corresponding to the base of the draft-tube, i.e. πD where D is the diameter of the draft-tube. The surface mixer draws water from the top 1.2 m of the water body, which emerges as a radial plume at the base of the draft-tube. The density of the inflow to the surface mixer is assumed to be less than or equal to the ambient water at the exit of the draft-tube. As the plume rises through the water column it entrains water from the surrounding environment, thus increasing the density of the plume. As the density increases the plume velocity decreases until the point of neutral buoyancy is reached where horizontal insertion occurs. The buoyancy flux ($m^4 s^{-3}$) of the plume is defined by:

$$B_P = g\frac{(\rho_{ambient} - \rho_{efflux})}{\rho_{efflux}}\frac{Q_P}{\pi D} \tag{7.1}$$

In which ρ_{efflux} is the density of the surface mixer efflux that is assumed to have the same properties as the *SML*, $\rho_{ambient}$ is the density of the water corresponding to the draft-tube exit depth and Q_P is the volume flux of the plume that is initially equal to the volumetric flow being pumped by the surface mixer impeller, Q_{mixer}. The plane plume equation for Q_P is based predominantly on the comprehensive experimental investigation of Kotsovinos and List (1977) and is given by:

$$Q_P = 3.32\left(\frac{\alpha}{2}\right)\sqrt[3]{B_P}(\pi D)z \tag{7.2}$$

where z is the depth and α is the entrainment coefficient for plane plumes (0.083) (Fischer *et al.*, 1979), that is divided by 2 as entrainment will not occur on the inside of the plume due to it rising against the external wall of the draft-tube. The coefficient in Eq. 7.2 implies that 33 % of the flux is turbulent transport while 66 % is due to the mean flow (Fischer *et al.*, 1979). In DYRESM the plume buoyancy flux is calculated at each layer (j) by:

$$B_j = g\frac{(\rho_j - \rho_{j-1})}{\rho_{j-1}}\frac{Q_{P_{j-1}}}{\pi D} \tag{7.3}$$

Starting at the discharge layer the subsequent volume flux is given by:

$$Q_{P_j} = 3.32\left(\frac{\alpha}{2}\right)\sqrt[3]{B_{P_j}}(\pi D)(z_j - z_{j-1}) + Q_{P_{j-1}} \tag{7.4}$$

where at the discharge layer $Q_{P_{j-1}} = Q_{mixer}$ and $\rho_{j-1} = \rho_{efflux}$.

The initial surface mixer algorithm used the following assumptions:

1. No initial momentum exists in the surface water entering the surface mixer.
2. The available impeller energy is always able to pump the surface water down to the outlet of the draft-tube.
3. The flow exiting the draft-tube has no jet characteristics.
4. The attributes of the internal draft-tube flow are the same as the surface water.

To test the surface mixer algorithm Myponga Reservoir was simulated from September-1999 to September-2000 using hourly averaged meteorological data generating a daily output at midday. A comparison of the measured temperature profile to the simulated data taken at 1200 midday on the 18-January-2000 is shown in Fig. 7.4. The measured temperature profile was taken from the Met 1, where the reservoir is at its deepest (36 m), see Chapter 3. The example shown in Fig. 7.4 demonstrates that with the use of the aerator algorithm only, a reasonable match between simulated and observed data was obtained resulting with a R^2 of 0.93 (*P-value* = 5E-13). However, when the surface mixer algorithm was used in conjunction with the aerator algorithm an improved fit was obtained (R^2 = 0.95, *P-value* = 4E-15). The addition of the surface mixer improved the match between the observed and simulated data at a depth of ~7 m, where the intrusion developed by the surface mixer was shown to impact upon the *SML*. Comparisons were made at daily intervals and the same degree of accuracy was observed. These comparisons are not shown as the surface mixer algorithm was improved and a detailed analysis is provided in Section 7.3.

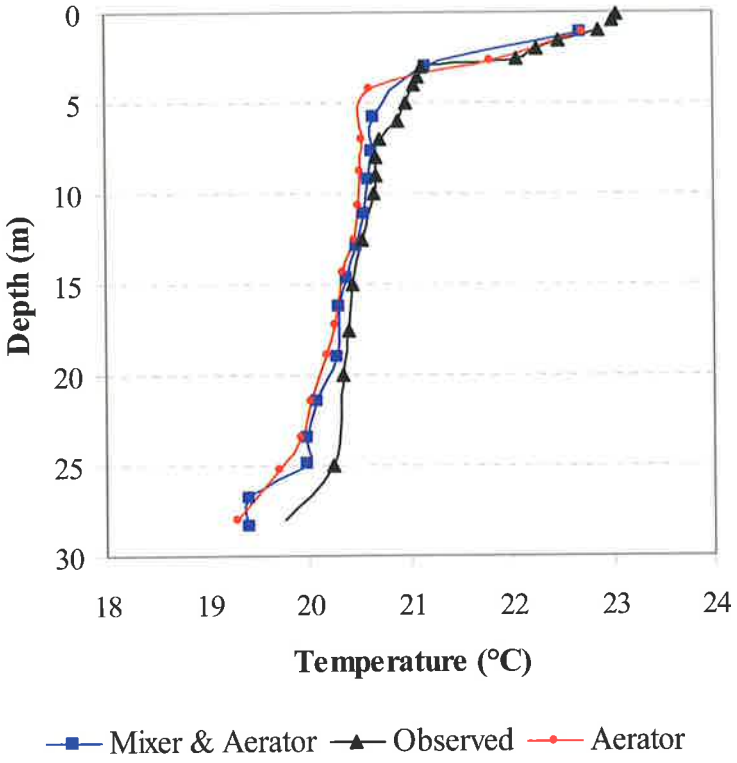

Figure 7.4 Simulated and observed temperature profiles for Myponga Reservoir at midday 18-January-2000, under artificially mixed conditions. Linear regressions were fitted to the (1) Mixer & Aerator/Observed results and (2) Aerator/Observed results. R^2 (1) = 0.96 (*P-value* = 4E-15) and R^2 (2) = 0.93 (*P-value* = 5E-13).

The validation of the surface mixer algorithm against temperature data was satisfactory, but the surface mixer algorithm did not permit the surface mixer efflux to penetrate below the depth of the draft-tube. Subsequently, the overall physical, biological and chemical impacts of the surface mixers could not be adequately investigated. The limitation with the original surface mixer algorithm was that the re-oxygenation and transport of phytoplankton into the hypolimnion could not be examined, as the simulated surface mixer efflux would not penetrate into the hypolimnion. Subsequently further profiling of the surface mixer efflux with the *ADVField* outlined in Chapter 3 showed that the efflux penetrated the water column to considerable depth and the surface mixer algorithm was modified to accommodate this.

7.3 STAGE TWO - MODIFIED SURFACE MIXER ALGORITHM

The improvement of the surface mixer algorithm was achieved by incorporating the calculation of the terminal depth, Eq. 7.5, from the ratio of initial momentum to initial buoyancy flux using Eq. 2.31, originally proposed by Turner (1966), which was validated against field data, presented in Chapter 6. The terminal depth was required to be included in the algorithm to ensure that the associated mixing, transport of phytoplankton and re-oxygenation of the hypolimnion is captured within the model.

$$z_m = 1.43\left(M_{efflux}\right)^{3/4}\left(B_{efflux}\right)^{-1/2} \tag{7.5}$$

Eqs 7.6 and 7.7 were employed to calculate the buoyancy and momentum fluxes respectively:

$$B_{efflux} = g\left(\frac{\rho_{ambient} - \rho_{efflux}}{\rho_{efflux}}\right)Q_{mixer} \tag{7.6}$$

and,

$$M_{efflux} = \frac{\pi}{4}D^2\left(z_{efflux}\right)^2 \tag{7.7}$$

where the velocity z_{efflux} is the mean axial velocity calculated from Q_{mixer}. The implementation of Eqs 7.5, 7.6 and 7.7 in DYRESM, calculates the terminal depth of the surface mixer efflux. The calculated depth is assigned to the depth of the draft-tube to initiate the depth at which the plume starts. This gives the surface mixer algorithm jet characteristics that include the initial entrainment of the efflux and radial spread as it penetrates to its terminal depth. If the calculated terminal depth is greater than the depth of the water body, then the terminal depth is assigned the value for the depth of the water body. The dilution of the surface mixer efflux is calculated using Eq. 6.8.

7.3.1 Detailed description of the surface mixer algorithm

The surface mixer algorithm flowchart, presented in Fig. 7.5, details the mathematical description of the flow exiting the surface mixer draft-tube. Initially the algorithm is invoked in the DYRESM configuration file by indicating with a TRUE/FALSE statement if artificial mixing is to be used during the simulation. If TRUE, the destratification file containing the initial conditions for the surface mixer is accessed. The destratification file requires the surface mixer dimensions; namely draft-tube diameter and length, and pumping capabilities including period of operation. At the start of each time-step, when the simulated surface mixer is in operation, the initial conditions are calculated and assigned, i.e. volume flux, $Q_{mixer} = Q_j$; momentum flux, M_j; buoyancy flux, B_j; surface temperature, T_N; discharge temperature, T_j; draft-tube diameter, D_j; depth of draft-tube exit, z_j (where the subscripts relate to the Lagrangian layer system within DYRESM).

Using the initial conditions the terminal depth of the surface mixer efflux is calculated (Eq. 7.5) and if the terminal depth is greater than the depth of the water body then the terminal depth is assigned to the maximum depth of the water body. As the surface mixer efflux penetrates to the terminal depth jet entrainment is calculated using Eq. 2.37. The volumetric flow is updated and the radial spread is calculated.

At the terminal depth the surface mixer efflux reverses direction and has plume characteristics. Buoyancy causes the plume to rise and dilution with ambient fluid occurs. At each layer the temperature of the plume is checked with the corresponding layer temperature until the temperatures are equal where the resulting plume layer volume is inserted. The layer thickness is adjusted and the existing DYRESM meteorological forcing functions are invoked. The surface mixer algorithm is repeated at each time-step whilst activated via the destratification file. The existing aerator algorithm operates concurrently with the surface mixer algorithm. Multiple surface mixers can be modelled simultaneously, with the capacity for each individual surface mixer having a unique configuration.

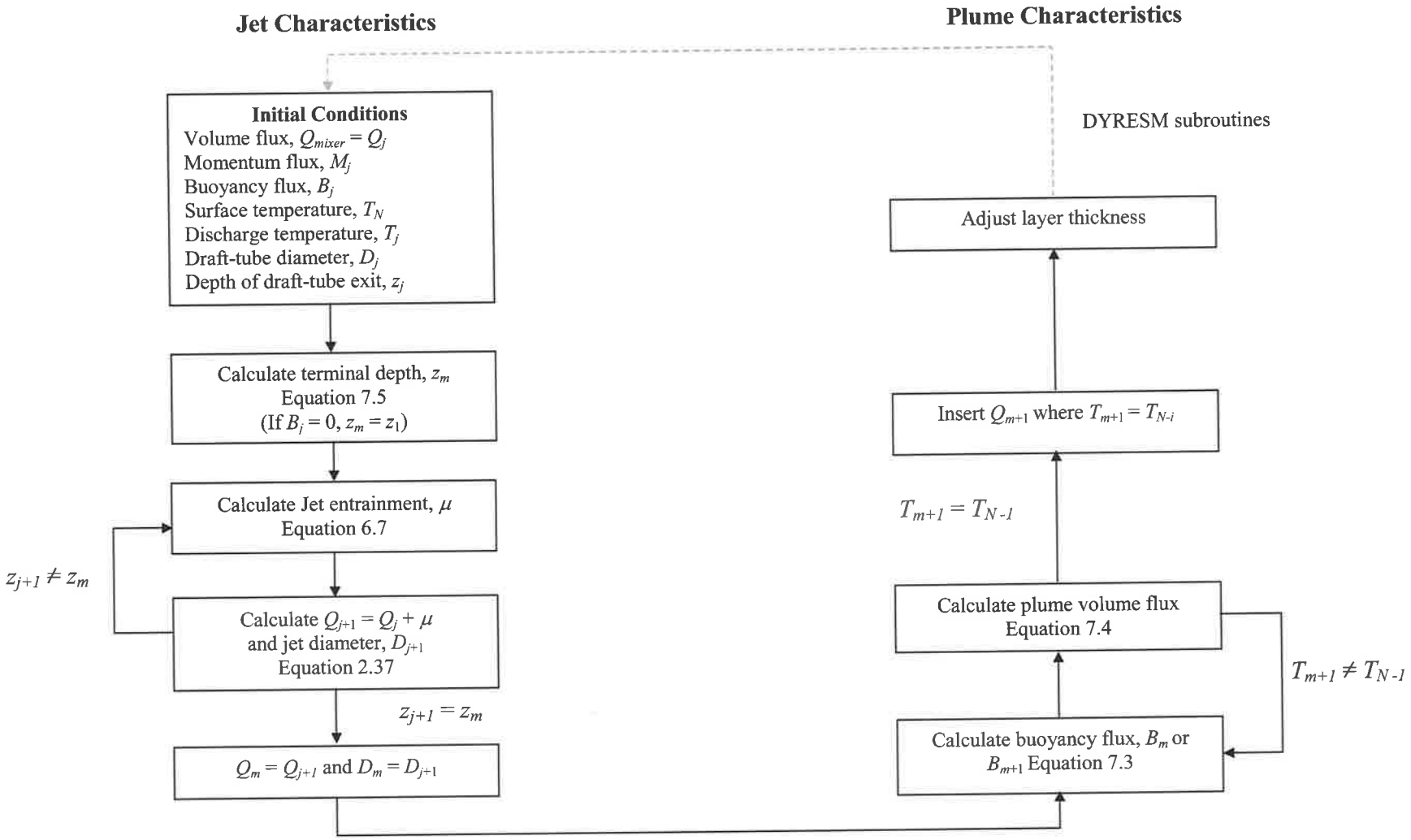

Figure 7.5 Surface mixer algorithm flowchart.

7.4 Simulation of Temperature Stratification at Myponga Reservoir

Myponga Reservoir was modelled with DYRESM with the artificial destratification algorithms (aerator and Stage 2 surface mixer algorithms) from 1-September-1999 to 1-September-2000. Sub-daily meteorological data was inputted into DYRESM with a time-step of 3600s.

For clarity averaged daily meteorological data is shown in Figs. 7.6, 7.7 and 7.8. The daily data depicted is typical meteorological data expected at 35°S latitude, where the shortwave radiation, daily temperature and average wind speed follow a similar seasonal cycle (shown as trend-lines in Figs. 7.6, 7.7 and 7.8). DYRESM requires shortwave and net longwave radiation, ambient air temperature and average wind speed at the appropriate time-step. The input files used in the DYRESM simulation are provided in Appendix D.

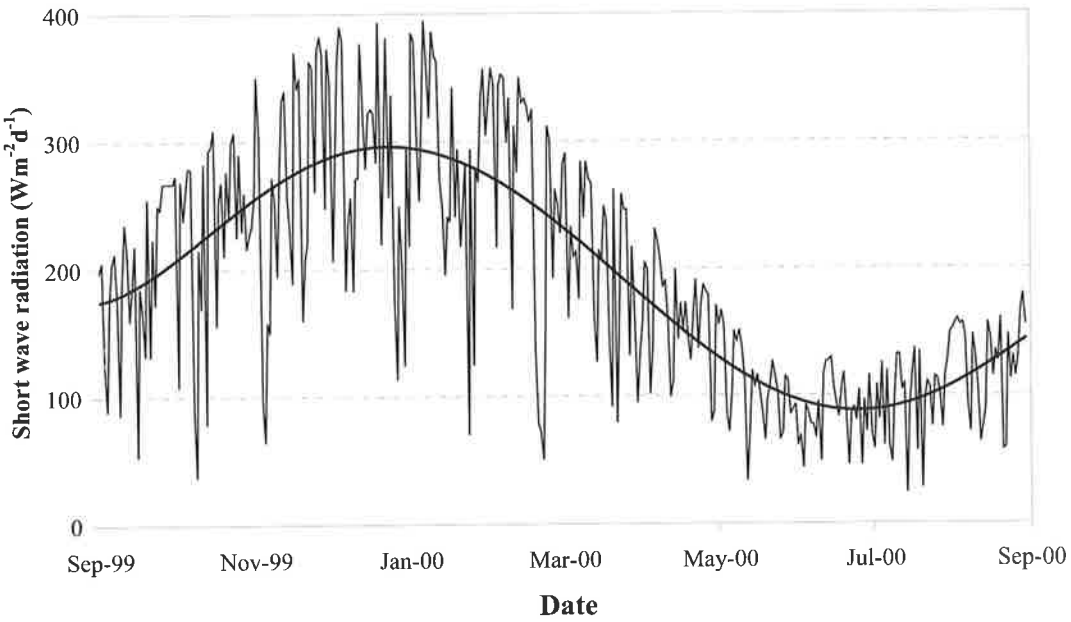

Figure 7.6 Daily average shortwave radiation data measured at Met 1, Myponga Reservoir, from September-1999 to September-2000.

The inflow was gauged on Myponga River and outflow data includes both spillway overflow and consumption (Fig. 7.9). The majority of consumption occurs during the

summer months, whilst spillway overflow occurs late winter and spring after periods of high rainfall and reduced consumption.

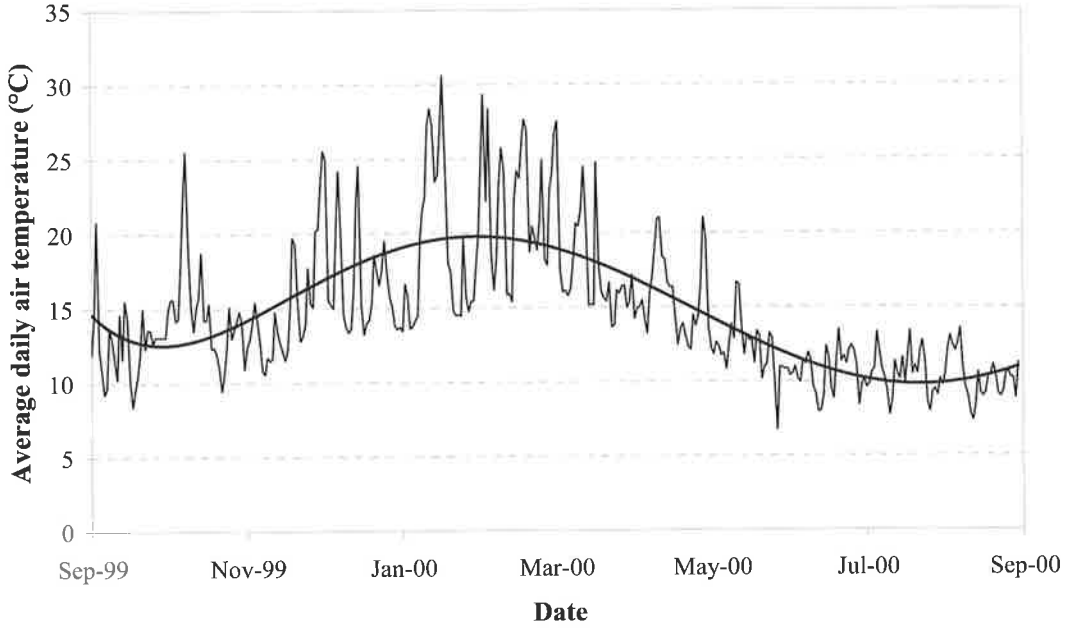

Figure 7.7 Daily average air temperature data measured at Met 1, Myponga Reservoir, from September-1999 to September-2000.

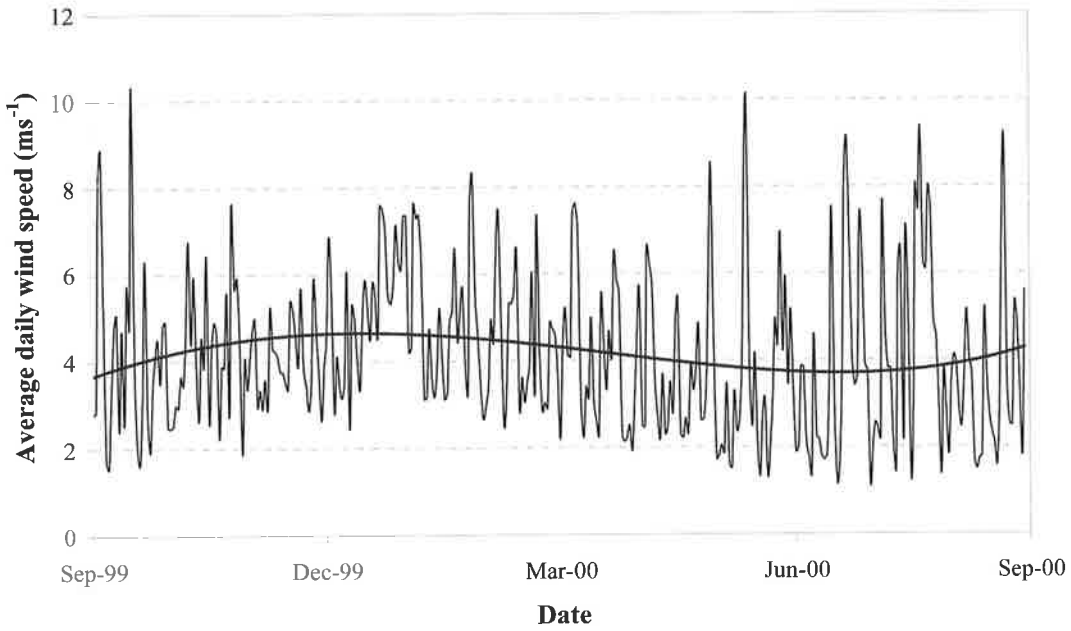

Figure 7.8 Daily average wind speed data measured at Met 1, Myponga Reservoir, from September-1999 to September-2000.

The simulated operation of the aerator and surface mixers were invoked on the same days as their actual operation in Myponga Reservoir during the simulated period. The days of operation for these devices are shown in Fig. 7.10, where the continuous line corresponds to the device being switched on. Also shown is the period when $CuSO_4$ dosing occurred, which importantly shows that artificial mixing devices were switched off during this period.

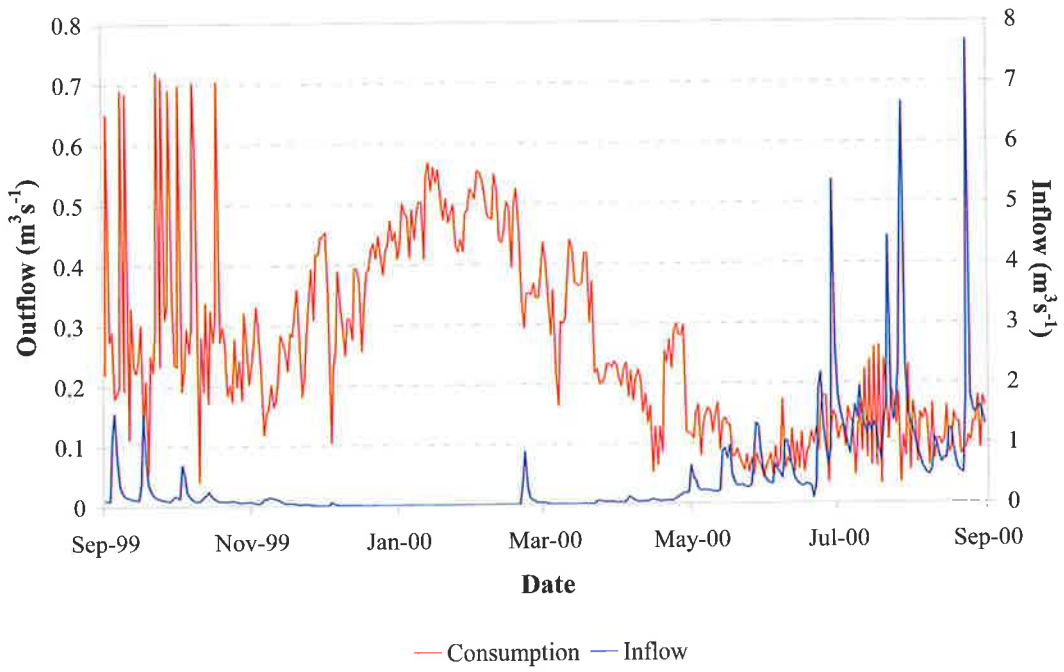

Figure 7.9 Myponga Reservoir inflow and outflow (consumption and spillway overflow).

The validation of the simulation, presented in Sections 7.4.1 and 7.4.2, enabled the surface mixer algorithm to be verified whilst giving insight of the impact of destratification at Myponga Reservoir on the annual heating and cooling cycle, whereupon CAEDYM could be invoked to investigate subsequent water quality issues. Upon successful validation the operation of the aerator and surface mixers could be manipulated to determine their effectiveness under different operational strategies. The specifications used to model the aerator and surface mixers (described in detail in Chapter 3) are shown in Table 7.1.

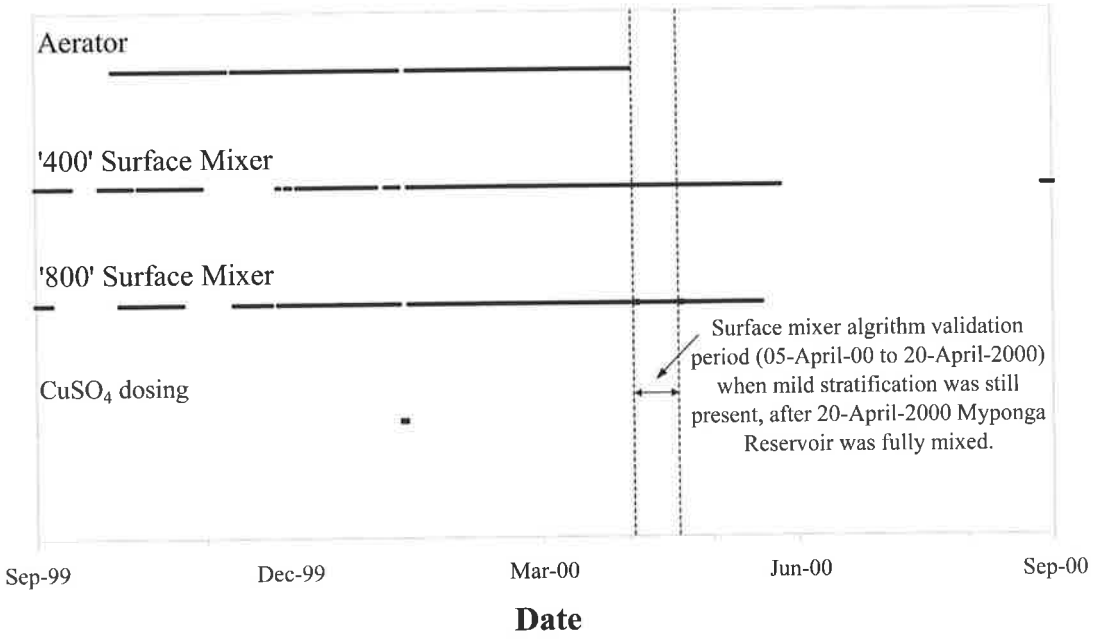

Figure 7.10 Operation schedule for artificial mixing and $CuSO_4$ dosing (denoted by solid lines) at Myponga Reservoir from 1-September-1999 to 1-September-2000.

Table 7.1 Artificial destratification system specifications.

Surface mixers (2)		**Aerator** (1)	
Draft-tube length	14.2 m	Diffuser height	0 m
Draft-tube diameter	4.9 m	Diffuser ports	160
Flow rate	3.5 m s^{-1}	Air flow rate	0.0468 m s^{-1}

7.4.1 Surface mixer algorithm validation

The validation of the surface mixer algorithm against field data was restricted to short periods throughout their operational history, as the aerator was always operated concurrently with the surface mixers when risk of stratification existed. At the time of the study the operational capabilities of the surface mixers was unproven, and management at Myponga Reservoir were not prepared to shutdown the aerator in case water quality became degraded. The chosen period to test the surface mixer algorithm was between 5-April-2000 and 20-April-2000 when the aerator was switched off, but surface heating was still evident. The water column was weakly stratified during this

period with a maximum temperature differential of 1.5 °C between the surface and sediment.

The simulated data closely matched the observed data; four comparisons during the modelled period are shown in Fig. 7.11. The depth of the modelled *SML* was captured in the simulation, however the simulated hypolimnion temperature profiles showed isothermal conditions which were not so pronounced in the field data, although the differences in temperature between the simulated and observed hypolimnetic regions are in the order of tenths of degrees. The depth at which the modelled surface mixer efflux reaches neutral buoyancy is between 5 to 7 m, which is evident in Fig. 7.11, closely matching the field data at the corresponding depth.

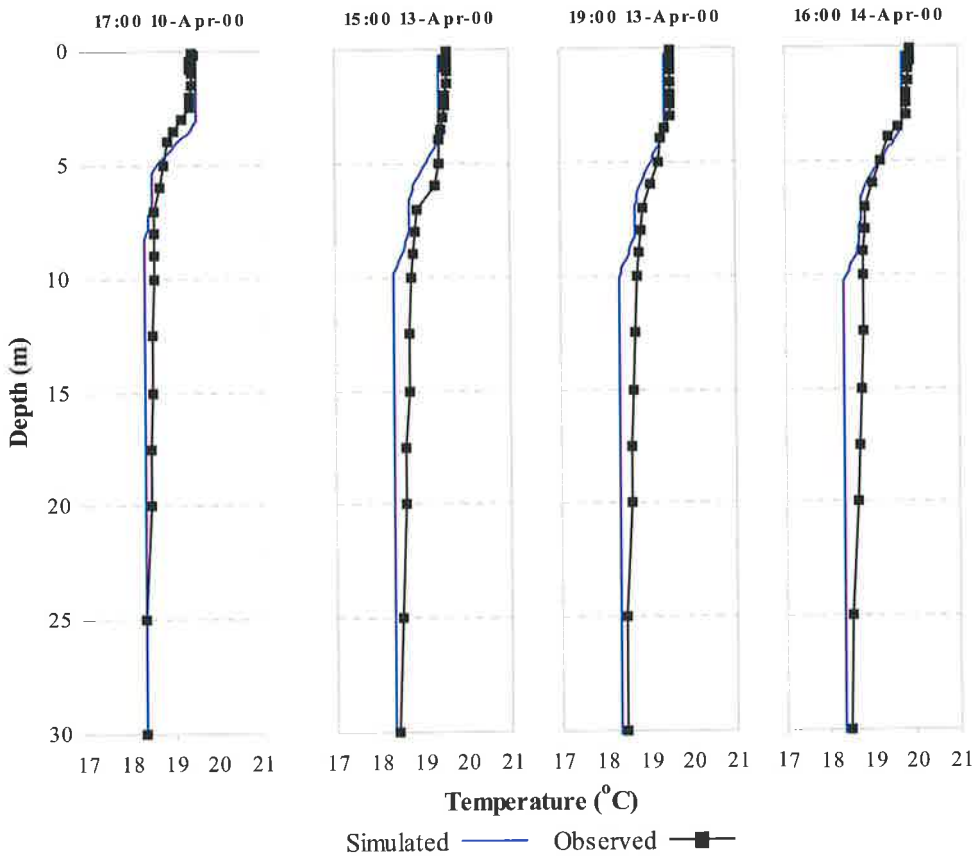

Figure 7.11 Comparison of selected observed and simulated temperature profiles between 5-April-2000 and 20-April-2000 when thermal stratification was present and the surface mixers were in operation, with R^2 and *P-values* of 0.96, 2E-08 (17:00 10-April-2000); 0.94, 3E-07 (15:00 13-April-2000); 0.95, 5E-08 (19:00 13-April-2000); and 0.94, 1E-08 (16:00 14-April-2000) respectively.

To further validate the surface mixer algorithm, temperature profile contour plots were used, which show comparisons between the midday simulated and observed field temperature data (taken from Met 1 thermistor data, Chapter 3) between 5-April-2000 and 1-May-2000, shown in Fig. 7.12.

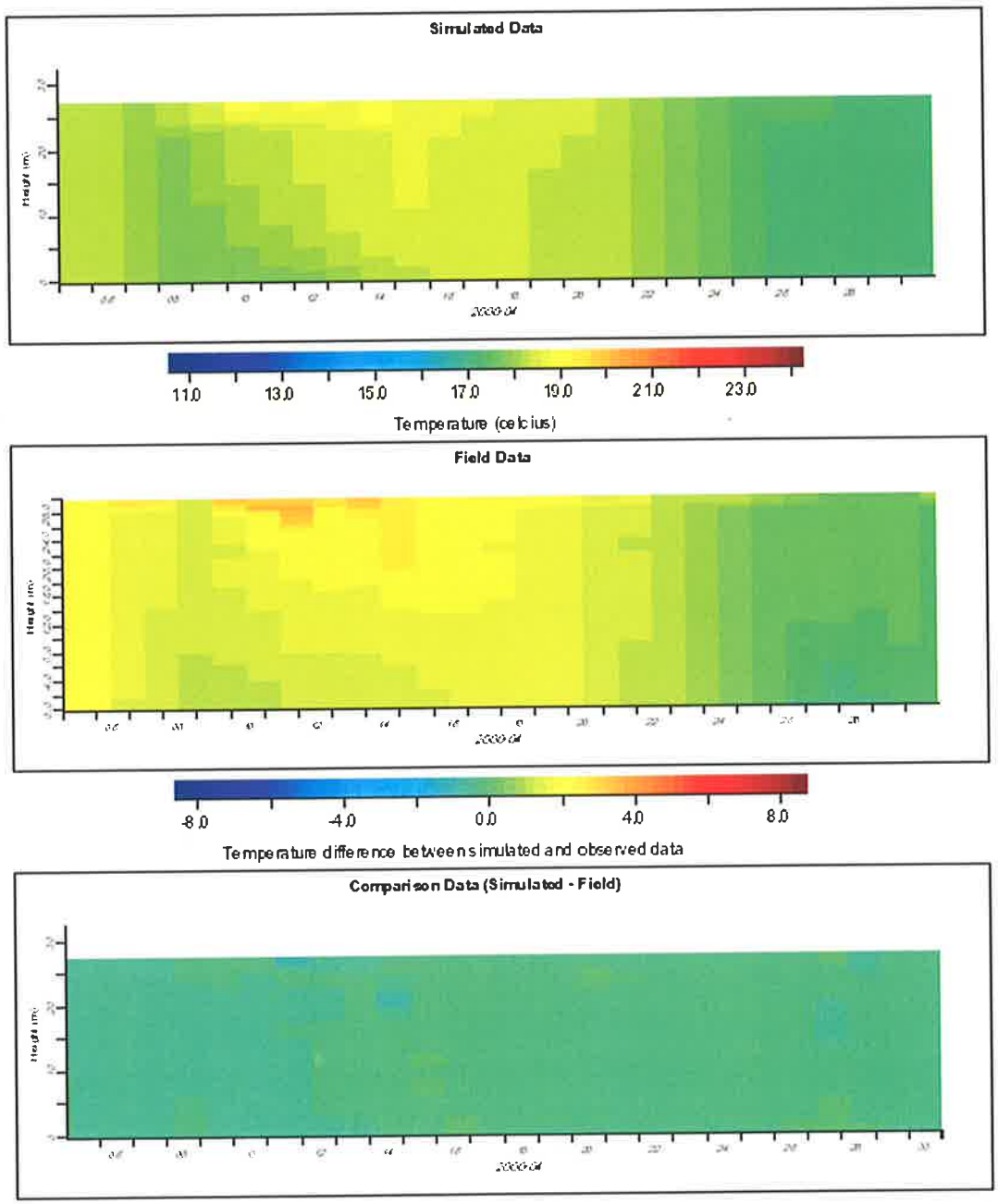

Figure 7.12 Daily temperature contours between the observed and simulated temperature, taken at midday when insolation is high, from 5-April-2000 to 1-May-2000.

The largest discrepancies occurred in the surface layer where temperatures differed up to ~ 0.5 °C. Deeper in the water column, temperature differences were less severe, ranging from 0 to 0.5 °C. Overall the temperature differences were less than 0.2 °C throughout the water column. As a final check of the surface mixer algorithm, the aerator and surface mixer algorithms were both switched off on the 5-April-2000 to determine if the resulting temperature structure would be significantly different when the simulated surface mixers were still operating. The subsequent temperature profile contours 5-April-2000 to 1-May-2000 are shown in Fig. 7.13.

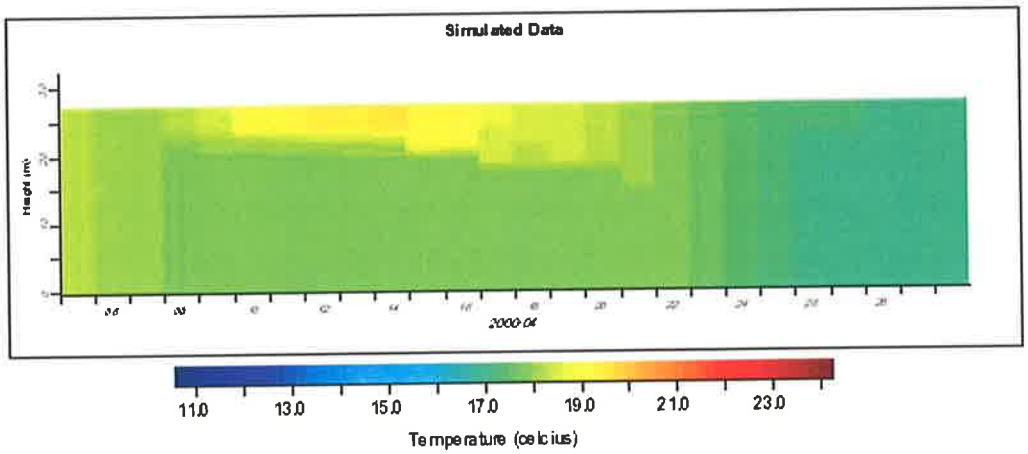

Figure 7.13 Daily simulated temperature contours from 5-April-2000 to 1-May-2000, with artificial mixing switched off on the 5-April-2000.

Without the operation of the simulated surface mixers after 5-April-2000 significant stratified conditions persisted up to the 20-April-2000, differing significantly from the data presented in Fig. 7.12, where weak stratification occurred.

The validation of the surface mixer algorithm based on the temperature profiles was satisfactory, high R^2 values and *P-values* << 0.01 were obtained when comparison of temperature profiles was undertaken. The temperature difference contour plot shown in Fig. 7.12 shows that the largest temperature differences were restricted to less than 0.5 °C and a high degree of accuracy was obtained. Due to DYRESM being a one-dimensional model and the measured temperature data being temporal, the simulation of the surface mixer algorithm was deemed to be sufficient as the overall temperature

structure was reproduced in the simulation with the depth of the thermocline consistently reproduced.

7.4.2 Validation of the simulated period from September-1999 to September-2000

The simulation output time was set to midday (43200 s, seconds from midnight) and compared with measured temperature data recorded at Met 1 for the entire modelled period. The observed and simulated temperature distribution contours are shown in Fig. 7.14, and selected temperature profiles are shown in Fig. 7.15. The annual thermal structure was satisfactorily modelled, with the annual heating and cooling cycle being reproduced. The heating of Myponga Reservoir through spring 1999 and early summer 2000 culminates with permanent stratification occurring for short periods (days to weeks) from January to April-2000, even though artificial mixing was operational. It is during these periods that the risk of cyanobacteria growth and depletion of oxygen in the hypolimnion is increased, which is investigated in the following chapter. Artificial mixing is in operation from early September to early May (Fig. 7.10). As solar insolation increases temperature gradients in the water column develop and minor diurnal stratification occurs. At the height of summer permanent stratification can occur.

The heating and cooling cycle at Myponga Reservoir is reproduced in the simulated data and the timing of permanent stratification is captured (Fig. 7.14). The comparison data confirms the accuracy of the simulation where temperature differences between the observed and simulated data were generally less than 1 °C. The results show that significant stratified conditions were limited to very short periods (days) under the current artificial mixing regime employed at Myponga Reservoir. The simulated data slightly underestimated the temperature in the lower regions of the water body, but did adequately capture the temperature dynamics and depth of the *SML* during the simulated period. As solar radiation decreased in magnitude, Myponga Reservoir begun to cool and the thermal structure was weakened, resulting in an isothermal structure. This was duplicated in both timing and magnitude in the simulation.

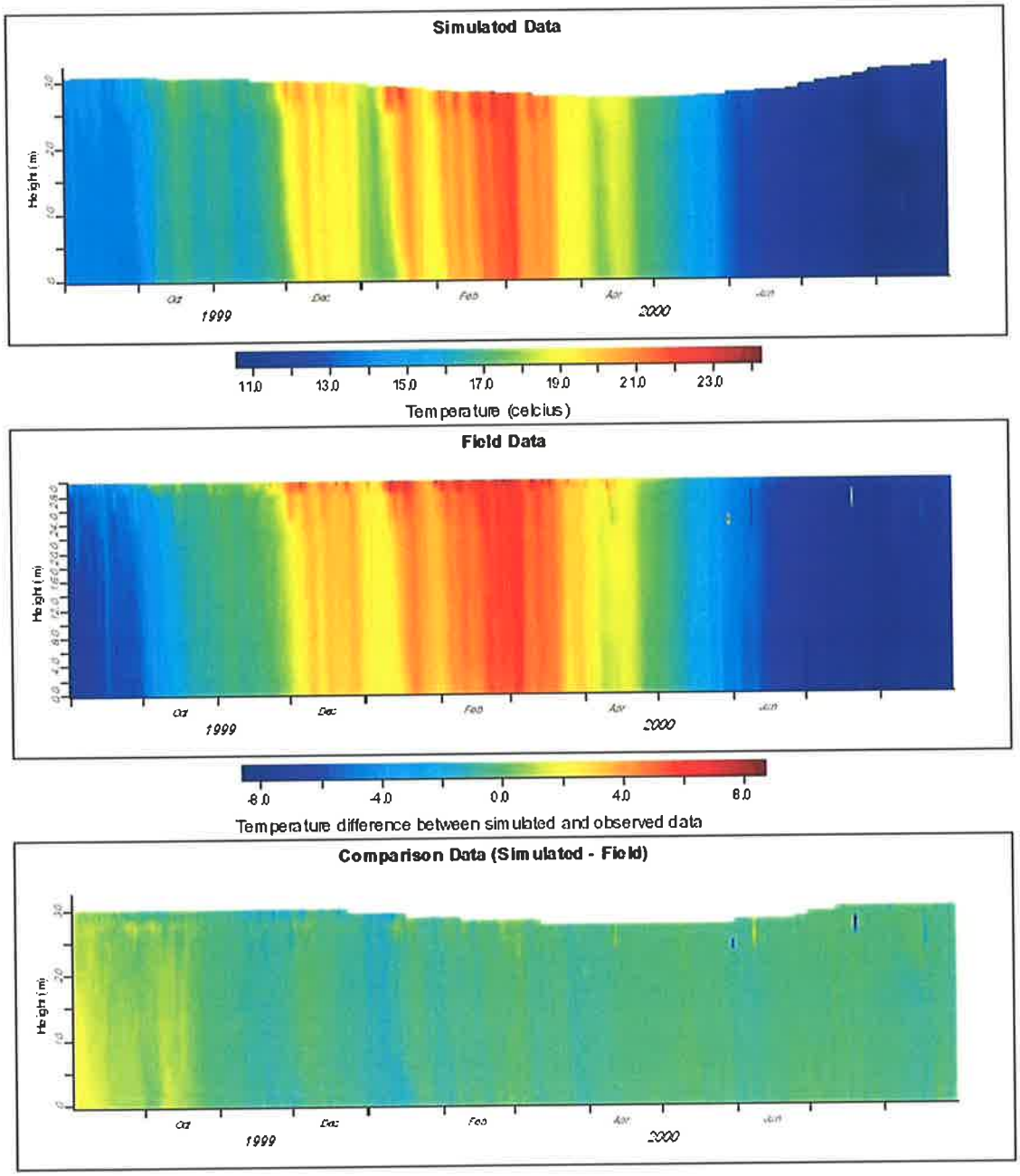

Figure 7.14 Simulated, Field and Comparison temperature data between September-1999 and September-2000. The lower plot shows the temperature discrepancy between the simulated and observed data. Note: the field data does not show the height change in the water level throughout the simulated period as the temperature was recorded from a floating platform.

To quantify the similarity between the simulated and observed temperature profiles, regression analysis was undertaken on the daily outputs and corresponding measured temperature data. Selected comparisons with an R^2 value greater than 0.90 are shown

in Fig. 7.15. Importantly, the use of the aerator and surface mixer algorithms enabled the depth of the thermocline and temperature gradient to be effectively simulated throughout the simulation period.

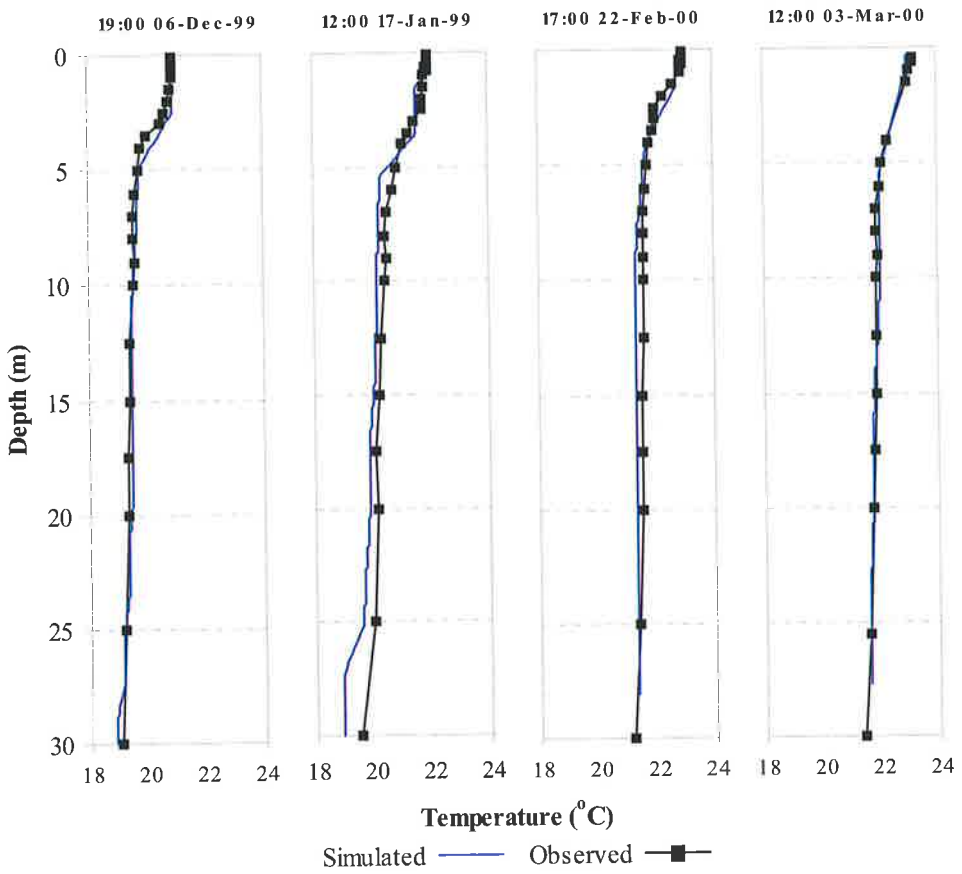

Figure 7.15 Comparison of selected observed and simulated temperature profiles during periods of artificial mixing between 1-September-1999 and 1-September-2000, with R^2 values and *P-values* of 0.97, 9E-12 (19:00 6-December-1999); 0.97, 3E-12 (12:00 17-January-2000); 0.92, 2E-08 (17:00 24-February-2000); and 0.97, 4E-11 (12:00 3-March-2000) respectively.

7.5 CONCLUSIONS

The validation of the surface mixer algorithm and the DYRESM simulation was restricted to Myponga Reservoir and in particular the comparison of temporal temperature data taken from Met 1. However, as the surface mixer algorithm is based on round jet analysis that is not site specific, the algorithm is deemed applicable to any water body. The observed temperature data was recorded at 24 discreet depths, see Chapter 2, in the water column and compared with interpolated data from the

DYRESM simulation output. The consistently high R^2 values obtained from comparison of observed and simulated temperature profiles throughout the modelled annual period provided the confirmation of a successful validation of the DYRESM simulation, which incorporated the surface mixer and aerator algorithms. The objective of numerical simulation of Myponga Reservoir was achieved, alleviating the need to assess the surface mixers solely on restricted field measurements.

The use of the parameters obtained in analysis of the surface mixer flow (Chapter 6) resulted in an improved algorithm, which was initially based on the limited propeller meter measurements. Knowledge gained from the entrainment characteristics from the swirling jet, and the penetration depth enabled the surface mixer algorithm to be enhanced.

The following chapter discusses the various management strategies with the use of artificial mixing and $CuSO_4$ dosing that could be employed at Myponga Reservoir. The operation of the surface mixers and aerator are analysed to determine the effectiveness of their individual and combined destratification abilities and impact upon cyanobacteria growth.

8. SIMULATING THE OPERATION OF THE AERATOR AND SURFACE MIXERS IN MYPONGA RESERVOIR

8.1 INTRODUCTION

The hydrodynamic state of a water body plays a decisive factor with the phytoplankton succession within a water body. By altering the hydrodynamic behaviour using artificial mixing the succession of phytoplankton can be manipulated to favour the growth of less problematic phytoplankton species and inhibit the growth of cyanobacteria, as discussed in Chapter 1. The validation of the surface mixer algorithm (Chapter 7) and the use of the existing DYRESM aerator algorithm, described previously, enabled the impact of artificial mixing using surface mixers or aerators, or a combination of both, upon cyanobacteria growth and dissolved oxygen concentration to be investigated.

The major objective for numerical simulation was to model the growth of cyanobacteria to determine if the surface mixers were able to inhibit their growth. To obtain realistic results, the model simulation needed to include competition for resources from phytoplankton groups. Consequently, the growth of the three dominant phytoplankton groups in Myponga Reservoir were simulated with the DYRESM-CAEDYM coupled hydrodynamic and ecological process model (presented in Chapter 2).

Additionally, as CAEDYM was able to model dissolved oxygen dynamics, the simulation of the surface mixers was also used to determine if they were able to maintain dissolved oxygen concentrations above 4 to 5 mgL^{-1} in the entire water column, as is necessary to prevent the release of iron and manganese from the sediment (Mortimer, 1941; Mortimer, 1942). A second aim was to investigate the capabilities of the existing aerator and surface mixers in order to determine the optimal artificial mixing operation in Myponga Reservoir.

The DYRESM-CAEDYM simulation of phytoplankton growth and dissolved oxygen dynamics was validated against field data measured at Myponga Reservoir between 1-September-1999 and 1-September-2000. Parameters used for phytoplankton growth in

the CAEDYM model are unique to each phytoplankton group growing under similar environmental conditions, and consequently are not universally applicable. Therefore the appropriate growth parameters must be obtained from phytoplankton that grow under the same conditions as that which are modelled, e.g. nutrient concentrations, light environment, temperatures etc. To adequately simulate the growth of the three dominant phytoplankton groups present in Myponga Reservoir an extensive literature search was required, to determine the appropriate parameters required for light and nutrient limited growth of the phytoplankton. The three-phytoplankton groups simulated were chlorophytes, cyanophytes and diatoms. The physical and biological characteristics of *Scenedesmus*, *Anabaena circinalis*, and *Nitzschia* were used to represent these groups respectively.

As stated the parameters for phytoplankton growth are unique to the conditions of the particular habitat that the phytoplankton exists in. Consequently, to obtain appropriate parameters for the simulated phytoplankton groups it was necessary to source data from similar phytoplankton groups that originated in a similar habitat to Myponga Reservoir. The parameters obtained and used for these groups are presented in Table 8.1.

The phytoplankton growth parameters listed in Table 8.1 were used in the CAEDYM growth functions described in Chapter 2. As CAEDYM is directly coupled to DYRESM, the hydrodynamic simulation did not require re-validation. Consequently, the CAEDYM phytoplankton growth and oxygen dynamics algorithms could be invoked once the appropriate parameterisation was completed. The DYRESM-CAEDYM simulation was run with the same meteorological forcing data that was used in Chapter 7.

The DYRESM-CAEDYM investigation was used to investigate the phytoplankton successional dominance and the degree of destratification under different operational regimes. The surface mixer algorithm enabled further insight into the impact of artificial mixing upon phytoplankton succession due to comprehensive hydrodynamic modelling.

Table 8.1 Parameter values used for phytoplankton growth in CAEDYM ([1]Field data, Chapter 4; [2]Westwood and Ganf, 2002; [3]Brookes *et al.* 1999a; [4]Kirk, 1994; [5]Reynolds 1984; [6]Reynolds *et al.*, 2001; [7]Bierman and Dolan, 1981; [8]Griffin *et al.*, 2001; [9]Riley and Stefan, 1987).

Notation	Units	Description	Parameter value		
			Diatom	Chlorophyte	Cyanophyte
base_ext	m^{-1}	Base extinction coefficient	1.56[1]		
Pmax	d^{-1}	Maximum potential growth rate of phytoplankton	0.62[5]	1.52[5]	0.75[2]
Ycc	mg C (mg Chl *a*)$^{-1}$	Mean ratio of C to Chl *a*	42[1,5]	42[1,5]	42[1,5]
Kr	d^{-1}	Respiration rate	0.051[5]	0.079[5]	0.074[5]
Kr	d^{-1}	$CuSO_4$ respiration % of *Pmax*	75 - 10		
Tsta	°C	Standard temperature	14	20[8]	20
Topt	°C	Optimum temperature	15	29[8]	33
Tmax	°C	Maximum temperature	27	35[8]	39
phsal	-	Type of water environment	Freshwater		
Algt	-	Light limitation	Non-photoinhibited light limitation		
I_K	µE m^{-2} s^{-1}	Parameter for initial slope of *PI* curve	16[4]	254[4]	62.5[2]
Kep	µg Chl a^{-1} m^{-1}	Specific attenuation coefficient	0.014[4]	0.022[4]	0.022[4]
K_P	mg L^{-1}	Half saturation constant for phosphorus	0.006[5]	0.0125[7]	0.0052[7]
K_N	mg L^{-1}	Half saturation constant for nitrogen	0.001[5]	0.014[5]	0
K_{Si}	mg L^{-1}	Half saturation constant for silicon	0.098[9]	0	0
phvel	-	Type of vertical migration	Constant velocity		
z_s	m s^{-1}	Constant settling velocity	-1.15E-6[6]	-1.2E-6[6]	0.17E-6[3]
Dia	µm	Diameter of phytoplankton	40[1]	76[1]	174[1]

8.2 CAEDYM CODE: NEW $CuSO_4$ DOSING ALGORITHM

To satisfactorily simulate the phytoplankton assembly at Myponga Reservoir the inclusion of $CuSO_4$ dosing was required on the 11 and 12-January-2000 (DYRESM-CAEDYM days 2000011 and 2000012). As with the PROTECH simulation study (Chapter 5) the $CuSO_4$ algorithm incorporated into CAEDYM reduced the total phytoplankton biomass in the water body over a period of two days. The simulated reduction of phytoplankton biomass was achieved by adding an extra function in the phytoplankton respiration subroutine in CAEDYM (Eq. 8.1) that was linked to the respiration rate, Eq. 2.76.

$$r' = r_{20^\circ C} \times \min\{f(I), f(N), f(P), f(Si), f(C), f(CuSO_4)\} \times f(T) \tag{8.1}$$

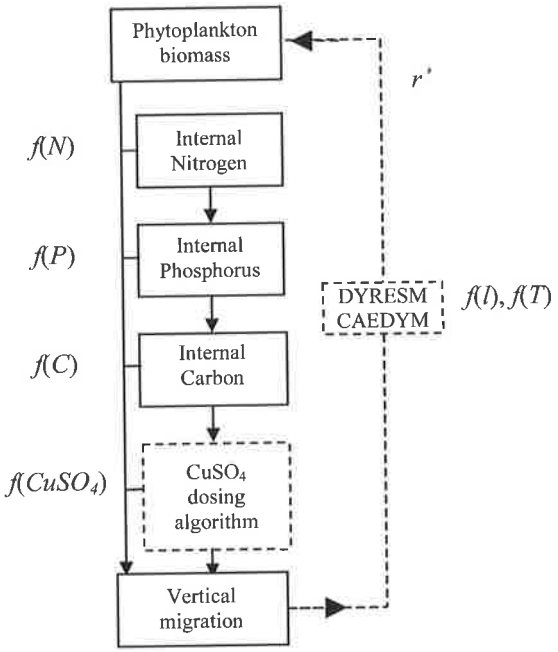

Figure 8.1 Flow diagram depicting the inclusion of the $CuSO_4$ dosing algorithm.

Within CAEDYM, as with many phytoplankton growth models, the loss rate is linked to respiration rate, *kr*. On the appropriate simulation time-step *kr* was increased to account for the indiscriminate action of $CuSO_4$ that causes lysis of phytoplankton. For example, the adopted *kr* value for chlorophytes was 0.079 (Reynolds, 1984), which

was initially increased to 75 % of the maximum potential rate growth of phytoplankton (*Pmax*, Table 8.1) on the first time-step on the corresponding dosing day, then decreased linearly to 10% of *Pmax* at the end of the second day after dosing. This procedure was developed using trial and error analysis, and repeated for the cyanophytes and diatoms.

8.3 VALIDATION

To undertake calibration and validation of the CAEDYM simulation the appropriate state variables were defined. The state variables are quantities that vary with time and are used to characterise the state of the reservoir at any time (Riley and Stefan, 1987). In the CAEDYM model set-up for Myponga Reservoir the state variables were biomass as Chl *a* concentration (μg Chl *a* L^{-1}) for chlorophytes, cyanophytes and diatoms; dissolved oxygen, temperature, phosphorus, nitrogen and silicon concentrations. The CAEDYM parameter file that contains the physiological constants used in the simulation is contained in the attached CD-ROM, entitled "Surface Mixers for Destratification and Management of *Anabaena circinalis* – Data".

A comprehensive calibration of the ecological component of DYRESM-Water Quality (the original incarnation of CAEDYM) was undertaken by Schladow and Hamilton (1997), using data collected from Prospect Reservoir, Western Australia. The calibration used a one-at-a-time parameter estimation method without confidence limits, which is obviously short of ideal. The main observation from their study was that the sensitive parameters identified were site specific.

As discussed in Chapter 4, Myponga Reservoir is highly coloured and has a high light extinction coefficient (~1.56 ln units). Myponga Reservoir field data demonstrated that significant phytoplankton growth occurs when the light and temperature conditions are favourable even though nutrient concentrations are sufficient for growth for relatively long periods. The calibration of the simulated phytoplankton growth in Myponga Reservoir was restricted to the maximum potential growth rate of phytoplankton (*Pmax*, Diatom 0.62, Chlorophyte 1.52, Cyanophyte 0.75 d^{-1}), the parameter for initial slope of each group's photosynthesis versus irradiance curve (I_K, 16, 254, 62.5 μE m^{-2} s^{-1}), respiration rate (*kr*, 75-10 % d^{-1}), settling velocity (z_s, -

1.15E-6, -1.2E-6, 0.17E-6 m s^{-1}) and the half saturation rates for nutrient uptake (K_P, 0.006, 0.0125, 0.0052; K_N, 0.001, 0.014, 0; and K_{Si}, 0.098, 0, 0 mg L^{-1}), Table 8.1.

These parameters were calibrated by trial-and-error adjustment for each phytoplankton group. The objective from this process was to maximise the correlation between the observed and simulated total and individual Chl *a* concentrations for the entire modelled period whilst maintaining the parameters within 10 % of their published values, thus maintaining the integrity of the physiological constants. During the calibration one parameter at a time was adjusted. The parameter values that gave the best correlation between the simulated and field data during the period September-1999 to September-2000 are given in Table 8.1.

The validation of the DYRESM-CAEDYM simulation for Myponga Reservoir was based on the thermal structure presented in Chapter 7, and the dissolved oxygen (DO) concentration (mg L^{-1}) and phytoplankton growth (as total Chl *a*, µg Chl *a* L^{-1}) data for the simulated period from September-1999 to September-2000. The matching of the DO data was achieved, where DO concentrations were maintained at levels greater than 4 to 5 mg L^{-1} throughout the entire simulated period as occurred in the observed data. When the reservoir was naturally fully mixed, DO was maintained at levels exceeding 5 mg L^{-1}, and during periods of high insolation when artificial mixing was used, the high levels of DO were maintained (Fig. 8.2).

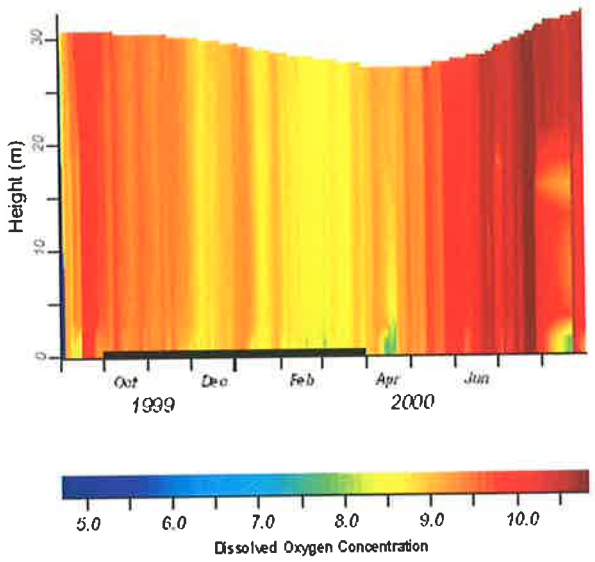

Figure 8.2 Simulated dissolved oxygen profiles for the period September-1999 to September-2000, under artificially mixed conditions (the period when surface mixers and aerator were operating is marked with a solid black line).

The observed phytoplankton data was obtained from integrated samples from the top 5 m of the water column. Subsequently the simulated data is presented in the same integrated format, i.e. simulated daily concentrations are averaged over the top 5 m. The comparison of measured (refer Chapter 4) and simulated total Chl *a* concentration for the simulated period, where a R^2 and *P-value* of 0.75 and 3E-09 respectively were obtained, is shown in Fig. 8.3. The correlation was the best achieved using the calibration method described above. The R^2 and *P-value* obtained indicated a reasonably strong correlation between observed and simulated data, which was supported by visual inspection that showed that the model followed observed trends, with a single summer peak occurring mid February-2000.

To maintain the calibration parameters within a reasonable range of their published values and accurately reproduce the total Chl *a* concentration for the modelled period proved to be extremely difficult. All of the parameters were found to be very sensitive, where slight changes in their values produced dramatic changes in the results.

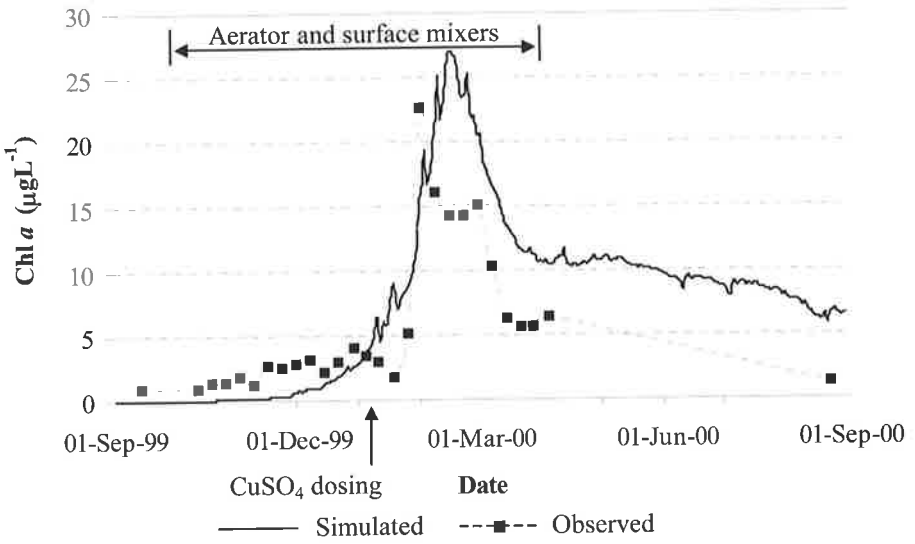

Figure 8.3 A comparison of observed and simulated total Chl *a* (µg Chl *a* L^{-1}), with simulated $CuSO_4$ dosing on DYRESM-CAEDYM day 2000011 and 2000012 (11 and 12-January-2000), and simulated surface mixers and aerator operating between DYRESM-CAEDYM days 1999274 and 2000092 (1-October-1999 to 1-April-2000). The R^2 and *P-value* for the comparison was 0.75 and 3E-09 respectively.

The model over predicted the total Chl *a* concentration for the simulated period, which could not be rectified without completely inhibiting the growth of the cyanophytes and diatoms due to the dominance of the chlorophytes. The artificial mixed conditions at Myponga Reservoir and the dominance of the chlorophytes, as seen in the field data, result in the minimal growth of cyanophytes, with the maximum concentration of *Anabaena circinalis* peaking at ~ 1.2 µg Chl *a* L^{-1} (~ 1600 cells mL^{-1}). Phytoplankton concentrations at this low level are inherently very difficult to simulate, especially when other simulated groups dominate and grow to concentrations that are orders of magnitude greater. Subsequently the model output was accepted as a reasonable representation of the phytoplankton assemblage observed in Myponga Reservoir under artificially mixed conditions, which included $CuSO_4$ dosing.

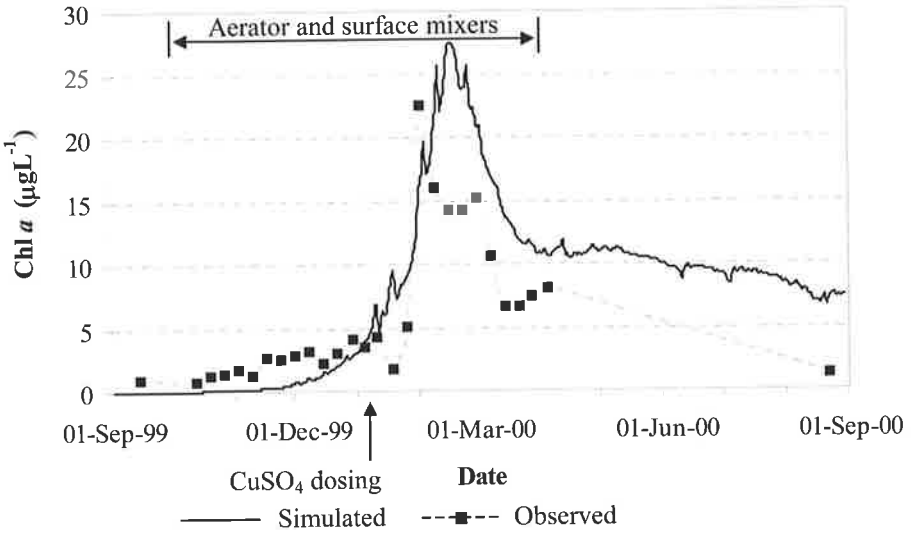

Figure 8.4 Observed and simulated chlorophyte (*Scenedesmus*) Chl *a* concentration (µg Chl *a* L^{-1}), with a R^2 and *P-value* of 0.73 and 4E-09 respectively.

Upon a reasonable comparison of the measured and simulated total Chl *a* data within the limitations of the model, the individual phytoplankton groups were analysed. The total Chl *a* concentration for the three simulated phytoplankton groups represented the entire phytoplankton assembly in Myponga Reservoir, i.e. the sum of the individual Chl *a* concentrations for the three groups was equal to the total Chl *a* concentration of the phytoplankton assembly. Using the individual and total Chl *a* concentrations the percentage contribution for each group was determined, which is summarised in Table 8.2 for the entire simulation investigation.

The observed phytoplankton assemblage at Myponga Reservoir was dominated by chlorophytes for the entire simulated period (96.3 % of the total biomass measured as Chl *a*) and this phenomena was reproduced in the simulation, see Fig. 8.4 (where an R^2 and *P-value* of 0.73 and 4E-09 respectively, was obtained), with the simulated chlorophytes representing 96.6 % of the total biomass measured as Chl *a*.

The best correlation for the simulation of *Anabaena circinalis* (cyanophyte) produced was a R^2 and *P-value* of 0.55 and 0.009 respectively. The comparison of measured and simulated Chl *a* for *Anabaena circinalis* is shown in Fig. 8.5, where a measured single peak of 1.2 µg Chl *a* L^{-1} (~1600 cells mL^{-1}) occurred on the 10-January-2000,

which was not reproduced in the simulation, as the simulated population did not recover after the $CuSO_4$ dosing algorithm was used. It should be noted that the observed cyanophyte concentration represented 0.5 % of the total biomass for the entire simulated period, and the simulated cyanophytes represented 0.8 % of the total biomass measured as Chl *a*.

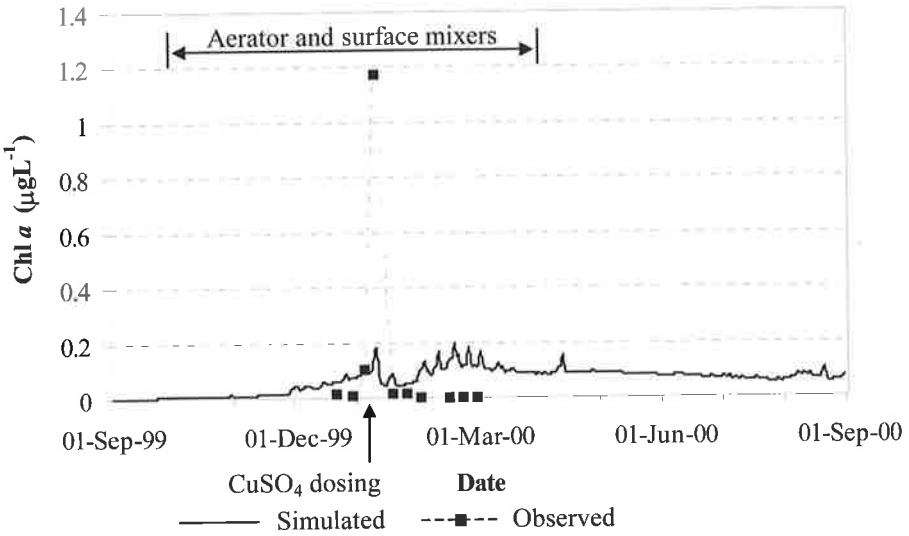

Figure 8.5 Comparison of the observed and simulated cyanophyte (*Anabaena circinalis*) Chl *a* concentration (µg Chl *a* L^{-1}), with a R^2 and *P-value* of 0.55 and 0.009 respectively.

The observed growth of diatoms was not reproduced in the simulation, Fig. 8.6, where the occurrence of a single peak that occurred during late March-early April was not captured in the model. The observed diatom concentration represented 3.2 % of the phytoplankton biomass in Myponga Reservoir, and the model output produced a similar result where simulated diatom growth represented 2.7 % of the total biomass measured as Chl *a* during the modelled period, but growth persisted at low concentrations throughout most of the simulated period.

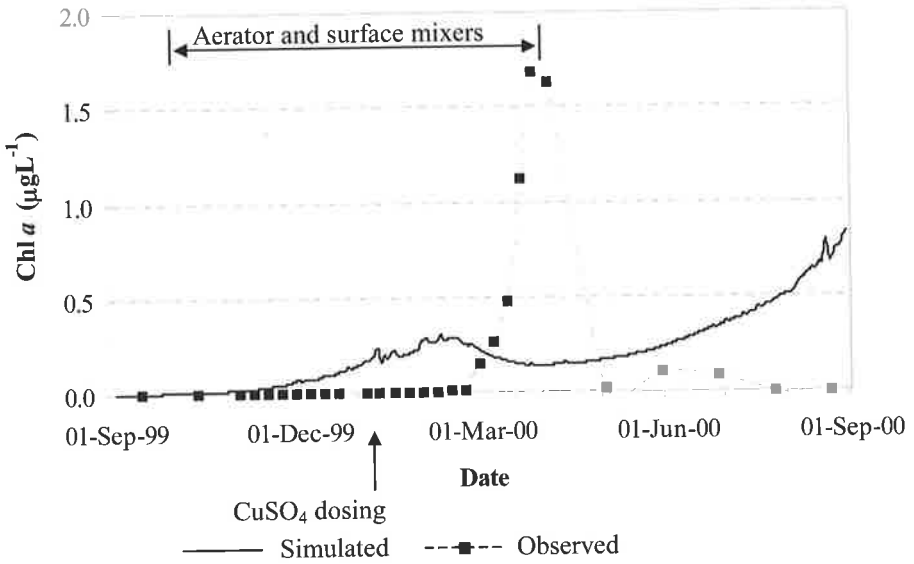

Figure 8.6 Observed and simulated diatom (*Nitzschia*) Chl *a* concentration (μg Chl *a* L^{-1}).

To further validate the DYRESM-CAEDYM simulation of the phytoplankton assembly, the modelled period was extended to March-2001 from September-2000, which corresponded to the end of the phytoplankton-sampling program. The physiological parameters presented in Table 8.1 were used for the extended simulation. The observed and simulated total Chl *a* concentrations for the extended period are shown in Fig. 8.7. The simulated biomass captures the timing of the summer peak that was observed in the field data, but did not simulate the unseasonal peak that occurred in December-2000. This peak was attributed to the phytoplankton *Chroomonas* (see Appendix B), which was not included in the model. The simulated growth of *Anabaena circinalis* from September-2000 to March-2001 produced a reasonable match with the field data (Fig. 8.8), although the simulated growth started earlier in the season than observed in the field.

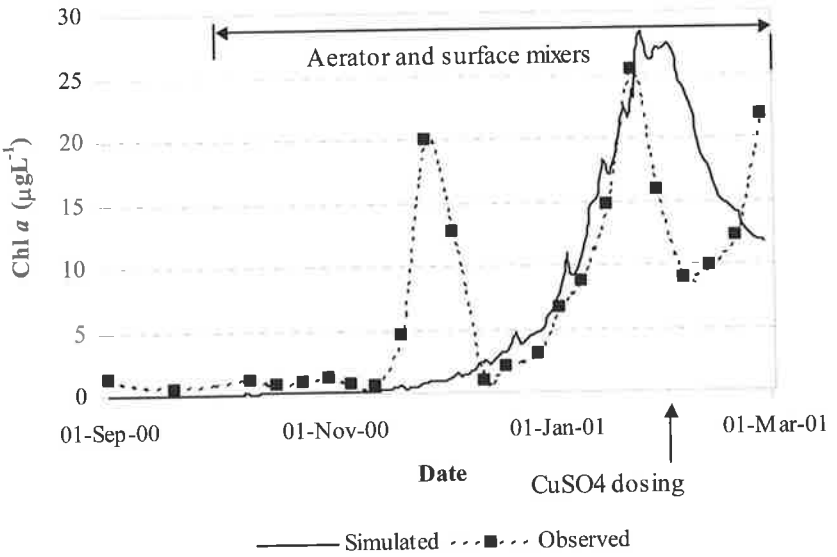

Figure 8.7 A comparison of observed and simulated total Chl *a* (µg Chl *a* L^{-1}), with simulated $CuSO_4$ dosing on DYRESM-CAEDYM day 2001031 (31-January-2000), and simulated surface mixers and aerator operating between DYRESM-CAEDYM days 2000275 and 2001059 (1-October-2000 to 28-February-2001).

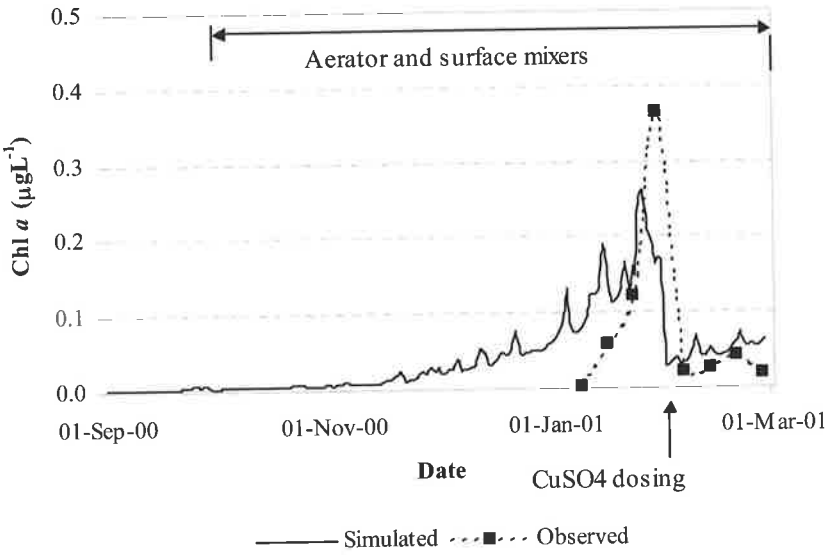

Figure 8.8 Comparison of the observed and simulated cyanophyte (*Anabaena circinalis*) Chl *a* concentration (µg Chl *a* L^{-1}) from 1-September-2000 to 1-March-2001.

The simulation of the 3 types of phytoplankton that were representative of the assembly in Myponga Reservoir from September-1999 to March-2001 produced reasonable results considering the restrictions of the model. The observed phytoplankton assembly consisted of more than 3 species, and other species will dominate the assembly given the right combination of nutrients, light and temperature, as demonstrated with the growth of *Chroomonas* during December-2000. The number of species simulated within CAEDYM requires to be increased, which would require intensive calibration, to achieve a better representation of the assembly in Myponga Reservoir.

As CAEDYM is a heavily parameterised model, calibration using a trial-and-error approach would be restrictive and laborious. To further improve the current and future simulations an efficient method to calibrate CAEDYM would be required. An appropriate method would be to use non-linear parameter fitting software, e.g. NLFIT (Kuczera and Parent, 1998), for model calibration. The task of increasing the number of simulated phytoplankton groups and subsequent calibration and analysis with appropriate software will be the focus of a proposed project to be supervised by the author David Lewis, Dr Martin Lambert (University of Adelaide), and Dr Justin Brookes (Cooperative Centre for Water Quality and Treatment).

8.4 SIMULATION OF VARIOUS MANAGEMENT STRAGEGIES

The CAEDYM model output compared with field data gave a reasonable representation of Myponga Reservoir's phytoplankton biomass as total Chl *a* for the entire assembly. The comparison of the individual groups showed a strong correlation with the chlorophytes, and a moderate correlation with cyanophytes (the target species). Consequently the model was used to determine the individual and combined impact of the surface mixers and aerator for destratification and control of cyanobacterial growth under the following management strategies[1]:

1. No artificial intervention
2. Aerator and surface mixers with no $CuSO_4$ dosing
3. Aerator only
4. Surface Mixers at measured flow rate (3.5 $m^3 s^{-1}$)
5. Surface mixers at design flow rate (5 $m^3 s^{-1}$)
6. Surface mixers at increased flow rate (8 $m^3 s^{-1}$)
7. Intermittent operation
8. Equivalent aerator energy input using surface mixers

8.5 RESULTS – EIGHT MANAGEMENT STRATEGIES

The various management strategies listed in section 8.4 are described individually with the pertinent results tabulated in Table 8.2. The reader is reminded that the objective for artificial mixing is to destratify Myponga Reservoir to maintain DO concentrations greater than 4 to 5 mg L^{-1} and to limit the growth of geosmin producing cyanophytes viz. *Anabaena circinalis*, to below 2000 cells mL^{-1}.

8.5.1 No artificial intervention (Strategy 1)

For the period 1-September-1999 to 1-September-2000 with no artificial mixing, the simulation of Myponga Reservoir (Fig. 8.9) illustrated that permanent stratification would exist for several months causing deleterious conditions to water quality where DO levels in the hypolimnion were significantly less than 4 mg L^{-1}. These anoxic conditions persisted for approximately six months from mid-spring to mid-autumn.

[1] **Note:** The observed data plotted in all the comparison plots, is the observed data recorded under normal operating conditions, and the simulated data from the respective strategy.

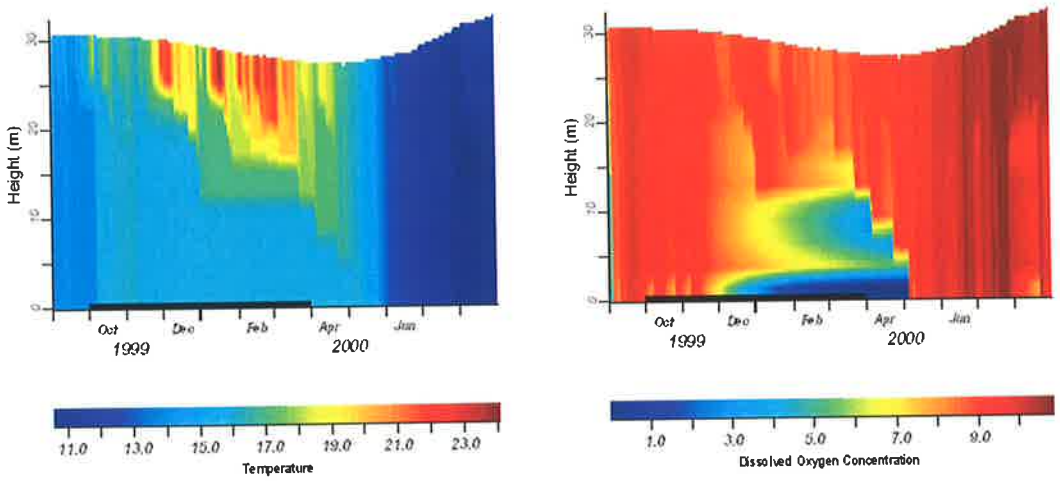

Figure 8.9 Simulated thermal structure and DO concentration for Myponga Reservoir with no artificial mixing.

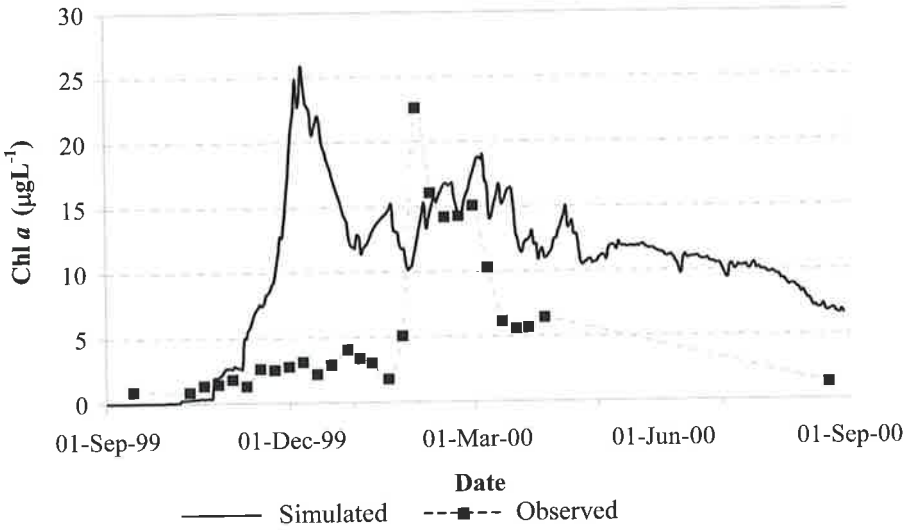

Figure 8.10 Simulated chlorophyte Chl *a* concentration (µg Chl *a* L^{-1}) with no artificial mixing compared with the observed data under normal operating conditions.

The growth of chlorophytes occurred late spring and dominated the phytoplankton assembly contributing to 91.3 % of the total biomass (Fig. 8.10). The cyanophyte growth was excessive during mid April (Fig. 8.11), where the concentration peaked at ~4400 cells mL^{-1} and had a mean concentration of ~ 1000 cells mL^{-1}. The simulation results highlight the potential degradation of water quality that could occur without

the use of artificial mixing. However, if the chlorophytes were to dominate earlier in the summer season, the associated consumption of nutrients could be advantageous leading to nutrient limited growth of other species later in the season.

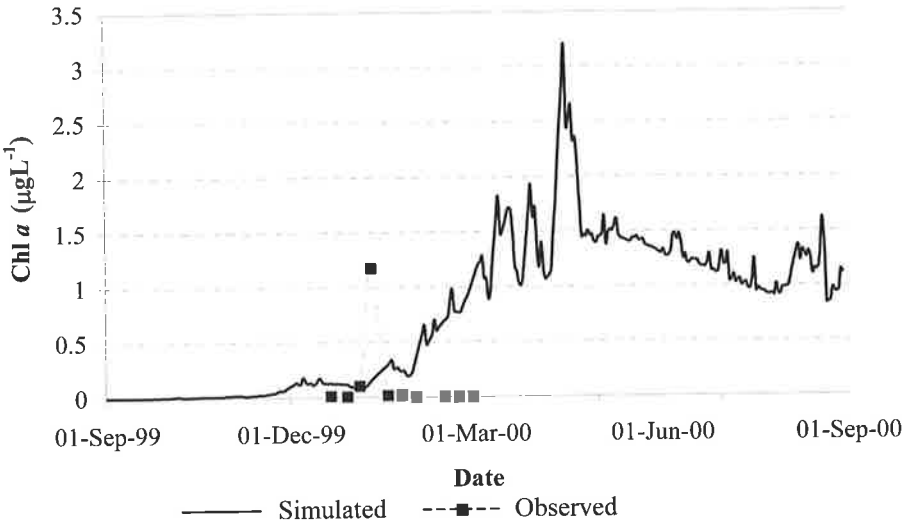

Figure 8.11 Simulated cyanophyte Chl *a* concentration (µg Chl *a* L^{-1}) with no artificial mixing compared with the observed data under normal operating conditions.

8.5.2 Artificial Mixing with no $CuSO_4$ dosing (Strategy 2)

The use of artificial mixing with no $CuSO_4$ dosing in the simulation resulted in a slightly increased phytoplankton biomass and a decreased correlation, $R^2 = 0.72$. The comparison is shown in Fig. 8.12, where the single simulated summer bloom occurred at the appropriate time, and the chlorophyte biomass as Chl *a* contributed 94.1 % of the total biomass for the simulated period. The simulated DO concentration was identical to the results shown in Fig. 8.2.

The reduced percentage contribution of chlorophytes occurred due to significantly increased growth of cyanophytes that contributed 2.8 % of the total biomass, which had a sustained concentration of ~ 300 cells ml^{-1} for approximately 6 months, and a maximum concentration of ~ 1100 cells mL^{-1} (~ 0.78 mg Chl *a* L^{-1}, Fig. 8.13).

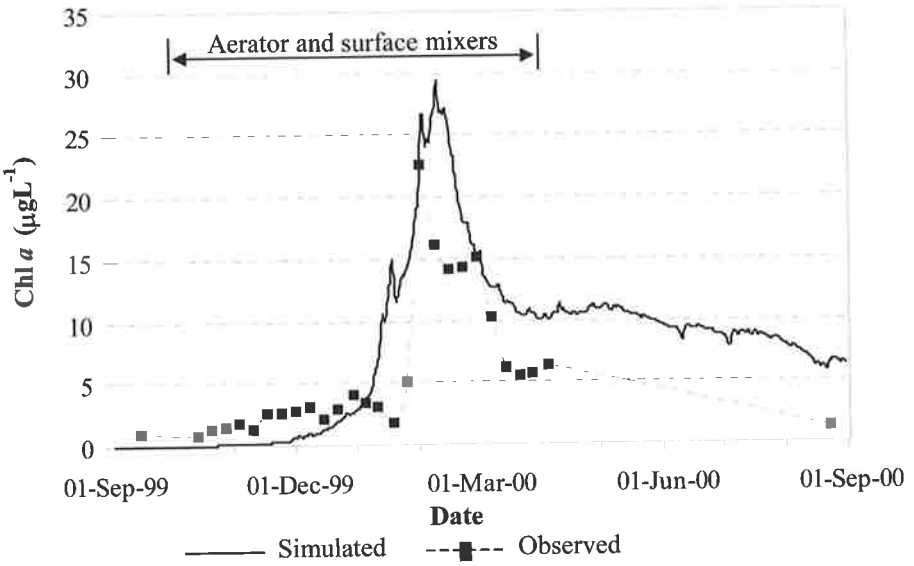

Figure 8.12 Simulated chlorophyte Chl *a* concentration (µg Chl *a* L^{-1}) with no $CuSO_4$ dosing compared with the observed data under normal operating conditions, $R^2 = 0.72$.

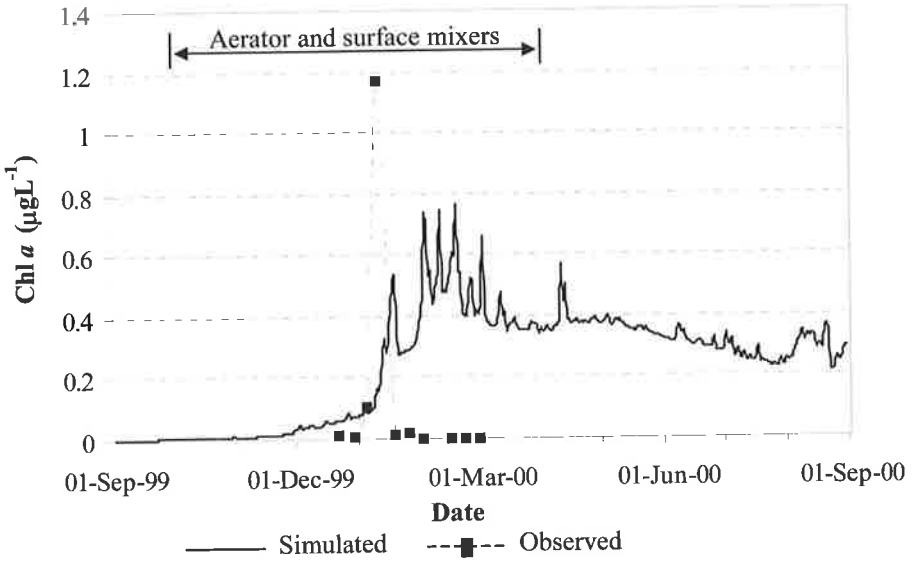

Figure 8.13 Simulated cyanophyte Chl *a* concentration (µg Chl *a* L^{-1}) with no $CuSO_4$ dosing compared with the observed data under normal operating conditions.

8.5.3 Aerator only (Strategy 3)

The DYRESM-CAEDYM model was run without the use of the surface mixer algorithms, using only the aerator algorithm that operated between 1-October-1999 and 1-April-2000.

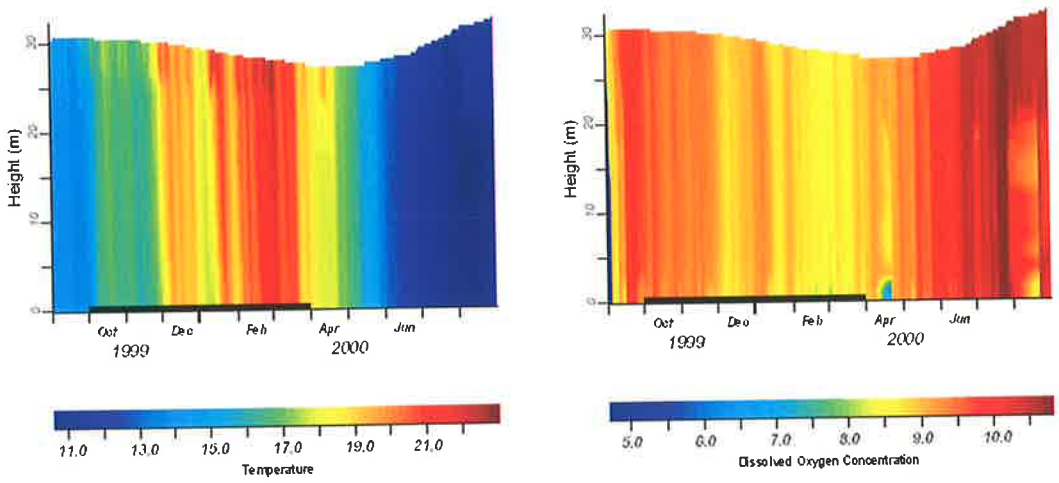

Figure 8.14 Temperature and dissolved oxygen profiles for the simulated period using the aerator only (period when aerator operating is marked with a solid black line).

The temperature profile and DO profiles indicate that mixed conditions were maintained for the majority of the simulated period (Fig. 8.14), with stratification limited to a couple of weeks during late February which corresponded with the increased growth of the cyanophytes (Fig. 8.16). Without the combined use of the surface mixers slightly more severe stratification occurred throughout the summer period. The DO concentrations were maintained greater than 4 to 5 mgL^{-1}. However some DO depletion is evident towards late April at the sediment surface.

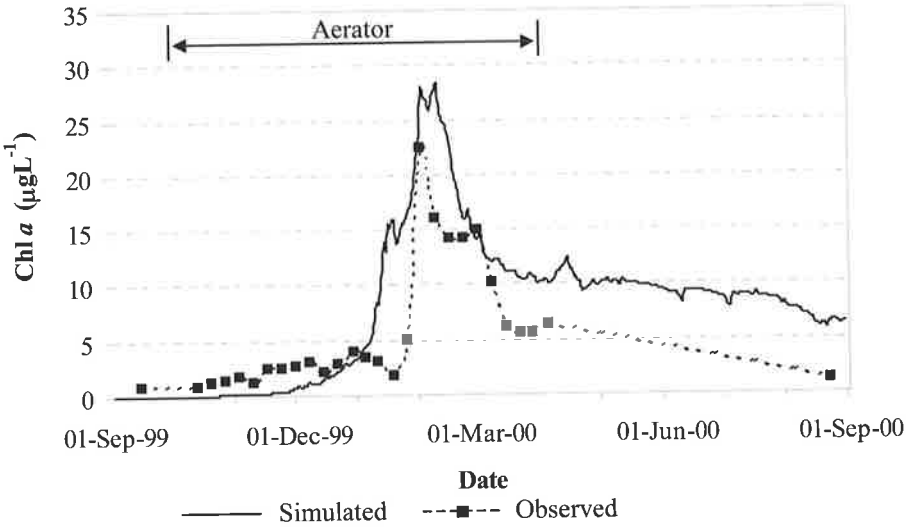

Figure 8.15 Simulated chlorophyte Chl *a* concentration (µg Chl *a* L^{-1}) with the use of the aerator only compared with the observed data under normal operating conditions.

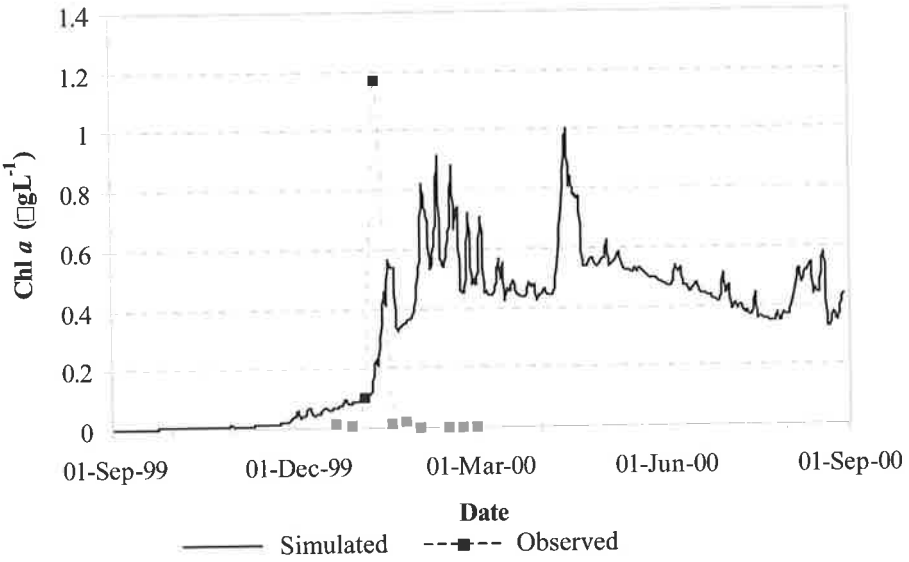

Figure 8.16 Simulated cyanophyte Chl *a* concentration (µg Chl *a* L^{-1}) with the use of the aerator only compared with the observed data under normal operating conditions.

The simulated growth of chlorophytes produced a lower total biomass (92.9 %) without the combined use of the surface mixers, and the timing of growth was unchanged compared growth under normal operating conditions (Fig. 8.15). The growth of the cyanophytes increased substantially and accounted for 4.0 % of the total biomass (Fig. 8.16). A maximum peak of ~1.0 µg Chl *a* L^{-1} occurring mid April,

which corresponded to a cell concentration of ~ 1400 cells mL^{-1}. As with the previous strategies, sustained growth of cyanophytes was maintained, but with a higher mean concentration of ~ 450 cells mL^{-1}.

8.5.4 Surface Mixers (Strategy 4)

The use of the surface mixers alone operating at their measured individual flow rate of 3.5 $m^3 s^{-1}$ were not capable of maintaining fully mixed conditions (Fig. 8.17). Significant stratification occurred during the summer months, which was reflected in the DO profile that shows concentrations levels falling to below 3.0 mg L^{-1} at the sediment surface. DO at this level would cause deleterious water quality conditions.

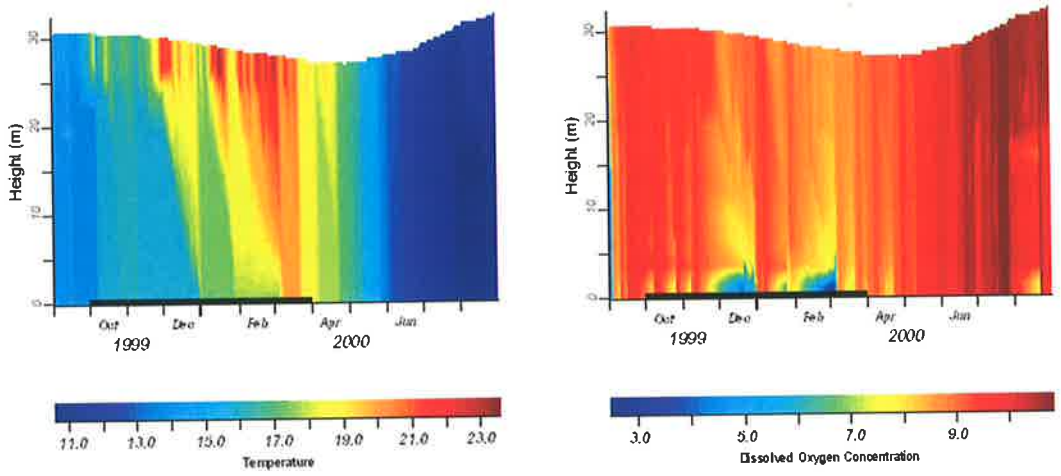

Figure 8.17 Temperature and dissolved oxygen profiles for the simulated period using two surface mixers at their measured flow rate of 3.5 $m^3 s^{-1}$ (period when surface mixers operating is marked with a solid black line).

The timing and magnitude of the simulated growth of chlorophytes altered significantly. The chlorophytes grew earlier in the summer period, peaking at the beginning of December-1999 (Fig. 8.18), which was similar to the simulated growth with no mixing (strategy 1). The cyanophyte growth started earlier than that in the previous scenarios, with persistent and significant growth occurring early autumn (Fig. 8.19). The maximum concentration of cyanophytes was ~ 2400 cells mL^{-1}, with a mean concentration of ~ 680 cells mL^{-1}. The sole use of the surface mixers operating at 3.5 $m^3 s^{-1}$ was not able to limit the growth of cyanophytes to manageable

levels and the associated production of geosmin with the sustained presence could become problematic and would require intervention in the filtration plant.

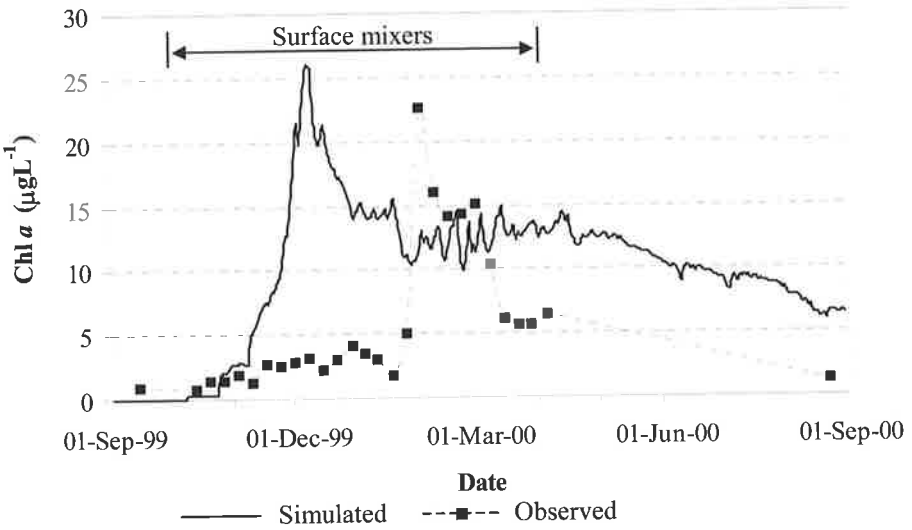

Figure 8.18 Simulated chlorophyte Chl *a* concentration (µg Chl *a* L^{-1}) with the use of the surface mixers operating at 3.5 $m^3 s^{-1}$ each compared with the observed data under normal operating conditions.

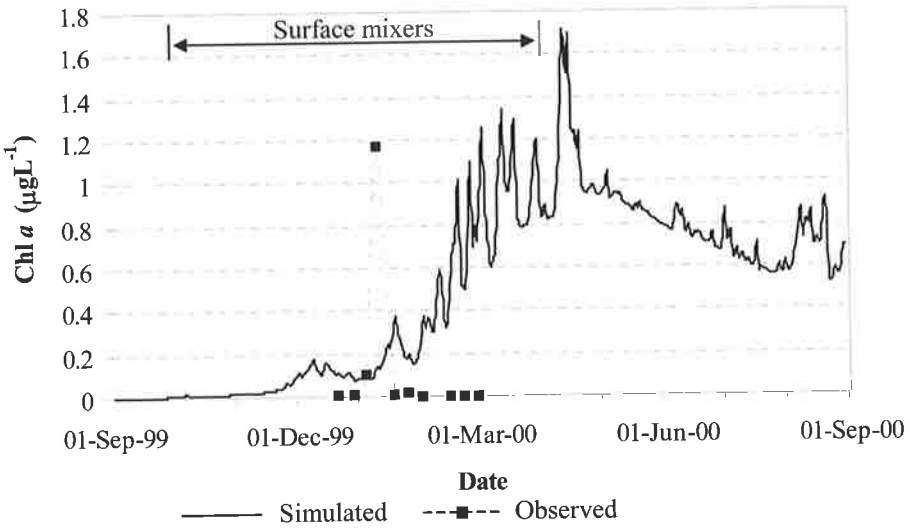

Figure 8.19 Simulated cyanophyte Chl *a* concentration (µg Chl *a* L^{-1}) with the use of the surface mixers operating at 3.5 $m^3 s^{-1}$ each compared with the observed data under normal operating conditions.

The stratified conditions that occur with the sole use of the surface mixers gave rise to the earlier growth of chlorophytes allowing the cyanophytes to dominate later in the season.

8.5.5 Surface mixers at 5 $m^3 s^{-1}$ (Strategy 5)

Increasing the flow rate of the surface mixers to 5$m^3 s^{-1}$ improved their destratification abilities (Fig. 8.20) and decreased the temperature gradient through the water column. DO was maintained at levels greater than 4 mgL^{-1} throughout the simulated period at the increased flow rate.

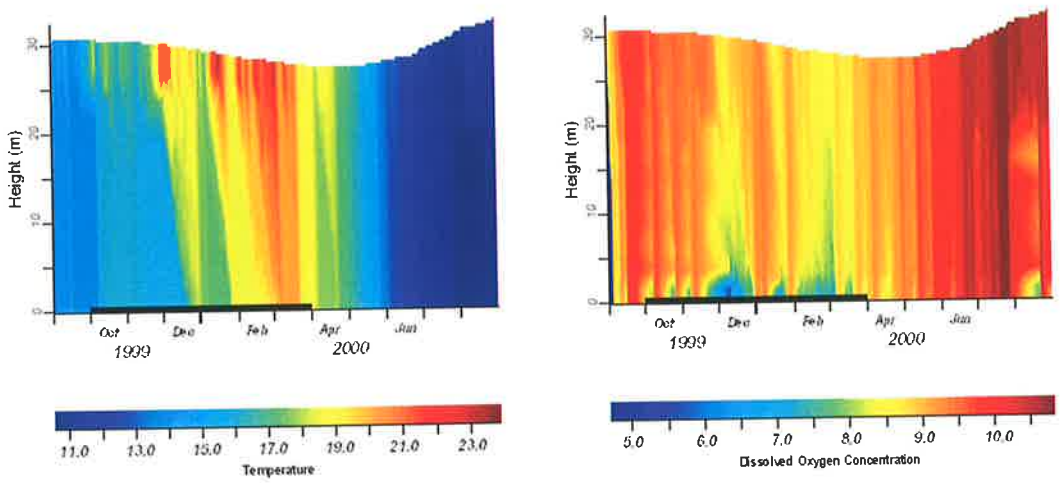

Figure 8.20 Temperature and dissolved oxygen profiles for the simulated period using the surface mixers at 5 $m^3 s^{-1}$ (period when surface mixers operating is marked with a solid black line).

As with the sole use of the surface mixers operating at 3.5 $m^3 s^{-1}$, the growth of chlorophytes occurred earlier in the season with similar magnitude (Fig. 8.21). The chlorophytes contributed 95.3 % of the total biomass as Chl *a*. When the two surface mixers operated at 5 $m^3 s^{-1}$, the cyanophyte growth peaked at a cell concentration of ~ 1500 cells mL^{-1} (1.12 µg Chl *a* L^{-1}) during mid April-2000, and persisted with a mean concentration of ~ 480 cells mL^{-1} (Fig. 8.22). The sustained growth of cyanophytes would require additional intervention to maintain water quality.

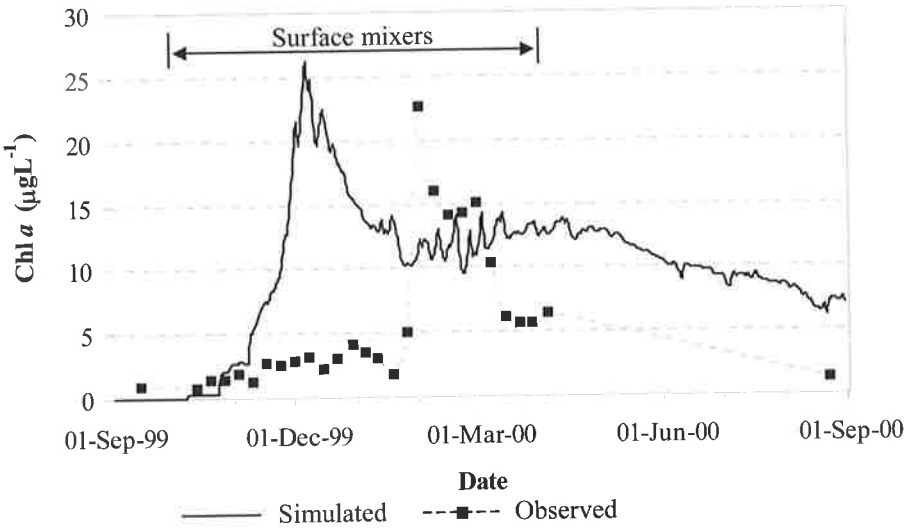

Figure 8.21 Simulated chlorophyte Chl *a* concentration (µg Chl *a* L^{-1}) with the use of the surface mixers operating at 5 $m^3 s^{-1}$ each compared with the observed data under normal operating conditions.

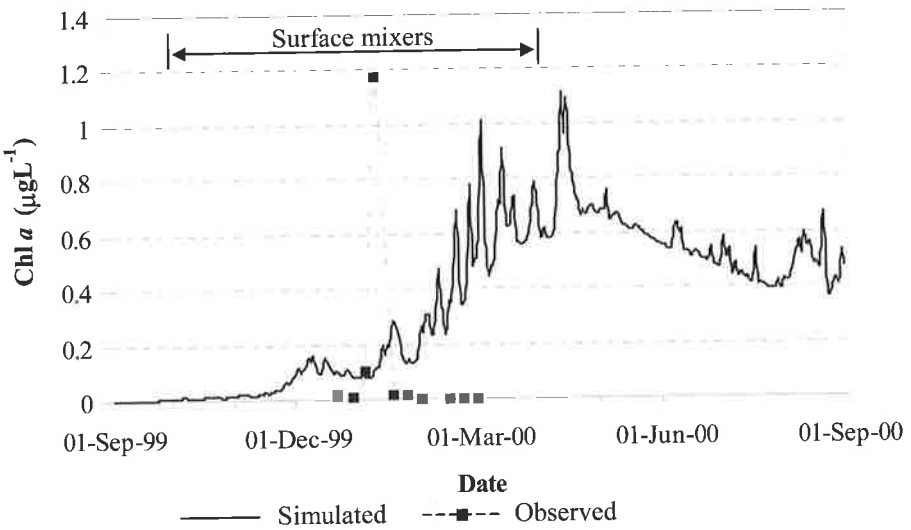

Figure 8.22 Simulated cyanophyte Chl *a* concentration (µg Chl *a* L^{-1}) with the use of the surface mixers operating at 5 $m^3 s^{-1}$ each compared with the observed data under normal operating conditions.

8.5.6 Surface mixers at $8m^3s^{-1}$ (Strategy 6)

The surface mixer flow rate was increased to 8 m^3 s^{-1}, which is the flow rate that the manufacturer claimed was observed in the current model (Elliott, 2002). The destratification ability with the surface mixers operating at 8 m^3 s^{-1} was increased, with the degree of stratification significantly reduced as compared with the lower surface mixer flow rates modelled in the previous scenarios. DO was also sufficiently maintained throughout the simulation (Fig. 8.23).

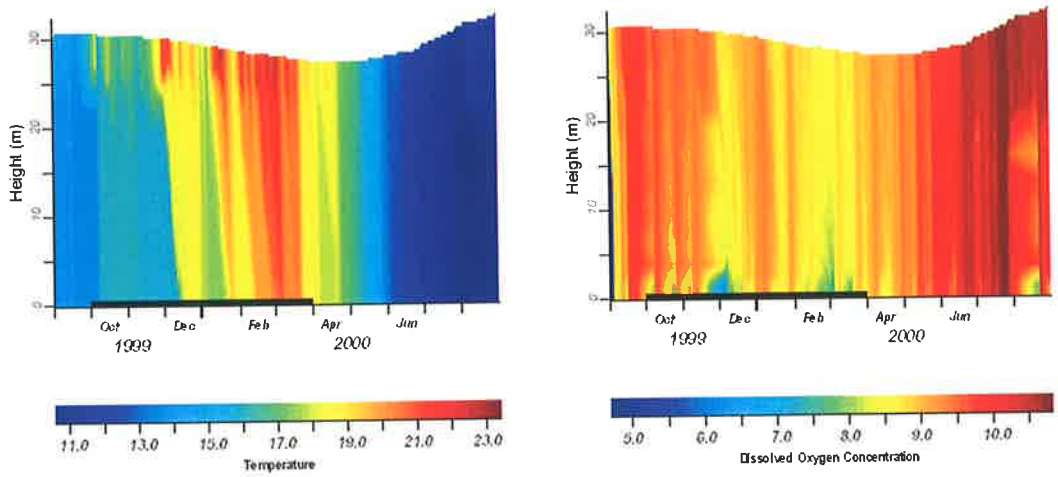

Figure 8.23 Temperature and dissolved oxygen profiles for the simulated period using the surface mixers at 8 m^3 s^{-1} (period when surface mixers operating is marked with a solid black line).

The timing and magnitude of chlorophyte growth was similar to when the surface mixers were operated at the lower flow rates (Strategies 4 and 5), with growth occurring late spring as depicted in Fig. 8.24. The chlorophytes maintained their dominance contributing to 96.4 % of the total biomass. The timing of cyanophyte growth was similar to strategies 4 and 5, however the mean concentration was significantly reduced to ~ 330 cells mL^{-1}, with a maximum peak of ~ 1000 cells mL^{-1} (0.73 µg Chl *a* L^{-1}) occurring mid-April (Fig. 8.25).

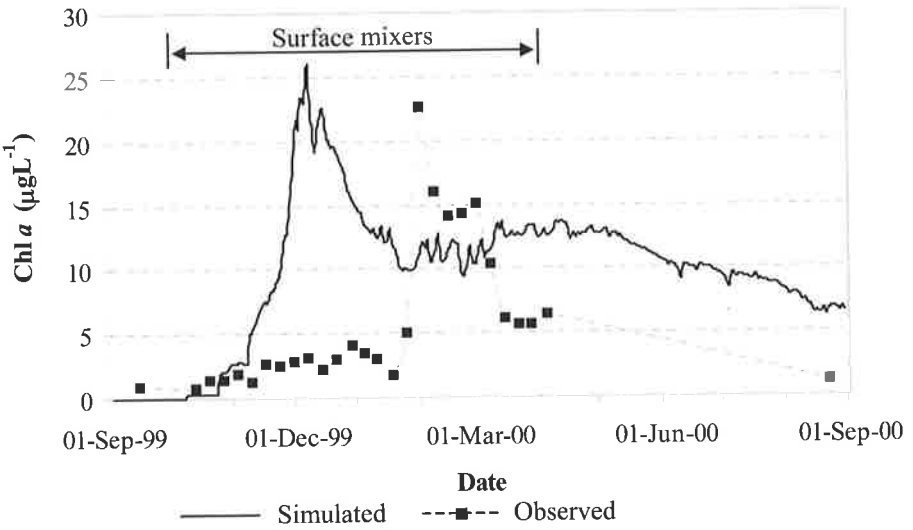

Figure 8.24 Simulated chlorophyte Chl *a* concentration (µg Chl *a* L^{-1}) with the use of the surface mixers operating at 8 $m^3 s^{-1}$ each compared with the observed data under normal operating conditions.

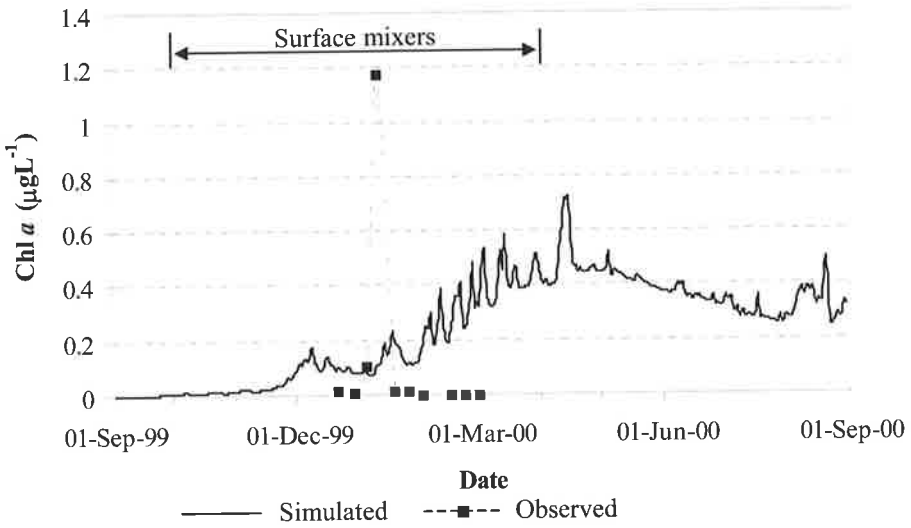

Figure 8.25 Simulated cyanophyte Chl *a* concentration (µg Chl *a* L^{-1}) with the use of the surface mixers operating at 8 $m^3 s^{-1}$ each compared with the observed data under normal operating conditions.

With the sole use of the surface mixers running at 8 $m^3 s^{-1}$, the growth of cyanophytes was maintained at manageable levels, and additional intervention could be avoided.

8.5.7 Intermittent operation (Strategy 7)

Reynolds *et al.* (1984) demonstrated that intermittent operation of artificial mixing could effectively manage the growth of phytoplankton. To test a similar scenario for Myponga Reservoir the aerator and surface mixers (at 3.5 $m^3 s^{-1}$) were operated intermittently in the model. The period of operation was from DYRESM day 1999335 to 2000110 (1-December-1999 to 19-April-2000). This period of operation was initially based on the corresponding dates of anoxic periods shown in Fig. 8.9, which was further refined to reduce the number of days that artificial mixing would be required, achieved by trial-and-error analysis. The surface mixers and aerators were switched on for an arbitrary period of 2 days every 4 days throughout the operational period. The temperature profile in Fig. 8.26 shows a similar trend as when the surface mixers and aerators were run continuously. Under intermittent mixing the DO concentration was adequately maintained throughout the modelled period.

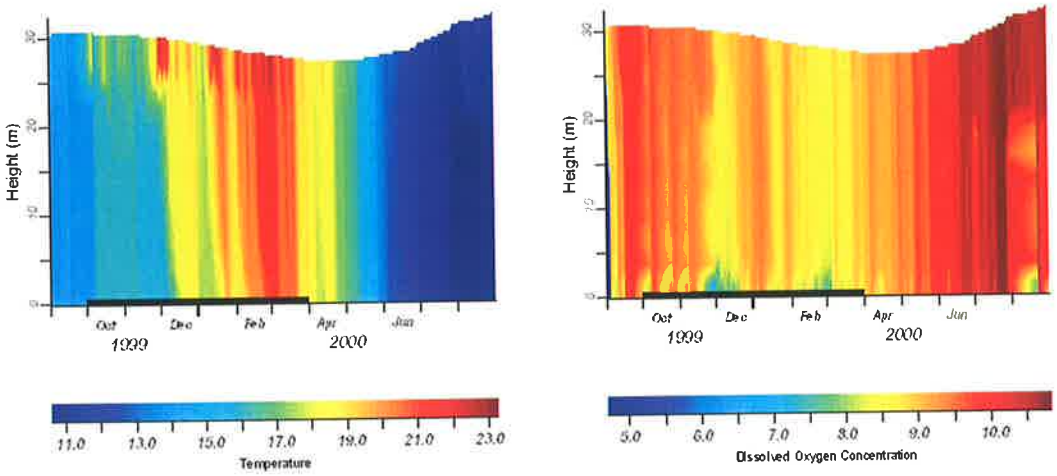

Figure 8.26 Temperature and dissolved oxygen profiles for the simulated period using intermittent mixing using both the surface mixers at 3.5 $m^3 s^{-1}$ and the aerator. The mixing devices operate intermittently (2 days on, 4 days off) throughout the period marked with a solid black line.

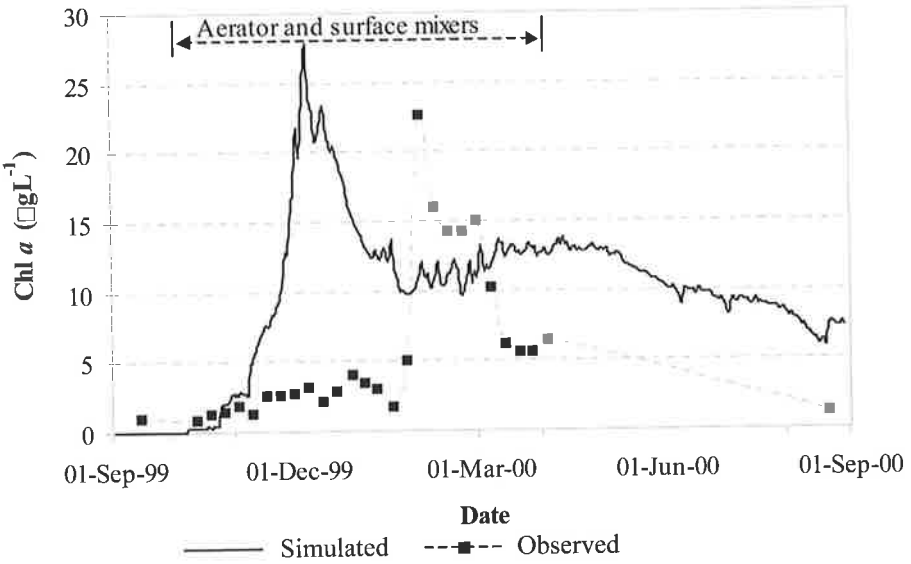

Figure 8.27 Simulated chlorophyte Chl *a* concentration (μg Chl *a* L^{-1}) with the use of the intermittent artificial mixing compared with the observed data under normal operating conditions.

The growth of chlorophytes occurred early December (Fig. 8.27), which was similar to the results that were produced when the sole use the surface mixers at various flow rates was used, contributing to 97.1 % of the total biomass. The growth of cyanophytes also occurred at a similar time as when the surface mixers were operated alone (Fig. 8.28). However, with intermittent mixing the magnitude of cyanophyte growth was significantly reduced with a maximum peak of ~ 670 cells mL^{-1} (0.48 μg Chl *a* L^{-1}) occurring mid April, with a mean concentration of 235 cells mL^{-1}.

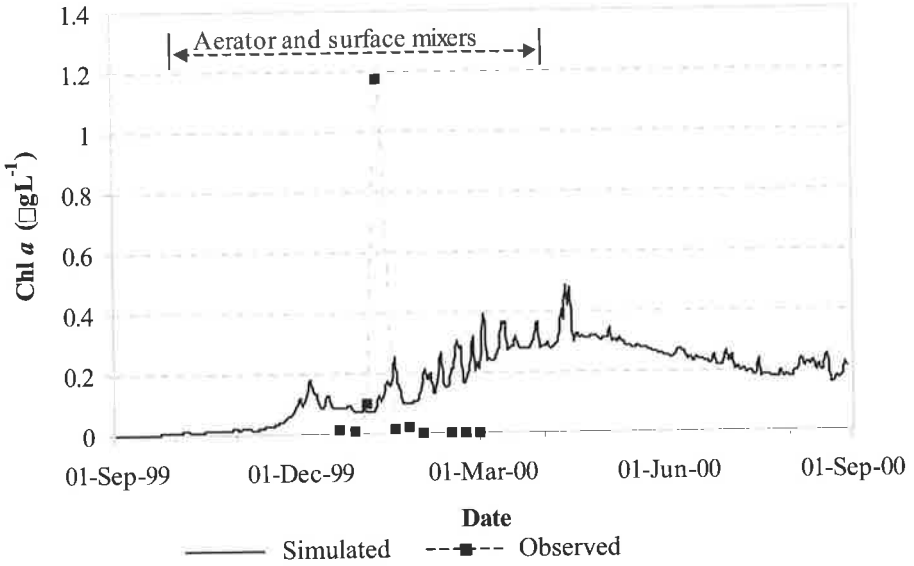

Figure 8.28 Simulated cyanophyte Chl *a* concentration (μg Chl *a* L^{-1}) with the use of the intermittent artificial mixing compared with the observed data under normal operating conditions.

The use of intermittent operation of the surface mixers and aerators gave encouraging results, which maintained stratified conditions and cyanophyte growth well below 2000 cells mL^{-1}.

8.5.8 Equivalent aerator energy input using surface mixers (Strategy 8)

The final strategy that was investigated was related to the energy requirements of the existing aerator at Myponga Reservoir, which is rated at 100 kW. The surface mixers are rated at 4 kW and therefore 25 surface mixers at 3.5 m^3s^{-1} would use the equivalent energy of the aerator. With 25 simulated surface mixers operating in Myponga Reservoir, fully mixed conditions and DO concentration above 4 to 5 mg L^{-1} were maintained (Fig. 8.29).

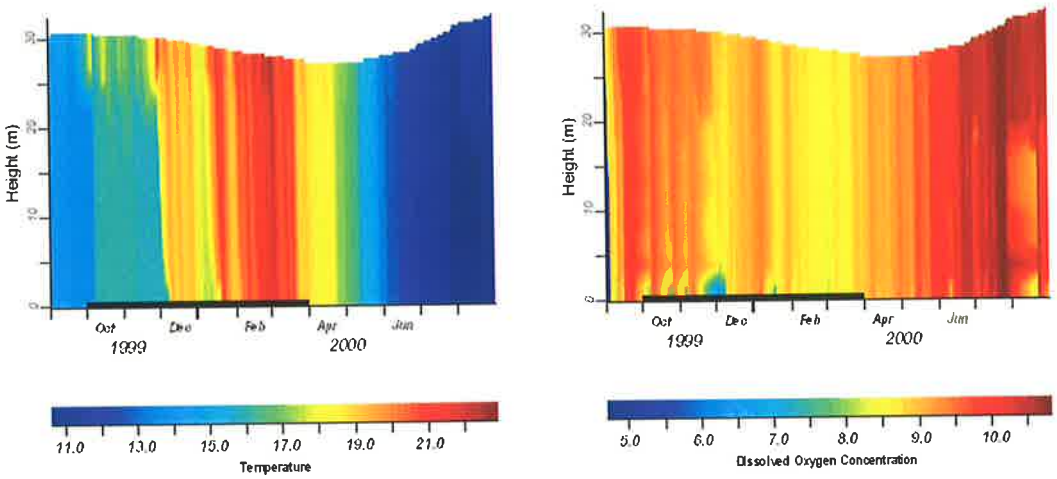

Figure 8.29 Simulated thermal structure and DO concentration for Myponga Reservoir with 25 surface mixers.

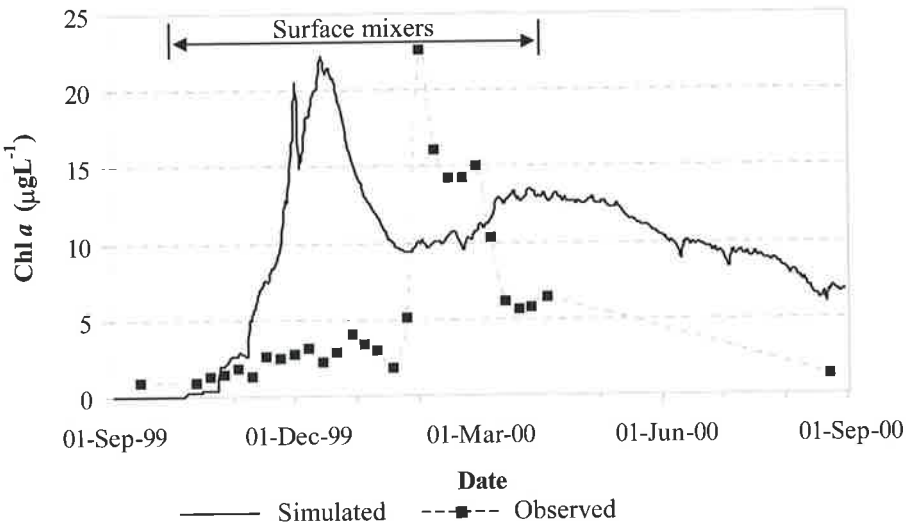

Figure 8.30 Simulated chlorophyte Chl *a* concentration (µg Chl *a* L^{-1}) with 25 surface mixers compared with the observed data under normal operating conditions.

Using this strategy, the growth of chlorophytes started early November (Fig. 8.30) and dominated the biomass with a 98.3 % contribution. The growth of cyanophytes was almost insignificant, but persisted all year with a mean concentration of ~ 80 cells mL^{-1} (~ 0.06 µg Chl *a* L^{-1}) and a maximum concentration of ~ 150 cells mL^{-1} (~ 0.11 µg Chl *a* L^{-1}, Fig. 8.31).

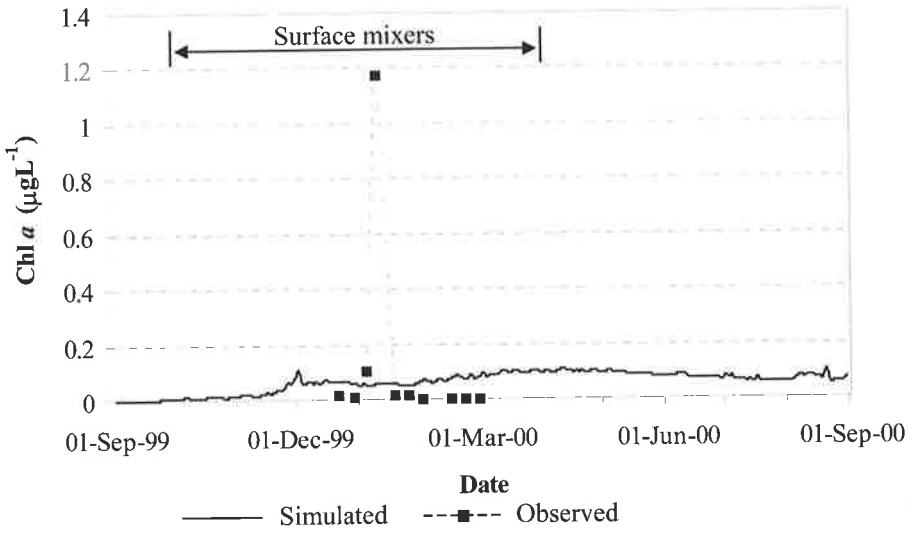

Figure 8.31 Simulated cyanophyte Chl *a* concentration (µg Chl *a* L^{-1}) with 100 kW of equivalent surface mixers compared with the observed data under normal operating conditions.

8.6 DISCUSSION

The effectiveness of the various operational strategies (listed below) used to limit the growth of cyanobacteria and maintain dissolved oxygen concentration in the water column are summarised in Table 8.2.

1. No artificial intervention
2. Aerator and surface mixers with no $CuSO_4$ dosing
3. Aerator only
4. Surface Mixers at measured flow rate (3.5 $m^3 s^{-1}$)
5. Surface mixers at design flow rate (5 $m^3 s^{-1}$)
6. Surface mixers at increased flow rate (8 $m^3 s^{-1}$)
7. Intermittent operation
8. Equivalent aerator energy input using surface mixers

The major result that can be concluded from the various operational strategies is that the chlorophytes dominated the phytoplankton assembly in all cases, and without any artificial mixing (strategy 1) the cyanophyte concentration would well exceed levels that would be detrimental to water quality (> 2000 cells mL^{-1}).

Table 8.2 Results from existing and simulated water quality management strategies.

Artificial mixing operation	Maximum cyanophyte concentration (cells.mL^{-1})	Days above 1000 cells.mL^{-1}	Minimum DO (mgL^{-1})	Simulated phytoplankton assembly composition		
				Chlorophytes	Cyanophytes	Diatoms
Existing - Field	1625	1	~5.00	96.30%	0.50%	3.20%
Existing - Sim	278	0	4.70	96.60%	0.70%	2.70%
Strategy 1	4444	196	1.00	91.30%	6.80%	1.90%
Strategy 2	1069	3	4.70	94.10%	2.90%	3.00%
Strategy 3	1389	16	4.70	92.90%	4.00%	3.10%
Strategy 4	2361	133	1.20	93.90%	4.70%	1.40%
Strategy 5	1556	21	4.70	95.30%	3.40%	1.30%
Strategy 6	1014	1	4.70	96.40%	2.40%	1.20%
Strategy 7	667	0	4.70	97.10%	1.70%	1.20%
Strategy 8	153	196	4.70	98.30%	0.60%	1.10%

The results from the simulation investigation give insight into the operational strategies that could be undertaken at Myponga Reservoir. The simulation employed for validation, which used the surface mixer, aerator and $CuSO_4$ dosing algorithm, produced similar results to the field data. The cyanophyte concentration was kept below 1000 cells mL^{-1}, and well mixed conditions and sufficient DO concentrations were maintained. If no artificial mixing or $CuSO_4$ dosing was undertaken, excessive growth of cyanophytes would occur and permanent stratification would lead to the presence of anoxic conditions. The sole use of the aerator without $CuSO_4$ dosing adequately maintained well mixed conditions and DO throughout the water column. However, the growth of cyanophytes could exceed 1000 cells mL^{-1} (for a total of 16 days) but did not reach the threshold of 2000 cells mL^{-1}.

When the aerator is coupled with the surface mixers (at 3.5 m^3 s^{-1}), the growth of cyanobacteria was further reduced with the peak concentration reduced from ~ 1400 cells mL^{-1} to ~ 1000 cells mL^{-1}. The current operation of the surface mixers (3.5 m^3 s^{-1}) used alone would not be able to destratify the water column and maintain DO at acceptable levels, and importantly the growth of the cyanophytes would exceed 2000 cells mL^{-1}. Increasing the flow rates of the surface mixers improve their destratification abilities and reduce the growth of the cyanophytes. With a surface mixer flow-rate of 8 m^3 s^{-1}, optimal results were achieved maintaining DO above 4 mg L^{-1} and limiting the maximum concentration of cyanophytes to ~ 1000 cells mL^{-1}.

Using intermittent mixing, the growth of cyanophytes was restricted to a maximum concentration of ~ 700 cells mL^{-1}, and well-mixed conditions were maintained. The use of $CuSO_4$ dosing would not be required under this strategy and operational costs would be reduced due to the increased downtime of the aerator and surface mixers. The use of 25 surface mixers, using the same energy as the existing aerator, adequately destratified Myponga Reservoir and almost completely inhibited the growth of cyanobacteria. Although the results were appealing, the practicality of using 25 surface mixers is unreasonable.

8.7 CONCLUSIONS

The addition of the surface mixer and $CuSO_4$ dosing algorithms to DYRESM-CAEDYM enabled the phytoplankton succession and dissolved oxygen concentration to be adequately simulated and validated against field data for the period 1-September-1999 to 1-September-2000. This enabled various management strategies to be investigated (section 8.4). The threat of cyanobacteria growth would exist during the period that coincides with the depleted oxygen levels in the hypolimnion when the physical structure of the water body is stable and the *SML* is shallow, and an adequate source of nutrient is available.

The current mixing program at Myponga Reservoir adequately maintains DO throughout the water column, and coupled with $CuSO_4$ dosing limits the growth of cyanobacteria (*Anabaena circinalis*) to a maximum concentration of ~ 1600 cells mL^{-1} (1.17 µg Chl *a* L^{-1}), contributing to 0.5% of the total biomass as Chl *a*. The simulation of the existing aerator, surface mixers and $CuSO_4$ dosing produced similar results, enforcing the need for intervention to maintain manageable levels of cyanobacterial growth and DO concentrations. The simulation showed that when the surface mixers and aerator are used without the use of $CuSO_4$ dosing (strategy 2) the cyanophytes would not grow to any significant concentration to be of concern. The sole use of the surface mixers was found to be adequate at maintaining water quality if the flow rate could be increased to 8 $m^3 s^{-1}$. However, at their current flow-rate (3.5 $m^3 s^{-1}$) they are not able to fully destratify Myponga Reservoir and limit the growth of cyanophytes to below 2000 cells mL^{-1}.

The use of intermittent artificial mixing would reduce operational costs as the aerator and surface mixers would operate 50 % less than the current operational schedule, and was shown to be an effective operational strategy. Using this technique, destratified conditions are maintained, DO concentrations are kept high and the growth of cyanobacteria is minimal and importantly, the use of $CuSO_4$ dosing is not necessary. Under the current operating conditions, the simulation demonstrated that the use of $CuSO_4$ dosing is superfluous, as cyanophyte concentrations did not exceed 2000 cells mL^{-1}. As demonstrated with PROTECH and DYRESM-CAEDYM, the current nutrient concentrations, light climate, meteorological forcing and artificial mixing operations at Myponga Reservoir do not favour excessive growth of cyanobacteria.

The simulation of Myponga Reservoir with the modified DYRESM-CAEDYM model demonstrates that modelling has the potential to be used as a tool to assess and optimise water quality management strategies. Upon successful simulation of the limnological processes in a water body, any myriad of strategies can be investigated. The modeller can alter meteorological conditions, nutrient loadings, timing and use of artificial mixing devices etc. to gain insight into the management of the water body. The addition of the surface mixer and $CuSO_4$ dosing algorithms has successfully been incorporated into the DYRESM-CAEDYM model and has extended its use.

9. CONCLUSIONS

9.1 CONCLUSIONS

The overall objectives for this research were to (1) gain insight into the limnological behaviour of Myponga Reservoir to ascertain if the surface mixers could be used as an effective management tool to improve water quality, (2) quantify the hydrodynamic behaviour of the surface mixers, and (3) use numerical modelling techniques to extend the assessment of the surface mixers beyond the analysis of field data.

9.1.1 Limnological behaviour of Myponga Reservoir

To adequately assess the surface mixers, the limnological behaviour of Myponga Reservoir was quantified. This was achieved with extensive field monitoring, which included the installation of meteorological monitoring stations, and the instigation of daily, weekly and monthly monitoring programs. The extensive physical, chemical and biological data collected at Myponga Reservoir gave important insight into the limnological processes that occur within the water body.

Myponga Reservoir is highly coloured (z_{eu} ~ 3 m) and is well mixed annually from late April to late September without the use of artificial mixing. On an annual basis, artificial mixing with an aerator and two surface mixers is used to limit the severity of stratification and limit the growth of cyanobacteria, where relatively well-mixed conditions are maintained. During periods of high insolation excessive surface heating occurs leading to diurnal stratification. Severe stratification can occur but is restricted to a couple of weeks coinciding with excessive insolation and average wind speeds < 4 m s^{-1}.

The integrity of the meteorological field data was validated by a heat budget, with the discrepancies attributed to instrument error and limitations with heat content calculations. Due to substantial wind mixing, differential heating and cooling; horizontal mixing in Myponga Reservoir occurs on diurnal time-scales, which enables the water in the side arm and main basin to be well-mixed creating relatively homogeneous habitats for phytoplankton growth. Modelling the growth of phytoplankton as a function of light and mixed depth showed that the two regions

would provide the capacity for a heterogeneous assembly to exist in Myponga Reservoir, but due to significant horizontal mixing between the two locations the phytoplankton assembly remains homogenous.

Based on the maximum Chl *a* concentration of 38 μg Chl *a* L^{-1}, measured between October-1998 and March-2001, Myponga Reservoir is categorised as a eutrophic system which requires intervention to maintain water quality. There is a lag between nutrient delivery to the reservoir and utilisation of the resource for cyanobacteria growth, which requires the right combination of light, heat and nutrient, which occurred rarely due to artificial mixing. The bulk of the nutrient load came from Myponga River as the internal nutrient load was suppressed by artificial destratification.

The combined use of the aerator and surface mixers installed in Myponga Reservoir were found to deepen the *SML* at Myponga Reservoir, which was maintained below the euphotic depth for the majority of the summer. Consequently, the growth of cyanobacteria was light-limited and, in general, a restrictive light environment existed for phytoplankton growth.

9.1.2 Hydrodynamic behaviour of the surface mixers

The impeller-induced jet generated by the surface mixers was examined during isothermal and stratified conditions. The surface mixers generated a large swirling jet with a Reynolds number in the order of 10^6 and a Swirl number of 0.2. Under isothermal conditions the streamwise flow quickly developed showing a typical Gaussian profile that is unique with swirling and non-swirling jets. The *ZFE* for the surface mixer flow was considerably shorter than that of swirling jets presented in the literature and achieved self-similarity ~ 2 m downstream of the draft-tube exit (0.5561 l_Q/z).

The radial spread for the surface mixer flow under isothermal conditions was approximately three times that of a non-swirling jet and spread linearly at a half angle of 14.4 °. The entrainment into the jet has been analysed and can be predicted under isothermal and stratified conditions. The terminal depth can be adequately predicted by using Eq. 2.64; and the significant parameters characterising the surface mixer jet

were quantified and include the radial spread of the jet, length of the *ZFE*, commencement of the *ZEF* and the location of the virtual origin. The successful characterisation of the hydrodynamic behaviour of the surface mixers has been achieved and enabled the development of a surface mixer algorithm that can be incorporated into existing hydrodynamic models and used to assess their impact upon the limnological behaviour of a water body.

9.1.3 Modelling the limnological impact of the surface mixers

The analysis of the surface mixer flow enabled algorithms to be developed that were incorporated into the one-dimensional ecological model PROTECH and the coupled hydrodynamic-ecological model DYRESM-CAEDYM. The capabilities of these models has been extended and provided an improved tool for water quality managers.

The PROTECH code was successfully modified to simulate the annual thermal and phytoplanktonic characteristics of Myponga Reservoir. This was achieved with the addition of surface mixer and $CuSO_4$ dosing algorithms, which were based on extensive field measurements and data analysis. The subsequent study demonstrated that artificial mixing via the surface mixers has a significant effect upon the total phytoplankton biomass in Myponga Reservoir. The simulation confirmed that the management practices put in place at Myponga Reservoir to control the phytoplankton community reduced the phytoplankton biomass, and demonstrated that the most important factor regulating the current phytoplankton content is that it is light limited.

The PROTECH simulation successfully reproduced the phytoplanktonic character of Myponga Reservoir and highlighted that the community was dominated by *R*-type phytoplankton under all the simulated conditions tested. The simulated action of $CuSO_4$ dosing and artificial mixing reduced the simulated phytoplankton biomass but had insignificant effects upon the actual phytoplankton succession. Thus it was concluded from the PROTECH study that regardless of the artificial controls imposed upon the reservoir, potentially harmful *CS*-types (*Anabaena circinalis*) would probably never be a significant health risk with the current practices undertaken in Myponga Reservoir.

Improved surface mixer and $CuSO_4$ dosing algorithms were successfully integrated into DYRESM-CAEDYM and were validated against field data for the simulated period from 1-September-1999 to 1-September-2000. The objective to simulate the thermal structure, dissolved oxygen concentration and phytoplankton assembly (3 dominant species) in Myponga Reservoir was achieved, alleviating the need to assess the surface mixers solely on restricted field measurements, and enabled different management strategies to be investigated. The individual and combined operation of the surface mixers and aerator was analysed to determine the effectiveness of their destratification abilities and, coupled with the $CuSO_4$ dosing algorithm, their impact upon cyanobacteria growth. The investigation confirmed that the threat of cyanobacteria growth would exist during periods that coincide with depleted oxygen levels in the hypolimnion when the physical structure of the water body is stable and an adequate source of nutrient is available. The DYRESM-CAEDYM model confirmed that the current mixing program at Myponga Reservoir adequately maintains DO throughout the water column, and coupled with $CuSO_4$ dosing limits the growth of cyanobacteria (*Anabaena circinalis*). The simulation of the existing aerator, surface mixers and $CuSO_4$ dosing produced similar results as the observed data, enforcing the need for intervention to maintain manageable levels of cyanobacterial growth and DO concentrations. The simulation showed that without the use of $CuSO_4$ dosing, cyanobacteria would not grow to any significant concentration to be of concern under the present limnological state.

The sole use of the aerator would adequately provide destratification requirements, and would also limit the growth of cyanobacteria. The current operation of the surface mixers used alone would not be able to destratify the water column and maintain DO at acceptable levels, and the growth of cyanobacteria would exceed 2000 cells mL^{-1}. Increasing the flow rates of the surface mixers improved their destratification abilities and reduced cyanobacteria growth to acceptable levels. Under the modelled conditions, the use of $CuSO_4$ dosing was superfluous as the growth of cyanobacteria could be maintained below 2000 cells mL^{-1} with the current operation of the aerator and surface mixers. The simulation of Myponga Reservoir with the modified DYRESM-CAEDYM model demonstrated that modelling is an effective tool to assess and optimise water quality management strategies. As demonstrated with PROTECH and DYRESM-CAEDYM, the current nutrient concentrations, light

climate and meteorological conditions at Myponga Reservoir do not favour the growth of cyanobacteria, thus alleviating the requirement to use $CuSO_4$ dosing.

It was concluded that the surface mixers are able to remove buoyant cyanobacteria from the surface water and transport them to below the draft-tube depth, and limit the severity of stratification. The penetration of the surface mixer jet was found to be a function of the surface water temperature and the ambient water temperature at the exit point of the draft-tube. Consequently, during periods of excessive solar insolation the jet issuing from the surface mixer draft-tube becomes buoyant and is not able to reach the sediment surface, thus limiting their destratification capabilities and reducing the time that entrained cyanobacteria remain below the surface. For the surface mixers to be effectively used for destratification and control of cyanobacteria, the flow-rate needs to be increased to at least 8 m^3 s^{-1}, as demonstrated in the DYRESM-CAEDYM simulation.

9.1.4 Summary

The results presented in this thesis describe the hydrodynamic behaviour of the surface mixers and their resultant impact upon cyanobacteria growth. The development of empirical relationships which reliably describe the hydrodynamic and geometric properties of large diameter impeller-induced swirling jets has added to the theory on jets and plumes and closed the gap that was identified in the literature. The publication of these results will enable large swirling jets with high Reynolds number generated from surface mixers to be effectively considered as a method of improving water quality in lakes and reservoirs.

9.2 RECOMMENDATIONS FOR FUTURE WORK

The development of the surface mixer algorithm, which was based on comprehensive flow measurements, was successfully incorporated into DYRESM. The algorithm was validated with the temperature data collected at Myponga Reservoir and the coupled ecological model CAEDYM was used to investigate the behaviour of the phytoplankton assembly under different management strategies. The simulation was found to produce a reasonable representation of the phytoplankton assembly at Myponga Reservoir, but highlighted a need for rigorous calibration of CAEDYM with

non-linear parameter fitting software. The only reported calibration study for CAEDYM was undertaken by Schladow and Hamilton (1997), using trial-and-error analysis, which was limited to site specificity. To satisfactorily calibrate CAEDYM, a sensitivity analysis that assesses the calibrated physiological parameters is required, which will determine if the resultant parameters match that published in the literature and produce a meaningful representation of phytoplankton growth.

The surface mixers at Myponga Reservoir have only been used in conjunction with the existing aerator. To confirm the results generated from the PROTECH and DYRESM-CAEDYM analysis, the surface mixers need to be operated without the aerator during periods that lead to degraded water quality. The use of $CuSO_4$ dosing to limit cyanobacteria growth in Myponga Reservoir is questioned, and numerical modelling suggests its use is unnecessary under the current operation and limnological behaviour of Myponga Reservoir. A contingency plan needs to be put in place to enable the use of $CuSO_4$ dosing to be withheld to support these findings.

The use of surface mixers for destratification and management of cyanobacterial growth is gaining popularity in Australian water bodies. To further validate the surface mixer algorithm that was incorporated in DYRESM-CAEDYM, more field data is required from other water bodies within Australia and internationally, where different meteorological conditions and bathymetry exist. This will increase the robustness of the surface mixer algorithm and improve confidence in its application.

10. REFERENCES

Albertson, M.L., Dai, Y.B., Jensen, R.A. and Rouse, H., 1950. Diffusion of submerged jets. Transactions of the American Society of Civil Engineers, 115(2409): 639-697.

Antenucci, J.P. and Imerito, A., 2000. The CWR Dynamic Reservoir Simulation Model DYRESM. Centre for Water Research, University of Western Australia, 38 pp.

Arnold, D.E., 1971. Ingestion, assimilation, survival, and reproduction by *Daphnia pulex* fed seven species of blue-green algae. Limnology & Oceanography, 16: 906-920.

Baines, W.D., Turner, J.S. and Campbell, I.H., 1990. Turbulent fountains in an open chamber. Journal of Fluid Mechanics, 212: 557-592.

Behrenfeld, M.J. and Falkowski, P.G., 1997. A consumers guide to phytoplankton primary productivity models. Limnology and Oceanography, 42: 1479-1491.

Berman, T. and Shteinman, B., 1998. Phytoplankton development and turbulent mixing in Lake Kinneret (1992-1996). Journal of Plankton Research, 20(4): 709-726.

Bierman, V.J. and Dolan, D.M., 1981. Modelling of phytoplankton - nutrient dynamics in Saginaw Bay, Lake Huron. Journal of Great Lakes Research, 7(4): 409-439.

Billant, P., Chomaz, J.M. and Huerre, P., 1998. Experimental study of vortex breakdown in swirling jets. Journal of Fluid Mechanics, 376: 183-219.

Bowmer, K.H., Padovan, A., Oliver, R.L., Korth, W. and Ganf, G.G., 1992. Physiology of geosmin production by *Anabaena circinalis* isolated from the Murrumbidgee River, Australia. Water Science and Technology, 25: 259-67.

Boyd, A.J., Filipe, V.L.L. and Bartholomae, C.H., 2001. Near-surface currents and hydrology off Southern Angola in July 1999. South African Journal of Science, 97(5/6): 219-222.

Bratley, P., Fox, B.L. and Schrage, L.E., 1987. A Guide to Simulation. Springer-Verlag, New York, NY., 397 pp.

Brookes, J.D., Burch, M.D. and Tarrant, P., 2000. Artificial destratification: Evidence for improved water quality. Water, 27(3): 18-22.

Brookes, J.D. and Ganf, G.G., 2001. Variations in the buoyancy response of *Microcystis aeruginosa* to nitrogen, phosphorus and light. Journal of Plankton Research, 23(12): 1399-1411.

Brookes, J.D., Ganf, G.G., Green, D. and Whittington, J., 1999a. The influence of light and nutrients on buoyancy, filament aggregation and floatation of *Anabaena circinalis*. Journal of Plankton Research, 21(2): 327-341.

Brookes, J.D., Lewis, D.M., Linden, L.G. and Burch, M.D., 2002. On-line monitoring of reservoirs for the management of water quality in reservoirs. Water, 29(5): 20-27.

Brookes, J.D., Sherman, B.S. and Burch, M., 1999b. Artificial Mixing for Destratification and Control of Cyanobacterial Growth in Reservoirs, Project 2.5.1. Sixth month milestone report, CRC Water Quality and Treatment, Adelaide.

Burch, M.D., Velzeboer, R.M.A., Chow, C.W.K., Stevens, H.C., Bee, C.M., and J. House, 1998. Evaluation of copper algicides for the control of algae and cyanobacteria. 130, Urban Water Research Association of Australia, Melbourne.

Carmichael, W.W., 1992. Cyanobacteria secondary metabolites- the cyanotoxins. Journal of Applied Bacteriology, 72: 445-459.

Carter Lund, H. and Lund, J.W.G., 1995. Freshwater Algae. Their microscopic world explored. Biopress Ltd, Bristol, Bristol, 360 pp.

Chigier, N.A. and Chervinsky, A., 1967. Experimental Investigation of Swirling Vortex Motion in Jets. Journal of Applied Mechanics, 34: 443-451.

Chorus, I. and Bartram, J. (Editors), 1999. Toxic Cyanobacteria in Water. E & FN Spoon, 416 pp.

Cotonnec, G., Brunet, C., Sautour, B. and Thoumelin, G., 2001. Nutritive value and selection of food particles by copepods during a spring bloom of *Phaeocystis sp.* in the English Channel, as determined by pigment and fatty acid analyses. Journal of Plankton Research, 23(7): 693-703.

Cowell, B.C., Dawes, C.J., Gardiner, W.E. and Scheda, S.M., 1987. The influence of whole lake aeration on the limnology of a hypereutrophic lake in central Florida. Hydrobiologia, 148: 3-24.

Crow, S.C. and Champagne, F.H., 1971. Orderly structure in jet turbulence. Journal of Fluid Mechanics, 48(3): 547-591.

de Jonge, V.N., Elliott, M. and Orive, E., 2002. Causes, historical development, effects and future challenges of a common environmental problem: eutrophication. Hydrobiologia, 475(1): 1-19.

Droop, M.R., 1973. Some thoughts on nutrient limitation in algae. Journal of Phycology, 9: 264-272.

Elliott, J.A., Irish, A.E., Reynolds, C.S. and Tett, P., 2000a. Modelling freshwater phytoplankton communities: an exercise in validation. Ecological Modelling, 128: 19-26.

Elliott, J.A., Reynolds, C.S. and Irish, A.E., 2000b. The diversity and succession of phytoplankton communities in disturbance-free environments using the model, PROTECH. Archiv für Hydrobiologie, 149: 241-258.

Elliott, J.A., Reynolds, C.S. and Irish, A.E., 2000c. An investigation of dominance in phytoplankton using the PROTECH model. Freshwater Biology, 46(1): 99-108.

Elliott, S., 2002. Personal Communication.

Falconer, I., 1999. An overview of problems caused by toxic blue-green algae (cyanobacteria) in drinking and recreational water. Environmental Toxicology, 14(1): 5-12.

Falconer, I., 2001. Toxic cyanobacterial bloom problems in Australian waters: risks and impacts on human health. Phycologia, 40(3): 228-233.

Fischer, H.B., List, J.L., Koh, R.C.Y., Imberger, J. and Brooks, N.H., 1979. Mixing in Inland and Coastal Waters. Academic Press, 483 pp.

Ganf, G.G., 1980. Factors controlling the growth of phytoplankton in Mt Bold Reservoir, South Australia. A.W.R.C. Technical report, Australian Government Publishing Service.

Gates, D.M., 1966. Spectral distribution of solar radiation on the Earth's surface. Science, 151: 523-529.

George, D.G., 2000. Remote sensing evidence for the episodic transport of phosphorus from the littoral zone of a thermally stratified lake. Freshwater Biology, 43(4): 571-578.

Ghazzawina, R., 1994. Self-similar solutions for axisymmetrical jets using 2 turbulence models. International Journal for Numerical Methods in Engineering, 37(11): 1915-1930.

Giussani, G., Debernardi, R. and Ruffoni, T., 1990. 3 Years of Experience in Biomanipulating a Small Eutrophic Lake - Lago-Di-Candia (Northern Italy). Hydrobiologia, 200: 357-366.

Gliwicz, Z.M. and Lampert, W., 1990. Food thresholds in daphnia species in the absence and presence of blue-green filaments. Ecology, 71(2): 691-702.

Griffin, S.L., Herzfeld, M. and Hamilton, D.P., 2001. Modelling the impact of zooplankton grazing on phytoplankton biomass during a dinoflagellate bloom in the Swan River Estuary, Western Australia. Ecological Engineering, 16(3): 373-394.

Gupta, A.K., Lilley, D.G. and Syred, N. (Editors), 1984. Swirl Flows. Energy and Engineering Science Series. Abacus Press, 475 pp.

Hamill, G.A. and Johnston, H.T., 1993. The Decay of Maximum Velocity within the Initial Stages of a Propeller Wash. Journal of Hydraulic Research, 31(5): 605-613.

Hamill, G.A., Johnston, H.T. and Stewart, D.P., 1999. Propeller wash scour near quay walls. Journal of Waterway Port Coastal & Ocean Engineering-ASCE, 125(4): 170-175.

Hamilton, D.P., 1999. Numerical modelling and reservoir management: applications of the DYRESM model. In: J.G. Tundisi and M. Straskraba (Editors), Theoretical Reservoir Ecology and its Applications. International Institute of Ecology, Brazilian Academy of Sciences and Backhuys Publishers, pp. 153-173.

Hamilton, D.P. and Schladow, G., 1995. Controlling the indirect effects of flow diversions on water quality in an Australian reservoir. Environment International, 21(5): 583-590.

Hamilton, D.P. and Schladow, S.G., 1997. Prediction of water quality in lakes and reservoirs. Part 1-Model description. Ecological Modelling, 96: 91-110.

Herzfeld, M. and Hamilton, D.P., 2000. The CWR Computational Aquatic Ecosystem Dynamics Model CAEDYM, The Centre for Water Research, University of Western Australia.

Hicks, B.B., 1972. Some evaluations of drag and bulk transfer coefficients over water. Boundary-layer Meteorology, 8: 201-213.

Hillebrand, H., Dürselen, C.D., Kirschtel, D., Zohary, T. and Pollingher, U., 1999. Biovolume calculation for pelagic and benthic microalgae. Journal of Phycology, 35(2): 403-424.

Hindell, J.S., Jenkins, G.P., Moran, S.M. and Keough, M.J., 2003. Swimming ability and behaviour of post-larvae of a temperate marine fish re-entrained in the pelagic environment. Oecologia, 135(1): 158-66.

Hocking, G.C., Sherman, B.S. and Patterson, J.C., 1988. Algorithm for selective withdrawal from stratified reservoir. Journal of the Hydraulic Division, ASCE, 114: 707-719.

Hodgkin, E.P. and Hamilton, B.H., 1993. Fertilizers and Eutrophication in South-Western Australia - Setting the Scene. Fertilizer Research, 36(2): 95-103.

Hoge, F.E. Wright, C.W., Swift, R.N., Yungel, J.K., Berry, R.E., and R. Mitchell, 1998. Fluorescence signatures of an iron-enriched phytoplankton community in the eastern equatorial Pacific Ocean. Deep-Sea Research, Part II: Topical Studies in Oceanography, 45(6): 1073-1082.

Holm, N.P., Ganf, G.G. and Shapiro, J., 1983. Feeding and assimilation of *Daphnia pulex* fed *Aphanizomenon flos-aquae*. Limnology and Oceanography, 28: 677-687.

Hooper, F.H., Ball, R.C. and Tanner, H.A., 1952. An experiment in the artificial circulation of a small Michigan lake. Transactions of the American Fisheries Society, 82: 222-241.

Humphries, S.E. and Imberger, J., 1982. The influence of the internal structure and dynamics of Burrinjuck Reservoir on phytoplankton blooms. ED 82-023, University of Western Australia, Nedlands.

Hyun, B.S. and Patel, V.C., 1991. Measurements in the flow around a marine propeller at the stern of an axisymmetric body. Part 1: Circumferentially-averaged flow. Experiments in Fluids, 11: 33-44.

Imberger, J., 1982. Reservoir dynamics modelling. In: M. O'Laughlin and P. Cullen (Editors), Predictions in Water Quality. Australian Academy of Science, Canberra, pp. 223-248.

Imberger, J. and Hamblin, P.F., 1982. Dynamics of lakes, reservoirs and cooling ponds. Annual Review of Fluid Mechanics, 14: 153-187.

Imberger, J., Patterson, J., Hebbert, B. and Loh, I., 1978. Dynamics of reservoir of medium size. Journal of the Hydraulics Division, 104(5): 725-743.

Imberger, J. and Patterson, J.C., 1981. A dynamic reservoir simulation model-DYRESM:5. In: H.B. Fischer (Editor), Transport Models for Inland and Coastal Waters. Academic Press, pp. 310-361.

Imberger, J. and Patterson, J.C., 1989. Physical Limnology, Advances in Applied Mechanics, pp. 303-475.

Imboden, D.M. and Wuest, A., 1995. Mixing mechanisms in lakes. In: D.M. Imboden, J. Gat, L. Chou and A. Lerman (Editors), Physics and chemistry of lakes. Springer-Verlag, pp. 83-138.

Imteaz, M.A. and Asaeda, T., 2000. Artificial mixing of lake water by bubble plume and effects of bubbling operations on algal bloom. Water Research, 34(6): 1919-1929.

Ismail, R., Kassim, M.A., Inman, M., Baharim, N.H. and Azman, S., 2002. Removal of iron and manganese by artificial destratification in a tropical climate (Upper Layang Reservoir, Malaysia). Water Science & Technology, 46(9): 179-183.

Jones, G.J., 1997. Limnological study of cyanobacterial dominance in three South-East Queensland reservoirs. In: R.R.D. Davis (Editor), Managing Algal Blooms: Outcomes from the CSIRO Blue-Green Algal Research Program. CSIRO Land and Water, Canberra, pp. 51-66.

Jonsson, L. and Rissler, S., 1991. The use of mixers for improving water quality in reservoirs, lakes, and harbours. In: A.A. Balkema (Editor), European Conference on Advances in Water Resources, Rotterdam, The Netherlands, pp. 407-416.

Jørgensen, S.E., 1986. Fundamentals of Ecological Modelling. Elsevier, Amsterdam, 391 pp.

Jørgensen, S.E., 1995a. The growth rate of zooplankton at the edge of chaos: ecological models. Journal of Theoretical Biology, 175(1): 13-21.

Jørgensen, S.E., 1995b. The state of the art of ecological modelling in limnology. Ecological Modelling, 78: 101-115.

Kim, D.S. and Watanabe, Y., 1993. The effect of long-wave ultraviolet radiation (UV-A) on the photosynthetic activity of natural-populations of fresh-water phytoplankton. Ecological Research, 8(2): 225-234.

Kirk, J.T.O., 1983. Light and photosynthesis in aquatic ecosystems. Cambridge University Press, Cambridge, 401 pp.

Kirk, J.T.O., 1994. Light and photosynthesis in aquatic systems. Cambridge University Press, 509 pp.

Kotsovinos, N.E. and List, E.J., 1977. Plane turbulent buoyant jets. Part 2. Turbulence structure. Journal of Fluid Mechanics, 81: 25-44.

Kuczera, G. and Parent, E., 1998. Monte Carlo assessment of parameter uncertainty in conceptual catchment models: The Metropolis algorithm. Journal of Hydrology, 211(1 - 4): 69 - 85.

Lewis, D.M., Antenucci, J.P., Brookes, J.D. and Lambert, M.F., 2001a. Numerical simulation of surface mixers used for artificial mixing in reservoirs., Environmental Engineering Research Event, Noosa, Queensland, Australia.

Lewis, D.M., Antenucci, J.P., Brookes, J.D. and Lambert, M.F., 2001b. Numerical simulation of surface mixers used for destratification of reservoirs. In: F. Ghassemi, D. Post, M. Sivapalan and R. Vertessy (Editors), International Congress on Modelling and Simulation, MODSIM, pp. 311-317.

Lewis, D.M., Antenucci, J.P., Brookes, J.D. and Lambert, M.F., 2002a. Surface mixing for destratification: simulating the impact. Water, 29: 27-29.

Lewis, D.M., Elliott, J.A., Lambert, M.F. and Reynolds, C.S., 2002b. The simulation of an Australian reservoir using a phytoplankton community model: PROTECH. Ecological Modelling, 150(1-2): 107-116.

Lewis, D.M., Elliott J.A., Brookes, J.D., Lambert, M.F., Irish, A.E., and C.S. Reynolds, 2003. Modelling the effects of artificial mixing and copper sulphate dosing on phytoplankton in an Australian reservoir. Lakes and Reservoirs: Research and Management, 8: 31-40.

Lewis, M.R., Cullen, J.J. and Platt, T., 1984. Relationships between vertical mixing and photoadaption of phytoplankton: similarity criteria. Marine Ecology, 15: 141-149.

Lewis, W.M.J., 1979. Spatial distribution of the phytoplankton in a tropical lake (Lake Lanao, Philippines). Internationale Revue der gesamten Hydrobiologie, 63: 619-635.

Linden, L.G., Burch, M.D., Brookes, J.D., Baker, P., Sherman, B.S. and D.M. Lewis, 2002. Artificial destratification and water quality in Happy Valley Reservoir. Report to Bulk Water Liaison Group, Cooperative Research Centre for Water Quality and Treatment, Adelaide.

Linden, L.G., Lewis, D.M., Burch, M.D. and Brookes, J.D., 2003. Nutrient load is determined by high flow episodes in the Mediterranean Myponga Reservoir. Marine and Freshwater Research, (In Review).

List, E.J., 1982. Turbulent jets and plumes. Annual Review of Fluid Mechanics, 14: 189-212.

Loague, K. and Green, R.E., 1991. Statistical and graphical methods for evaluating solute transport methods: Overview and application. Journal of Contaminant Hydrology, 7: 51-73.

Lorenzen, C.J., 1967. Determination of chlorophyll and phaeopigments - spectrophotometric equations. Limnology and Oceanography, 12: 343-346.

Lorenzen, M.W., 1972. The role of artificial mixing in eutrophication control. PhD Thesis, Harvard University, Cambridge, 186 pp.

MacIntyre, S., 1993. Vertical mixing in a shallow, eutrophic lake: possible consequences for the light climate of phytoplankton. Limnology and Oceanography, 38(4): 798-817.

MacIntyre, S., 1996. Turbulent eddies and their implications for phytoplankton within the euphotic zone of Lake Biwa, Japan. Japan Journal of Limnology, 57(4): 395-410.

MacIntyre, S., Romero, J.R. and Kling, G.W., 2002. Spatial-temporal variability in surface layer deepening and lateral advection in an embayment of Lake Victoria, East Africa. Limnology and Oceanography, 47(3): 656-671.

Mayer, D.G. and Butler, D.G., 1993. Statistical Validation. Ecological Modelling, 68: 21-32.

McAuliffe, T.A. and Rosich, R.S., 1989. Review of artificial destratification of water storages in Australia, Urban Water Research Association of Australia, Melbourne.

McKinion, J.M. and Baker, D.N., 1982. Modelling, experimentation, verification and validation: Closing the feedback loop. Transactions of the American Society of Agricultural Engineers, 25: 647 - 653.

McLaughlin, D.K. and Givens, M.R., 1978. A hydraulic model study of propeller-type lake destratification pumps. A-075-OKLA, School of Mechanical and Aerospace Engineering Oklahoma State University, Stillwater, Oklahoma.

Monismith, S.G. and Fong, D.A., 1996. A simple model of mixing in stratified tidal flows. Journal of Geophysical Research - Oceans, 101(12): 28583-28595.

Monismith, S.G., Imberger, J. and Morison, M.L., 1990. Convective motions in the sidearm of a small reservoir. Limnology and Oceanography, 35: 1676-1702.

Mortimer, C.H., 1941. The exchange of dissolved substances between mud and water in lakes. I. Journal of Ecology, 29: 280-329.

Mortimer, C.H., 1942. The exchange of dissolved substances between mud and water in lakes. II. Journal of Ecology, 30: 147-201.

Morton, B.R., 1968. Similarity and breakdown in swirling turbulent jets. Mechanical and Chemical Engineering Transactions, MC4(2): 241-246.

Morton, B.R., Taylor, G. and Turner, J.S., 1956. Turbulent gravitational convection from maintained and instantaneous sources. Proceedings of the Royal Society of London, 234: 1-23.

Pahl-Wostl, C. and Imboden, D.M., 1990. DYPHORA - A dynamic model for the rate of photosynthesis of algae. Journal of Plankton Research, 12: 1207-1221.

Park, S.H. and Shin, H.D., 1993. Measurements of entrainment characteristics of swirling jets. Int. J. Heat Mass Transfer, 36(16): 4009-4018.

Pasciak, W.J. and Gavis, J., 1974. Transport limitation of nutrient uptake in phytoplankton. Limnology and Oceanography, 19: 881-889.

Patterson, J.C., 1991. Modelling the effects of motion on primary production in the mixed layer of lakes. Aquatic Sciences, 53(2/3): 218-238.

Patterson, J.C., Hamblin, P.F. and Imberger, J., 1984. Classification and dynamic simulation of the vertical density structure of lakes. Limnology and Oceanography, 29(4): 845-861.

Patterson, J.C., Hamilton, D.P. and Ferris, J.M., 1994. Modelling of cyanobacteria blooms in the mixed layer of lakes and reservoirs. Australian Journal of Marine and Freshwater Research, 45: 829-845.

Patterson, J.C. and Imberger, J., 1989. Simulation of bubble plume destratification systems in reservoirs. Aquatic Sciences, 51(1): 3-18.

Persson, P.E., 1983. Off-flavours in aquatic ecosystems - An introduction. Water Science & Technology, 15: 1-11.

Peterson, J. and Bayazitoglu, Y., 1992. Measurements of Velocity and Turbulence in Vertical Axisymmetrical Isothermal and Buoyant Jets. Journal of Heat Transfer-Transactions of the ASME, 114(1): 135-142.

Petersson, P., 1996. Laser doppler velocity measurements in an impeller-generated turbulent jet. 3195, Lund Institute of Technology, Lund University, Sweden.

Petersson, P., Larson, M. and Jonsson, L., 1996. Measurements of the velocity field downstream of an impeller. Journal of Fluids Engineering - Transactions of the ASME, 118(3): 602-610.

Petersson, P., Larson, M. and Jonsson, L., 2000. Development of a turbulent jet generated by a mixer in weak co-flow and counter-flow. International Journal of Heat & Fluid Flow, 21(1): 1-10.

Pitts, W.M., 1991. Reynolds-number effects on the mixing behaviour of axisymmetrical turbulent jets. Experiments in Fluids, 11(2-3): 135-141.

Pratte, B.D. and Keffer, J.F., 1972. The swirling turbulent jet. Journal of Basic Engineering, 94(4): 739-748.

Priestley, C.H.B. and Ball, F.K., 1955. Continuous convection from an isolated source of heat. Quarterly journal of the Royal Meteorological Society, 81(348): 144-157.

Psenner, R., 1994. Environmental Impacts on Freshwaters - Acidification as a Global Problem. Science of the Total Environment, 143(1): 53-61.

Quintero, J.E. and Garton, J.E., 1973. A low energy lake destratifier. Transactions of the American Society of Agricultural Engineering, 16(5): 973-978.

Redalje, D.G., Lohrenz, S.E., Verity, P.G. and Flagg, C.N., 2002. Phytoplankton dynamics within a discrete water mass off Cape Hatteras, North Carolina: the Lagrangian experiment. Deep-Sea Research, Part II: Topical Studies in Oceanography, 49(20): 4511-4531.

Reynolds, C.S., 1984. The Ecology of Freshwater Phytoplankton. Cambridge University Press, Cambridge, 384 pp.

Reynolds, C.S., 1988. Functional morphology and the adaptive strategies of freshwater phytoplankton. In: C.D. Sandgren (Editor), Growth and Reproductive Strategies of Freshwater Phytoplankton. Cambridge University Press, New York, pp. 388-433.

Reynolds, C.S., 1989. Physical determinants of seasonal change in the species composition of phytoplankton. In: U. Sommer (Editor), Phytoplankton Ecology: succession in plankton communities. Springer Verlag, New York, pp. 9-56.

Reynolds, C.S., 1997a. The Pelagic Environment. In: O. Kinne (Editor), Vegetation Processes in the Pelagic: A Model for Ecosystem Theory. Excellence in Ecology. Ecology Institute, Oldendorf/Luhe, pp. 21-70.

Reynolds, C.S. (Editor), 1997b. Vegetation Processes in the Pelagic: A Model for Ecosystem Theory. Excellence in Ecology, 9. Ecology Institute, Oldendorf/Luhe, 371 pp.

Reynolds, C.S. and Irish, A.E., 1997. Modelling phytoplankton dynamics in lakes and reservoirs: the problem of in-situ growth rates. Hydrobiologia, 349: 5-17.

Reynolds, C.S., 1999. Personal communication.

Reynolds, C.S., Irish, A.E. and Elliott, J.A., 2001. The ecological basis for simulating phytoplankton responses to environmental change. Ecological Modelling, 140: 271-291.

Reynolds, C.S. and Walsby, A.E., 1975. Water-blooms. Biological Reviews of the Cambridge Philosophical Society, 50(4): 437-481.

Reynolds, C.S., Wiseman, S.W. and Clarke, M.J.O., 1984. Growth and loss-rate responses of phytoplankton to intermittent artificial mixing and their potential application to the control of planktonic algal biomass. Journal of Applied Ecology, 21: 11-39.

Ricou, F.P. and Spalding, D.B., 1961. Measurements of entrainment by axisymmetrical turbulent jets. Journal of Fluid Mechanics, 11: 21-32.

Riley, G.A., 1957. Phytoplankton of the North Central Sargasso Sea. Limnology and Oceanography, 2: 272-270.

Riley, M.J. and Stefan, H.G., 1987. Dynamic lake water quality simulation model "MINLAKE", University of Minnesota, St. Paul, Minnesota.

Rodi, W., 1982. Turbulent Buoyant jets and plumes. Pergamon Press, 184 pp.

Rosler, R.S. and Bankoff, S.G., 1963. Large-scale turbulence characteristics of a submerged water jet. American Institute of Chemical Engineers Journal, 9(5): 672-676.

Rouse, H., Yih, C.S. and Humphreys, H.W., 1952. Gravitational convection from a boundary source. Tellus, 4: 201-210.

Rykiel, E.J., 1996. Testing ecological models: the meaning of validation. Ecological Modelling, 90: 229-244.

Sami, S., Carmody, T. and Rouse, H., 1967. Jet diffusion in the region of flow establishment. Journal of Fluid Mechanics, 27: 231-252.

Schladow, S.G. and Fisher, I.H., 1995. The physical response of temperate lakes to artificial destratification. Limnology and Oceanography, 40(2): 359-373.

Schladow, S.G. and Hamilton, D.P., 1995. Effect of major flow diversion on sediment nutrient release in a stratified reservoir. Marine and Freshwater Research, 46: 189-195.

Schladow, S.G. and Hamilton, D.P., 1997. Prediction of water quality in lakes and reservoirs: Part II - Model calibration, sensitivity analysis and application. Ecological Modelling, 96: 111-123.

Sherman, B.S., Webster, I.T., Jones, G.J. and Oliver, R.L., 1998. Transitions between *Aulacoseira* and *Anabaena* dominance in a turbid weir pool. Limnology and Oceanography, 43: 1902-1915.

Sherman, B.S., Whittington, J. and Oliver, R., 2000. The impact of artificial mixing on water quality in Chaffey Reservoir. Archiv fur Hydrobiologie, 55: 15-29.

Sivonen, K. and Jones, G., 1999. Cyanobacterial Toxins. In: I. Chorus and J. Bartram (Editors), Toxic Cyanobacteria in Water. E & F. N. Spoon, pp. 41-111.

Spigel, R.H. and Imberger, J., 1980. The classification of mixed layer dynamics in lakes of small to medium size. Journal of Physical Oceanography, 10(7): 1104-1121.

Spigel, R.H. and Imberger, J., 1987. Mixing processes relevant to phytoplankton dynamics in lakes. New Zealand Journal of Marine and Freshwater Research, 21: 361-377.

Steel, J.A. and Duncan, A., 1999. Modelling the ecological aspects of bankside reservoirs and implications for management. Hydrobiologia, 396: 133-147.

Steichen, J.M., 1970. The effect of lake destratification on water quality parameters. PhD Thesis, Oklahoma State University, Stillwater, Oklahoma, 108 pp.

Steinberg, C., 1983. Effects of artificial destratification on the phytoplankton populations in a small lake. Journal of Plankton Research, 5(6): 855-864.

Stephens, R. and Imberger, J., 1993. Reservoir destratification via mechanical mixers. Journal of hydraulic engineering, 119(4): 438-457.

Suter, P.J. and Kilmore, G., 1990. Mechanical mixers: an alternative destratification technique, Myponga Reservoir, South Australia. Journal of the Australian Water and Wastewater Association, February: 32-35.

Thomas, D., Kotz, S. and Rixon, S., 1999. Watercourse survey and management recommendations for the Myponga River catchment, Environmental Protection Agency, Adelaide, South Australia.

Tikkanen, T. and Willen, T., 1992. Vaxtplanktonflora. Ord & Bildmkarna AB, Stockholm.

Townsend, A.A., 1976. The Structure of Turbulent Shear Flow. Cambridge monographs on mechanics and applied mathematics. Cambridge University Press, 429 pp.

Turner, J.S., 1966. Jets and plumes with negative or reversing buoyancy. Journal of Fluid Mechanics, 26(4): 779-792.

Turner, J.S., 1973. Buoyancy Effects in Fluids. Cambridge University Press, 367 pp.

Tyson, W.C. and Mobley, M.H., 1996. Surface water pump velocities at Cherokee Dam, Tennessee Valley Authority, Norris, Tennessee.

Velzeboer, R.M.A., Cugley, J.A. and Patterson, J.C., 1991. Modelling optimum conditions for reservoir destratification using mechanical mixers. 24, Urban Water Research Association of Australia.

Viner, A.B., 1983. The effect of vertical mixing on the phytoplankton of Lake Rotongaio (July 1979-January 1981). N.Z. J. of Marine and Freshwater Research, 17: 407-422.

Visser, P.M., Ibelings, B.W., Vanderveer, B., Koedood, J. and Mur, L.R., 1996. Artificial mixing prevents nuisance blooms of the cyanobacterium *Microcystis* in Lake Nieuwe Meer, the Netherlands. Freshwater Biology, 36(2): 435-450.

Visser, P.M., Ketelaars, H.A.M. and Mur, L.R., 1995. Reduced growth of the cyanobacterium *Microcystis* in an artificially mixed lake and reservoir. Water Science & Technology, 32(4): 53-54.

Wahl, T.L., 2000. Analyzing ADV data using WinADV. In: R.H. Hotchkiss and M. Glade (Editors), 2000 Joint Conference on Water Resources Engineering and Water Resources Planning and Management. American Society of Civil Engineers, Minneapolis, Minnesota, pp. 4000.

Walsby, A.E., 1997. Modelling the daily integral of photosynthesis by phytoplankton: its dependence on the mean depth of the population. Hydrobiologia, 349: 65-74.

Wanninkhof, R., 1992. Relationship between wind speed and gas exchange over the ocean. Journal of Geophysical Research, 97: 7373-7382.

Webb, W.L. and Newton, M., 1974. Carbon dioxide exchange of *Alnus rubra*: a mathematical model. Oecologia, 17(281-291).

Wells, M.G. and Sherman, B.S., 2001. Stratification produced by surface cooling in lakes with significant shallow regions. Limnology and Oceanography, 46(7): 1747-1759.

Westwood, K. and Ganf, G.G., 2002. Effect of mixing patterns and light dose on growth of *Anabaena circinalis* in a turbid lowland river. River Management and Application (In Review).

Wetzel, R.G., 2001. Limnology - Lake and River Ecosystems. Academic Press, Florida, 1006 pp.

Whitaker, J., Barica, J., Kling, H. and Buckley, M., 1978. Efficacy of copper sulphate in the suppression of *Aphanizomenon flos-aquae* blooms in prairie lakes. Environmental Pollution, 15(185-194).

APPENDIX A. FIELD SITE INFORMATION

Table A.1 Thermistor locations below surface (m).

Myponga 1 Main Basin	Myponga 2 Side arm
0.1	0.1
0.2	0.2
0.4	0.3
0.6	0.4
0.8	0.5
1.0	0.6
1.5	0.8
2.0	1.0
2.5	1.2
3.0	1.4
3.5	1.6
4.0	1.8
5.0	2.0
6.0	2.5
7.0	3.0
8.0	3.5
9.0	4.0
10.0	5.0
12.5	6.0
15.0	7.0
17.5	8.0
20.0	9.0
25.0	10.0
30.0	12.5
	15.0

Table A.2 Australian case studies (McAuliffe and Rosich, 1989).

Aroona Reservoir	Greaves Creek Reservoir	Little Bass Reservoir	Running Creek Reservoir
Avon Dam	Happy Valley Reservoir	Little Nerang Creek Dam	Solomon Dam
Barossa Reservoir	Harding Reservoir	Little Para Reservoir	Split Rock Dam
Bullarto Reservoir	Hindmarsh Reservoir	Lyell Reservoir	Sugarloaf (Winneke) Reservoir
Callide Dam	Hinze Dam	Lower Cascade Reservoir	Suma Park Reservoir
Carcoar Dam	Kangaroo Creek Reservoir	Malpas Reservoir	Tarago Reservoir
Chaffey Dam	Korumburra No 1	Mangrove Creek Reservoir	Thomsons Creek Reservoir
Chichester Dam	Lake Bullen Merri	Mardi Dam	Thomson Dam
Dartmouth Dam	Lake Eppalock	Myponga Reservoir	Upper Cordeaux Reservoir
Deep Creek Reservoir	Lake Manchester	North Pine Dam	Warren Reservoir
Enoggera Dam	Lake Medlow	Porters Creek Reservoir	Windamere Dam
Glenbawn Dam	Lake Morris	Prospect Reservoir	Wombat Reservoir
Glennies Creek Reservoir	Lance Creek Reservoir	Rocky Creek Dam	Woodford Creek Reservoir

APPENDIX B. FIELD DATA

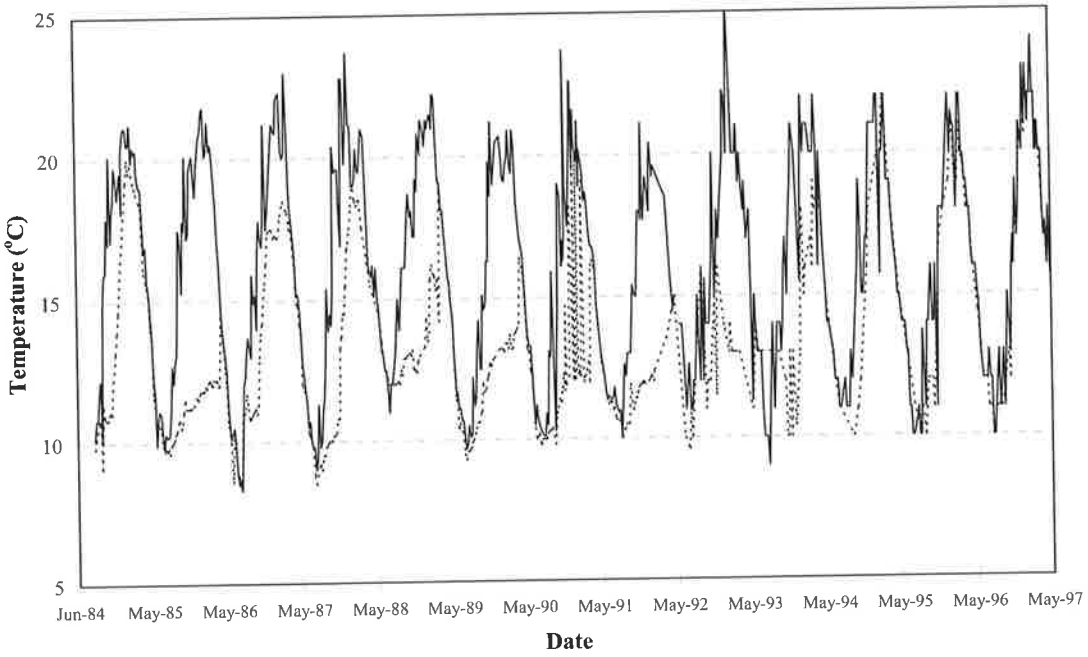

Figure B.1 Historical thermistor data for Myponga Reservoir, recorded at the water surface (solid line) and a depth of 30m (dashed line) from 1984 to 1998.

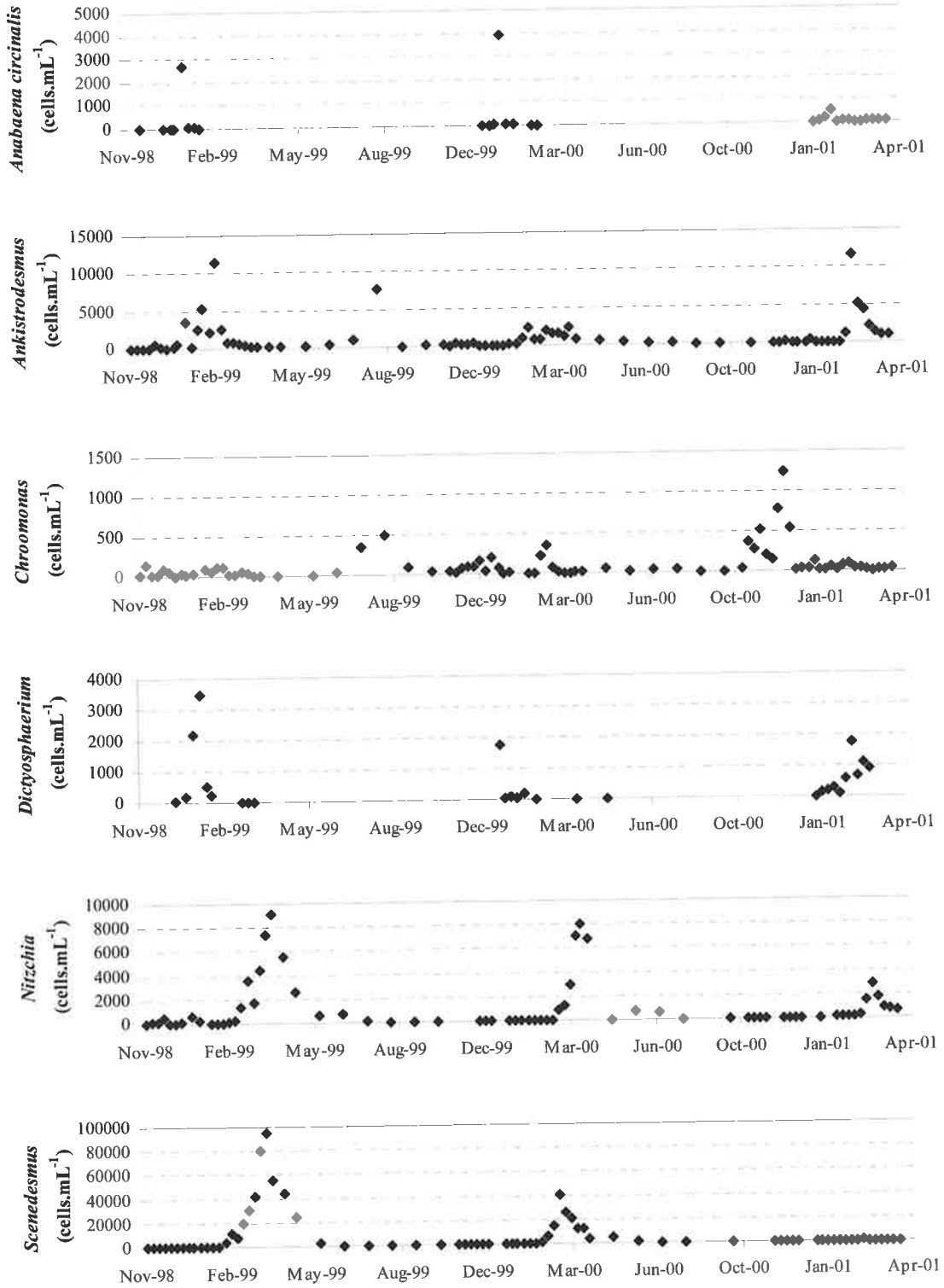

Figure B.2 Individual dominant phytoplankton species concentration at Location 1.

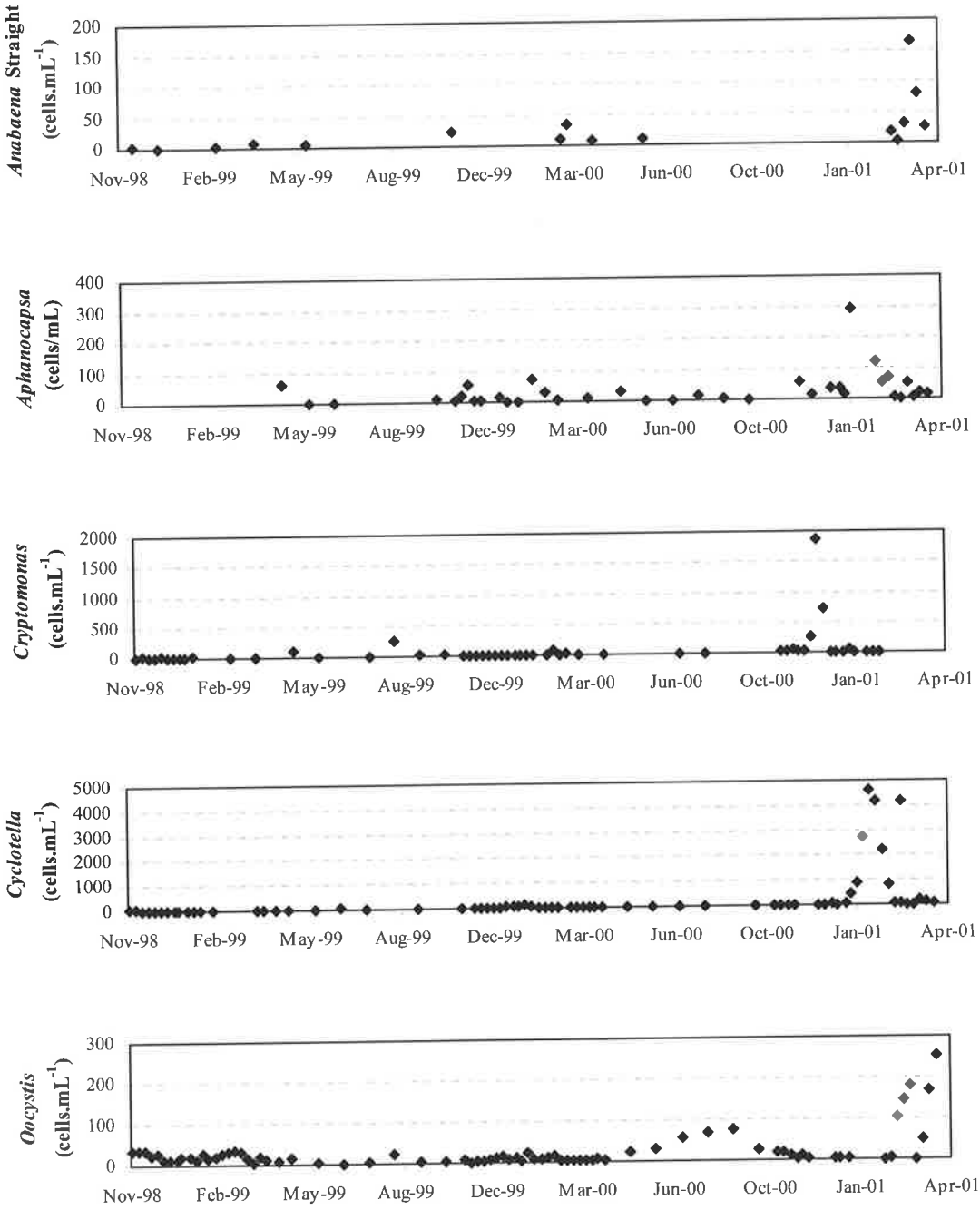

Figure B.3 Individual phytoplankton species concentration at Location 1.

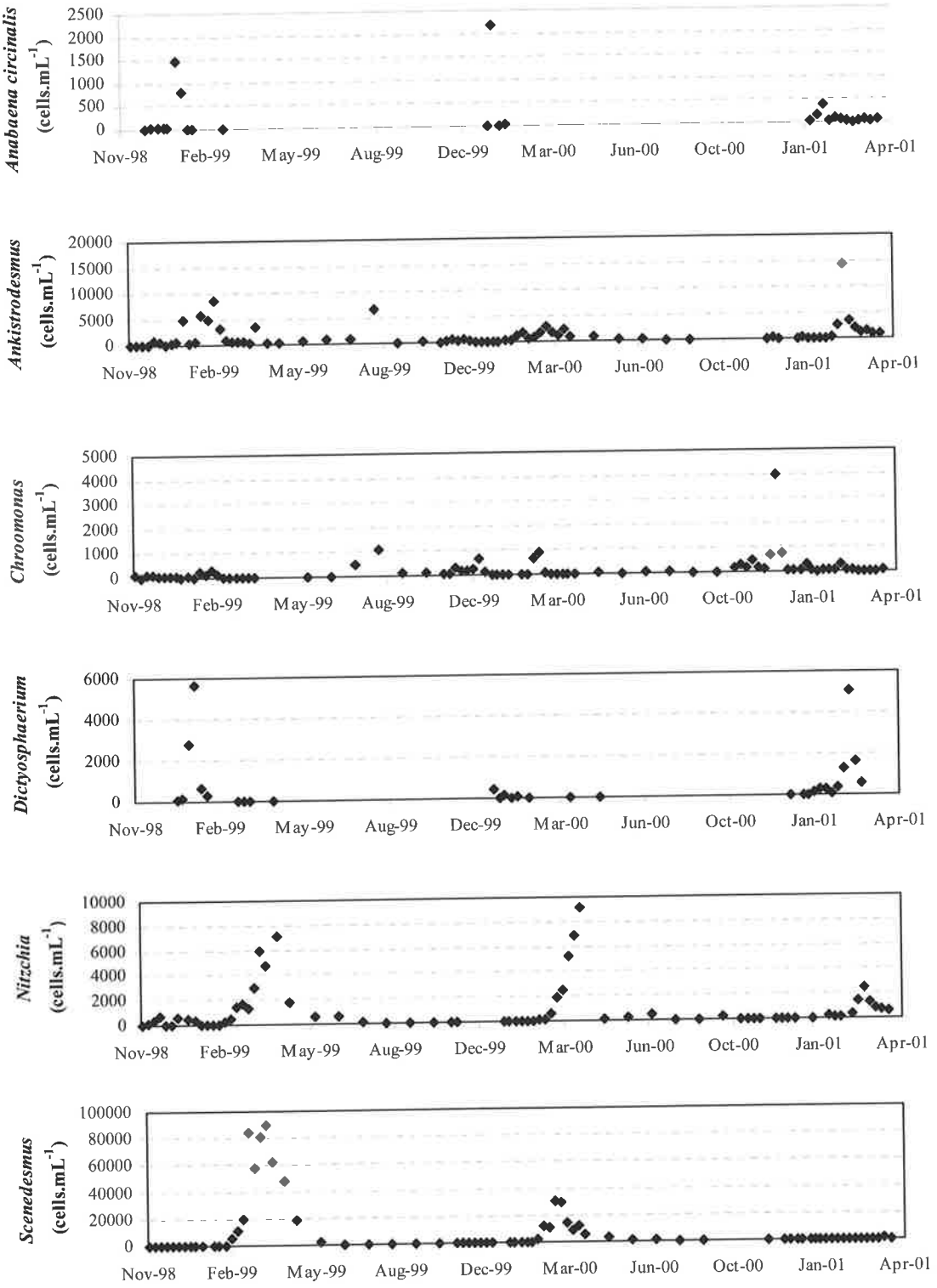

Figure B.4 Individual dominant phytoplankton species concentration at Location 4.

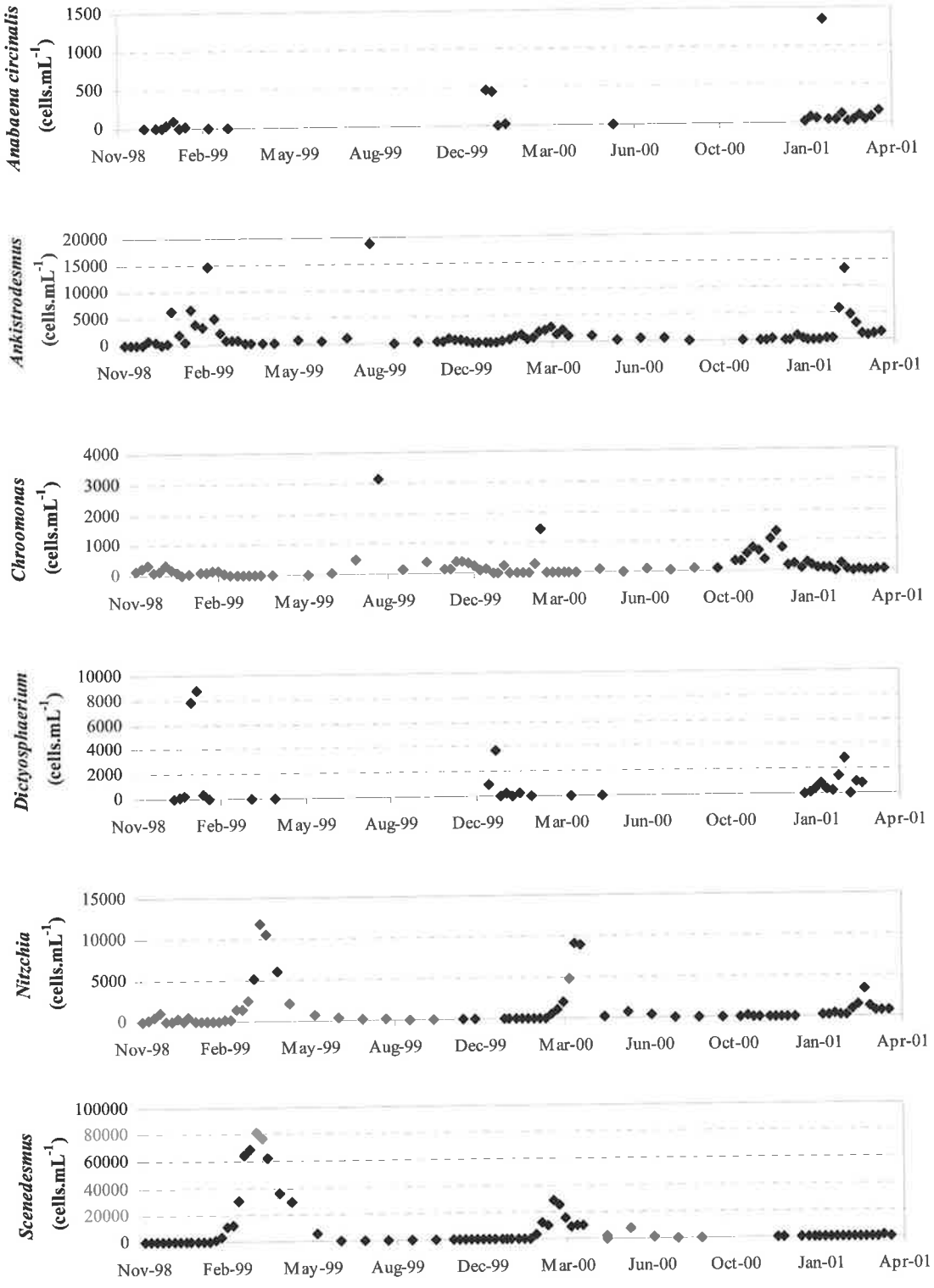

Figure B.5 Individual dominant phytoplankton species concentration at Location 7.

APPENDIX C. PROTECH INPUT FILES

The following PROTECH files are presented in Appendix C:

- Morphometry data (Depths.dat)
- Phytoplankton species and dimensions (Algae.des)
- Initial density profile (Site.des)

The time step used for the PROTECH simulation was inputted hourly, therefore due to the file size the following files are available on CD-ROM, entitled "Surface Mixers for Destratification and Management of *Anabaena circinalis* – Data":

- Cloud.dat
- Outflow.dat
- Outflowmixer.dat
- Pnloads.dat
- Pumps.dat
- Wind.dat
- Sediment.dat

C.1 DEPTHS

```
100   0      0
103   65     146.5
106   139    445.7
109   200    951.1
112   305    1703.7
115   414    2778.2
118   533    4194.8
121   681    6011.7
124   882    8349.1
127   1128   11355.8
130   1483   15260
133   1969   20421.4
136   2709   27409.3
```

C.2 ALGAE

```
diatom=F : 8.000E+01 : Scenedesmus
grazed=T : 9.080E+02 : Scenedesmus
Nfixer=F : 1.000E+03 : Scenedesmus
diatom=F : 6.000E+00 : Pseudanabaena
Grazed=F : 1.010E+02 : Pseudanabaena
Nfixer=F : 7.540E+01 : Pseudanabaena
diatom=T : 4.500E+01 : Nitzschia
Grazed=T : 5.910E+02 : Nitzschia
Nfixer=F : 5.660E+02 : Nitzschia
diatom=F : 8.000E+00 : Monoraphidium
Grazed=T : 1.260E+02 : Monoraphidium
Nfixer=F : 1.010E+02 : Monoraphidium
diatom=F : 1.250E+01 : Chroomonas
Grazed=T : 2.920E+02 : Chroomonas
Nfixer=F : 1.180E+02 : Chroomonas
diatom=F : 2.100E+01 : Cryptomonas
Grazed=T : 1.030E+03 : Cryptomonas
Nfixer=F : 2.710E+03 : Cryptomonas
diatom=F : 5.000E+00 : Chlamydomonas
grazed=T : 1.120E+02 : Chlamydomonas
Nfixer=F : 6.000E+01 : Chlamydomonas
diatom=F : 7.500E+01 : Anabaena
grazed=F : 6.200E+03 : Anabaena
Nfixer=T : 2.900E+04 : Anabaena
```

C.3 FIELD

```
Myponga Reservoir          : Title
      1           1        : nSeg (no. of segments), nTim
                             (no.of time steps/day)
      30.6                 : starting depth
      5586.0      1        : Maximum length of water body
      2           16.6     : 0 pumping outflow, 1 spill (river) &
                             pumping level metres
      2           15.0     : 0 jetting inflow; 1 spill inflow (river) :
                             if + then above mud;  - then depth below
                             surface waters
      1.0         0.5      : Summer and Autumn Wedderburn testing
                             constants
      0.4                  : Wstep testing constant
      0.3                  : Mixing Factor, Stable Water Column Surface
                             Cooling
      FALSE                : True if starting lake nutrients on next
                             line
      1                    : number of river inflows,  number of outlets
      MyCreek              : names of inflows (max 7 characters each)
      0           364      : iSkip (no. of days skipped), maxD (no. of
                             days run)
FlowWin=1.00 FlowSpr=1.00 FlowSum=1.00 FlowAut=1.00
HeatWin=1.00 HeatSpr=1.00 HeatSum=1.00 HeatAut=1.00
WindWin=1.00 WindSpr=1.00 WindSum=1.00 WindAut=1.00
1.000E+00 1.000E+00 1.000E+00 : tChlws,tChleq,tChlss
                          (total Chlorophyll levels)
0.014E-00 0.152E-00 0.207E-00 0.142E-00 0.142E-00 0.142E-00 0.142E-00
0.159E-00
      5.0                : length of integrated sampler
      0.000E+00          : pbirdi (input of phosphate by birds, kg/d)
      0                  : number of rivers to be phosphorus stripped
                           (max 10)
0.829E+00 : epsw (baseline epsilon)
1.055E+00 : resp (rate adjustment for respiration - 5.5% of temp
                  growth rate)
rpflag=1  rnflag=1  rsflag=1   gflag=0   fflag=1   mflag=0
rflag1=0       0.0
4                     : No. elements in starting profile: Temp P N Si
 100.0 11.84 65.5 937.5 7000
 105.6 11.89 65.5 937.5 7000
 110.6 11.89 65.5 937.5 7000
 115.6 12.02 65.5 937.5 7000
 120.6 12.27 65.5 937.5 7000
 125.6 12.56 65.5 937.5 7000
 126.6 12.87 65.5 937.5 7000
 130.6 13.58 65.5 937.5 7000
```

APPENDIX D. DYRESM – CAEDYM INPUT FILES

The following DYRESM – CAEDYM files are presented in Appendix D:

- DYRESM Configuration (Myponga.cfg)
- DYRESM Parameters (Myponga.par)
- CAEDYM Configuration (Myponga.con)
- Physical data and lake morphometry (Myponga.stg)
- CAEDYM Hardwire parameters (Harwire.hw)
- Initial profile (Myponga.pro)

A 10-minute time step was used in the simulation of Myponga Reservoir and subsequently large input files were required. The following files are available on accompanying CD-ROM, entitled "Surface Mixers for Destratification and Management of *Anabaena circinalis* – Data":

- Meteorological data (Myponga.met)
- Stream Inflow (Myponga.inf)
- Withdrawals (Myponga.wdr)
- Artificial mixing (Myponga.mix)
- Field data (Myponga.fld)
- CAEDYM Initialisation (Myponga.int)
- CAEDYM Water quality constants and parameters (Myponga.dat)

D.1 DYRESM CONFIGURATION

```
<#4>
! Myponga configuration file
1999244                 # Simulation start day
365                     # Simulation length (unit=day; max=3652day)
.true.                  # Run CAEDYM (.TRUE. or .FALSE.)
1                       # Output Interval per day
1.56                    # Light extinction coefficient
0                       # Benthic Boundary Thickness
1.5                     # Min layer thickness (m)
3.0                     # Max layer thickness (m)
3600                    # Time Step (s)
5                       # Number of Output Selections
TEMPTURE CYANO CHLOR FDIAT DO       # List of Output Selections
.true.  CONTINUOUS_OP   # Activate bubbler (.TRUE. or .FALSE.)
.FALSE.                  # Activate non-neutral atmospheric stability
(.TRUE. or .FALSE.)
```

D.2 DYRESM PARAMETER

```
<#5>
Parameters File.
1.3E-3          # bulk aerodynamic momentum transport coefficient
0.08            # mean albedo of water
0.96            # emissivity of a water surface
3.00            # critical wind speed [m s^-1]
46800           # time of day for output (in seconds)
2.0E0-3         # entrainment coefficient constant
0.012           # bubbler entrainment coefficient
0.083           # buoyant plume entrainment coefficient
0.06            # shear production efficiency (0.08) (eta_K)
0.20            # potential energy mixing efficiency (eta_P)
0.06            # wind stirring efficiency (0.06)    (eta_S)
1.0E+7          # effective surface area coefficient
200             # vertical mix coefficient
```

D.3 CAEDYM CONFIGURATION

```
11          ! Transport scheme invoked (0 = external advection)
 0          ! Open boundary condition type (0 = no open boundaries)
 2          ! Method of sediment nutrient flux calculation
 F          ! Simulate colour / tracer
 F          ! Simulate iron
 F          ! Simulate manganese
 F          ! Simulate aluminium
 F          ! Simulate pH
 F          ! Simulate turbulence quantities
 F          ! Print progress messages
 T          ! Print debug information
 Myponga.int     ! Initialisation file
 Myponga.dat     ! Constants file
 NULL       ! Inflow forcing file
 NULL
! 3D forcing file
 1.0        ! Print time step (days)
 60.0       ! Time series time step (minutes)
 1.0        ! Benthic time step (days)
 3          ! Number of phytoplankton groups to simulate
 2 4 7      ! Phytoplankton groups to simulate
 0          ! Number of zooplankton groups to simulate
 0          ! Number of jellyfish groups to simulate
 0          ! Number of fish groups to simulate
 0          ! Number of seagrass groups to simulate
 0          ! Number of macroalgae groups to simulate
 0          ! Number of invertebrate groups to simulate
 1  1  -2.0      ! Time series location
 0          ! Phytoplankton time series group
 0          ! Zooplankton time series group
 0          ! Jellyfish time series group
 0          ! Fish time series group
 0          ! Seagrass time series group
 0          ! Macroalgae time series group
 0          ! Invertebrate time series group
 0          ! Number of salinity divisions for time series output
 -1.  10. 25. 99. ! Salinity bounds for time series output
!Myponga configuration
```

D.4 PHYSICAL DATA AND LAKE MORPHOMETRY

```
<#3>
Myponga Reservoir morphometry
-35.24                          # latitude
100                             # height above MSL
1                               # number of inflows
SURF 88.8   0.24   0.016  Myponga Ck    # 1/2-angle, slope, drag coeff,
name
0.0                                # zero-ht elevation (i.e., bottom
elev.)
33.1                            # crest elevation [m]
1                               # number of outlets
19.31                           # outlet heights
11                                # number of stg survey points after
header line
   Elev [m]       A [m^2]
        3          127200
        6          205100
        9          289900
       12          389300
       15          501000
       18          641600
       21          839300
       24         1108000
       27         1448000
       30         1932000
       33.1       3200000
```

D.5 INITIAL PROFILE

```
Myponga Reservoir.  Initial profile.     01 Sep 1999    Met station 1
14      # number of initial profile points
Height (m)      T (Cel)      S (pss)
     0.7         13.66        0.422
     5.7         13.66        0.422
    10.7         13.67        0.422
    13.2         13.67        0.422
    15.7         13.71        0.422
    18.2         13.71        0.422
    20.7         13.72        0.422
    28.2         13.72        0.422
    28.7         13.79        0.422
    29.2         13.79        0.422
    29.7         13.84        0.422
    30.4         13.84        0.422
    30.5         13.87        0.422
    30.6         13.87        0.422
```

D.6 HARDWIRE

```
1       !number of phytoplankton groups that contain internal nitrogen
        stores
2       !array containing the actual phytoplankton groups with
        internal nitrogen stores
1       !number of phytoplankton groups which contain internal
        phosphorus stores
2       !array containing the actual phytoplankton groups with internal
        nitrogen    stores
0       !number of phytoplankton groups which contain internal carbon
        stores
0       !number of fish groups that are planktonic feeders
0       !number of fish groups that do not have adult/juvenile size
        classes
0       !3D forcing variables subject to error analysis
1.00E-03 !minimum allowable biomass for phytoplankton
1.00E-03 !minimum allowable biomass for zooplankton
1.00E-02 !minimum allowable biomass for all other species
T       !specification method for configuration file
0       !type of water system for the simulation
0       !experimental configuration flag
T       !sediment oxygen flux model
T       !output method for sediment oxygen
T       !resuspension
T       !sparse location where inflow concentrations are written
T       !motile phytoplankton direction they are advected
T       !vertical migration / settling is performed
T       !vertical extent to which non-motile phytoplankton may settle
T       !vertical extent to which motile phytoplankton may settle
T       !horizontal area to which 3D forcing is applied
T       !nutrient pool contributed by phytoplankton excretion is
        directed to
1       !Along-river init: Start sparse coordinate; lower bank
442     !Along-river init: Start sparse coordinate; upper bank
4       !Along-river init: Initial search direction, start edge"
1423    !Along-river init: End sparse coordinate; lower bank
1476    !Along-river init: End sparse coordinate; upper bank
4       !Along-river init: Initial search direction, end edge"
```